DOC.20041025.0004

QA: QA

MDL-WIS-PA-000003 REV 01

October 2004

Seismic Consequence Abstraction

Prepared for:
U.S. Department of Energy
Office of Civilian Radioactive Waste Management
Office of Repository Development
1551 Hillshire Drive
Las Vegas, Nevada 89134-6321

Prepared by:
Bechtel SAIC Company, LLC
1180 Town Center Drive
Las Vegas, Nevada 89144

Under Contract Number
DE-AC28-01RW12101

DISCLAIMER

This report was prepared as an account of work sponsored by an agency of the United States Government. Neither the United States Government nor any agency thereof, nor any of their employees, nor any of their contractors, subcontractors or their employees, makes any warranty, express or implied, or assumes any legal liability or responsibility for the accuracy, completeness, or any third party's use or the results of such use of any information, apparatus, product, or process disclosed, or represents that its use would not infringe privately owned rights. Reference herein to any specific commercial product, process, or service by trade name, trademark, manufacturer, or otherwise, does not necessarily constitute or imply its endorsement, recommendation, or favoring by the United States Government or any agency thereof or its contractors or subcontractors. The views and opinions of authors expressed herein do not necessarily state or reflect those of the United States Government or any agency thereof.

QA: QA

Seismic Consequence Abstraction

MDL-WIS-PA-000003 REV 01

October 2004

OCRWM	MODEL SIGNATURE PAGE/CHANGE HISTORY	Page iii 1. Total Pages: 267

2. Type of Mathematical Model

☐ Process Model ☒ Abstraction Model ☐ System Model

Describe Intended Use of Model

This abstraction defines the damage to the waste package, drip shield, and cladding from seismic hazards and defines the methodology for using these abstractions in the seismic scenario for TSPA-LA.

3. Title

Seismic Consequence Abstraction

4. DI (including Rev. No., if applicable):

MDL-WIS-PA-000003 REV 01

5. Total Appendices	6. No. of Pages in Each Appendix
Eight (8)	A-10; B-10; C-12; D-10; E-12; F-22; G-4; H-2, 1 CD

	Printed Name	Signature	Date
7. Originator	Michael Gross		10/22/04
8. Independent Technical Reviewer	Rob Howard		22 OCT 04
9. Checker	Jim Kam		10/22/04
10. QER	Darrell Svalstad		10/25/04
11. Responsible Manager/Lead	Mark Board		10/25/04
12. Responsible Manager	Mark Board		10/25/04

13. Remarks

Errata 1 (DC 38392) was addressed in REV 01.

Change History

14. Revision No.	15. Description of Change
REV 00	Initial Issue.
REV 01	Initial abstractions have been modified for: 1. Damaged area on the waste package and drip shield is represented as a network of stress corrosion cracks, rather than a "plug" of material that can separate from an EBS component. 2. The effective area of the crack network for diffusive transport is defined. Arguments are provided to demonstrate that the physical morphology of the crack network will not allow a significant advective flux to pass through the drip shield or waste package. 3. A distribution for the maximum value of peak ground velocity is described and incorporated into the computational methodology for the seismic scenario. 4. Minor changes to the fault displacement damage abstraction because of changes in waste package design for the outer diameter of the outer barrier. 5. Changes in waste package temperature and waste package relative humidity if a drift collapses in the lithophysal zones are incorporated into the seismic scenario. The entire document was revised because of extensive changes. Changes to this version are too extensive to be indicated by change bars.

INTENTIONALLY LEFT BLANK

CONTENTS

Page

CONTENTS (Continued)

Page

CONTENTS (Continued)

Page

INTENTIONALLY LEFT BLANK

FIGURES

Page

FIGURES (Continued)

Page

TABLES

Page

TABLES (Continued)

Page

ACRONYMS

BWR	boiling water reactor
CDSP	codisposal
CSNF	commercial spent nuclear fuel
DHLW	defense high-level radioactive waste
DOE	U.S. Department of Energy
EBS	engineered barrier system
ECRB	Enhanced Characterization of the Repository Block
FEPs	features, events, and processes
HLW	high-level radioactive waste
LA	license application
MSTHM	Multiscale Thermohydrologic Model
MT	metric ton (= 1,000 kg)
NRC	U.S. Nuclear Regulatory Commission
PGV	peak ground velocity
PSHA	Probabilistic Seismic Hazard Analysis
PWR	pressurized water reactor
RMEI	reasonably maximally exposed individual
SCC	stress corrosion crack
SNF	spent nuclear fuel
SR	site recommendation
TSPA	Total System Performance Assessment
TWP	technical work plan
UCL	upper confidence limit

INTENTIONALLY LEFT BLANK

1. PURPOSE

The primary purpose of this model report is to develop abstractions for the response of engineered barrier system (EBS) components to seismic hazards at a geologic repository at Yucca Mountain, Nevada, and to define the methodology for using these abstractions in a seismic scenario class for the Total System Performance Assessment - License Application (TSPA-LA). A secondary purpose of this model report is to provide information for criticality studies related to seismic hazards. The seismic hazards addressed herein are vibratory ground motion, fault displacement, and rockfall due to ground motion. The EBS components are the drip shield, the waste package, and the fuel cladding. The requirements for development of the abstractions and the associated algorithms for the seismic scenario class are defined in *Technical Work Plan For: Regulatory Integration Modeling of Drift Degradation, Waste Package and Drip Shield Vibratory Motion and Seismic Consequences* (BSC 2004 [DIRS 171520]).

The development of these abstractions will provide a more complete representation of flow into and transport from the EBS under disruptive events. The results from this development will also address portions of integrated subissue ENG2, Mechanical Disruption of Engineered Barriers, including the acceptance criteria for this subissue defined in Section 2.2.1.3.2.3 of the *Yucca Mountain Review Plan, Final Report* (NRC 2003 [DIRS 163274]).

1.1 SCOPE

The scope of this report is limited to abstracting the mechanical response of EBS components to seismic hazards during the postclosure period and defining algorithms for the seismic scenario class. The abstractions are based on the results from structural response calculations of EBS components to vibratory ground motion and from analyses for fault displacement. The structural response calculations are not documented in this report; rather, the results from these design calculations provide the input data that the abstractions are based on. The major design calculations and model report that provide input information for the abstractions are identified in Table 1-1 and Section 6.1.2. The sources for direct input data and corroborating input data are identified in Tables 4-1 and 6.1-1, respectively. The outputs from this document are identified in Section 8.1.

Table 1-1. Major References for Seismic Damage Abstractions

Damage Process	Calculation Report
Damage to the waste package from vibratory ground motion.	*Structural Calculations of Waste Package Exposed to Vibratory Ground Motion* 000-00C-WIS0-01400-000-00A (BSC 2004 [DIRS 167083]).
Calculation of damaged area caused by end-to-end impacts of adjacent waste packages for a predefined set of impact velocities and impact angles.	*21-PWR Waste Package Side and End Impacts* 000-00C-DSU0-01000-000-00B (BSC 2003 [DIRS 162293])
Acceleration of the fuel assemblies from end-to-end waste package impacts.	*Maximum Accelerations on the Fuel Assemblies of a 21-WR Waste Package During End Impacts* 000-0C-SU0-1100-000-00A (BSC 2003 [DIRS 162602]).
Damage to the drip shield from vibratory ground motion.	*Structural Calculations of Drip Shield Exposed to Vibratory Ground Motion* 000-00C-PEC0-00100-000-00 (BSC 2003 [DIRS 163425]).
Damage to the drip shield from impact of large rock blocks.	*Drip Shield Structural Response to Rock Fall* 000-0C-SE0-00300-000-00A (BSC 2004 [DIRS 168993]).
Damage Process	**Model Report**
Rockfall induced by vibratory ground motion.	*Drift Degradation Analysis* ANL-EBS-MD-000027 REV 03 (BSC 2004 [DIRS 166107]).

PWR = pressurized water reactor

The damage abstractions for EBS components include both model abstractions and scientific analyses. The abstractions for damage to the waste package and drip shield in response to vibratory ground motion are treated as models because they rely on analyses of structural response over a range of ground motions that is wider than typically covered by seismic designs for buildings or nuclear power plants. These model abstractions have been validated to the requirements in AP-SIII.10Q, *Models*, through an independent technical review and through a comparison of the abstraction to computational data. The abstractions for damage to the cladding and for damage from fault displacement are considered scientific analyses because the cladding abstraction uses a simple, bounding approach and because the damage abstraction for fault displacement is based on design clearances between EBS components. Similarly, the abstractions for flow diversion (also called flux splitting) on the drip shield and waste package after a seismic event are also simple scientific analyses of potential flow patterns through stress corrosion cracks or through the area exposed by drip shield separation. Although scientific analyses are not validated to the requirements in AP-SIII.10Q, *Models*, Section 6.10 provides a discussion of verification for these abstractions.

This report does not address the performance of naval spent nuclear fuel (SNF) during seismic events. The Naval Nuclear Propulsion Program Technical Support Document for the License Application will provide the seismic analysis for naval SNF.

1.2 LIMITATIONS

The major limitations of the postclosure abstractions for the seismic scenario class are as follows:

- The structural response calculations include degradation of the waste package and drip shield over a 20,000-year time frame, which includes the initial 10,000-year regulatory period (Assumption 5.5). The 20,000-year duration for the seismic analyses is designed

to demonstrate that repository performance remains robust well after the 10,000-year regulatory period has ended. Calculations of the seismic scenario class beyond 20,000 years may require new structural response calculations with additional levels of structural degradation.

- Coupled effects from multiple seismic events are not considered because seismic hazards with the potential to have a significant impact on engineered barriers are anticipated to occur very rarely, if at all, during the 10,000-year regulatory period. More specifically, seismic hazards with the greatest potential to damage the engineered barriers correspond to very large disruptive events with annual exceedance frequencies much less than 10^{-4} per year (see Section 6.5 and Assumption 5.1 in this report), so there is only a very small probability that multiple events with the potential to induce significant damage will occur over a 10,000 year or 20,000-year period.

- Spatial variability has not been represented in the damage abstractions for EBS components under ground motion (Sections 6.5.3, 6.5.6, and 6.5.6). In other words, damage to the waste package, drip shield, and fuel rod cladding from vibratory ground motion is constant throughout the repository.

- Structural response calculations for the waste package do not include any initial backfill around the drip shield at the time of the seismic event (Section 6.5.1.1). This representation is consistent with the present design that does not include an engineered backfill, is consistent with the results from drift degradation analyses under nominal repository conditions, and is consistent with rockfall analyses that indicate complete drift collapse does not occur until a peak ground velocity exceeds 2 m/s (BSC 2004 [DIRS 166107], Section 6.4.2.2.2) in the lithophysal regions of the repository.

- Structural response calculations are based on the 21-pressurized water reactor (PWR) waste package (Section 6.5.1.1). The 21-PWR waste package is the most common package type in the repository (BSC 2004 [DIRS 169472], Table 11). The design for the 21-PWR package is very similar to the design of the 44-boiling water reactor (BWR) package, and these two package types account for almost 65 percent of the packages in the inventory for TSPA-LA (BSC 2004 [DIRS 169472], Table 11, for the 21-PWR absorber plate, 21-PWR control rod, and 44-BWR absorber plate). It is reasonable to base damage estimates on the 21-PWR waste package because it is the dominant package design in the repository.

- The hazard curve for peak ground velocity at the emplacement drifts (defined in Section 6.4.3) has peak ground velocity (PGV) values that exceed 5 m/s for annual exceedance frequencies below 10^{-7} per year (see Table 6.4-1 in Section 6.4.3). These PGV values are extremely large and may not be physically realizable for the seismic sources and geologic conditions in and around Yucca Mountain. A distribution for the maximum feasible or bounding values for PGV has been developed and included in TSPA-LA, based on an analysis of geologic conditions and other corroborating evidence at the repository site (Section 6.4.4).

- The ground motion time histories[1] for structural response calculations were created using different approaches for intercomponent variability and for spectral conditioning. The results from a limited sensitivity study indicate that the current damage abstraction for the waste package bounds the expected damage changes from these different approaches. Section 6.4.2 provides a discussion on the methodology for defining the suites of ground motions that are used in the structural response calculations, and Section 6.5.1.5 summarizes the results of the sensitivity study.

[1] A ground motion time history defines the three-dimensional motion of the earth during a seismic event. Each ground motion time history defines the displacement, velocity, and acceleration in three component directions as a function of time at a specific repository location. The three components of each ground motion time history are applied simultaneously to determine structural response of EBS components. Ground motion amplitude is identified by the first horizontal component of the peak ground velocity (PGV), usually referred to as horizontal PGV or simply PGV in this document. Note that the peak velocities for the second horizontal and vertical components of ground motion are not fixed, but will vary substantially even when the first horizontal PGV component is at a fixed value. The process to generate the ground motion time histories is summarized in Section 6.4.2.

2. QUALITY ASSURANCE

Preparation of this model report and its supporting technical activities has been performed in accordance with the appropriate requirements of the quality assurance program. This document is also prepared in accordance with the applicable technical work plan (TWP) (BSC 2004 [DIRS 171520]), which directs the work identified in work package ARTM05. Analysis and modeling activities performed under this TWP are subject to the requirements of the Quality Assurance Requirements and Description document because they are associated with the characterization of the waste form and waste package in support of performance assessment (BSC 2004 [DIRS 171520], Section 8). The technical work plan was prepared in accordance with AP-2.27Q, *Planning for Science Activities*. Input information for this model report are identified and tracked in accordance with AP-3.15Q, *Managing Technical Product Inputs*. No qualified software was used to develop the abstractions documented in this report, so LP-SI.11Q-BSC, *Software Management,* is not applicable. The model(s) and scientific analyses in this document are not structures, systems, or components (SSCs) so the quality level classification from AP-2.22Q, *Classification Analysis and Maintenance of the Q-List*, is not applicable. The methods used to control the electronic management of data, as required by AP-SV.1Q, *Control of the Electronic Management of Information*, are identified in Section 8 of the technical work plan.

This model report presents information on the impacts by seismic events on engineered barriers that are important to waste isolation performance in the Yucca Mountain Repository. The following SSCs have been determined to be important to waste isolation, and have SSCs that are credited for prevention or mitigation of safety category event sequences so that they meet the performance objectives in 10 CFR 63.111.

Systems/Subsystems Classified as Safety Category

- Commercial and naval spent nuclear fuel cladding
- U.S. Department of Energy (DOE) and commercial waste packages
- Post emplacement drip shield
- Naval spent nuclear fuel waste package.

The listed SSCs and their safety category are based on the *Q-List* (BSC 2004 [DIRS 168361], p. A-4).

This document is prepared in accordance with AP-SIII.10Q, *Models*, and reviewed in accordance with AP-2.14Q, *Document Review*, as directed in the TWP.

INTENTIONALLY LEFT BLANK

3. USE OF SOFTWARE

3.1 QUALIFIED SOFTWARE

No qualified software is used to develop the seismic consequence abstractions. These abstractions are based on the results of structural response calculations that are performed with qualified software and that are documented in separate design calculation reports identified in Table 1-1. These abstractions are also based on the results of (1) rockfall calculations that are performed with qualified software (Table 1-1), and (2) thermohydraulic calculations and seepage calculations that are performed with qualified software and that are documented in separate model reports identified in Sections 6.8.1 and 6.8.3. These qualified software packages are not directly used in the abstraction process and hence are not listed here.

3.2 OTHER SOFTWARE

Microsoft Excel for Windows, Version 97 SR-2, has been used to develop the abstractions for damage from seismic hazards. The standard functions in Microsoft Excel, including its statistical package, are sufficient for these analyses. No macros, codes, or software routines are required for or developed during this work. Relevant Microsoft Excel files are included as appendices to this report. As used to develop abstractions, Microsoft Excel 97 SR-2 is not required to be qualified or documented in accordance with LP-SI.11Q-BSC, *Software Management*.

The formulas, listing of inputs, and listing of outputs for the Microsoft Excel spreadsheets are presented in Appendices A, B, and E of this model report.

INTENTIONALLY LEFT BLANK

4. INPUTS

4.1 DIRECT INPUT

Table 4-1 presents the direct input information for abstraction of damage to EBS components from seismic hazards. The information in Table 4-1 has been categorized into six areas that are relevant to the abstractions in this report: (1) ratio of crack area to damaged area[2] for a network of stress corrosion cracks, (2) damage to the waste package from vibratory ground motion, (3) damage to the cladding from vibratory ground motion, (4) damage to the drip shield from vibratory ground motion, (5) damage to the waste package, drip shield, and cladding from fault displacement, and (6) input information for the seismic scenario class. The numerical values in Table 4-1 are presented with the same number of significant figures as presented in the source. The technical product inputs identified in Table 4-1 are appropriate for the development of model abstractions and scientific analyses for the seismic scenario class.

For project-historical reasons, the sources in Table 4-1 generally identify ground motion levels by the value of the annual exceedance frequency. This report identifies ground motion level by the value of horizontal peak ground velocity (PGV), rather than exceedance frequency, because PGV is a unique and unambiguous measure of the amplitude of the ground motions. The rationale for using PGV, rather than exceedance frequency, is explained further in Section 6.1.3. For the reader's convenience, the following list identifies the correspondence between the values of annual exceedance frequency in the sources for Table 4-1 and the values of PGV in Tables 4-1 and 6.1-1 of this report:

- PGV of 0.19 m/s corresponds to the 5×10^{-4} per year exceedance frequency in the sources.
- PGV of 0.384 m/s corresponds to the 10^{-4} per year exceedance frequency in the sources.
- PGV of 1.05 m/s corresponds to the 10^{-5} per year exceedance frequency in the sources[3].
- PGV of 2.44 m/s corresponds to the 10^{-6} per year exceedance frequency in the sources.
- PGV of 5.35 m/s corresponds to the 10^{-7} per year exceedance frequency in the sources.

Section 8.2 identifies the uncertainties in input information and parameters for the damage analyses of EBS components and explains how these uncertainties are propagated into the abstractions for the seismic scenario class.

[2] The area of material that exceeds the residual stress threshold for accelerated stress corrosion cracking is referred to as the "damaged area" throughout this report. The basis for this damage mechanism is explained in Section 6.3.1.

[3] Three preliminary ground motions corresponding to the 10^{-5} per year exceedance frequency were developed before the exact PGV value of 1.05 m/s was available. The approximate value of PGV corresponding to the 10^{-5} per year exceedance frequency was estimated to be 0.992 m/s, based on the scaled hazard curve (see Figure 6.4-2 and Appendix A). The PGV value of 0.992 m/s is used to describe these preliminary ground motions, when appropriate.

Table 4-1. Direct Input Information for Seismic Consequence Abstractions

Input Information	Value	Source
Effective Transport Area for a Network of Stress Corrosion Cracks:		
Ratio of crack area to damaged area for a densely packed network of stress corrosion cracks in Alloy 22 at room temperature.	0.00328 to 0.0131	DTN: MO0403SPASCRKD.000 [DIRS 168105]; see values under Crack Area Density at room temperature
Damage to the Waste Package from Vibratory Ground Motion:		
Damage statistics for the waste package, based on a sampling of vibratory ground motions at the 10^{-6} per year hazard level.	See Table 16 In source	BSC 2004 [DIRS 169990], Table 16
Damage statistics for the waste package, based on a sampling of vibratory ground motions at the 10^{-7} per year hazard level.	See Table 17 In first source; see BSC 2004 [DIRS 171717] for Realization 11	BSC 2004 [DIRS 169990], Table 17; BSC 2004 [DIRS 171717] for Realization 11
Damage to the Cladding from Vibratory Ground Motion:		
Maximum peak acceleration of fuel assemblies due to waste package-to-waste package impacts.	See Table 14 In source	BSC 2004 [DIRS 167369], Table 14
Average peak acceleration of fuel assemblies due to waste package-to-waste package impacts.	See Table 15 In source	BSC 2004 [DIRS 167369], Table 15
Statistics for axial impact velocities between adjacent waste packages, based on a sampling of vibratory ground motions at the 2.44 m/s (10^{-6} per year) PGV level.	See Tables 6.1.2-1 through 6.1.2-15	BSC 2004 [DIRS 167083], Tables 6.1.2-1 to 6.1.2-15
Statistics for axial impact velocities between adjacent waste packages, based on a sampling of vibratory ground motions at the 5.35 m/s (10^{-7} per year) PGV level.	See Tables 6.2.2-1 through 6.2.2-15	BSC 2004 [DIRS 167083], Tables 6.2.2-1 to 6.2.2-15
Axial impact velocity between adjacent waste packages for the single vibratory ground motion at the 0.190 PGV level, corresponding to an annual exceedance frequency of 5×10^{-4} per year.	Relative displacement of waste package and pallet nodes is less than $\pm$0.01 mm	BSC 2004 [DIRS 167083], Figures 10 and 11
Axial impact velocity between adjacent waste packages for the single vibratory ground motion at the 0.384 m/s PGV level, corresponding to an annual exceedance frequency of 1×10^{-4} per year.	Relative displacement of waste package and pallet nodes is less than $\pm$0.07 mm	BSC 2004 [DIRS 167083], Figures 20 and 21
Damage to the Drip Shield from Vibratory Ground Motion:		
Damage to the drip shield due to impact by single rock blocks from the 2.44 m/s (10^{-6} per year) PGV level.	See Table 2	BSC 2004 [DIRS 169220], Table 2
Damage to the drip shield due to impact by maximum rock block from the 5.35 m/s (10^{-7} per year) PGV level.	See Table 3	BSC 2004 [DIRS 169220], Table 3
Damage to the drip shield for the single vibratory ground motion at the 0.190 m/s PGV level, corresponding to an annual exceedance frequency of 5×10^{-4} per year.	No damage	BSC 2004 [DIRS 169220], Calculation Results I
Damage statistics for the area of the drip shield exceeding the residual stress threshold at 10^{-6} per year.	See Table 4	BSC 2004 [DIRS 169220], Table 4

Table 4-1. Direct Input Information for Seismic Consequence Abstractions (Continued)

Input Information	Value	Source
Damage statistics for the drip shield in an unfilled drift, based on a sampling of vibratory ground motions at the 5.35 m/s PGV level, corresponding to the 10^{-7} per year exceedance frequency.	Drip shield separates for the analyzed ground motions	BSC 2004 [DIRS 169220], Calculation Results III
Kinematic studies of drip shield motion for an open drift and for a drift partly and completely filled with rockfall.	Drip shields do not separate for an open drift. Frictional forces from small amount of rockfall stabilizes drip shield motion and prevents separation.	BSC 2004 [DIRS 169753], Section 5.3
Damage to the Waste Package, Drip Shield and Cladding from Fault Displacement:		
Drift Diameter.	5.5 m	BSC 2004 [DIRS 169058], Figure 1
Height of Steel Invert Structure (maximum thickness of invert).	863.6 mm	BSC 2004 [DIRS 170074]
Drip Shield Nominal Height – Exterior.	2885.62 mm	BSC 2004 [DIRS 169220], Table 1
Drip Shield Height – Interior.	2716 mm	BSC 2004 [DIRS 168489], Figure 1
Clearance between Interior Height of Drip Shield and the 5 DHLW Waste Packages.	367.1 mm	BSC 2004 [DIRS 168489], Figure 1
Outside Diameter of 44-BWR Waste Package Outer Barrier.	1675.1 mm	BSC 2004 [DIRS 169472], Table 1, to drawing 000-MW0-DSU0-00502-000-00A with source data
Outside Diameter of 24-BWR Waste Package Outer Barrier.	1294.1 mm	BSC 2004 [DIRS 169472], Table 1, to drawing 000-MW0-DSU0-00602-000-00A with source data
Outside Diameter of 21-PWR Waste Package Outer Barrier.	1637 mm	BSC 2004 [DIRS 169472], Table 1, to drawing 000-MW0-DSU0-00402-000-00B with source data
Outside Diameter of 12-PWR Waste Package Outer Barrier.	1313.2 mm	BSC 2004 [DIRS 169472], Table 1, to drawing 000-MW0-DSU0-00302-000-00A with source data
Outside Diameter of Naval-Long Waste Package Outer Barrier.	1863.7 mm	BSC 2004 [DIRS 169472], Table 1, to drawing 000-MW0-DNF0-00102-000-00A with source data
Outside Diameter of Naval-Short Waste Package Outer Barrier.	1863.7 mm	BSC 2004 [DIRS 169472], Table 1, to drawing 000-MW0-DNF0-00202-000-00A with source data
Outside Diameter of 5 DHLW/DOE SNF - Short Waste Package Outer Barrier.	2044.7 mm	BSC 2004 [DIRS 169472], Table 1, to drawing 000-MW0-DS00-00102-000-00A with source data

Table 4-1. Direct Input Information for Seismic Consequence Abstractions (Continued)

Input Information	Value	Source
Outside Diameter of 5 DHLW/DOE SNF - Long Waste Package Outer Barrier.	2044.7 mm	BSC 2004 [DIRS 169472], Table 1, to drawing 000-MW0-DS00-00202-000-00A with source data
Outside Diameter of 2-MCO/2-DHLW Waste Package Outer Barrier.	1749.4 mm	BSC 2004 [DIRS 169472], Table 1, to drawing 000-MW0-DS00-00302-000-00A with source data
44-BWR Waste Package Nominal Length.	5024.4 mm	BSC 2004 [DIRS 169472], Table 1
24-BWR Waste Package Nominal Length.	5024.4[4] mm	BSC 2004 [DIRS 169472], Table 1
21-PWR Waste Package Nominal Length.	5024.4 mm	BSC 2004 [DIRS 169472], Table 1
12-PWR Waste Package Nominal Length.	5560.4 mm	BSC 2004 [DIRS 169472], Table 1
Naval-Long Waste Package Nominal Length.	5837.4 mm	BSC 2004 [DIRS 169472], Table 1
Naval-Short Waste Package Nominal Length.	5202.2 mm	BSC 2004 [DIRS 169472], Table 1
5 DHLW/ DOE SNF - Short Waste Package Nominal Length.	3452.8 mm	BSC 2004 [DIRS 169472], Table 1
5 DHLW/DOE SNF - Long Waste Package Nominal Length.	5059.4 mm	BSC 2004 [DIRS 169472], Table 1
2-MCO/2-DHLW Waste Package Nominal Length.	5059.4 mm	BSC 2004 [DIRS 169472], Table 1
Clearance between Top of 21-PWR Waste Package and Underside of Drip Shield Peripheral Bulkhead.	806.2 mm	BSC 2004 [DIRS 170074]
Clearance between Top of 12-PWR Waste Package and Underside of Drip Shield Peripheral Bulkhead.	1132.1 mm	BSC 2004 [DIRS 170074]
Clearance between Top of 44-BWR Waste Package and Underside of Drip Shield Peripheral Bulkhead.	765.2 mm	BSC 2004 [DIRS 170074]
Clearance between Top of Naval Waste Package and Underside of Drip Shield Peripheral Bulkhead.	562.1 mm	BSC 2004 [DIRS 170074]
Clearance between Top of 5 DHLW/DOE Waste Package and Underside of Drip Shield Peripheral Bulkhead.	367.1 mm	BSC 2004 [DIRS 170074]
Emplacement Drift Numbers and Rock Type Intersected by the Sundance fault. - Rock type or types identified in parentheses.	1-6 (Tptpll) 1-7 (Tptpll/Tptpmn) 1-8 (Tptpmn) 2-1 (Tptpmn)	DTN: MO0012MWDGFM02.002 [DIRS 153777], File in Earthvision: Horizon *from/usr6/restored/ism4/Faults/f00 Sundance.2grd*

[4] Table 1 of the *D&E/PA/C IED Typical Waste Package Components Assembly* report (BSC 2004 [DIRS 169472]) has 5024.5 mm as the length of the 24-BWR waste package. This appears to be a conversion error, because 197.81-in = 5024.4 mm, not 5024.5 mm as stated in Table 1 of the reference. The corrected value is listed in Table 4-1.

Table 4-1. Direct Input Information for Seismic Consequence Abstractions (Continued)

Input Information	Value	Source
Emplacement Drift Numbers and Rock Type Intersected by the Drill Hole Wash fault. - Rock type or types identified in parentheses.	4-1 (Tptpll) 4-2 (Tptpll) 3-4 W (Tptpll) 3-5 W (Tptpll) 3-6 W (Tptpll) 3-7 W (Tptpll) 3-8 W (Tptpll) 3-9 W (Tptpll) 3-10 E (Tptpmn) 3-11 E (Tptpmn) 3-12 E (Tptpmn) 3-13 E (RHHtop/ Tptpmn) 3-14 E (RHHtop) 3-15 E (RHHtop) 3-16 E (RHHtop) 3-17 E (RHHtop)	BSC 2004 [DIRS 168180], Table 9 for drift numbers; DTN: MO0012MWDGFM02.002 [DIRS 153777], for rock type; RHHtop is the lowermost portion of the Tptpul. File in Earthvision: Horizon *from/usr6/restored/ism4/Faults/f00drill.2grd*
Emplacement Drift Numbers and Rock Type Intersected by the Pagany Wash Fault. - Rock type or types identified in parentheses.	3-1 W (Tptpll) 3-1 E (Tptpll) 3-2 E (Tptpll) 3-3 E (Tptpll) 3-4 E (Tptpll) 3-5 E (Tptpmn) 3-6 E (Tptpmn) 3-7 E (Tptpmn)	BSC 2004 [DIRS 168180], Table 9 for drift numbers; DTN: MO0012MWDGFM02.002 [DIRS 153777], for rock type; File in Earthvision: Horizon *from/usr6/restored/ism4/Faults/f00pagany.2grd*
Emplacement Drift Numbers and Rock Type Intersected by the Sever Wash Fault. - Rock type or types identified in parentheses.	3-2 E (Tptpll) 3-3 E (Tptpll)	BSC 2004 [DIRS 168180], Table 9 for drift numbers; DTN: MO0012MWDGFM02.002 [DIRS 153777], for rock strata; File in Earthvision: Horizon *from/usr6/restored/ism4/Faults/f00sever.2grd*
Emplacement Drift Numbers Intersected by the western splay off the main Ghost Dance Fault.	2-17, 2-18, 2-19, 2-20, 2-21, 2-22, 2-23, 2-24, 2-25, 2-26, and 2-27	BSC 2004 [DIRS 168180], Table 9
Fault Displacement Hazard at Site 3 – on the Drill Hole Wash Fault.	See source file for data	DTN: MO0401MWDRPSHA.000 [DIRS 166962], file: *./displ/tot_haz/s3.frac_mean.gz*
Fault Displacement Hazard at Site 5 – on the Sundance Fault.	See source file for data	DTN: MO0401MWDRPSHA.000 [DIRS 166962], file: *./displ/tot_haz/s5.frac_mean.gz*
Fault Displacement Hazard at Site 7a – a generic repository location, approximately 100 meters east of the Solitario Canyon fault, with a hypothetical small fault with 2-meter offset.	See source file for data	DTN: MO0401MWDRPSHA.000 [DIRS 166962], file: *./displ/tot_haz/s7a.frac_mean.gz*

Table 4-1. Direct Input Information for Seismic Consequence Abstractions (Continued)

Input Information	Value	Source
Fault Displacement Hazard at Site 8a – a generic repository location, midway between the Solitario Canyon and Ghost Dance faults, with a hypothetical small fault with a 2 meter offset.	See source file for data	DTN: MO0401MWDRPSHA.000 [DIRS 166962], file: *./displ/tot_haz/s8a.frac_mean.gz*
Fault Displacement Hazard at Sites 7b and 7c – generic repository locations, approximately 100 meters east of the Solitario Canyon fault. Site 7b has a hypothetical shear with 10-cm offset and site 7c has a hypothetical fracture with no cumulative displacement.	See source files for data	DTN: MO0401MWDRPSHA.000 [DIRS 166962], files: *./displ/tot_haz/s7b.frac_mean.gz* and *./displ/tot_haz/s7c.frac_mean.gz*
Fault Displacement Hazard at Sites 8b and 8c – generic repository locations, midway between the Solitario Canyon and Ghost Dance faults. Site 8b has a hypothetical shear with 10 cm offset and site 8c has a hypothetical fracture with no cumulative displacement.	See source files for data	DTN: MO0401MWDRPSHA.000 [DIRS 166962], files: *./displ/tot_haz/s8b.frac_mean.gz* and *./displ/tot_haz/s8c.frac_mean.gz*
Nominal Quantity for LA of 21-PWR Waste Packages with Absorber Plates.	4299	BSC 2004 [DIRS 169472], Table 11
Nominal Quantity for LA of 21-PWR Waste Packages with Control Rods.	95	BSC 2004 [DIRS 169472], Table 11
Nominal Quantity for LA of 12-PWR Long Waste Packages with Absorber Plates.	163	BSC 2004 [DIRS 169472], Table 11
Nominal Quantity for LA of 44-BWR Waste Packages with Absorber Plates.	2831	BSC 2004 [DIRS 169472], Table 11
Nominal Quantity for LA of 24-BWR Waste Packages with Absorber Plates.	84	BSC 2004 [DIRS 169472], Table 11
Nominal Quantity for LA of 5 HLW Short/1 DOE SNF Short Waste Package.	1147	BSC 2004 [DIRS 169472], Table 11
Nominal Quantity for LA of 5 HLW Long/1 DOE SNF Long Waste Package.	1406	BSC 2004 [DIRS 169472], Table 11
Nominal Quantity for LA of 2 MCO/2 HLW Waste Package.	149	BSC 2004 [DIRS 169472], Table 11
Nominal Quantity for LA of 5 HLW Long/1 DOE SNF Short Waste Package.	31	BSC 2004 [DIRS 169472], Table 11
Nominal Quantity for LA of 5 HLW Long Only Waste Package.	679	BSC 2004 [DIRS 169472], Table 11
Nominal Quantity for LA of Naval Short Waste Package.	144	BSC 2004 [DIRS 169472], Table 11
Nominal Quantity for LA of Naval Long Waste Package.	156	BSC 2004 [DIRS 169472], Table 11
Parameters for the Seismic Scenario:		
Horizontal PGV at Point B for the 10^{-5} per year mean annual exceedance frequency.	1.05 m/s	DTN: MO0401SEPPGVRL.022 [DIRS 169099]
Horizontal PGV at Point B for the 10^{-6} per year mean annual exceedance frequency.	2.44 m/s	DTN: MO0303DPGVB106.002 [DIRS 162712]

Table 4-1. Direct Input Information for Seismic Consequence Abstractions (Continued)

Input Information	Value	Source
Horizontal PGV at Point B for the 10^{-7} per year mean annual exceedance frequency.	5.35 m/s	DTN: MO0210PGVPB107.000 [DIRS 162713]
Mean hazard curve for horizontal PGV at Point A, a reference rock outcrop at the repository elevation.	See source file: *h_vel_extended.frac_mean* in the DTN	DTN: MO03061E9PSHA1.000 [DIRS 163721]
Distribution type and limits for the maximum value of PGV at Point B.	Uniform; Lower Bound = 1.5 m/s; Upper Bound = 5 m/s	DTN: MO0404BPVELEMP.000 [DIRS 171052]

BWR = boiling water reactor; DHLW = defense high-level radioactive waste; DOE = U.S. Department of Energy; LA = license application; PWR = pressurized water reactor; SNF spent nuclear fuel; MCO = multicanister overpack.

4.2 CRITERIA

General programmatic requirements for this document are listed in *Technical Work Plan For: Regulatory Integration Modeling of Drift Degradation, Waste Package and Drip Shield Vibratory Motion and Seismic Consequences* (BSC 2004 [DIRS 171520]). The TWP specifies that this document and the analyses described herein must adhere to the requirements of AP-SIII.10Q, *Models.* The TWP specifies that this document must discuss the barrier function of the EBS components (waste package, drip shield, and emplacement pallet) that may be affected by seismically-induced hazards. The TWP also specifies that the acceptance criteria in *Yucca Mountain Review Plan, Final Report* (NRC 2003 [DIRS 163274]) must be addressed.

The general requirements to be satisfied by the TSPA are stated in 10 CFR 63.114 [DIRS 156605]. Technical requirements to be satisfied by the TSPA are identified in the *Yucca Mountain Project Requirements Document* (Canori and Leitner 2003 [DIRS 166275]). The requirement that pertains to this model report and its link to 10 CFR Part 63 [DIRS 156605], is defined in Section 3.4 of Canori and Leitner (2003 [DIRS 166275]) as follows:

- **PRD-002/T-015: Requirements for Performance Assessment**

  10 CFR 63.114 [DIRS 156605], specifies technical requirements to be used in a performance assessment to demonstrate compliance to 10 CFR 63.113 [DIRS 156605]. It includes requirements for calculations, including data related to site geology, hydrology, and geochemistry; the need to account for uncertainty and variability in model parameters, the need to consider alternative conceptual models, and technical bases for inclusion or exclusion of specific features, events, and processes (FEPs), deterioration or degradation processes of engineered barriers, and all the models used in performance assessment.

The acceptance criteria that are relevant to requirement PRD-002/T-015 and that will be used by the U.S. Nuclear Regulatory Commission (NRC) to determine whether the technical requirements have been met for seismic consequence abstractions are found in Section 2.2.1.3.2.3 of *Yucca Mountain Review Plan, Final Report* (NRC 2003 [DIRS 163274]). The five general acceptance criteria in Section 2.2.1.3.2.3 are listed below, along with the

subcriteria specifically addressed by this report. Where a subcriterion includes several components, only some components may be addressed. Section 8.2 provides a detailed discussion of how the seismic abstractions and the seismic scenario class meet the applicable acceptance criteria from *Yucca Mountain Review Plan, Final Report* (NRC 2003 [DIRS 163274]).

Acceptance Criteria from Section 2.2.1.3.2.3, *Mechanical Disruption of Engineered Barriers*

Acceptance Criterion 1: System Description and Model Integration Are Adequate.

(1) Total system performance assessment adequately incorporates important design features, physical phenomena, and couplings, and uses consistent and appropriate assumptions throughout the mechanical disruption of engineered barrier abstraction process.

(2) The description of geological and engineering aspects of design features, physical phenomena, and couplings, that may affect mechanical disruption of engineered barriers, is adequate. For example, the description may include materials used in the construction of engineered barrier components, environmental effects (e.g., temperature, water chemistry, humidity, radiation, etc.) on these materials, and mechanical-failure processes and concomitant failure criteria used to assess the performance capabilities of these materials. Conditions and assumptions in the abstraction of mechanical disruption of engineered barriers are readily identified and consistent with the body of data presented in the description.

(3) The abstraction of mechanical disruption of engineered barriers uses assumptions, technical bases, data, and models that are appropriate and consistent with other related U.S. Department of Energy abstractions. For example, assumptions used for mechanical disruption of engineered barriers are consistent with the abstraction of degradation of engineered barriers (Section 2.2.1.3.1 of the Yucca Mountain Review Plan). The descriptions and technical bases provide transparent and traceable support for the abstraction of mechanical disruption of engineered barriers.

(4) Boundary and initial conditions used in the total system performance assessment abstraction of mechanical disruption of engineered barriers are propagated throughout its abstraction approaches.

(5) Sufficient data and technical bases to assess the degree to which features, events, and processes have been included in this abstraction are provided.

Subcriterion (6) is not discussed here because it is related to transient criticality and beyond the scope of this report. Subcriterion (7) is not discussed here because there are no activities related to peer review or qualification of existing data discussed in this report.

Acceptance Criterion 2: Data Are Sufficient for Model Justification.

(1) Geological and engineering values, used in the license application to evaluate mechanical disruption of engineered barriers, are adequately justified. Adequate descriptions of how the data were used, interpreted, and appropriately synthesized into the parameters are provided.

(3) Data on geology of the natural system, engineering materials, and initial manufacturing defects, used in the total system performance assessment abstraction, are based on appropriate techniques. These techniques may include laboratory experiments, site-specific field measurements, natural analog research, and process-level modeling studies. As appropriate, sensitivity or uncertainty analyses used to support the U.S. Department of Energy total system performance assessment abstraction are adequate to determine the possible need for additional data.

(4) Engineered barrier mechanical failure models for disruption events are adequate. For example, these models may consider effects of prolonged exposure to the expected emplacement drift environment, material test results not specifically designed or performed for the Yucca Mountain site, and engineered barrier component fabrication flaws.

Subcriterion (2) is not discussed here because data collection activities related to the geology of the natural system engineering materials, and initial manufacturing defects are beyond the scope of this report.

Acceptance Criterion 3: Data Uncertainty Is Characterized and Propagated Through the Model Abstraction.

(1) Models use parameter values, assumed ranges, probability distributions, and bounding assumptions that are technically defensible, reasonably account for uncertainties and variabilities, and do not result in an under-representation of the risk estimate.

(2) Process-level models used to represent mechanically disruptive events, within the emplacement drifts at the proposed Yucca Mountain repository, are adequate. Parameter values are adequately constrained by Yucca Mountain site data, such that the effects of mechanically disruptive events on engineered barrier integrity are not underestimated. Parameters within conceptual models for mechanically disruptive events are consistent with the range of characteristics observed at Yucca Mountain.

(3) Uncertainty is adequately represented in parameter development for conceptual models, process-level models, and alternative conceptual models considered in developing the assessment abstraction of mechanical disruption of engineered barriers. This may be done either through sensitivity analyses or use of conservative limits; and Review Plan for Safety Analysis Report 2.2-33.

Subcriterion (4) is not discussed here because an expert elicitation was not performed during the development of the seismic damage abstractions.

Acceptance Criterion 4: Model Uncertainty Is Characterized and Propagated Through the Model Abstraction.

(2) Consideration of conceptual model uncertainty is consistent with available site characterization data, laboratory experiments, field measurements, natural analog information and process-level modeling studies; and the treatment of conceptual model uncertainty does not result in an under-representation of the risk estimate.

(3) Appropriate alternative modeling approaches are investigated that are consistent with available data and current scientific knowledge, and appropriately consider their results and limitations using tests and analyses that are sensitive to the processes modeled.

Subcriterion (1) is not discussed here because alternate modeling approaches for features, events, and processes is beyond the scope of this report.

Acceptance Criterion 5: Model Abstraction Output Is Supported by Objective Comparisons.

(1) Models implemented in this total system performance assessment abstraction provide results consistent with output from detailed process-level models and/or empirical observations (laboratory and field testings and/or natural analogs).

(2) Outputs of mechanical disruption of engineered barrier abstractions reasonably produce or bound the results of corresponding process-level models, empirical observations, or both.

(3) Well-documented procedures, that have been accepted by the scientific community to construct and test the mathematical and numerical models, are used to simulate mechanical disruption of engineered barriers.

Subcriterion (4) is not discussed here because sensitivity studies or bounding analyses are not provided to TSPA within this report.

4.3 CODES, STANDARDS, AND REGULATIONS

No codes, standards, and regulations are applicable to the development of the seismic consequence abstractions. The regulation that is applicable to the development of these abstractions is 10 CFR Part 63, *Energy: Disposal of High-Level Radioactive Wastes in a Geologic Repository at Yucca Mountain, Nevada* [DIRS 156605], specifically 10 CFR 63.114 and 10 CFR 63.115.

5. ASSUMPTIONS

5.1 DAMAGE THRESHOLD FROM VIBRATORY GROUND MOTION LIES BETWEEN HORIZONTAL PEAK GROUND VELOCITIES OF 0.384 M/S AND 1 M/S

Assumption: There is no damage to EBS components until the repository experiences ground motions with PGV larger than 0.384 m/s. More specifically, the abstractions for damage to the waste package, drip shield and cladding from vibratory ground motion assume that damage becomes nonzero for ground motions with PGV values between 0.384 m/s and 1 m/s.

Basis: Structural analyses for the waste package and drip shield have been performed using a single set of vibratory ground motions (with two horizontal components and one vertical component) with horizontal PGV of 0.190 m/s and 0.384 m/s. The results of these analyses demonstrate that the response of the waste package and drip shield are always in the elastic regime (BSC 2004 [DIRS 167083], Sections 6.3 and 6.4; BSC 2003 [DIRS 163425], Section 6.1), with no damage to the structures. There will also be no failure of the cladding because waste package displacements are very small (BSC 2004 [DIRS 167083], Sections 6.3 and 6.4), with no impacts or significant acceleration that could fail the cladding.

The seismic consequence abstractions for TSPA-LA assume that damage to EBS components from vibratory ground motion becomes nonzero for ground motions with PGV values between 0.384 m/s and 1 m/s.

Confirmation Status: This assumption is verified by results from structural response calculations for ground motions with PGV values at 1.05 m/s (BSC 2004 [DIRS 171717]).

Use In Model: The abstraction for damage to the waste package in Sections 6.5.1 and 6.5.3 represents the upper bound for damage as a linear function of PGV. This linear function first becomes positive (i.e., damage first becomes nonzero) for a value of PGV that lies between 0.384 m/s and 1 m/s. This assumption is also used in Section 6.5.6 to set the lower bound for damage to the cladding.

5.2 PAGANY WASH AND SEVER WASH FAULT DISPLACEMENTS

Assumption: The fault displacement hazard curves for the Pagany Wash fault and for the Sever Wash fault are identical to the fault displacement hazard curve for the Drill Hole Wash fault.

Basis: The assumption of equivalency is justified by the results of field investigations that are summarized by Menges and Whitney (1996 [DIRS 106342], Section 4.2.4.10). The reasoning that supports the assumption of equivalency is as follows:

1. Previous geologic studies have consolidated discussion of the three faults based on similar characteristics and apparent similarity in fault development in response to the extensional environment. These faults are characterized as northwest-trending faults that are extensional structures related to the left-oblique component of displacement along the north-trending faults. They are, generally,

strike-slip faults with a right lateral movement (Menges and Whitney 1996 [DIRS 106342], Section 4.2.4.10 and Table 4.2.1.2).

2. The field data for the three sites includes surface exposures and trench studies for Pagany Wash fault and Sever Wash fault, and drill core data for the Drill Hole Wash fault. Because of the existence of subsurface data, and consistent with the choice of representative locations used by the expert elicitation panel as presented in the Probabilistic Seismic Hazard Analysis (PSHA) (CRWMS 1998 [DIRS 103731], Section 4.3.2), it is reasonable to use the response of the Drill Hole Wash fault as the basis for the seismic hazard.

3. None of the faults suggest displacement in Quaternary alluvial terraces, so it is appropriate to assume a low probability of significant displacement for these three faults.

4. The scale of vertical displacement is less than 5 to 10 meters for each structure (Menges and Whitney 1996 [DIRS 106342], Table 4.2.1.2), consistent with a maximum displacement of approximately 2 meters for a single low probability event (CRWMS M&O 1998 [DIRS 103731], Figure 8.4).

5. Total fault length, an important factor in seismic hazard assessment, is similar for the three faults and ranges from 2 km for the Drill Hole Wash fault to 4 km for the other faults.

6. Spatial orientation to the Solitario Canyon and Bow Ridge faults, also an important factor in a hazard assessment, is similar for the three faults as illustrated in Figure 4.2.2 and described in Section 4.2.4.10 of Menges and Whitney (1996 [DIRS 106342]). Spatial orientation to more distant seismic sources is also similar.

It is, therefore, reasonable to treat the Drill Hole Wash fault, the Sever Wash fault, and the Pagany Wash fault in a similar manner with regard to the potential seismic hazard.

Confirmation Status: This assumption does not require confirmation. *Probabilistic Seismic Hazard Analyses for Fault Displacement and Vibratory Ground Motion at Yucca Mountain, Nevada* (PSHA) (CRWMS M&O 1998 [DIRS 103731]) defines fault displacement hazards at 15 faulting conditions within the immediate vicinity of Yucca Mountain. The PSHA did not characterize closely spaced faults separately because their displacements during a seismic event are expected to be similar. Assumption 5.2 follows the same approach used during the PSHA to characterize the response at representative fault locations (CRWMS M&O 1998 [DIRS 103731], Section 4.3.2).

Use In Model: This assumption is used in Section 6.7.3.

5.3 DERIVING THE FORMULA FOR MEAN DOSE

Assumption: In deriving the formula for mean dose, the probability distribution of the dose is assumed to be a function of the time of occurrence and the amplitude of the horizontal PGV for the seismic event (Appendix F). More specifically, the likelihood of dose time histories for the reasonably maximally exposed individual at time τ from a seismic event occurring at a time, *t*, prior to τ, depends only on the time of occurrence of the event and on PGV at the waste emplacement drifts associated with the seismic event.

Basis: This assumption is a reasonable representation of the functional relationship between the probability distribution on dose (e.g., median, mean, 95^{th} percentile, etc.) and the parameters of a seismic event (time of occurrence of the event and the amplitude (PGV) of the event) at the emplacement drifts. This assumption simplifies the mathematical derivation for mean dose presented in Appendix F without being overly restrictive.

Confirmation Status: This assumption does not require confirmation because event time and PGV are reasonable parameters for defining the dose time history for the seismic scenario class are valid.

Use In Model: This assumption is used in Appendix F.

5.4 RANDOMNESS OF SEISMIC EVENTS

Assumption: Seismic events occur in a random manner, following a Poisson process, over long periods of time.

Basis: The assumption that the behavior of the earth is generally random (i.e., a Poisson process) is a common assumption in many PSHAs. In other words, earthquakes are considered as independent events with regard to magnitude, time and location. This assumption is similar to Assumption 6.4.2 in *Characterize Framework for Seismicity and Structural Deformation at Yucca Mountain, Nevada* (BSC 2004 [DIRS 168030]). Although there may be cases where sufficient data and information exists to depart from this assumption, the Poisson process is generally an effective representation of nature and represents a compromise between the complexity of natural processes, availability of information, and the sensitivity of results of engineering relevance.

Confirmation Status: This assumption does not require confirmation because it is a common engineering assumption in seismic hazard analysis and because it is an implicit assumption in the development of hazard curves for the seismic scenario (BSC 2004 [DIRS 168030], Section 6.4.2).

Use In Model: This assumption is used in Section 6.9 and Appendix F.

5.5 SUMMARY OF MAJOR ASSUMPTIONS IN SUPPORTING CALCULATIONS

The seismic consequence abstractions are based on the results from analyses for the structural response of EBS components to vibratory ground motion, from the effective transport area through the dense network of stress corrosion cracks that is postulated to exist within the

damaged areas on EBS components, and from analyses of rockfall induced by vibratory ground motion. The structural response calculations and rockfall calculations (Table 1-1) are not described in this report; rather, the results from these design calculations and scientific analyses provide the input data that the abstractions are based on. These supporting calculations include several major assumptions that are not directly used in the abstraction process, but are noteworthy enough to deserve repeating here. Similarly, the major assumptions for the determination of the effective transport area through a crack network are also summarized here.

The structural response calculations for the waste package and drip shield incorporate assumptions for structural thickness (degradation) and for material properties of Alloy 22 and of Titanium Grade 7. The thicknesses of the drip shield plates and the waste package outer shell have been reduced by 2-mm to represent the potential degradation of these structures by general corrosion over the first 10,000 years after repository closure. The material properties of Alloy 22 and of Titanium Grade 7 have been evaluated at an elevated temperature (150°C) that provides conservative values for mechanical properties over 98.5 percent of the 10,000-year duration for an unfilled drift. The rationale for the temperature assumption is discussed below. The rationale for the thickness reduction is discussed in more detail in several design calculations (BSC 2004 [DIRS 167083], Assumption 3.21; BSC 2003 [DIRS 163425], Assumption 3.10).

A temperature of 150°C is appropriate and reasonable for evaluation of material properties at the time of the seismic event. This value (150°C) is conservative for evaluation of material properties during 98.5 percent of the first 10,000 years after repository closure. This result is based on a thermal analysis for an unfilled drift with three infiltration levels and five host-rock units (BSC 2004 [DIRS 169565], Figures 6.3-7 to 6.3-11). Results are presented for waste package temperature, which also provides an upper bound for the drip shield temperature. The peak waste package temperature ranges from 147.4°C to 177.8°C (BSC 2004 [DIRS 169565], Table 6.3-8). The waste package temperature time histories demonstrate that temperature exceeds 150°C for, at most, the first 150 years after ventilation ceases. In some cases, the temperature never exceeds 150°C for certain infiltration levels and host rock units. Since the time period when temperature exceeds 150°C is not greater than 150 years, it follows that evaluating material properties such as the yield strength at 150°C is conservative for at least 98.5 percent of the 10,000-year regulatory period.

The rockfall calculations for the lithophysal zones also make a key assumption. In the lithophysal zone, the block size distribution is assumed to be a function of the inter-lithophysal fracture density and the lithophysae spacing (BSC 2004 [DIRS 166107], Assumption 5.2.2). This assumption is relevant to the abstraction process because the size, mass, and velocity of the fragmented rock are related to the potential damage to the drip shield and waste package from tunnel collapse in the lithophysal zone, as discussed in Sections 6.6.2 and 6.6.3 of this document.

The effective cross-sectional area for transport through a network of stress corrosion cracks is a distribution of values based on two conceptual models (BSC 2004 [DIRS 169985], Section 6.5; DTN: MO0403SPASCRKD.000 [DIRS 168105]). The first conceptual model is based on a hexagonal array of randomly oriented cracks, while the second conceptual model is based on a hexagonal array of cracks in parallel rows. The use of a distribution directly represents the uncertainty in these two alternate conceptual models in TSPA.

Both conceptual models assume a hexagonal array of cracks because this leads to the closest packing of crack centers on a surface. Both conceptual models are based on recommendations from previous analyses (BSC 2004 [DIRS 169985], Sections 6.5.1 and 6.5.2) regarding the estimated length, intercrack spacing, and crack opening shape and size for the weld region in the waste package lid. For example, the spacing between crack centers is at least the wall thickness because cracks with more closely spaced centers will be arrested before penetrating completely through the wall thickness. In addition, the cross-sectional area of a crack is assumed constant through the wall thickness, although cracks tend to narrow at the crack tip (see Figure 6.3.2 in this report). The minimum spacing between crack centers and the constant cross-sectional area are conservative features of either model.

INTENTIONALLY LEFT BLANK

6. MODEL DISCUSSION

6.1 INTRODUCTION

6.1.1 Background

The U.S. Department of Energy (DOE) is implementing a comprehensive seismic evaluation strategy for a geologic repository at Yucca Mountain. This strategy began during the site recommendation (SR) period with a probabilistic seismic hazard analysis for the repository site. In the probabilistic seismic hazard analyses, the DOE has developed (1) ground motion hazard curves for the Yucca Mountain site, and (2) fault displacement hazard curves for fifteen faulting conditions mapped within the immediate vicinity of Yucca Mountain (CRWMS M&O 1998 [DIRS 103731], Sections 7 and 8).

The results from *Probabilistic Seismic Hazard Analyses for Fault Displacement and Vibratory Ground Motion at Yucca Mountain, Nevada* (CRWMS M&O 1998 [DIRS 103731]) were used to support screening decisions for FEPs relevant to potential seismic effects on the repository. With the exception of seismic ground motion effects on fuel rod cladding, FEPs related to ground motion were screened out of the Total System Performance Assessment for the Site Recommendation (TSPA-SR) on the basis of median ground motion hazard (BSC 2004 [DIRS 168789], Section 6.2.6). A key assumption for the TSPA-SR screening decision was that the median hazard curve, rather than the mean hazard curve, was appropriate for the analysis. The ground motions and fault displacement amplitudes from the median hazard curves were low enough that their expected damage to the engineered barriers was not significant, even down to the lowest annual exceedance frequency of 10^{-8} per year. This result supported the decision to screen out seismic effects, except for fuel rod cladding, from TSPA-SR.

The Nuclear Regulatory Commission (NRC) subsequently expressed concern about the potential impacts of larger amplitude earthquakes on EBS components during the postclosure period. These concerns resulted in agreements that were reached between the NRC staff and the DOE during the NRC/DOE Technical Exchange on Structural Deformation and Seismicity KTI, held on October 11-12, 2000 (Gardner 2000 [DIRS 154287]).

The DOE's seismic analysis approach for the License Application is outlined in a letter report, *Approach to Postclosure Seismic Analyses for a Potential Geologic Repository at Yucca Mountain, Nevada* (Brocoum 2001 [DIRS 159576], enclosure). The strategy outlined in the letter report responds to the NRC's concerns on seismic issues. Specifically, the DOE agreed to either provide technical justification for the use of median fault displacement and ground motion hazard curves as the basis for screening seismic FEPs for the TSPA-LA, or to adopt mean values as the basis for screening seismic FEPs, or to evaluate and implement an alternative approach. The DOE has adopted mean hazard curves for vibratory ground motion and for fault displacement in screening FEPs for TSPA-LA and in developing the seismic consequence abstractions for TSPA-LA.

6.1.2 Information Sources and Outputs

This report presents the abstractions for damage to EBS components due to seismic hazards and the computational methodology for the seismic scenario class for TSPA-LA. These abstractions and the computational methodology are the outputs from this model report. The intended use of this output is to define the seismic scenario class for TSPA-LA. The report includes discussion of:

- The criteria for determining the damaged areas of the waste package and drip shield under vibratory ground motions
- The morphology and abstraction of these damaged areas as a function of the seismic hazard
- Damage to EBS components from fault displacement
- The abstraction of cladding failure in response to waste package impacts
- The algorithms for including the damage abstractions in the seismic scenario class
- Post-seismic event changes in seepage, temperature, and relative humidity due to tunnel collapse and in EBS flow pathways due to accelerated localized corrosion of Alloy 22.

Figure 6.1-1 illustrates the major components of the EBS in a typical emplacement drift. The major EBS components are the waste package, the drip shield, and the fuel rod cladding (the cladding is not shown in Figure 6.1-1). These are important components because they provide barriers to the release of radionuclides from the EBS into the unsaturated zone. Figure 6.1-1 also shows the steel sets that will be added as ground support in some drifts. Steel sets are not considered in postclosure seismic analysis because rapid corrosion of mild steel is anticipated to limit their effectiveness in the postclosure repository environment.

The effectiveness of these barriers is potentially compromised by the direct effects from an earthquake, including vibratory ground motion, fault displacement, and rockfall induced by ground motion. The effectiveness of these barriers is also potentially compromised by indirect effects after an earthquake, including changes in seepage, temperature, and relative humidity if an emplacement drift collapses completely during a very low probability earthquake.

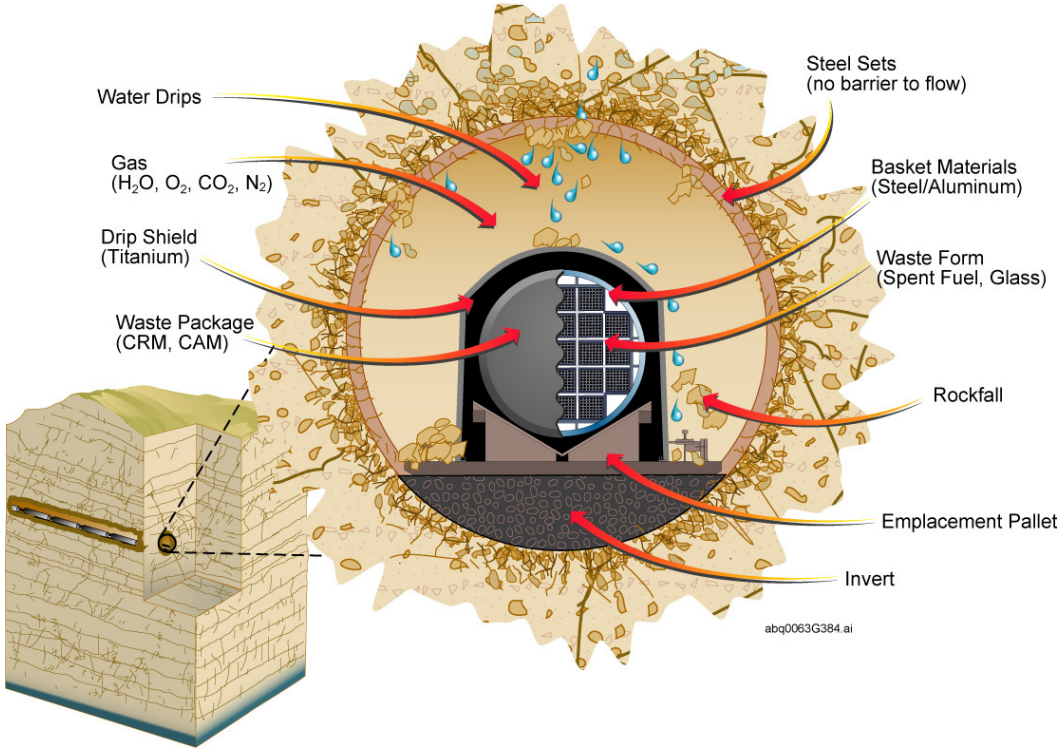

Figure 6.1-1. Schematic Diagram of the EBS Components in a Typical Emplacement Drift

Mathematically, the response of the EBS components to ground motion and fault displacement can be represented by the following vector, $\vec{A}$, that provides a conceptual representation of the major input parameters, the key damage mechanisms, and the post-seismic event changes for the seismic scenario class. In effect, Sections 6.3 through 6.9 of this report provide a definition, an abstraction, or a computational algorithm for each term on the right-hand side of this vector:

$$\vec{A} = (t, v_{hazard}, v_{bound}, \vec{d}, fWPA_{|V}, fDSA_{|V}, fCLD_{|V}, nPWRFD_{|D}, aPWRFD, nBWRFD_{|D}, aBWRFD, nHLWFD_{|D}, aHLWFD, nHLWFD_{|D}, aHLWFD, aLHLWFD, cSEEP_{v,t}, cTEMP_{v,t}, cRH_{v,t}, cFLUX_{v,t}),$$

(Eq. 6-1)

where t is the time (year) after repository closure when the seismic hazard occurs;

v_{hazard} is the amplitude of the ground motion from the hazard curve, measured in terms of horizontal PGV (m/s);

v_{bound} is a distribution representing the bounding value for the first horizontal PGV component at the emplacement drifts (m/s);

$\vec{d}$ is a vector of displacements for known faults that intersect emplacement drifts (m);

$fWPA_{|V}$ is the fraction (%) of waste package surface area damaged by ground motion. The abstraction for damage to the waste package is defined in Sections 6.5.1 through 6.5.3, based on information in *Structural Calculations of Waste Package Exposed to Vibratory Ground Motion* (BSC 2004 [DIRS 167083]);

$fDSA_{|V}$ is the fraction (%) of drip shield surface area damaged by ground motion. The abstraction for damage to the drip shield from ground motion is defined in Sections 6.5.4, 6.5.5, and D1 through D3, based on information in *Structural Calculations of Drip Shield Exposed to Vibratory Ground Motion* (BSC 2003 [DIRS 163425]);

$fCLD_V$ is the fraction (%) of cladding perforated by the vibratory ground motion. The abstraction for damage to the cladding is defined in Section 6.5.6, based on information in *Maximum Accelerations on the Fuel Assemblies of a 21-PWR Waste Package During End Impacts* (BSC 2003 [DIRS 162602]) and in *Structural Calculations of Waste Package Exposed to Vibratory Ground Motion* (BSC 2004 [DIRS 167083]);

$nPWRFD_{|D}$ is the number (dimensionless, denoted by "-") of PWR waste packages failed due to fault displacement. The abstraction for the number of failed waste packages is defined in Section 6.7.5, based on design information and on the mean hazard curves in the probabilistic seismic hazard analyses (DTN: MO0401MWDRPSHA.000 [DIRS 166962]);

$aPWRRD$ is the damaged area (m^2) on PWR waste packages and their associated drip shield and cladding resulting from fault displacement. The abstraction for waste package damaged area and for damage to drip shield and cladding is defined in Section 6.7.5;

$nBWRFD_{|D}$ is the number (-) of BWR waste packages failed due to fault displacement. The abstraction for the number of failed waste packages is defined in Section 6.7.5, based on design information and on the mean hazard curves in the probabilistic seismic hazard analyses (DTN: MO0401MWDRPSHA.000 [DIRS 166962]);

$aBWRRD$ is the damaged area (m^2) on BWR waste packages and their associated drip shields and cladding resulting from fault displacement. The abstraction for damaged area and for damage to drip shield and cladding is defined in Section 6.7.5;

$nNVLFD_{|D}$ is the number (-) of Naval waste packages failed due to fault displacement. The abstraction for the number of failed waste packages is defined in Section 6.7.5, based on design information and on the mean hazard curves in the probabilistic seismic hazard analyses (DTN: MO0401MWDRPSHA.000 [DIRS 166962]);

$aNVLRD$ is the damaged area (m^2) on Naval waste packages and their associated drip shields and cladding resulting from fault displacement. The abstraction for damaged area and for damage to drip shields is defined in Section 6.7.5;

$nHLWFD_{|D}$ is the number (-) of HLW waste packages failed due to fault displacement. The abstraction for the number of failed waste packages is defined in Section 6.7.5, based on design information and on the mean hazard curves in the probabilistic seismic hazard analyses (DTN: MO0401MWDRPSHA.000 [DIRS 166962]);

$aHLWRD$ is the damaged area (m^2) on HLW waste packages and their associated drip shields and cladding resulting from fault displacement. The abstraction for damaged area and for damage to drip shields is defined in Section 6.7.5;

$cSEEP_v$ is an indicator variable (-) for the change in seepage flux in the lithophysal zone after the seismic event that collapses the emplacement drifts, as described in Section 6.8.1;

$cTEMP_{v,t}$ is an indicator variable (-) for the change in temperature on the waste packages in the lithophysal zone after a seismic event that collapses the emplacement drifts, as described in Section 6.8.3;

$cRH_{v,t}$ is an indicator variable (-) for the change in relative humidity on the waste packages in the lithophysal zone after a seismic event that collapses the emplacement drifts, as described in Section 6.8.3;

$cFLX_{v,t}$ is an indicator variable (-) for the change in flux splitting on the waste package (i.e., the fraction of seepage flux that enters a waste package after falling onto the outer surface of the package) if localized corrosion occurs after the seismic hazard. The flux splitting algorithms are described in Sections 6.8.2 and D4 in Appendix D.

In the above notation, a subscript "|V" or "|D" indicates a parameter that has a distribution that is conditional on (i.e., is a function of) the final value for PGV, denoted here as v, or on the fault displacements, $\vec{d}$, respectively. The subscripts "v" and "t" indicate variables that are functions of the final value of PGV, v, or time of the event, t, respectively.

The levels of ground motion and fault displacement are based on the mean hazard curves defined in DTN: MO0401MWDRPSHA.000 [DIRS 166962], (data files defined in Table 4-1 of this report), based on the *Probabilistic Seismic Hazard Analyses for Fault Displacement and Vibratory Ground Motion at Yucca Mountain, Nevada* (PSHA) (CRWMS M&O 1998 [DIRS 103731]). The response of the EBS components incorporates an allowance for corrosion and degradation of the waste package and drip shield over the 10,000-year regulatory period for

the repository (Assumption 5.5). The seismic scenario class has been designed to accurately represent the seismic hazards that cause significant structural damage, and considers hazards with an annual exceedance probability of 10^{-8} per year or greater, per 10 CFR 63.114(d) [DIRS 156605].

6.1.3 Terminology

The terminology for the seismic hazard curves and for the suite of ground motions corresponding to a given exceedance frequency is explained here. In addition, the difference between a damage abstraction and a response surface is briefly explained.

A mean hazard curve defines the relationship between the mean estimate of the mean annual frequency of exceedance and the amplitude of the seismic effect, either for vibratory ground motion (measured by PGV) or for fault displacement (measured by a vertical displacement). The mean annual exceedance frequency represents the mean value of the frequency in any year with which future seismic events will exceed a given value of the PGV or fault displacement.

The mean annual exceedance frequency spans many orders of magnitude, from a minimum of 10^{-8} per year to a maximum of 1 per year (or greater). The mean frequency is defined as the number of observed events, divided by the time interval of observation. It varies randomly from one observation to the next. We use the mean of this random number as a measure of how likely an event is over any future year. When the mean annual exceedance frequency of interest is much less than 1, as it is here, the mean annual exceedance frequency and the annual exceedance probability are essentially equal.[5] This report uses the term exceedance frequency because it is more general, although the annual exceedance frequency and annual exceedance probability are interchangeable for the very infrequent seismic hazards considered in this study. All hazard curves in this report are based on the mean annual exceedance frequency.

The effect of vibratory ground motion on the EBS components is assessed for a set of ground motions with a given value of the horizontal PGV. Sets of 17 three-component ground motions have been developed for a PGV of 2.44 m/s and for a PGV of 5.35 m/s. These ground motion sets are often referred to in this project and in some of its reports as the 10^{-6} per year and the 10^{-7} per year ground motions (respectively) because PGV values of 2.44 m/s and 5.35 m/s correspond to these frequency values on the hazard curve at Point B (the emplacement drifts). Unfortunately, this convenient terminology is extremely misleading because a seismic event with a PGV of 2.44 m/s will not occur with a frequency of 10^{-6} per year. The correspondence of 2.44 m/s with 10^{-6} per year on the mean hazard curve means that all ground motion events with PGV greater than 2.44 m/s occur with a mean annual frequency of 10^{-6} per year. In other words, the ensemble of seismic ground motions with PGV exceeding 2.44 m/s will occur with a mean frequency of 10^{-6} per year. To make an additional point, the probability of encountering an earthquake with a PGV of *exactly* 2.44 m/s is infinitesimally small, and will certainly not occur with a frequency of 10^{-6} per year.

[5] The probability of one or more events for a Poisson process (Assumption 5.4) with annual rate λ over duration T is given by $(1 - e^{-\lambda T})$. When λ is small enough, the probability that one or more events occur in an interval T becomes $(1 - e^{-\lambda T}) = 1 - (1 - \lambda T + (\lambda T)^2 - \ldots) \approx \lambda T$, so the annual probability for one or more events is given by $(\lambda T)/T = \lambda$, the annual frequency of events. A typical criterion for the accuracy of this expansion is for $\lambda T \leq 0.1$.

In this report, ground motions are identified by the appropriate value of PGV. The value of PGV provides a unique and unambiguous identifier for each set of ground motions, even when multiple hazard curves have been developed for a site. In fact, the multiple hazard curves in Figures 6.4-2 and 6.4-3 (Sections 6.4.3 and 6.4.4) illustrate the problem with identifying ground motion amplitude by exceedance frequency because a given value of PGV can be associated with multiple values of the exceedance frequency.

The value of PGV refers to the peak ground velocity of the first horizontal component of the ground motions. The use of PGV is appropriate for parameterizing the damaged area as a function of ground motion amplitude, and does not imply that the second horizontal and vertical velocity components have the same PGV value. In fact, ground motion time histories that preserve intercomponent variability (see discussion in Section 6.4.2) have substantial variability in the PGV values among the three components of the ground motion.

Finally, the damage abstractions for EBS components are defined in a different manner than fragility curves or than response surfaces. A fragility curve is defined as the probability of a binary event; for example, a fragility curve can define the probability of damaged area exceeding 1 percent of the surface area of the waste package, as a function of PGV. While it is possible to produce a family of fragility curves for multiple damage levels, such as for 0.2 percent, 0.5 percent, 1 percent, 2 percent, and so on, this is an awkward methodology to incorporate into a Monte Carlo approach, such as the TSPA for the Yucca Mountain Project. A typical response surface represents the mean damage and its standard deviation, often as normal or lognormal distributions whose parameters are functions of the amplitude of the ground motion or fault displacement. A response surface is more amenable to a Monte Carlo approach, provided the deviation about the mean is sampled in an appropriate manner. The damage abstractions for the seismic scenario class are similar to a response surface, but usually define upper and lower bounds of a distribution as a function of ground motion amplitude, rather than that of the mean. For example, the damage abstraction for the waste package is based on a uniform distribution with an upper bound that is a function of PGV and with a lower bound at zero. So the upper bound of the uniform distribution is defined in a similar fashion as the mean of a response surface. While the use of a uniform distribution is not typical for fragility analyses or response surfaces, this approach does provide a simple, transparent, and accurate approach for representing the variability and uncertainty in seismically-induced damage based on Monte Carlo sampling for TSPA.

6.1.4 Corroborating Information

The abstractions for damage to EBS components from seismic hazards are based on the direct input information in Table 4-1 of Section 4.1 and on the corroborating information in Table 6.1-1.

Table 6.1-1. Corroborating Input Information for Seismic Consequence Abstractions

Input Information	Value	Source
Seismic Failure Criteria:		
Residual stress threshold for initiation of stress corrosion cracking on a smooth surface of Alloy 22	90 percent of the yield strength of Alloy 22	BSC 2004 [DIRS 169985], Section 6.2.1, 2nd paragraph on page 6-7
Residual stress threshold for initiation of stress corrosion cracking on a smooth surface of Titanium Grade 7	50 percent of the yield strength of Titanium Grade 7	BSC 2004 [DIRS 169985], Section 6.2.1, 2nd paragraph on page 6-7
Damage to the Waste Package from Ground Motion:		
Preliminary damage statistics for the waste package, based on three vibratory ground motions with a PGV of 0.992 m/s, corresponding to an annual exceedance frequency near 1×10^{-5} per year	See Table XI-2	BSC 2004 [DIRS 167083], Table XI-2
Damage to the waste package for the single vibratory ground motion at the 0.190 m/s and 0.384 m/s PGV levels, corresponding to annual exceedance frequencies of 5×10^{-4} per year and of 1×10^{-4} per year	No damage	BSC 2004 [DIRS 167083], Section 6.3, last paragraph, and Section 6.4, last paragraph
Rockfall Induced by Ground Motion in the Lithophysal Zone:		
Damage statistics for a tunnel in the lithophysal zone, based on a sampling of vibratory ground motions at the 2.44 m/s (10^{-6} per year) PGV level	Tunnel collapses for ground motions with PGV > 2 m/s	BSC 2004 [DIRS 166107], Section 6.4.2.2.2, 4th bullet under subheading Discussion
Damage to a tunnel in the lithophysal zone for the single vibratory ground motion at the 0.190 m/s PGV level	No rockfall for rock mass categories 2-5; minor, low-energy rockfall for rock mass category 1	BSC 2004 [DIRS 166107], Section 6.4.2.2.1
Damage to the Waste Package and Drip Shield from Fault Displacement:		
Fault Displacement Hazard at Site 2 – on the Solitario Canyon fault	See Figure 8-3	CRWMS M&O 1998 [DIRS 103731], Figure 8-3
Fault Displacement Hazard at Site 4 – on the Ghost Dance fault	See Figure 8-5	CRWMS M&O 1998 [DIRS 103731], Figure 8-5
Fault Displacement Features of the Sever Wash fault and the Pagany Wash fault	Similar to Drill Hole Wash fault	Menges and Whitney 1996 [DIRS 106342], Section 4.2.4.10, and Section 5.2 of this report
PGV level for complete drift collapse in lower lithophysal	2.0 m/s	BSC 2004 [DIRS 166107], Section 6.4.2.2.2, 4th bullet under subheading Discussion
Subsurface facility layout and numbering of emplacement drifts	Figure 1	BSC 2004 [DIRS 164519], Figure 1
Alternate conceptual model for probability-weighted number of waste package failures from fault displacement	1.91×10^{-4} to 1.91×10^{-6}	Waiting et al. 2003 [DIRS 164449]
Alternate conceptual model for number of fault intersections with emplacement drifts	191	Waiting et al. 2003 [DIRS 164449]
Parameters for the Seismic Scenario:		
Horizontal PGV at Point B for the single ground motion corresponding to the 5×10^{-4} per year mean annual exceedance frequency	19.00 cm/s (rounded to 0.190 m/s)	BSC 2004 [DIRS 166107] Table X-1

Table 6.1-1. Corroborating Input Information for Seismic Consequence Abstractions (Continued)

Input Information	Value	Source
Horizontal PGV at Point B for the single ground motion corresponding to the 1×10^{-4} per year mean annual exceedance frequency	38.38 cm/s (rounded to 0.384 m/s)	BSC 2004 [DIRS 166107] Table X-1
Changes Due to Drift Collapse:		
Seepage abstraction if ground motion amplitude (PGV) is large enough to collapse the drifts	See file *ResponseSurfaceSMPACollapsedDrift.dat* in DTN	DTN: LB0307SEEPDRCL.002 [DIRS 164337]
Change in temperature of waste package if seismic hazard is large enough to collapse the drifts	See files: *Twp_dhlw-l1_3case.dat*, *Twp_dhlw-s1_3case.dat, Twp_bwr1-1_3case.dat, Twp_bwr1-2_3case.dat, Twp_bwr2-1_3case.dat, Twp_pwr1-1_3case.dat, Twp_pwr1-2_3case.dat,* and *Twp_pwr2-1_3case.dat* in DTN	DTN: LL040310323122.044 [DIRS 168769]
Change in relative humidity on the waste package if seismic hazard is large enough to collapse the drifts	See files: *RHwp_dhlw-s1_3case.dat, RHwp_dhlw-l1_3case.dat, RHwp_bwr1-1_3case.dat, RHwp_bwr1-2_3case.dat, RHwp_bwr2-1_3case.dat, RHwp_pwr1-1_3case.dat, RHwp_pwr1-2_3case.dat*, and *RHwp_pwr2-1 3case.dat* in DTN	DTN: LL040310323122.044 [DIRS 168769]

6.2 RELEVANT FEPS FOR THE SEISMIC SCENARIO CLASS

The development of a comprehensive list of FEPs potentially relevant to postclosure performance of the potential Yucca Mountain repository is an ongoing, iterative process based on site-specific information, design, and regulations. The content of this report is relevant to the list of seismic-related FEPs extracted from the LA FEP list (DTN: MO0407SEPFEPLA.000 [DIRS 170760]) and shown in Tables 6.2-1 and 6.2-2. The damage abstractions for the waste package and cladding provide the basis for screening of the listed FEPs, based on the relevant sections of this report identified in Tables 6.2-1 and 6.2-2. This report provides the justification for changing the screening decision for FEP 1.2.03.02.0B from Include, as currently indicated in DTN MO0407SEPFEPLA.000 [DIRS 170760] and in the relevant TWP for this activity (BSC 2004 [DIRS 171520], Table 2-2), to Exclude. Table 6.2-1 identifies the TSPA-LA FEPs

that are included in the seismic scenario class and the section in this report where each FEP is addressed. Table 6.2-2 identifies the TSPA-LA FEPs that are excluded from the seismic scenario class and the section in this report where the screening argument is discussed.

The seismic scenario class is based on two modeling cases: (1) a case with mechanical damage alone, and (2) a case with mechanical damage and localized corrosion. Either case has a single seismic event that occurs at a randomly chosen time in each realization of the TSPA-LA. Seismic events with PGV levels greater than 0.384 m/s (exceedance frequencies less than 10^{-4} per year on the hazard curve at Point B, the emplacement drifts) are considered here because the associated ground motions and fault displacements have the potential to cause damage to the EBS components (see Assumption 5.1). The response of the drip shield, waste package, and cladding to this single seismic event is represented through damage abstractions for the EBS components under vibratory ground motion and fault displacement. The areas on the EBS components that exceed a residual stress threshold are susceptible to accelerated stress corrosion cracking, resulting in a network of stress corrosion cracks that has the potential to provide a pathway for transport through the engineered barriers. Once radionuclides are released from the EBS, flow and transport in the unsaturated zone and the saturated zone are based on the same models and algorithms as for the nominal scenario class, with the exception of: (1) changes in the in-drift environment caused by drift collapse in the lithophysal zones of the repository and (2) the flux splitting for the waste package (i.e., the fraction of the liquid flux onto the waste package that can flow inside and contact the waste form) if accelerated localized corrosion can occur. Biosphere calculations are also unchanged from those for the nominal scenario class.

Table 6.2-1. FEPs Included in Seismic Consequence Abstractions, their Disposition in TSPA-LA, and the Relevant Sections of this Report

FEP #	FEP Name	Section Where FEP is Addressed
1.2.02.03.0A	Fault displacement damages EBS components	Section 6.7 defines the damage abstraction for the EBS components in response to fault displacement. Step 9 in Section 6.9.2 provides an algorithmic description and definition of output parameters for the fault displacement damage abstraction for the EBS components. Table 6.9-1 summarizes the 20 output variables for TSPA-LA that specifically relate to damage from fault displacement.
1.2.03.02.0A	Seismic ground motion damages EBS components	Sections 6.5.1 through 6.5.3 define the damage abstraction for the waste package in response to vibratory ground motion. Steps 3 through 5 in Section 6.9.2 provide an algorithmic description and definition of output parameters for the damage abstractions for this barrier. Table 6.9-1 summarizes the 8 output variables for TSPA-LA that specifically relates to damage to the waste package from vibratory ground motion. Sections 6.5.4 and 6.5.5 provide the basis for screening out damage to the drip shield from vibratory ground motion for the TSPA-LA. However, the validation testing for the TSPA-LA model retains an abstraction for drip shield separation from vibratory ground motion because the technical basis for excluding separation was established after the start of model validation activities. This abstraction is described in Appendix D, Sections D1 though D3. Steps 6 and 7 in Section 6.9.2 provide an algorithmic description and definition of output parameters for the abstraction for drip shield separation. Table 6.9-1 summarizes the 4 output variables for TSPA-LA that specifically relate to damage from drip shield separation.

Table 6.2-1. FEPs Included in Seismic Consequence Abstractions, their Disposition in TSPA-LA, and the Relevant Sections of this Report (Continued)

FEP #	FEP Name	Section Where FEP is Addressed
		Section 6.5.7 defines the damage abstraction for the cladding under vibratory ground motion. Step 8 in Section 6.9.2 defines the algorithm for the damage abstraction for cladding in the TSPA-LA. Table 6.9-1 identifies the single output variable for the abstraction of cladding damage.
1.2.03.02.0D	Seismic-induced drift collapse alters in-drift thermohydrology	Section 6.9.2 summarizes the changes in the in-drift environment after a seismic event. Steps 12, 13 and 14 in Section 6.9.2 summarize the methodology for the post-seismic event changes for TSPA.

Table 6.2-2. FEPs Excluded from Seismic Consequence Abstractions and the Relevant Sections of this Report

FEP #	FEP Name	Section Where FEP is Addressed
1.2.03.02.0B	Seismic-induced rockfall damages EBS components	Damage to EBS components from seismically-induced rockfall in the nonlithophysal zones is analyzed but not abstracted into the seismic scenario class for TSPA-LA. In the nonlithophysal zones, large rock blocks can be shaken free from the walls and drop onto the drip shield under the influence of gravity. Section 6.6.1 provides a description of the rock block calculations and the drip shield structural response calculations for impacts by rock blocks. Analysis of rockfall in the lithophysal zones is discussed under FEP 1.2.03.02.0C (the next FEP in this table). The damage to the drip shield from the impact of large rock blocks is not included TSPA-LA. Damaged areas on the drip shield are susceptible to accelerated stress corrosion cracking (see Section 6.3.3). However, the quantity of liquid that can adjectively flow through the resulting crack network and impinge on the waste package will be insignificant, as discussed in Section 6.3.6. In this situation, damage to the drip shield from rock blocks is not included in the seismic scenario class for TSPA-LA. Damage to the waste package or cladding from rock blocks is also not included in the seismic scenario class for TSPA-LA. The drip shield remains intact until a seismic event occurs during the first 10,000 to 20,000 years after repository closure. In addition, the drip shield will not separate in response to vibratory ground motions (see Section 6.5.5). In its intact state, the drip shield will deflect blocks away from the waste package without collapsing or contacting the waste package, even for the largest blocks (see Section 6.6.1.2). It follows that the drip shield provides protection from rockfall for the waste package and cladding, so this damage mechanism is not included in TSPA-LA.

Table 6.2-2. FEPs Excluded from Seismic Consequence Abstractions and the Relevant Sections of this Report (Continued)

FEP #	FEP Name	Section Where FEP is Addressed
1.2.03.02.0C	Seismic-induced drift collapse damages EBS components	Section 6.6.1 describes the rock block analyses and the structural response of the drip shield in response to rock block impacts. Section 6.5.5 presents the screening argument for excluding drip shield separation from TPSA-LA. Step 6 in Section 6.9.2 summarizes the rationale for not including damage from rock block impacts induced by vibratory ground motion in TSPA-LA. Damage to EBS components from seismically-induced rockfall in the lithophysal zones is analyzed but not abstracted into the seismic scenario class for TSPA-LA. Vibratory ground motion can cause failure of the host rock around the emplacement drifts, but is anticipated to cause insignificant damage to the drip shield, waste package, and cladding. The lithophysal rock will fragment into small rock fragments that have little capability to damage the drip shield, either from individual impacts or from their static load, as discussed in Sections 6.6.2 and 6.6.2.1, respectively. Damage to EBS components from lithophysal rockfall is not included in TSPA on this basis. Section 6.6.2 describes the rockfall calculations and the structural response of the drip shield in response to the static load from rockfall. Step 6 in Section 6.9.2 summarizes the rationale for not including damage from rock block impacts induced by vibratory ground motion in the seismic scenario for TSPA-LA.

6.3 FAILURE MECHANISM, RESIDUAL STRESS THRESHOLDS, AND FAILURE MORPHOLOGY FOR THE WASTE PACKAGE AND DRIP SHIELD

6.3.1 Failure Mechanisms Under Seismic Loads

Mechanical processes that occur during a significant seismic event (i.e., an event with PGV greater than 0.384 m/s; see Assumption 5.1) have the potential to compromise the functionality of the waste packages, drip shields, and fuel rod cladding as barriers to radionuclide release. These mechanical processes include impacts caused directly by vibratory ground motion during an earthquake, impacts caused by rock blocks and rockfall induced by vibratory ground motions, and mechanical loading from fault displacement.

Under significant vibratory ground motions, impacts can occur between adjacent waste packages and between the waste package and its emplacement pallet, the surrounding drip shield, and the invert. Impacts can also occur between the drip shield and the emplacement pallet, the invert, and even the drift wall. Rockfall induced by vibratory ground motions can result in impacts on the drip shield in the postclosure period and impacts on the waste packages in the preclosure period, when drip shields are not yet in place. Rockfall induced by vibratory ground motion in the lithophysal zones may collapse the drifts, resulting in static loads from the mass of rubblized rock surrounding the drip shield. Finally, mechanical loads may be generated by fault displacement within the repository block. In this case, EBS components may become pinned if fault displacement is greater than the available clearances between components.

These mechanical processes are associated with a number of potential failure mechanisms, each of which is discussed below:

- Peak dynamic loads have the potential to result in immediate puncture or tearing of an EBS component if the localized strain exceeds the ultimate tensile strain. A puncture

provides a potential pathway for seepage to flow into and radionuclide transport out of an EBS component.

- Impact-related dynamic loads may dent a component, resulting in permanent structural deformation with residual stress. High levels of residual tensile stress may lead to local degradation from accelerated corrosion processes. Areas that are breached from corrosion processes provide a potential pathway for flow into and radionuclide transport out of an EBS component.
- Static loads from rockfall may collapse or buckle the drip shields. Buckling or collapse represents a change in the physical shape of the drip shield, potentially compromising its ability to deflect seepage and rockfall away from the waste package.
- Impacts between adjacent waste packages impose dynamic loads on waste package internals. These dynamic loads may result in buckled fuel rods and perforated cladding. Failure of cladding provides a potential pathway for release of radionuclides from fuel rods.
- Large displacements on known faults in the repository block may shear waste packages and drip shields if the EBS components become pinned by the fault response. Sheared components provide potential pathways for flow into and radionuclide transport out of the damaged components.

Immediate puncture or tearing of waste packages is very unlikely because Alloy 22 and Titanium Grade 7 are ductile metals that require very high dynamic loads to reach their ultimate tensile strain. The potential for immediate breach through tensile or shear failure is included in the constitutive model for the structural response calculations supporting the seismic scenario class; however, the computational meshes are generally too coarse to realistically simulate a small, localized puncture. Supporting calculations for waste package drops on the emplacement pallet or the calculations for waste package response under vibratory ground motion indicate that the maximum stress intensity for the impact velocities observed in the vibratory ground motion calculations is significantly below the ultimate tensile strength (BSC 2003 [DIRS 165497] and BSC 2003 [DIRS 167083, Sections 6.1.4 and 6.2.4]). In this situation, a localized puncture or tearing is very unlikely from impact processes caused by vibratory ground motions and is not included in the seismic scenario class.

The presence of high residual tensile stress has the potential to result in accelerated stress corrosion cracking (Sections 6.3.2 and 6.3.3). This combined mechanical-corrosion failure mechanism is expected to be the most likely cause of failure for the waste package and drip shield from impact processes caused by vibratory ground motions and by rockfall induced by vibratory ground motions. The areas that exceed the residual tensile stress threshold are referred to as the damaged area throughout this document. The effective area for flow and transport through the damaged areas will be substantially less than the damaged area because the cross-sectional area of the stress corrosion cracks is much less than the total surface area that exceeds the residual stress threshold, as derived in Sections 6.3.5 and 6.3.6.

Application of a residual tensile stress threshold for seismic failures is nonmechanistic in the sense that detailed calculations with accelerated corrosion rates or crack propagation are not used to determine the actual failure time after a seismic event. Rather, a network of stress corrosion

cracks is considered to immediately form once the residual tensile stress threshold is exceeded, providing potential pathways for flow and transport through the areas exceeding the residual tensile stress threshold. The residual tensile stress threshold is often referred to as the residual stress threshold or more simply the stress threshold, with the understanding that the principal residual stress must always be tensile to initiate an accelerated corrosion process.

Figure 6.3-1 is a simplified illustration of how residual stress is generated by permanent (plastic) deformation in a simple uniaxial strain model. The loading path in Figure 6.3-1 has three phases: (1) elastic loading until reaching the elastic yield limit, (2) plastic loading above the elastic yield limit, and (3) elastic unloading when the external load reduces the local stress. Figure 6.3-1 also shows that plastic deformation does not always generate a damaged area because the final residual stress state may be compressive or, if tensile, may be below the tensile threshold to initiate accelerated localized corrosion or stress corrosion cracking.

The static loads from rockfall may initiate plastic deformation, potentially leading to buckling or collapse of the drip shield (Section 6.6.2.2). The appropriate failure criterion for the onset of plastic deformation is the elastic yield strength, which corresponds to the point at the top of the elastic loading path in Figure 6.3-1. The physical configuration of the drip shield can change when local stresses exceed the elastic yield strength, resulting in plastic deformation of the structure. It is important to differentiate between the two failure criteria for the drip shield. For impact loading, an area may be damaged as a flow barrier when it exceeds the residual stress threshold of Titanium Grade 7, as discussed in Section 6.3.3. This failure is a combined mechanical-corrosion response of a cold-worked material to dynamic impacts. For plastic deformation from static loading of the drip shield, failure is determined by the elastic yield strength at the onset of plastic yielding, as discussed in Section 6.6.2.2. These criteria are applied separately and independently because the appropriate failure mechanisms are distinct physical responses to different loading conditions and failure modes.

The dynamic loads on fuel rods from end-to-end impacts of adjacent waste packages have the potential to buckle the fuel rods and fail the cladding. The primary cladding failure mechanism is perforation due to accelerations when the waste package impacts the emplacement pallet or when there is an end-to-end impact of adjacent waste packages (see discussion in Section 6.5.6). The *g*-loads required to buckle fuel rods are estimated from a simple analytic model based on Euler buckling of a column (Chun et al. 1987). It is estimated that the cladding fails when the impact accelerations are in the range of 82 *g* to 252 *g* for axial impacts and 63 *g* to 211 *g* for lateral impacts (Chun et al. 1987 [DIRS 144357], Table 4).

Large displacements on known faults in the repository block have the potential to shear waste packages and drip shields if the EBS components become pinned by the fault response. The response of EBS components to fault displacement is discussed in Section 6.7. Given the complexity of the response of EBS components and the invert to a fault displacement, a simplified failure criterion has been applied to determine shear failure in a collapsed drift. If the fault displacement is greater than the clearance between the top of a waste package and the underside of the drip shield, the waste package is modeled as failing from shear. This simple failure criterion is appropriate because shear failure from fault displacement only occurs from extremely low frequency, high amplitude fault displacements, corresponding to an annual exceedance frequency of less than or equal to 10^{-7} per year.

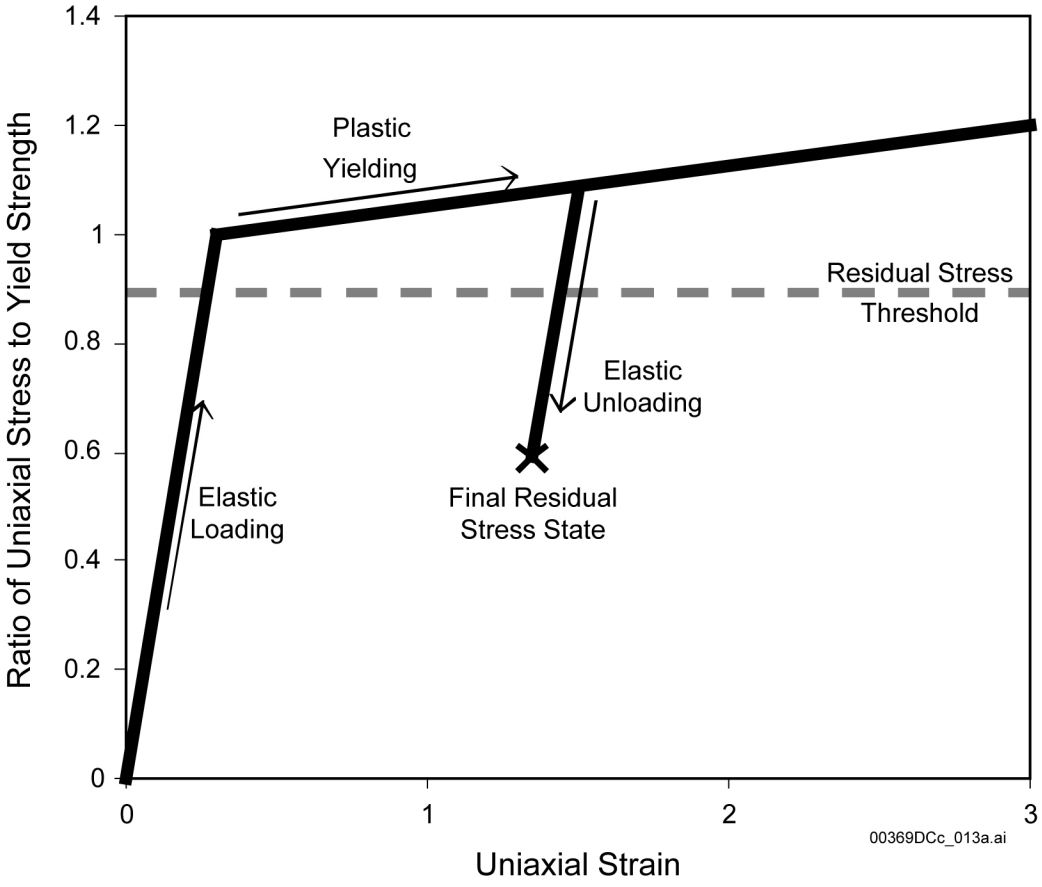

Figure 6.3-1. Permanent Deformation from Plastic Yielding Generates Residual Stress

Accelerated stress corrosion cracking from high residual stress is expected to be the most likely cause of failure for the waste package from impact processes in the seismic scenario class. The residual stress thresholds for seismic response are similar to the criteria for initiation of stress corrosion cracking on smooth surfaces of Alloy 22 (BSC 2004 [DIRS 169985], Section 6.2.1, with thresholds defined on page 6-7). The use of a stress corrosion cracking initiation criterion is appropriate for seismic analysis because regions where the residual stress from mechanical damage exceeds the tensile failure criterion are expected to be extensively cold-worked and, hence, potentially subject to enhanced stress corrosion cracking.

A residual stress threshold is a conservative failure criterion because detailed corrosion models will have a delay time until failure. This approach is appropriate because it is consistent with other tensile failure criteria (BSC 2004 [DIRS 169985], Section 6.2.1, second paragraph on page 6-7) and because it is easily applied to the output from structural response calculations.

6.3.2 Residual Stress Damage Threshold for the Waste Package

The residual stress threshold for failure of the waste package is represented by a uniform distribution with a lower bound of 80 percent of the yield strength of Alloy 22 and an upper bound of 90 percent of the yield strength of Alloy 22. The upper bound is based on experimental data and conservatively incorporates a safety factor of 2.2 because of the very long lifetime of

the waste package (BSC 2004 [DIRS 169985], Section 6.2.1, second paragraph on page 6-7). The lower bound is introduced to evaluate the sensitivity of damaged area to potential uncertainty in the residual stress threshold. This residual stress criterion (80 to 90 percent of the yield strength) is also consistent with the failure criterion for initiation of stress corrosion cracking in other waste package analyses.

In practice, the damage to the waste package has been evaluated at the extremes of the uniform distribution. The results from each structural response calculation are postprocessed to determine the elements in the outer shell of the waste package whose residual stress exceeds 80 percent of the yield strength of Alloy 22 and to determine the elements in the outer shell of the waste package whose residual stress exceeds 90 percent of the yield strength of Alloy 22. These elements are then converted into an area susceptible to accelerated stress corrosion cracking at the 80 and 90 percent criteria. The appropriate areas at intermediate values of the residual stress threshold can then be defined by linear interpolation between the extremes. The elements that exceed 90 percent of the yield strength are always a subset of the elements that exceed 80 percent of the yield strength. In other words, the damaged area for the 90 percent residual stress threshold is always less than or equal to the damaged area for the 80 percent residual stress threshold.

6.3.3 Residual Stress Damage Threshold for the Drip Shield

For the drip shield barrier, the residual stress threshold for failure is represented by a fixed lower bound of 50 percent of the yield strength of the drip shield plate material (Titanium Grade 7) (BSC 2004 [DIRS 169985], Section 6.2.1, second paragraph on page 6-7). The fixed bound is based on experimental data and conservatively incorporates a safety factor of 2.2 because of the long lifetime of the drip shield (BSC 2004 [DIRS 169985], Section 6.2.1, second paragraph on page 6-7). The following discussion is abridged from *Stress Corrosion Cracking of the Drip Shield, the Waste Package Outer Barrier, and the Stainless Steel Structural Material* (BSC 2004 [DIRS 169985], Section 6.2.1), where a more detailed discussion of the experimental data and the technical basis for this threshold can be found.

There is extensive experimental data for Titanium Grade 7 that justifies the use of 50 percent of yield strength as a stress corrosion cracking initiation criterion. These data include long-term constant load tests in a concentrated brine environment (~15 percent Basic Saturated Water, designated as J-13) at 105°C with specimens loaded to stresses of 110 to 140 percent of the yield strength. Some specimens failed relatively early (≤168 hours) at applied stresses in excess of 110 percent of yield strength. At 110 percent of yield strength, there is a mixture of failure and non-failure run out times from about 200 hours for first failure to greater than several thousand hours without failure. These data are consistent with a failure threshold that is less than 110 percent of yield strength.

A second source of information regarding the stress corrosion cracking initiation criterion for Titanium Grade 7 comes from U-bend tests. Initiation of stress corrosion cracking is not observed in fixed deflection U-bend tests on Titanium Grade 7 exposed for one year and Titanium Grade 16 (an analogous titanium/palladium alloy) exposed for five years to a range of relevant aqueous environments at 60°C and 90°C in the Lawrence Livermore National Laboratory Long Term Corrosion Test Facility. These U-bend tests are more representative of

secondary residual stress loading that might result from deformation following seismic loadings. These U-bend specimens are deflected and then restrained to give apex strains (cold work level) of greater than 10 percent, which results in sustained stress levels near the yield strength. A very conservative value of 50 percent of yield strength is selected as a threshold criterion for Titanium Grade 7, even though the initiation of stress corrosion cracking is not observed for residual stresses greater than yield strength.

6.3.4 Morphology of Damage on the Waste Package

The material for the waste package outer corrosion barrier, Alloy 22, has been shown to be potentially susceptible to stress corrosion cracking under environmental conditions that are relevant to the repository. The stress corrosion cracking mode (morphology) is transgranular stress corrosion cracking (TGSCC), rather than the intergranular stress corrosion cracking which is commonly observed in pressurized systems, such as pipelines or light water reactor components (Andresen et al. 2001 [DIRS 167840]). The primary issue for the seismic scenario class is to define the effective area and transport mode (advective or diffusive) resulting from seismically-induced deformation and the associated TGSCC through the outer corrosion barrier of the waste package. The conditions leading to TGSCC and the potential geometry of the crack system have therefore been investigated (Herrera 2004 [DIRS 168133]), and are summarized below.

Seismically-induced deformation has the potential to initiate and propagate cracks on the outer shell of the waste package. A range of aqueous brine type environments may form on the waste package outer corrosion barrier, producing the requisite concurrent conditions for accelerated stress corrosion cracking: (1) high residual tensile stress, (2) an environment that supports corrosion, and (3) a material that has been cold worked during the seismic event. Once initiated, the strain fields (residual stresses) produced by the seismically-induced impacts can drive crack growth. Depending on the stress distribution, cracks may propagate through-wall if the stress intensity factor remains positive. If multiple cracks are initiated in the same general area, it is theoretically possible, but very unlikely, that multiple cracks can intersect or coalesce, creating a continuous crack around the deformed region.

There is a very low probability that a residual stress profile would be created that would allow an initiated stress corrosion crack to propagate both through-wall and circumscribing a dent or deformed area. Any through-wall residual stress fields resulting from seismic impact loads would be a secondary type stress (displacement controlled). There is no significant stress from other sources, such as stress induced by internal pressure. In addition, stresses and strains are generally of higher magnitude at the outer surface and tend to decrease through the thickness for the deformation-induced damage from a seismic event. In this situation, any crack that initiates and propagates may arrest before penetrating the full thickness of the outer barrier and is highly unlikely to have a positive stress intensity factor throughout that could result in both through-wall and 360° cracking around the entire dent (BSC 2004 [DIRS 169985], Sections B6.1 and B6.3).

Even postulating that a through-wall crack occurs and circumscribes the dented area, the nature of stress corrosion cracking will preclude the dented area from falling out. Cracks in Alloy 22 are transgranular, but whether transgranular or intergranular, the crack path has complex local

branches with a roughness and tortuosity, as illustrated in Figure 6.3-2 (Herrera 2004 [DIRS 168133] Figure 2-1), that make it geometrically impossible for an inner "plug" to disengage from the vessel in the absence of a superimposed primary load (i.e., significant internal pressure). Any internal pressure that develops from heat up to about 150°C and/or corrosion-generated gas with the small amount of internal water vapor that is available would not be sufficient to force the dented area from the wall.

This analysis (Herrera 2004 [DIRS 168133]) is consistent with many years of experience with stress corrosion cracks in light water reactor components and other internally pressurized systems. A number of incidents of stress corrosion cracking have been observed in light water reactors involving both austenitic stainless steels and nickel-based alloys (Herrera 2004 [DIRS 168133] Appendix A). The observed stress corrosion cracking has been extensive in many of these incidents, sometimes becoming fully circumferential in response to weld-induced residual tensile stress and pressure-induced primary stresses. Even under these conditions, which are more severe than in the post-seismic environment, there has not been a documented case where any section of material dropped out as a result of the observed cracking (Herrera 2004 [DIRS 168133] Section 7.0).

6.3.5 Effective Area for Flow and Transport Through the Waste Package

Since the most probable failure mechanism from a seismic event is accelerated stress corrosion cracking and since the damaged areas that exceed the residual stress failure for Alloy 22 are expected to remain physically intact, it is reasonable to represent these areas as a dense network of stress corrosion cracks, rather than as a plug of material that separates from the outer barrier. The effective area for transport through the crack network has been estimated with the following procedure.

The range of crack densities and crack widths has been estimated for four closely spaced networks of cracks (Herrera 2004 [DIRS 168133] Section 6.2; DTN: MO0403SPASCRKD.000 [DIRS 168105]). Figure 6.3-3 presents one of these hexagonal arrays, with parallel rows of randomly oriented cracks. In this approach, centers of through-wall cracks are located in a densely packed hexagonal array and are separated by at least a wall thickness. The wall thickness is anticipated to be the minimum possible separation because stress relief from propagation of adjacent cracks relieves the local stress intensity factor, preventing tighter spacing between through-wall cracks. The width of each crack is estimated by assuming an elliptical opening with constant through-wall stress given by the elastic yield strength. This is a conservative approach because the crack tips tend to narrow at the inner surface (see Figure 6.3-2) and because stress relief from adjacent cracks will again tend to reduce the local stress levels at a crack.

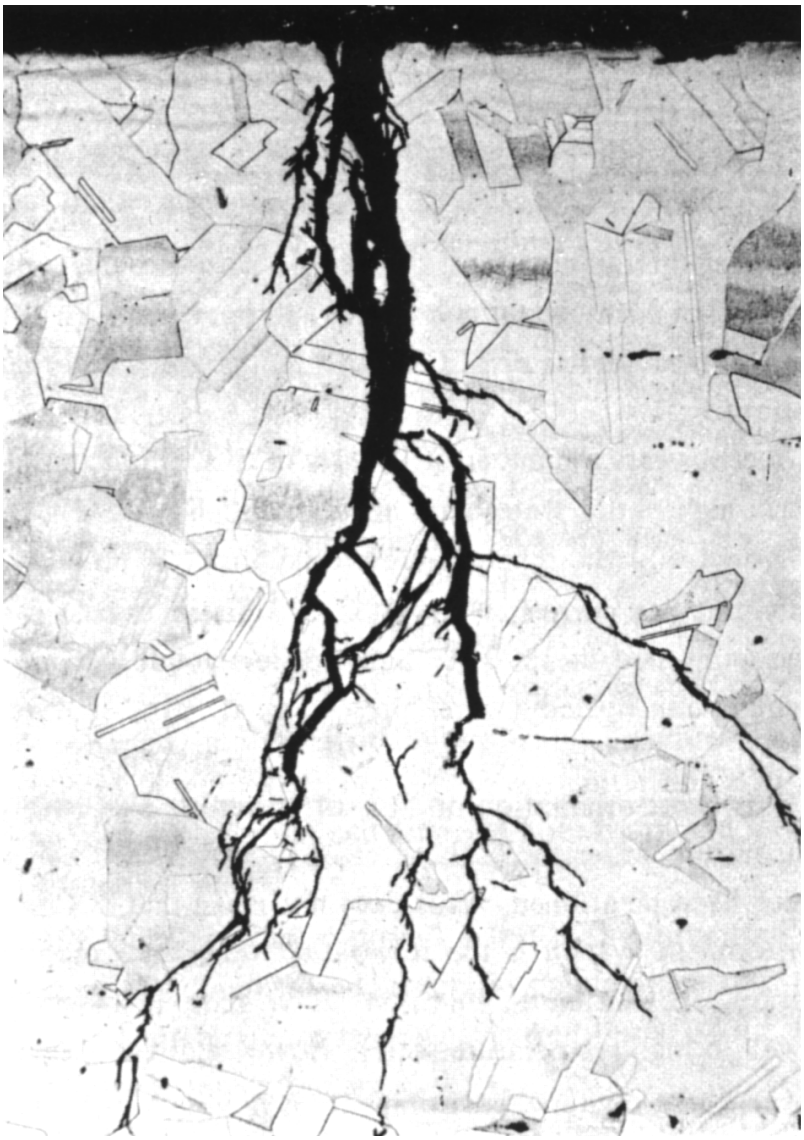

Source: Herrera 2004 [168133], Figure 2-1.

Figure 6.3-2. Typical Example of TGSCC in Stainless Steel

The hexagonal network of closely spaced cracks is a convenient conceptual model for estimating a range of crack densities and crack opening areas for TSPA-LA. However, this crack geometry is not commonly observed in industrial systems. Rather, an axisymmetric dent often produces cracks that are oriented circumferentially around the center of the dent because the circumferential direction is normal to the main stress gradients in the radial direction. An analysis for circumferential cracks (Herrera 2004 [DIRS 168133] Section 6.3) indicates that the effective area of a typical circumferential crack network is within the range of uncertainty from the hexagonal model.

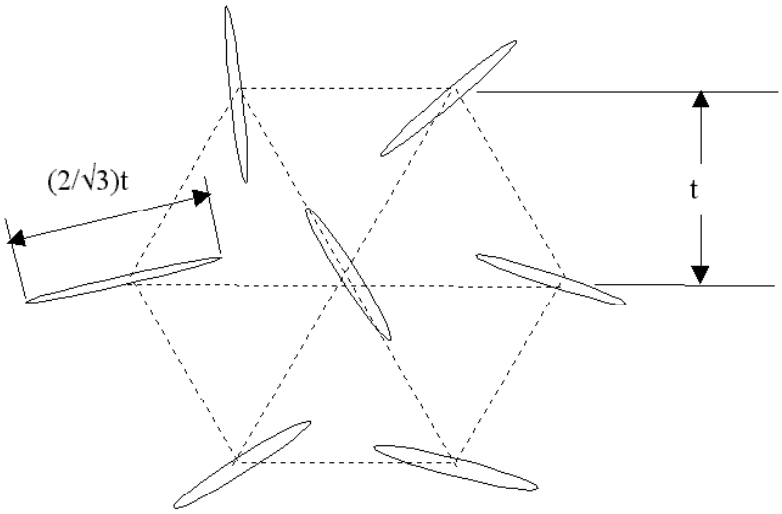

Source: Herrera 2004 [DIRS 168133], Figure 6-2.

NOTE: (Not drawn to scale).

Figure 6.3-3. Parallel Rows of Randomly Oriented Flaws, with Row Spacing Equal to Wall Thickness

The effective cross-sectional area for transport out of the waste package per unit damaged area is given by the product of the crack density per unit surface area, ρ_{SCC}, and the gap area per crack, A_{SCC}. The product $\rho_{SCC}A_{SCC}$ ranges from 0.00328 to 0.0131 (Herrera 2004 [DIRS 168133], Table 6-1) for the four crack networks. Stated differently, the effective transport area through the crack network is a factor of 76 to 305 less than the failed surface area that exceeds the residual stress threshold. The product has been evaluated using material properties for room temperature because this is slightly more conservative than material properties at 150°C.

The network of stress corrosion cracks on the waste package have high tortuosity and surface roughness, and narrow to very small apertures at the crack tip(s) (see Figure 6.3-2). This physical morphology has the potential to eliminate advective flux through the cracks because of infilling of small apertures with corrosion products, because of high surface tension when a narrow aperture is bridged by a single droplet, and because there is minimal head gradient or pressure gradient driving flow through the narrow apertures.

Evaporation-induced precipitation of calcite and other minerals may also occur within the cracks on the waste package, fostering crack plugging. When the drip shields are intact, the waters contacting the waste packages may be limited to condensate from the underside of the drip shields. This water can, however, interact with dust deposits containing soluble mineral species which are available for precipitation within the cracks, leading to plugging.

Even in the absence of crack plugging, the physical morphology of the crack network on the waste package prevents advective flow of liquid. However, it does provide a potential pathway for diffusive transport of radionuclides out of the waste package. The effective area for diffusive transport from the waste package is determined by the product of two random parameters, $\rho_{SCC}A_{SCC}$. The first parameter is the factor defining the ratio of effective area for diffusive transport to damaged area on the waste package. This factor is determined in each realization of

the seismic scenario class by sampling a uniform distribution with a lower bound of 0.00328 and an upper bound of 0.0131. The second parameter is the damaged area on the waste package, which is a random distribution whose upper bound is a function of PGV of the seismic disturbance. The product of these two parameters determines the effective area for diffusive transport from the waste package in each realization.

6.3.6 Effective Area for Flow Through the Drip Shield

The Titanium Grade 7 plates of the drip shield are also subject to the formation of residual stresses from seismic ground motions and from rockfall induced by seismic ground motions. As with Alloy 22, the most probable failure mechanism for Titanium Grade 7 after a seismic event is accelerated stress corrosion cracking, rather than immediate puncture or tearing of the drip shield. The deformed or dented region is expected to remain physically intact because individual cracks are complex, branching structures with high surface roughness and tortuosity. In this situation, the areas that exceed the residual stress failure criterion for Titanium Grade 7 are represented as a network of stress corrosion cracks, rather than as a plug of material that separates from the drip shield plates.

Further, the quantity of liquid that has the potential to flow through the drip shield and impinge on the waste package is reduced to an insignificant level because of the small crack apertures near crack tips and the high tortuosity and surface roughness of the cracks. In addition, flow through these cracks will be limited because of the infilling of cracks with corrosion products, because head gradients and pressure gradients driving flow through a crack are very small, because of high surface tension when a narrow aperture is bridged by a single droplet, and because of the potential for crack plugging from evaporation-induced precipitation over a period of a few hundred years.

Crack plugging will occur over time because the small heat flux across the drip shield will evaporate slowly flowing seepage, causing a scale deposit to form around the mouth of the crack and also within the crack. A detailed calculation of the expected rate of crack plugging due to evaporation-induced precipitation of calcite has been performed for a pore water of typical composition dripping onto a drip shield (BSC 2001 [DIRS 156807]). Cracks are sealed within a few hundred years when water is allowed to flow through the cracks at the expected (very low) rate for thin film flow (BSC 2001 [DIRS 156807] Section 6.3). Once a crack is plugged with precipitates, the magnitude of the liquid flux through the crack is negligible because of the lack of a significant pressure head or gradient to drive liquid through the crack, and because of the observed high tortuosity and roughness of the crack geometry (Herrera 2004 [DIRS 168133], Section 2 and Figures 2-1 and 2-2).

The formation of scale deposits, primarily calcium carbonate (calcite), is well documented in flow systems in seawater environments and in heat exchangers with natural brines, such as in desalination plants (carrying ~6% NaCl solutions) and in potash plants (carrying greater than 12 percent mixtures of NaCl/KCl). In these plants, mineral deposits form rapidly at elevated temperatures and must be regularly removed to avoid loss of heat exchanger efficiency. In the case of seepage based on the J-13 groundwater from Yucca Mountain, calcite precipitation is the first stage of the concentration process (BSC 2001 [155640], Section 6.7.1), but occurs more

slowly then in these plants because lower temperatures reduce the evaporation rates. Other minerals also precipitate from J-13 groundwater, such as amorphous silica.

Given these features and processes, advective flow through crack networks in the drip shield is not included in the seismic scenario class for TSPA-LA.

6.4 GROUND MOTIONS AT THE EMPLACEMENT DRIFTS

6.4.1 Probabilistic Seismic Hazard Analysis

A PSHA was performed to assess the seismic hazards of vibratory ground motion and fault displacement at Yucca Mountain. The PSHA (CRWMS M&O 1998 [DIRS 103731]) provides quantitative hazard results to support an assessment of the repository's long-term performance and to form the basis for developing seismic design criteria for the license application. Key attributes of the PSHA methodology for Yucca Mountain are (1) utilization of an extensive geologic and seismologic database developed over a 20-year period in the Yucca Mountain region; (2) explicit consideration and quantification of uncertainties regarding alternative seismic-source, ground-motion, and fault-displacement models; and (3) use of a formal, structured expert elicitation process to capture the informed scientific community's views of key inputs to the PSHA.

The PSHA methodology for vibratory ground motions has become standard practice for deriving vibratory ground motion hazards for design purposes. Less commonly, probabilistic fault displacement analyses are conducted to provide quantitative assessments of the location and amount of differential ground displacement that might occur. Both analyses provide hazard curves, which express the annual frequency of exceeding various amounts of ground motion (or fault displacement). The resulting seismic hazard curves represent the integration over all relevant earthquake sources and magnitudes of the frequency of future earthquake occurrence and, given an occurrence, its effect at a site of interest.

The basic elements of a PSHA for vibratory ground motions are:

a) Identification of seismic sources that contribute to the vibratory ground motion hazard at Yucca Mountain and characterization of their geometry;

b) Characterization of seismic sources by the recurrence rate of earthquakes of various magnitudes and the maximum magnitude;

c) Attenuation relations that define a specified ground motion parameter (such as peak ground velocity) as a function of magnitude, source-to-site distance, local site conditions, and, in some cases, seismic source characteristics;

d) Integration of the seismic source characterization and ground motion attenuation evaluations, including associated uncertainties, into a seismic hazard curve and associated uncertainty distribution.

Probabilistic fault displacement hazard analysis follows a similar path:

a) Identification of fault sources of fault displacement (principal faults);

b) Characterization of the frequency, size, and locations of displacements on principal faults;

c) Characterization of the amounts and locations of subsidiary displacements as a function of distance from principal faults and magnitudes;

d) Integration of source characterization and distance distribution, including associated uncertainties, into a fault displacement hazard curve and associated uncertainty distribution.

The PSHA incorporates both variability and uncertainty. Variability, also termed randomness or aleatory uncertainty, is the natural randomness in a process. For discrete variables, the randomness is parameterized by the probability of each possible value. For continuous variables, the randomness is parameterized by the probability density function. An example of variability is the amplitude of ground motion that would occur at a particular location from repeated earthquakes having exactly the same magnitude at exactly the same distance (say, magnitude 6 at 25 km distance). Variations in ground motion amplitude are expected due to unknowable complexities in earthquake-to-earthquake source properties and in the propagation path.

Uncertainty, also termed epistemic uncertainty, is the scientific uncertainty in the model of the process. It is due to limited data and knowledge. The uncertainty is characterized by alternative models. For discrete random variables, the epistemic uncertainty is modeled by alternative probability distributions. For continuous random variables, the uncertainty is modeled by alternative probability density functions. Examples of uncertainty are alternative ground motion attenuation relations that express the amplitude of ground motion at a particular site as a function of distance to the source and earthquake magnitude. Unlike variability, uncertainty is potentially reducible with additional knowledge and data.

Given the input evaluations, the hazard calculation method integrates over all values of the variables and estimates the annual frequency of exceedance of any ground-shaking amplitude at the site. The hazard curve quantifies the variability of the earthquake occurrence and ground-shaking attenuation. In addition to the variability of the seismic hazard, however, is uncertainty about the seismotectonic environment of a site. Significant advances in development of methodology to quantify uncertainty in seismic hazard have been made in the past 20 years (Budnitz et al. 1997 [DIRS 103635]). These advances involve the development of alternative interpretations of the seismotectonic environment of a site by multiple experts and the structured characterization of uncertainty. Evaluations by multiple experts are made within a structured expert elicitation process designed to minimize uncertainty due to uneven or incomplete knowledge and understanding (Budnitz et al. 1997 [DIRS 103635]). The weighted alternative interpretations are expressed by use of logic trees. Each pathway through the logic tree represents a weighted interpretation of the seismotectonic environment of the site for which a

seismic hazard curve is computed. The result of computing the hazard for all relevant pathways is a distribution of hazard curves representing the full variability and uncertainty in the hazard at a site.

The seismic scenario class for TSPA-LA uses the mean hazard curves for peak ground velocity and for fault displacement. Each mean hazard curve, which is defined as an average of the distribution of hazard curves referred to in the preceding paragraph, typically lies above the 80^{th} percentile of the distribution because the average is dominated by the larger values of the distribution. The use of the mean hazard curves simplifies the Monte Carlo sampling process for TSPA and provides an accurate representation for the mean dose to the reasonably maximally exposed individual, as required to demonstrate acceptable repository performance over 10,000 years.

6.4.2 Site-Specific Ground Motions

Site-specific ground motions are needed for the structural response calculations and rockfall calculations supporting postclosure performance assessment. Ground motion results from the PSHA are for a hypothetical reference rock outcrop and do not reflect site-specific soil and rock properties at the locations for which the ground motions are needed (e.g., the emplacement area level). The PSHA was conducted in this fashion because the site-specific rock and soil properties were not characterized at the time of the PSHA. Thus, further analyses are carried out to modify the PSHA results to reflect the appropriate site-specific conditions for the site of interest. These site-specific analyses are briefly described here, based on the detailed description in (BSC 2003 [DIRS 166274]).

Postclosure performance assessment requirements determine the location and the annual exceedance probabilities for which site-specific ground motions are needed. For analyses supporting postclosure performance assessment, site-specific ground motions are developed for the waste emplacement level. Selection of annual exceedance probabilities is motivated by the requirement to "consider only events that have at least one chance in 10,000 of occurring over 10,000 years" (10 CFR 63.114(d) [DIRS 156605]). To address this requirement, ground motions are developed for annual exceedance probabilities of 1×10^{-5}, 1×10^{-6}, and 1×10^{-7} per year. Analyses using the developed ground motions form the basis for evaluating repository performance for seismic events with annual exceedance probabilities from 1×10^{-4} per year to as low as 1×10^{-8} per year.

A detailed site response model provides the basis for development of seismic time histories at the emplacement drifts (BSC 2003 [DIRS 166274]). Different approaches are used for developing time histories depending on how they will be used (e.g., in design or in evaluating postclosure repository performance). For Yucca Mountain, three approaches have been used to develop time histories: spectral conditioning, scaling to peak ground velocity, and scaling to peak ground velocity preceded by spectral conditioning. The spectral-matching approach is used primarily to develop time histories that will be used in design analyses and is not discussed further here.

The peak-ground-velocity scaling approaches are used to develop time histories for postclosure analyses. The goal of these analyses is to determine how the EBS components perform under earthquake loads that are significantly beyond their design basis. In addition to determining the consequences of these low-probability ground motions, another goal is to evaluate the variability in the consequences. Because much of the variability in consequences will be driven by random variability in the ground motion, the time histories for postclosure analyses are developed to capture and represent that random variability.

Peak ground velocity is selected as the scaling parameter because damage to underground structures has been correlated with peak ground velocity (McGarr 1984 [DIRS 163996] page 206). PGV is appropriate for structural damage caused by sliding or impact under earthquake loads (Newmark and Rosenblueth 1971 [DIRS 151246], Sections 11.3.5 and 11.4). Finally, PGV is also appropriate for the response of a rock mass to dynamic loading because the change in stress across a weak compression wave[6] is directly proportional to the particle velocity. The abstractions in this document therefore use the horizontal PGV as the measure of the amplitude of the ground motion. Alternate measures, such as peak ground acceleration or the spectral acceleration at a given frequency, are anticipated to give similar results.

In the PGV-scaling approach, the earthquake recordings are scaled such that their peak ground velocity matches the peak ground velocity determined in the site-response analysis for a location of interest. The records may be scaled such that both horizontal components match the target horizontal peak ground velocity and the vertical component matches the target vertical peak ground velocity. Alternatively, one horizontal component may be scaled to the target horizontal peak ground velocity and the scaling of the other components done in a manner to maintain the intercomponent variability of the original recordings. Both of these methods have been used at Yucca Mountain.

For each annual exceedance frequency of interest, 17 sets of time histories are developed. Each set of time histories consists of acceleration, velocity and displacement in each of two horizontal component directions and in the vertical component direction. The site-specific time histories are based on actual recordings of strong ground motion from earthquakes in the western United States and around the world (McGuire et al. 2001 [DIRS 157510], Appendix B). Recordings are selected to represent those earthquakes that dominate the seismic hazard at a given annual probability of exceedance. In other words, the recordings used as a basis for the time histories are selected to have a range of magnitudes and distances that corresponds to the magnitudes and distances of earthquakes contributing to the seismic hazard at the given annual exceedance frequency. By basing the time histories on actual earthquake recordings and choosing records consistent with the seismic hazard, the resulting time histories exhibit realistic phase characteristics and durations.

A variation of the PGV-scaling approach involves spectrally conditioning the original strong-ground-motion records before using them to develop time histories. Spectral conditioning modifies the original strong motion records such that their response spectra reflect to a greater degree the site conditions at Yucca Mountain. Conditioning can be done with respect to the

[6] A compression wave, also known as a p-wave, has particle velocity in the same direction as the direction of wave propagation. The wave is weak if the wave velocity is equal to the acoustic (compressional) velocity in the medium. An acoustic wave in air is an example of a weak compression wave.

PSHA reference rock outcrop conditions or to the waste emplacement level conditions that reflect the site response. Conditioning can be thought of as a weak spectral match. A strong spectral match is not desired in this case because it would tend to reduce the random variability of the original recordings.

For the annual exceedance frequency of 1×10^{-6} per year, two suites of 17 sets of time histories each were developed. The 17 sets of recorded strong ground motion that form part of the basis for the time histories were selected to represent the range of magnitudes and distances consistent with the range indicated by the PSHA. The first suite consists of time histories for which both horizontal components were scaled to the site-specific horizontal peak ground velocity and the vertical component was scaled to the site-specific vertical peak ground velocity. The observed intercomponent variability is therefore not maintained for the first suite. Also, the records used to generate the time histories were not spectrally conditioned prior to scaling.

A second suite of time histories for an annual frequency of exceedance of 1×10^{-6} was developed by first spectrally conditioning the records to weakly match Yucca Mountain site conditions based on the response spectra for the PSHA reference rock outcrop. Specifically, the ratios between mean response spectra for average western U.S. conditions and mean response spectra for the PSHA reference rock outcrop at Yucca Mountain were determined. The western U.S. response spectra are considered typical of the strong motion records forming the basis for Yucca Mountain time histories. These ratios, or transfer functions, were then applied to the response spectrum for each of the strong ground motion records to be used in generating time histories. Finally, the modified response spectra formed targets for weak spectral matches of the original records. Following this conditioning, the records were scaled to the site-specific peak ground velocity. In this case, only one horizontal component was scaled to the peak ground velocity and the other components were scaled to preserve the intercomponent variability of the original records.

Two suites of 17 sets of time histories were also developed for an annual exceedance frequency of 1×10^{-7}. For both of these suites, the records forming the basis for the time histories were spectrally conditioned prior to scaling. In one case, they were spectrally conditioned to weakly match the response spectra for the PSHA reference rock outcrop, similar to the approach for the second suite of ground motions for 1×10^{-6} annual exceedance frequency. In the second case, they were conditioned to the site-specific response spectra for the waste emplacement area.

Analyses of rockfall and EBS structural response used the most current suite of ground motions that were available when the calculations were performed. The EBS structural response calculations for the 10^{-6} per year ground motions were performed with the first suite of ground motions, wherein the time histories are scaled to the known values of PGV in the horizontal and vertical directions; intercomponent variability was not preserved. The EBS structural response calculations for the 10^{-7} per year ground motions were again performed with the first suite of ground motions that were spectrally conditioned to the reference rock outcrop and preserved the intercomponent variability of the original records.

6.4.3 PGV Hazard Curve at the Emplacement Drifts

The horizontal PGV values have been defined for the 10^{-5} per year, 10^{-6} per year and 10^{-7} per year mean annual exceedance frequencies at the emplacement drifts (called Point B in the probabilistic seismic hazard analysis). The horizontal PGV value corresponding to the 10^{-5} per year point on the hazard curve is 1.05 m/s (DTN: MO0401SEPPGVRL.022 [DIRS 169099]). The horizontal PGV value corresponding to the 10^{-6} per year point on the hazard curve is 2.44 m/s (DTN: MO0303DPGVB106.002 [DIRS 162712]). The horizontal PGV value corresponding to the 10^{-7} per year point on the hazard curve is 5.35 m/s (DTN: MO0210PGVPB107.000 [DIRS 162713]). The location of Point B is illustrated in Figure 6.4-1.

TSPA requires a mean hazard curve at the emplacement drifts (Point B) for a wide range of exceedance frequencies. The three values of horizontal PGV that are available at Point B are insufficient to define the hazard curve over its full range, which is typically 10^{-4} per year to 10^{-8} per year. A solution to this problem is to scale the Point A (a reference rock outcrop at the repository elevation, as shown in Figure 6.4-1) hazard curve so that it minimizes the sum of the squares of the residuals with respect to the three known values at Point B. This approach, known as a least squares fit, is reasonable because it preserves the shape of the Point A hazard curve while reproducing the known values at Point B within a small error. The shape of the hazard curves at Points A and B will be approximately the same if the deaggregation of earthquake sources over the frequency range of interest remains similar at the two points. This is a reasonable approximation over the frequency range of interest.

The scaling analysis is presented in Appendix A[7], based on the Point A hazard curve defined by the probabilistic seismic hazard analyses expert elicitation (DTN: MO03061E9PSHA1.000 [DIRS 163721], file: *h_vel_extended.frac_mean*; see page A-5 in Appendix A for scaling of these data points). A scaling factor of 0.7959 results in errors of +1.6 percent, +7.5 percent, and – .8 percent with respect to the three known values at Point B. The scaled hazard curve at Point B is illustrated in Figure 6.4-2. PGV values at other annual exceedance frequencies can be determined by interpolation, with the resulting values shown in Table 6.4-1.

6.4.4 Modified Hazard Curve for Extreme Ground Motions

The hazard curves in Figure 6.4-2 are unbounded, in the sense that PGV continues to increase (albeit more slowly) with decreasing values of the exceedance frequency. This general behavior leads to PGV values that exceed 5 m/s for annual exceedance frequencies below 10^{-7} per year, as shown in Table 6.4-1. These PGV values are extremely large and may not be physically realizable for the seismic sources and geologic conditions in and around Yucca Mountain. In particular, the physical properties of the lithophysal rocks at the emplacement drift level are expected to provide physical limits on the PGV experienced at that location (Point B) (BSC 2004 [DIRS 170137]).

[7] The analysis in Appendix A scales the logarithm of annual exceedance frequency as a linear function of PGV. This approach is consistent with typical plots of hazard curves, although a log-log fit to the individual points on the hazard curve often produces a more accurate fit. The difference between log-linear and log-log approaches is not significant over this frequency range, as discussed in Appendix A.

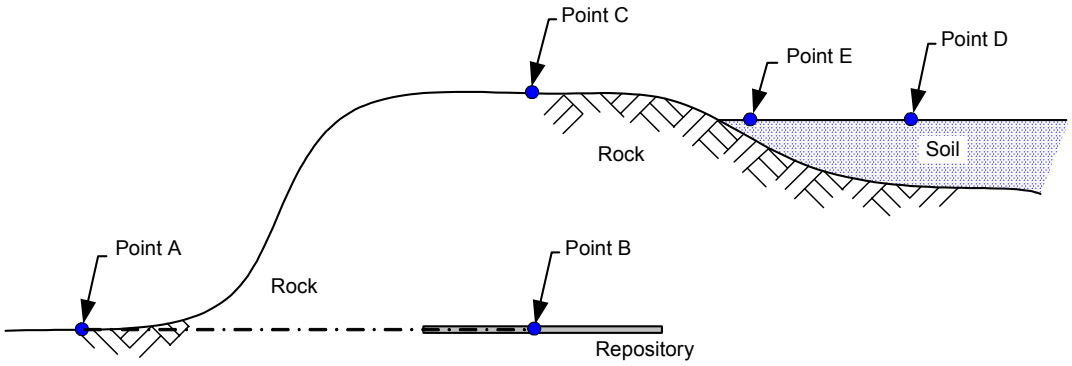

Modified from CRWMS M&O 1998

LEGEND

Point "A" - Reference rock outcrop
Point "B" - Repository elevation
Point "C" - At rock surface
Point "D" - At surface of significant soil layer over rock
Point "E" - At surface of shallow soil layer over rock

Figure 6.4-1. Schematic Diagram Showing Location of Points A and B

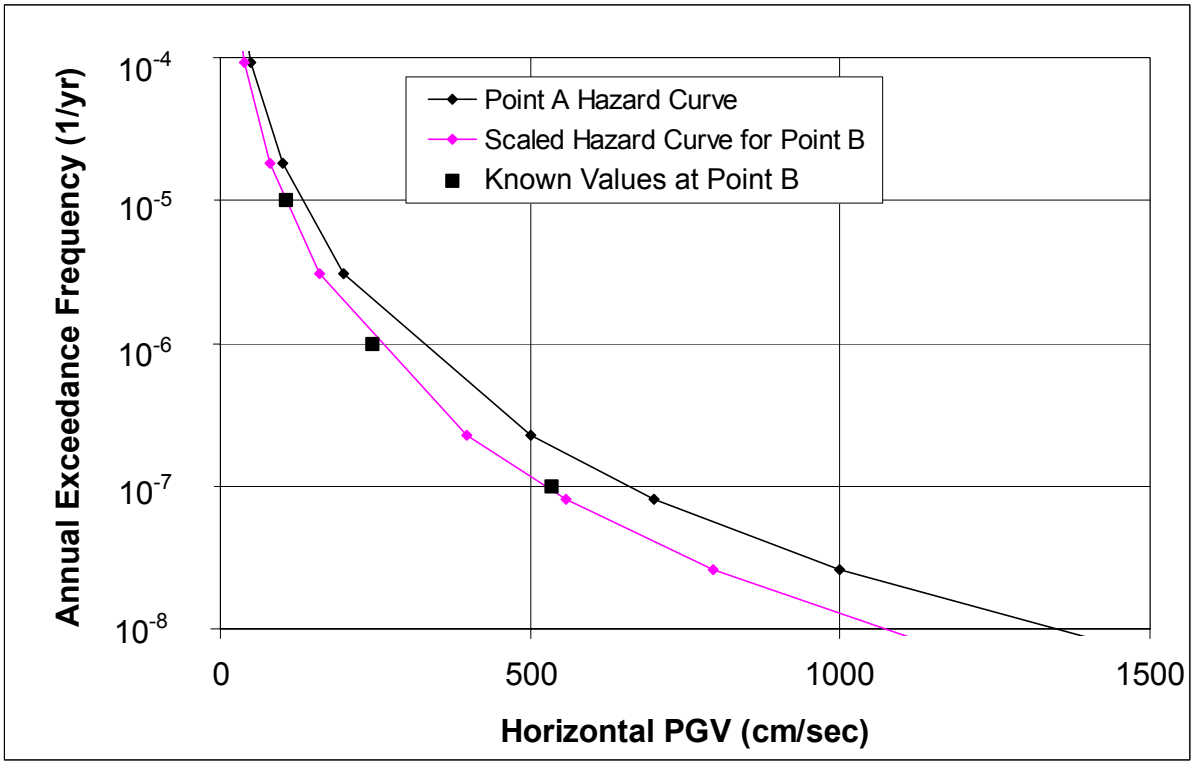

NOTE: Calculation in Appendix A.

Figure 6.4-2. Hazard Curve for Point B is Generated by Scaling the Point A Hazard Curve

Table 6.4-1. Calculated Values of PGV on the Point B Hazard Curve

Annual Exceedance Frequency (1/yr)	Horizontal PGV [a] (cm/s)
5×10^{-4}	18.1
10^{-4}	38.7
5×10^{-5}	55.0
10^{-5}	106.6 [b]
10^{-6}	262.3 [b]
10^{-7}	525.5 [b]
10^{-8}	1072.

[a] All values calculated in Appendix A.
[b] These calculated values have errors of +1.6, +7.5 and –1.8 percent with respect to the known values at Point B of 105 cm/s (10^{-5} per year), 244 cm/s (10^{-6} per year) and 535 cm/s (10^{-7} per year), respectively. Error at 10^{-5} per year based on exact calculation in spreadsheet in Appendix A; small difference from using 106.6 cm/s in this table is due to round off.

This viewpoint is supported by analysis of lithophysae at Yucca Mountain. If extreme ground motions with PGV of 5 m/s or above occurred at Yucca Mountain, the resulting ground motions would have damaged the lithophysal strata, either by generating fractures between adjacent lithophysae or ultimately by crushing the lithophysae. Geologic evidence indicates that lithophysal strata have remained intact over the lifetime of Yucca Mountain, estimated at 12.8 million years (Sawyer et al. 1994 [DIRS 100075]). It follows that extreme ground motions have not occurred during the past 12.8 million years (BSC 2004 [DIRS 170137]).

While past experience cannot be used to eliminate the potential for extreme seismic events in the future, it can provide a basis for estimating the annual frequency of extreme seismic events in the future. Analysis of the geologic conditions and other corroborating evidence from the Yucca Mountain repository site, such as precariously perched rocks, provides a basis for estimating the maximum feasible or bounding value of PGV at the emplacement drifts. This estimate is represented as a distribution because of the high uncertainty in estimating extreme values of seismic sources, ground motion attenuation, and limits on future behavior. The distribution adopted for TSPA-LA has a lower bound of 1.5 m/s, an upper bound of 5 m/s and the distribution type is uniform (DTN: MO0404BPVELEMP.000 [DIRS 171052]). This shape is more conservative (i.e., results in more events with higher values of PGV) than the anticipated distribution at the repository (BSC 2004 [DIRS 170137]).

The uniform distribution for the bounding value of PGV can be combined with the existing hazard curve at Point B to generate a new composite hazard curve for the repository horizon. The ground motion can exceed a particular value, x, only if both the bounding value of PGV (defined by the uniform distribution just discussed) is greater than x and the ground motion from the original unbounded analysis (as defined by the original PSHA hazard curve) is greater than x. Mathematically, the annual probability (hazard) that the composite PGV value is greater than a given value, x, is defined by the product of the probability that the bounding value for PGV has a value greater than x and the annual probability that the original unbounded motion has a PGV value greater than x. (Remember that annual exceedance frequency and annual exceedance probability are essentially equal for low frequency events.) The detailed calculations are shown in Appendix A, and result in the modified mean hazard curve shown in Figure 6.4-3.

The combined hazard curve in Figure 6.4-3 is not used directly by TSPA-LA. Rather, the scaled hazard curve at Point B and the uniform distribution for the bounding value of PGV are independently sampled, and the final value of PGV is determined as the minimum of the two sampled values. This approach ensures that the value of PGV from the hazard curve is always less than the relevant bound for PGV in each realization of the TSPA-LA calculations. With this bound, the PGV amplitude for ground motion never exceeds 5.35 m/s, which corresponds to the 10^{-7} annual exceedance frequency on the scaled hazard curve at Point B. Since the bound on PGV does not apply to the hazard curves for fault displacement, the damage abstraction for fault displacement still considers annual exceedance frequencies greater than or equal to 10^{-8} per year.

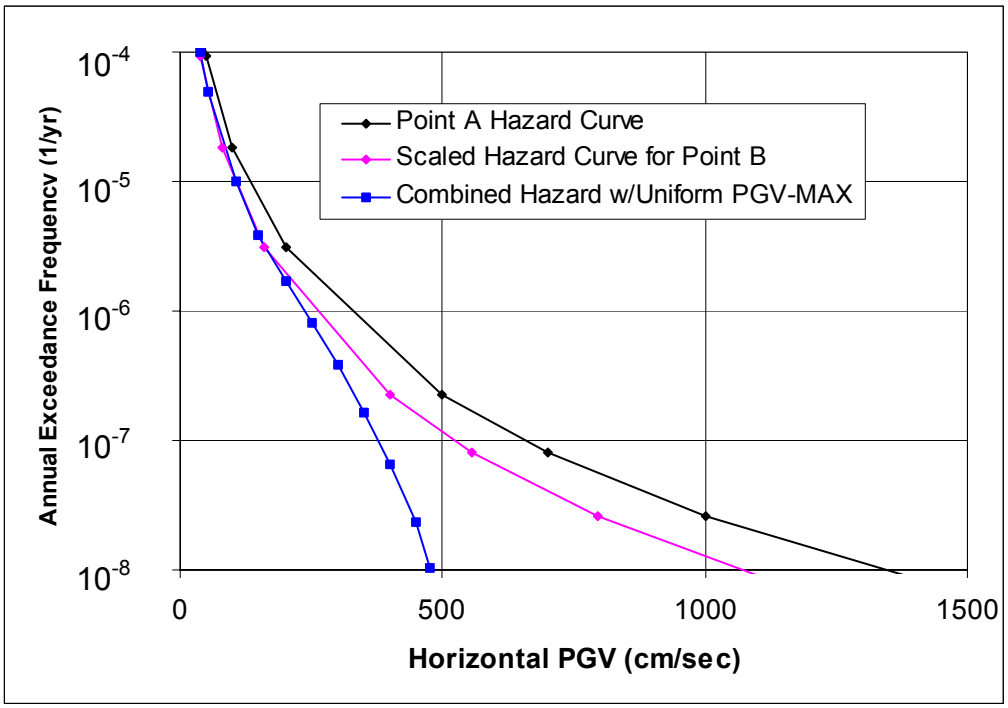

NOTE: Calculation in Appendix A.

Figure 6.4-3. Combined Mean Hazard Curve for the Scaled Hazard Curve at Point B and a Uniform Distribution for the Bounding Value of PGV

6.5 DAMAGED AREA ABSTRACTIONS FOR VIBRATORY GROUND MOTION

This section defines the damaged area abstractions for the waste package and drip shield from vibratory ground motion. The response of the rock mass and emplacement drifts to vibratory ground motion and the potential for rockfall induced by vibratory ground motion to cause mechanical damage to the drip shield, waste package, and cladding is discussed in Section 6.6.

6.5.1 Initial Abstraction for Waste Package Damage from Ground Motion

This abstraction defines the damage to the waste package from vibratory ground motion. To this end, structural response calculations have been performed to determine the damage from impact(s) between the waste package and emplacement pallet and from impact(s) between

adjacent waste packages (BSC 2004 [DIRS 167083]; BSC 2004 [DIRS 171717]). The potential for damage from impacts between the waste package and drip shield is included in the analysis, but produces negligible damage because the drip shield is unrestrained and can move freely. In particular, the drift is unfilled at the time of the seismic event and the potential coupling between rockfall and the dynamic motion of the EBS components during the seismic event is not included in the analyses.

In this section, the term "damage" is synonymous with a damaged area that exceeds the residual stress threshold for Alloy 22, resulting in enhanced susceptibility to accelerated stress corrosion cracking and the formation of pathways for radionuclide transport from the waste package. Permanent structural deformation does not always result in "damage" because the residual stress may be below the threshold for Alloy 22. No damage is equivalent to 0 percent damaged area on the surface of the package, so there is no transport of radionuclides from the waste package.

6.5.1.1 Structural Response Calculations

A set of 15 calculations for dynamic waste package structural response are performed for the suite of ground motions with a PGV of 2.44 m/s (BSC 2004 [DIRS 167083], Section 6.1). A similar set of calculations is also performed for a PGV of 5.35 m/s (BSC 2004 [DIRS 167083], Section 6.2). These values for PGV correspond to the peak of the first horizontal velocity component, which is always in a horizontal plane and perpendicular to the longitudinal direction for the structural response calculations (the longitudinal direction runs along the centerline of the drift). The stochastic (uncertain) input parameters for the 15 simulations are the 15 sets of three-component ground motion time histories, the metal-to-metal friction coefficient, and the metal-to-rock friction coefficient. A Monte Carlo sampling scheme defines the appropriate combinations of ground motion and friction coefficients (BSC 2004 [DIRS 169059], Section 6.4) for each PGV level. The same sets of ground motion time histories (accelerograms) are also used for the analyses of drip shield damage from vibratory ground motions described in Section 6.6.1.

The EBS structural response calculations used the most current suite of ground motions that were available when the calculations were performed. The EBS structural response calculations at 2.44 m/s PGV level were performed with a suite of ground motions wherein the time histories are scaled to the target values of PGV in the horizontal and vertical directions; intercomponent variability was not preserved. The EBS structural response calculations at the 5.35 m/s PGV level were performed with a suite of ground motions that were spectrally conditioned to the reference rock outcrop and preserved the intercomponent variability of the original records. The EBS structural response calculations at the 1 m/s PGV level are performed with three preliminary ground motions that were scaled from the 2.44 m/s PGV level to the 0.992 m/s level. This scaling is based on the scaled hazard curve at Point B (see Figure 6.4-3 and Appendix A). These preliminary ground motions do not include intercomponent variability. Section 6.4.2 has further details on the methodology for deriving site-specific ground motions.

The structural response calculations do not represent the dynamic response of the invert to the ground motion. The invert is represented as an elastic body whose surface responds instantaneously and uniformly to the given ground motion. In other words, the ground motion time histories for the three components of motion are applied directly to the surface of the invert.

This is a reasonable approach for small amplitude ground motions because the invert is compacted under the weight of the waste packages and drip shield and because any remaining steel framework in the invert will tend to provide some integrity. These effects will result in an invert that tends to move as a single unit. For high amplitude ground motions, the invert ballast is likely to be thrown up and redistributed, allowing the heavy EBS components to settle on the bottom of the drift, directly in contact with the rock floor. In this case, applying the ground motions directly to the surface of the invert is again a reasonable approach because the surface of the invert is in direct contact with the emplacement pallet and drip shield.

The damage to the waste package is determined by comparing the residual first principal stress on the waste package outer shell to the failure criterion defined in Section 6.3.2. More specifically, two residual stress thresholds are used to define the damaged area on the outer shell of the waste package. The two stress thresholds are 80 and 90 percent of the yield strength of Alloy 22. These values correspond to the lower and upper bound of the uniform distribution for the residual stress threshold defined in Section 6.3.2. The area on the outer shell of the waste package for which the residual first principal stress exceeds the residual stress threshold is referred to as the "damaged area" throughout this document.

6.5.1.2 Waste Package Damage

The damaged areas for 14 different realizations with PGV of 2.44 m/s are summarized in Table 6.5-1 (BSC 2004 [DIRS 169990], Table 16). The results for Realization 8 are not presented in Table 6.5-1 because an input error[8] was discovered for this calculation during the checking process. The mean damage and standard deviation of the damage is also presented in this table. The mean damage for the 80 percent residual stress threshold is approximately twice as large as the mean damage for the 90 percent residual stress threshold. Note also that the variability in damage (i.e., the ratio of the maximum damage to the minimum damage for a given ground motion level) from the ground motions is approximately a factor of 10 at a given residual stress threshold. The uncertainty in damage is dominated by the uncertainty in the details of the ground motion at a given PGV level, rather than by the uncertainty in the residual stress threshold.

The results in Table 6.5-1 also demonstrate that the cumulative damage area is dominated by the contribution from end-to-end impacts of adjacent waste packages. In particular, the damaged area from waste package to pallet impacts is much smaller than the damage due to the end-to-end impacts of adjacent waste packages, with the exception of realization number 14. The damage from end-to-end impacts is the dominant contribution to total damage because the adjacent waste package is conservatively represented as a rigid wall anchored to the invert. The rigid wall is useful for computational simplicity, but overestimates the damage from end-to-end impacts. The rigid wall boundary condition overestimates damage because it corresponds to the end-to-end impact of waste packages with equal but opposite velocities. In the repository system, adjacent

[8] The three initial velocity components do not correspond to the beginning of the acceleration time history for Realization 8. Consequently, the velocity and displacement time histories are not appropriately specified, so the results from this realization are not included in the abstraction process. Eliminating one data point out of 15 will have only a minor impact on the abstraction because the exponent in Equation 6.5-1 increases by less than 8 percent when the number of data points decreases from 15 to 14 and because the abstraction conservatively bounds the results for both uniform and lognormal distributions of data, as discussed in Section 6.5.3.

packages are unlikely to impact with equal and opposite velocities because of the uniformity of ground motion over the 10-meter size scale of two waste packages and because of mass and friction coefficients of adjacent waste packages are likely to be different. The damage from multiple end-to-end impacts may also be overestimated because the potential for stress waves caused by a late impact to relax the residual stress generated by earlier impacts is ignored in estimating total damaged area.

The damaged areas for 14 different realizations for a PGV of 5.35 m/s are summarized in Table 6.5-2 (BSC 2004 [DIRS 169990], Table 17). The results for realization 2 are not presented in Table 6.5-2. The kinematics of the waste package in realization 2 result in impacts between package and pallet that are outside the finely meshed region of the outer shell, thereby reducing the numerical accuracy of the damage calculation for this realization. The mean damage for the 80 percent residual stress threshold is again approximately twice as large as the mean damage for the 90 percent residual stress threshold. The variability in damage from the ground motions is the dominant uncertainty because it is more than a factor of 10 at a given residual stress threshold. Finally, the damaged area from waste package to pallet impacts is much smaller than the damage due to the end-to-end impacts of adjacent waste packages, with the exception of realization numbers 1, 4, and 14.

6.5.1.3 Initial Abstraction

The failure criterion for Alloy 22 is defined as a uniform distribution between 80 and 90 percent of the yield strength (Section 6.3.1). In other words, there is uncertainty in the value of the appropriate residual stress threshold for Alloy 22. Tables 6.5-1 and 6.5-2 present damage values at the two extremes (80 percent and 90 percent) of the residual stress threshold. Since the damaged area is defined by the elements of the finite-element grid whose residual stress exceeds the value of the residual stress threshold, it follows that the damaged area for the 90 percent threshold is always less than or equal to the damaged area for the 80 percent threshold.

Table 6.5-1. Damaged Area from Vibratory Ground Motions with a PGV of 2.44 m/s

Realization Number[a]	Ground Motion Number	Damaged Area on the Waste Package					
		Waste Package to Pallet Interaction (m^2; % of total OS[d] area)		Waste Package to Waste Package Interaction (m^2; % of total OS[d] area)		Cumulative Damage (m^2; % of total OS[d] area)	
		80% Yield Strength	90% Yield Strength	80% Yield Strength	90% Yield Strength	80% Yield Strength	90% Yield Strength
1	7	0.0029; 0.010%	0.0014; 0.0050%	0.023; 0.082%	0.012; 0.043%	0.026; 0.092%	0.013; 0.046%
2	16[b]	0; 0	0; 0	0.017; 0.060%	0.0089; 0.032%	0.017; 0.060%	0.0089; 0.032%
3	4	0.0050; 0.018%	0; 0	0.19; 0.67%	0.083; 0.29%	0.20; 0.71%	0.083; 0.29%
4	8	0.030; 0.11%	0.0064; 0.023%	0.12; 0.43%	0.061; 0.22%	0.15; 0.53%	0.067; 0.24%
5	11	0.0015; 0.0053%	0; 0	0.15; 0.53%	0.066; 0.23%	0.15; 0.53%	0.066; 0.23%
6	1	0.025; 0.089%	0.0028; 0.0099%	0.15; 0.53%	0.063; 0.22%	0.18; 0.64%	0.066; 0.23%

Table 6.5-1. Damaged Area from Vibratory Ground Motions with a PGV of 2.44 m/s (Continued)

Realization Number[a]	Ground Motion Number	Damaged Area on the Waste Package					
		Waste Package to Pallet Interaction (m^2; % of total OS[d] area)		Waste Package to Waste Package Interaction (m^2; % of total OS[d] area)		Cumulative Damage (m^2; % of total OS[d] area)	
		80% Yield Strength	90% Yield Strength	80% Yield Strength	90% Yield Strength	80% Yield Strength	90% Yield Strength
7	2	0.017; 0.060%	0; 0	0.11; 0.39%	0.057; 0.20%	0.13; 0.46%	0.057; 0.20%
9	10	0.0035; 0.012%	0; 0	0.12; 0.43%	0.062; 0.22%	0.12; 0.43%	0.062; 0.22%
10	9	0; 0	0; 0	0.014; 0.050%	0.0071; 0.025%	0.014; 0.050%	0.0071; 0.025%
11	5	0.012; 0.043%	0.0037; 0.013%	0.074; 0.26%	0.032; 0.11%	0.086; 0.30%	0.036; 0.13%
12	6	0.0039; 0.014%	0; 0	0.073; 0.26%	0.036; 0.13%	0.077; 0.27%	0.036; 0.13%
13	12	0; 0	0; 0	0.032; 0.11%	0.016; 0.057%	0.032; 0.11%	0.016; 0.057%
14	14	0.010; 0.035%	0.0043; 0.015%	0.0056; 0.020%	0.0029; 0.010%	0.016; 0.057%	0.0072; 0.026%
15	3	0.0078; 0.028%	0.0015; 0.0053%	0.020; 0.071%	0.010; 0.035%	0.028; 0.099%	0.012; 0.043%
				Mean Value[c, e]		0.310%	0.136%
				Standard Deviation[c]		0.237%	0.097%
				Minimum Value[c]		0.050%	0.025%
				Maximum Value[c]		0.710%	0.290%

Source: BSC 2004 [DIRS 169990], Table 16.

[a] Only 14 realizations are presented in this table. Results for realization 8 are not presented because of an error in the input file for this calculation.

[b] Calculations are performed with 15 ground motions numbered 1, 2, 3, …, 14, and 16. Seventeen sets of ground motion time histories were initially developed from which 15 sets were selected for postclosure analyses. Two extra sets were developed to allow for substitutions if any of the sets were found to be inappropriate. For example, the response spectrum for the vertical component of ground motion #15 is an outlier when plotted with the other 16 response spectra. It exhibits anomalously low values at high frequencies (greater than about 2 Hz) and anomalously high values at low frequencies (less than about 0.2 Hz). Ground motion #16 was substituted for ground motion #15 for all computational suites at 2.44 m/s PGV level and at 5.35 m/s PGV level because of its anomalous response spectrum.

[c] Mean, standard deviation, minimum and maximum damage areas calculated in Appendix B.

[d] = outer surface of waste package.

[e] The mean value of percent damaged area for end-to-end impacts is 0.278 percent and 0.130 percent at stress thresholds of 80 percent and 90 percent of yield strength, respectively. These values represent 89.7 percent and 95.7 percent, of the total mean cumulative mean damage for the two residual stress thresholds.

Table 6.5-2. Damaged Area from Vibratory Ground Motions with a PGV of 5.35 m/s

Realization Number [a]	Ground Motion Number	Damaged Area on the Waste Package					
		Waste Package to Pallet Interaction (m^2; % of total OS[c] area)		Waste Package to Waste Package Interaction (m^2; % of total OS[c] area)		Cumulative Damage (m^2; % of total OS[c] area)	
		80% Yield Strength	90% Yield Strength	80% Yield Strength	90% Yield Strength	80% Yield Strength	90% Yield Strength
1	7	0.20; 0.71%	0.17; 0.60%	0.16; 0.57%	0.086; 0.30%	0.36; 1.28%	0.26; 0.92%
3	4	0.096; 0.34%	0.083; 0.29%	0.42; 1.49%	0.17; 0.60%	0.52; 1.84%	0.25; 0.89%
4	8	0.12; 0.43%	0.096; 0.34%	0.11; 0.39%	0.050; 0.18%	0.23; 0.82%	0.15; 0.53%
5	11	0.093; 0.33%	0.071; 0.25%	0.18; 0.64%	0.080; 0.28%	0.27; 0.96%	0.15; 0.53%
6	1	0.046; 0.16%	0.024; 0.085%	0.42; 1.49%	0.15; 0.53%	0.47; 1.67%	0.17; 0.60%
7	2	0.038; 0.13%	0.028; 0.099%	0.32; 1.13%	0.12; 0.43%	0.36; 1.28%	0.15; 0.53%
8	13	0.095; 0.34%	0.068; 0.24%	0.32; 1.13%	0.14; 0.50%	0.42; 1.49%	0.21; 0.74%
9	10	0.0052; 0.018%	0.0035; 0.012%	0.034; 0.12%	0.017; 0.060%	0.039; 0.14%	0.021; 0.074%
10	9	0.16; 0.57%	0.14; 0.50%	0.33; 1.17%	0.15; 0.53%	0.49; 1.74%	0.29; 1.03%
11	5	0.032; 0.11%	0.0070; 0.025%	0.17; 0.59%	0.072; 0.26%	0.20; 0.70%	0.079; 0.28%
12	6	0.062; 0.22%	0.041; 0.15%	0.10; 0.35%	0.044; 0.16%	0.16; 0.57%	0.085; 0.30%
13	12	0.027; 0.096%	0.018; 0.064%	0.12; 0.43%	0.053; 0.19%	0.15; 0.53%	0.071; 0.25%
14	14	0.020; 0.071%	0.016; 0.057%	0.0077; 0.027%	0.0040; 0.014%	0.028; 0.099%	0.020; 0.071%
15	3	0.0045; 0.016%	0; 0%	0.29; 1.03%	0.14; 0.50%	0.29; 1.03%	0.14; 0.50%
				Mean Value[b, d]		1.011%	0.518%
				Standard Deviation[b]		0.567%	0.303%
				Minimum Value[b]		0.099%	0.071%
				Maximum Value[b]		1.84%	1.03%

Sources: BSC 2004 [DIRS 169990], Table 17, and BSC 2004 [DIRS 171717] for Realization 11.

[a] Only 14 realizations are presented in this table. Results for realization 2 are not presented because the kinematics of the waste package are such that the impacts between package and pallet occur outside the finely meshed region of the outer shell.

[b] Mean, standard deviation, minimum and maximum damage calculated in Appendix B.

[c] = outer surface of waste package.

[d] The mean value of percent damaged area for end-to-end impacts is 0.788 percent and 0.333 percent at stress thresholds of 80 percent and 90 percent of yield strength, respectively. These values represent 76.0 percent and 63.5 percent, of the total mean cumulative mean damage for the two residual stress thresholds.

The residual stress threshold could be retained as a stochastic parameter whose value is sampled for TSPA-LA. In this situation, the damage at intermediate values of the residual stress threshold could be defined by linear interpolation between the damage at the extreme values. However, the uncertainty in damaged area is dominated by the ground motions, rather than the residual stress threshold, as discussed above. In this situation, it is reasonable to simplify the damage abstraction for the waste package by averaging the damaged areas at the two extremes (80 percent and 90 percent). In effect, this corresponds to a failure criterion for the average (85 percent) value of the residual stress thresholds. The average damage values are calculated in Appendix B.

A number of distributions are considered as potential fits to the damage area for the 14 realizations with damage information. A uniform distribution provides an excellent description of the damage and is simple to define and implement in a Monte Carlo sampling scheme. Figure 6.5-1 compares the damage results for the 5.35 m/s PGV level to the cumulative distribution function for a uniform distribution, which is simply a straight line. In comparing the damage results to the cumulative distribution function, the damage values have been sorted in ascending order and each point is assigned equal weight.

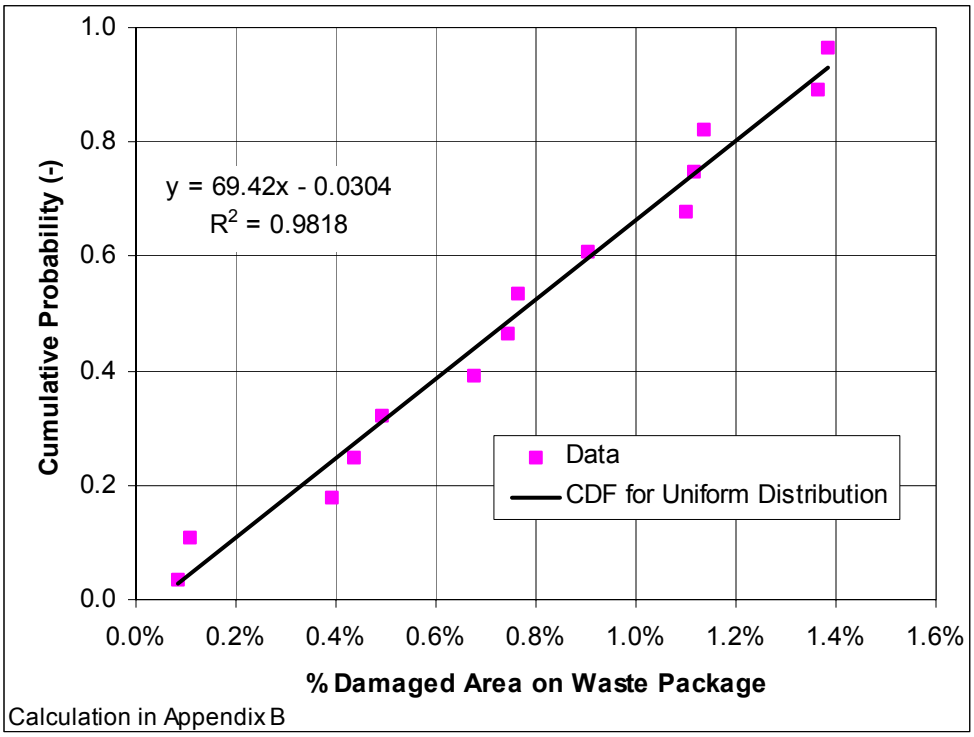

NOTE: (-)=dimensionless, CDF = cumulative distribution function.

Figure 6.5-1. Comparison of Damage Results for PGV of 5.35 m/s to a Cumulative Distribution Function for a Uniform Distribution

The straight line for the least squares fit to the results has been determined by Microsoft Excel's statistical package. This straight line provides an excellent fit to the results, judging by the fact that the square of the residuals, R^2, is 0.9818. An R^2 value of 1.0 is a perfect correlation and a value of 0.0 is no correlation. The fact that a straight line provides an excellent fit to the damage data confirms that a uniform distribution is a reasonable representation for the damage abstraction.

A uniform distribution also provides a very good description of the damage data for the PGV of 2.44 m/s. Figure 6.5-2 compares the damage results for a PGV of 2.44 m/s to the straight line for the least squares fit. The square of the residuals with the straight line, 0.946, is slightly less than that in Figure 6.5-1 but still quite close to 1.0. Again, a uniform distribution is a reasonable representation of these damage results.

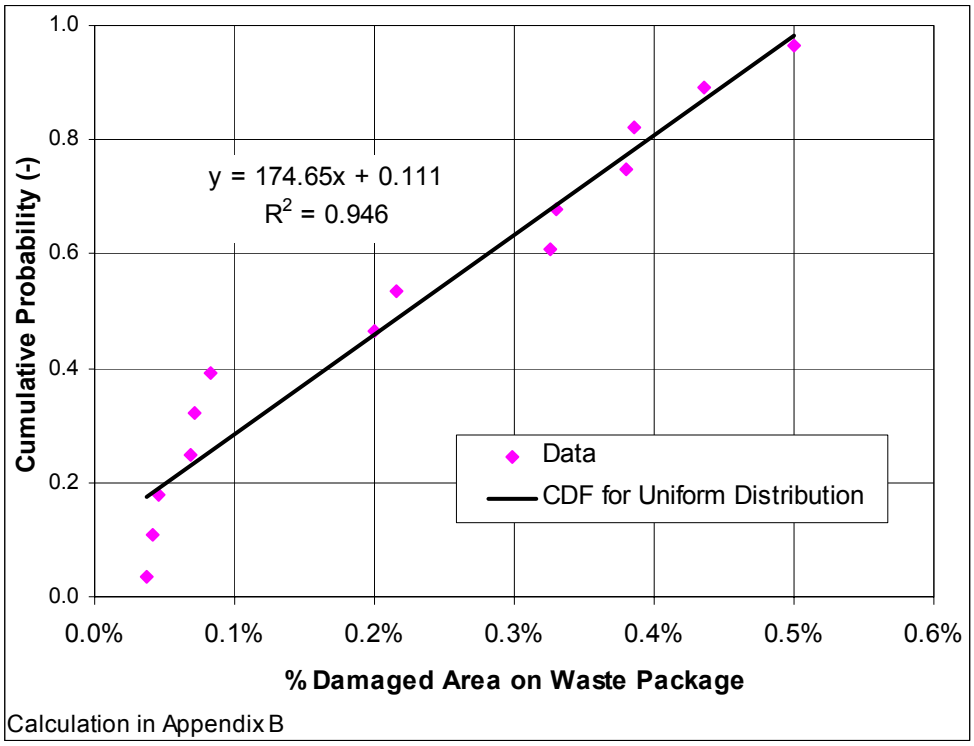

NOTE: (-)=dimensionless, CDF = Cumulative Distribution Function.

Figure 6.5-2. Comparison of Damage Results for PGV of 2.44 m/s to a Cumulative Distribution Function for a Uniform Distribution

The linear fits in Figures 6.5-1 and 6.5-2 provide preliminary estimates of the upper and lower bounds for the damaged area, based on the results in Tables 6.5-1 and 6.5-2. Of course, basing the upper and lower bounds solely on the 14 data points in each of Tables 6.5-1 and 6.5-2 may not capture the full range of variability from a more extensive sampling. To compensate for this effect, a statistical procedure has been used to calculate the upper bounds at the 95 percent confidence level. Rossman et al. (1998 [DIRS 162631]) describe a Bayesian procedure for calculating the 95 percent upper confidence limit (95%UCL) for the upper bound of a uniform distribution as follows:

$$95\%UCL = \alpha^{-\frac{1}{n-1}} \max(X), \qquad \text{(Eq. 6.5-1)}$$

where α is the significance level (i.e., $\alpha = 0.05$ at the desired, conservative 95 percent confidence level), n is the sample size, and X is the uncertain quantity of interest (i.e., the percent damaged area). Using Equation 6.5-1, the Bayesian upper bound for the uniform distribution of damaged area is calculated (see Appendix B) to be 0.63 percent at a PGV of 2.44 m/s and 1.74 percent at a PGV of 5.35 m/s. This formula for calculating the Bayesian upper bound uses what is called the flat prior that indicates maximal uncertainty about the upper bound based on the sampled values. Other prior distributions tend to represent increased prior certainty about the value of the parameter, and thus produce lower posterior estimates (Rossman et al. 1998 [DIRS 162631]). The selection of the flat prior is then a conservative choice.

Estimation of the lower bound of the uniform distribution also must be considered carefully. Figure 6.5-1 shows that the least squares fit for the 5.35 m/s PGV has a minimum damage value of less than 0.1 percent at a cumulative probability of 0.0. This minimum damage value is about a factor of 15 less than the damage of 1.5 percent at a cumulative probability of 1.0. Figure 6.5-2 shows that the least squares fit for the 2.44 m/s PGV has negative damage at a cumulative probability of 0.0. This is physically impossible, and is probably caused by the cluster of six points with damage values between 0.0 and 0.1 percent.

In this situation, it is reasonable to set the lower bound of the uniform distribution to 0 percent at all PGV levels. Zero percent is the minimum value for the least squares fit at the 2.44 PGV level. A zero percent minimum value produces a negligible deviation for the least squares fit for the minimum value at the 5.35 m/s PGV level.[9] Zero percent is also a reasonable lower bound for the preliminary damage results at the 0.992 m/s PGV level presented in Section 6.5.2.

[9] The least squares fit in Figure 6.5-1 can be modified to constrain the straight line to go through the origin. In this case, the trendline is y = 66.332x with an R^2 of 0.9793. This R^2 value is essentially identical to the value in Figure 6.5-1, 0.9818, for the unconstrained fit. This result confirms that a lower limit of 0 percent damage at 5.35 m/s PGV level is very reasonable. For Figure 6.5-2, the trendline that goes through the origin is y = 207.46x with an R^2 of 0.8953, about 5 percent lower than the unconstrained value for R^2 of 0.946 in Figure 6.5-2. So, a lower limit of 0 percent damage at 2.44 m/s PGV level is again a reasonable approach. The constraint to the linear fit is really moot here because the increase in damage for upper bounds at a 95 percent confidence level is much greater than the changes for a constrained or an unconstrained fit.

The complete damage abstraction for the TSPA-LA calculations is then a uniform distribution for the damage area, with a lower bound of zero and an upper bound given by a relationship between the (Bayesian 95 percent confidence level) upper bound versus the value of the horizontal PGV. A linear fit to the Bayesian upper bound produces the following relationship:

$$D_{ub} = 0.383 \times PGV - 0.305 \quad \text{for PGV} > 0.796 \text{ m/s}, \qquad \text{(Eq. 6.5-2)}$$
$$= 0 \quad \text{otherwise.}$$

where D_{ub} = Bayesian upper bound of the uniform distribution for the percent damaged area on the surface of the waste package. The unit of D_{ub} in Equation 6.5-2 is percent, so it is necessary to divide by 100 to convert D_{ub} into the fraction of the waste package surface area that is damaged. The calculation of the slope and y-intercept of the linear fit is documented in Appendix B.

Figure 6.5-3 compares the data for percent damaged area on the surface of the waste package with the linear fit (Equation 3) to the Bayesian upper bound at the 95 percent confidence limit. Note that there is no damage to the waste package for PGV less than 0.796 m/s, corresponding to an exceedance frequency of 1.8×10^{-5} per year (Table A-1 in Appendix A).

The damage to the waste package is applied to all waste packages in the repository, except for those packages that experience early time failures from manufacturing defects or from defects that occur during emplacement. There is no spatial variability for damage to the waste package.

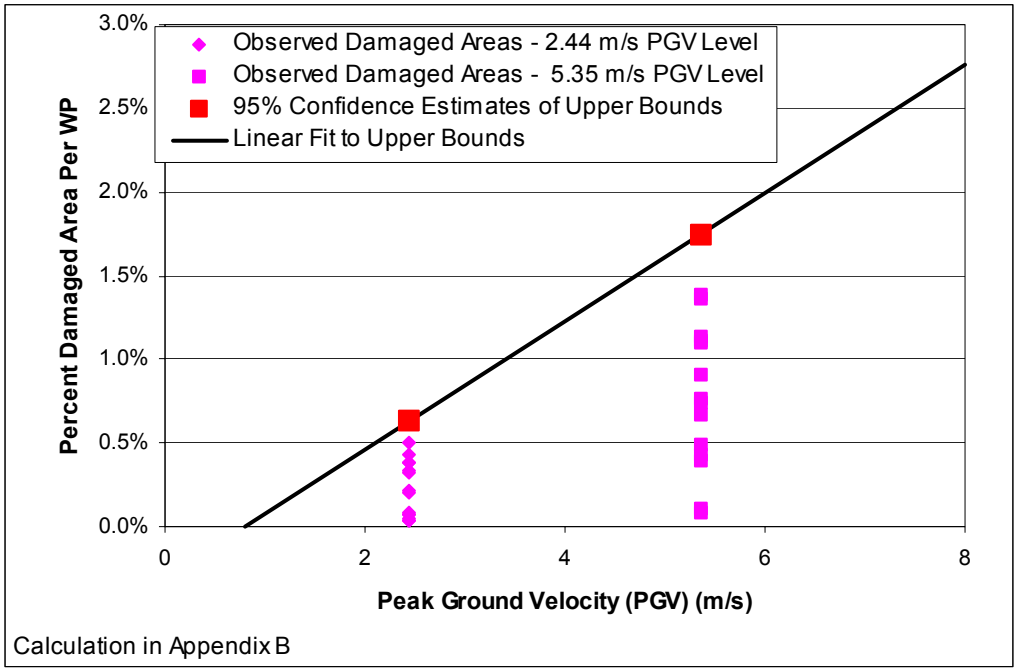

NOTE: The lower bound of damage distribution is 0 percent at all values of PGV.

Figure 6.5-3. Linear Fit to 95 Percent Confidence Estimate for Upper Bound of Damage Distribution

6.5.1.4 Corroborating Information for a PGV Near 1 m/s

Three simulations have been performed using ground motions with a PGV near 1 m/s. These simulations provide added confirmation that the upper bound for the damage, as shown in Figure 6.5-3, is tending to zero in a linear fashion. The approximate ground motions are created by scaling the three acceleration components of selected ground motions with PGV of 2.44 m/s. The factor for this scaling is defined by the ratio of the PGVs for the 10^{-5} to the 10^{-6} annual exceedance frequencies on the scaled hazard curve in Figure 6.4-2.[10] The numerical value of the scaling factor, 0.4066, is calculated in Appendix A of this report and available through DTN: MO0305SPASFEGM.000. The PGV for the scaled ground motions is given by (0.4066)(2.44 m/s) = 0.992 m/s.

This procedure is not exact because the deaggregation of seismic sources for the 2.44 m/s PGV and for the 1 m/s PGV is different and because the scaled hazard curve has a small error with respect to the known PGV value of 2.44 m/s at Point B. However, it provides a reasonable approach for preliminary calculations that can corroborate the abstraction in Figure 6.5-3. Ground motions number 1, 2, and 10, corresponding to realizations 6, 7, and 9, respectively, are selected (and scaled) for these calculations. These three ground motions are characterized by the highest intensity (energy) among the set of 15 ground motions for the 2.44 m/s PGV and have high levels of damage, although not the maximum damage (see Table 6.5-1). The damage results for these three ground motions (BSC 2004 [DIRS 167083], Attachment XI, Table XI-2) are summarized in Table 6.5-3.

The damage results for the three additional ground motions at PGV of 0.992 m/s can be added to the abstraction in Figure 6.5-3. The Bayesian upper bound at the 95 percent confidence limit can also be calculated for the three points in Table 6.5-3 and results in a value of 0.114 percent (calculation in Appendix B) for a residual stress threshold of 85 percent of the yield strength. Figure 6.5-4 shows that the linear equation for the upper bound, based on the results for PGV of 2.44 m/s and 5.35 m/s, is also a reasonable fit at PGV of 0.992 m/s, and that a lower bound of 0 percent damage is reasonable at this level. While there are only three data points for PGV near 1 m/s, these points do provide additional confidence in the extrapolation of the abstraction for the upper bound of waste package damage to values of PGV near and below 1 m/s.

6.5.1.5 Sensitivity Studies for Damage to the Waste Package

The data in Tables 6.5-1 and 6.5-2 are supported by three sensitivity studies identified in Table 6.5-4. These studies were performed after the major structural response calculations for the waste package (BSC 2004 [DIRS 167083]; BSC 2003 [DIRS 162293]) were completed.

[10] This scaling factor was necessary because a set of 17 ground motions for the 10^{-5} per year exceedance frequency and the corresponding value of PGV at Point B were not available at the time these analyses were performed. The ratio of PGV values from the scaled hazard curve in Figure 6.4-2 was the most reasonable approach to defining approximate ground motions for a PGV level near 1 m/s at that time.

Table 6.5-3. Damaged Area from Vibratory Ground Motions with a PGV of 0.992 m/s

Realization Number	Ground Motion Number	Cumulative Damage (m^2; % of total OS area)		
		80% Yield Strength	90% Yield Strength	85% Yield Strength
6	1	0.0060; 0.021	0; 0	0.0030; 0.0105
7	2	0; 0	0; 0	0; 0
9	10	0.0106; 0.038	0.0037; 0.013	0.00715; 0.0255

Source: BSC 2004 [DIRS 167083], Attachment XI, Table XI-2.

NOTE: OS = outer surface of waste package.

Damage at 85 percent of yield strength is the average of the values at 80 percent and 90 percent of yield strength.

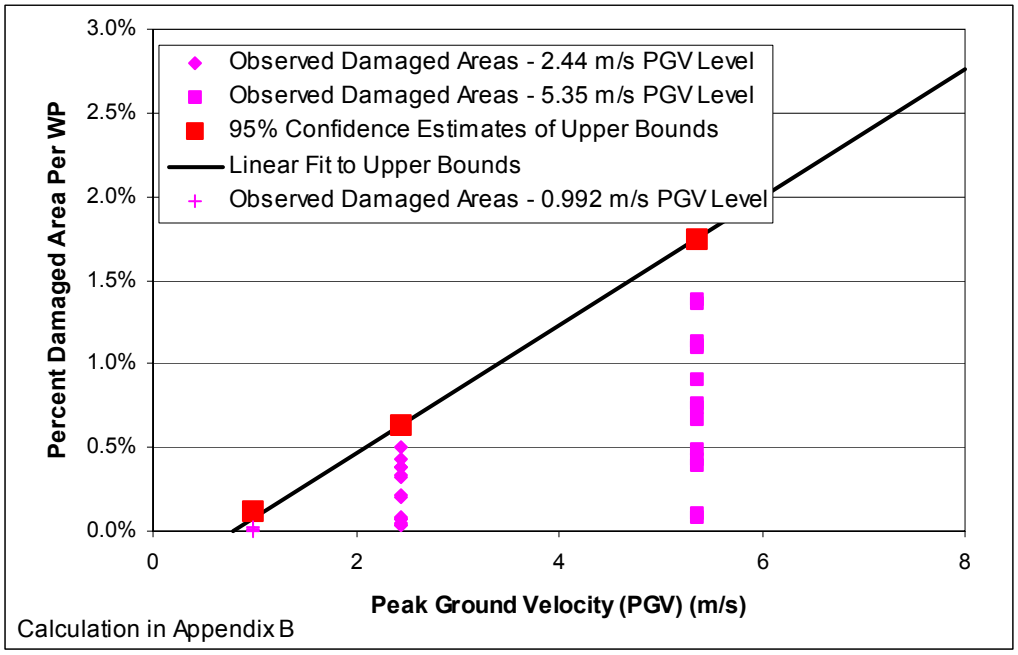

Figure 6.5-4. Comparison of Linear Fit to Bayesian Upper Bound of Damage with the Estimated Damage for a PGV near 1 m/s

Table 6.5-4. Sensitivity Studies for Abstraction of Waste Package Damage

Topic	Calculation Report
Sensitivity of damaged area caused by end-to-end impacts of adjacent waste packages to mesh refinement.	*21-PWR Waste Package End Impacts – A Mesh Study,* 000-00C-WIS0-02100-000-00A (BSC 2004 [DIRS 170844])
Sensitivity of damaged area to spectral matching and intercomponent variability of ground motion time histories for the 2.44 m/s PGV level.	*Additional Structural Calculations of Waste Package Exposed to Vibratory Ground Motion,* 000-00C-WIS0-01700-000-00A (BSC 2004 [DIRS 171717])
Sensitivity of damaged area to interpolation scheme for impact angles between 0 degree and 1 degree.	*Alternative Damaged Area Evaluation for Waste Package Exposed to Vibratory Ground Motion,* 000-00C-WIS0-01900-000-00A (BSC 2004 [DIRS 170843])

Tables 6.5-1 and 6.5-2 demonstrate that the majority of the damage to the waste package results from end-to-end impacts. *21-PWR Waste Package End Impacts – A Mesh Study* (BSC 2004 [DIRS 170844]) is a sensitivity study of damaged area in response to end-to-end impacts with refined finite-element meshes. Two refined meshes were considered during this study. The first mesh refinement increases the number of elements from 50,726 to 335,102, while the second mesh refinement has 1,198,942 elements (BSC 2004 [DIRS 170844], Section 6). The first mesh refinement results in average decreases of 29 percent and 36 percent in damaged area for thresholds of 80 percent and 90 percent of the yield strength, respectively (BSC 2004 [DIRS 170844], Section 6). The second mesh refinement further decreases the damaged area by 5 percent and 20 percent for thresholds of 80 percent and 90 percent of the yield strength, respectively (BSC 2004 [DIRS 170844], Section 6). Tables 6.5-1 and 6.5-2, which are based on the initial mesh documented in (BSC 2004 [DIRS 167083]), have significantly larger values of damaged area than either of the two refined meshes, and provide a conservative bias to the abstraction for waste package damage.

The structural response calculations for the 2.44 m/s PGV level reported in Table 6.5-1 used ground motion time histories that are scaled to target values of PGV in the horizontal and vertical directions; intercomponent variability was not preserved. *Additional Structural Calculations of Waste Package Exposed to Vibratory Ground Motion* (BSC 2004 [DIRS 171717]) documents a set of four calculations using ground motions that did preserve the intercomponent variability. The four ground motions are based on realizations 3, 4, 6, and 15 in Table 6.5-1. Realizations 3, 6 and 4 have the largest damaged areas for the calculations listed in Table 6.5-1. Realization 15 has large increases in the peak velocities for the second horizontal and vertical velocity components, 165 percent and 167 percent, respectively (BSC 2004 [DIRS 171717], Section 5 and Table 5-1). The damaged areas with the four new ground motions are summarized in Figure 6.5-5.

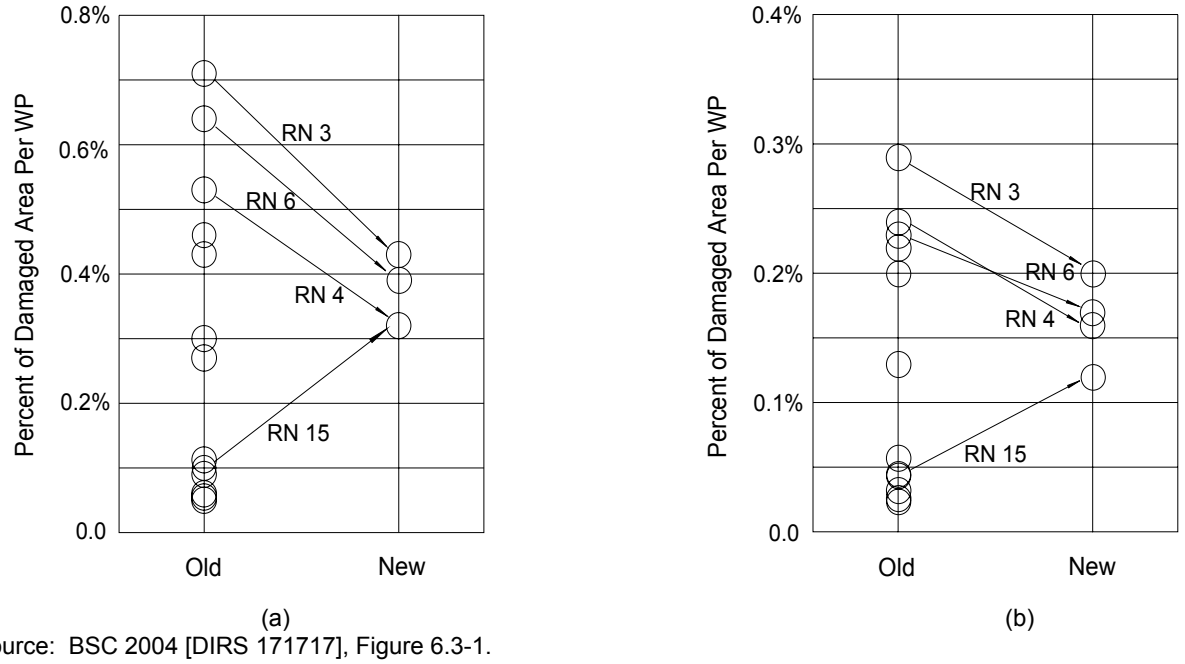

Source: BSC 2004 [DIRS 171717], Figure 6.3-1.

Figure 6.5-5. Schematic Representation of Scatter and Change of Damaged Area for Two Stress Thresholds: (a) 80 Percent of Yield Strength and (b) 90 Percent of Yield Strength

An analysis of the changes in damaged areas is presented in *Additional Structural Calculations of Waste Package Exposed to Vibratory Ground Motion* (BSC 2004 [DIRS 171717], Section 6.3), based on a detailed examination of the velocity time histories and the end impact parameters, which provide the major contribution to waste package damage. For the purposes of developing abstractions, the new results with ground motions that preserve intercomponent variability indicate that the original calculations for damaged areas provide a reasonable range of response that easily encompasses the new results. In this situation, it is reasonable to base the damage abstraction for TSPA-LA on the original calculations, which do not have intercomponent variability at the 2.44 m/s PGV level.

Alternative Damaged Area Evaluation for Waste Package Exposed to Vibratory Ground Motion (BSC 2004 [DIRS 170843]) is a study of the effect of low-angle impacts between a waste package and the longitudinal boundary on the damaged areas presented in Tables 6.5-1 and 6.5-2. The motivation for this analysis is that zero degree impacts are an idealized situation that may occur very infrequently, so interpolating with the damaged areas for zero degrees may bias the results. Comparing results with the new and old interpolation schemes at the 2.44 m/s PGV level (BSC 2004 [DIRS 170843], Section 6.1.3) indicates that while the change in the cumulative damaged area is significant in some low-damage realizations (most notably, realizations 2, 12, 13 and 14), the increase of the mean damaged area is 10 percent and 7 percent for the lower and upper damage thresholds, respectively. The maximum damaged area is changed only for the lower damage threshold, and even that increase (from 0.20 percent to 0.21 percent) is somewhat exaggerated due to the rounding off to two significant digits. Comparing results at the 5.35 m/s PGV level (BSC 2004 [DIRS 170843], Section 6.2.3) indicates that while the change in the cumulative damaged area is significant in some low-damage realizations (most notably realization 9) the increase of the mean damaged area is 4 percent and 2 percent for the lower and upper damage thresholds, respectively. The maximum damaged area is changed only for the lower damage threshold, from 1.84 percent to 1.88 percent of the total outer corrosion barrier surface area. These changes due to interpolation are less than the increase to define an upper bound for damage at the 95 percent confidence limit (Figure 6.5-4) and are less than the changes for the alternate conceptual damage model, discussed in the next section. The interpolation scheme does not produce a significant bias in the damage abstraction.

6.5.2 Fragility Analysis of Waste Package Damage

An independent technical review of this model abstraction has been performed by Dr. Robert P. Kennedy of RPK Structural Mechanics Consulting. The result of Dr. Kennedy's review is presented in Appendix C and briefly summarized here.

Dr. Kennedy presents an alternate analysis of the damage information for the waste package. This alternative analysis is structured around a fragility approach. In a fragility approach, one often asks: "What is the probability that the damage will exceed a given level for a given value of PGV?" Following this approach, a lognormally distributed approximation of the damage surface is fit by trial and error. The following lognormal distribution provides a good fit to the damage results in terms of exceedance probability (Equation C-9 in Appendix C):

Median:	$PGV_{50} = (5.7 \text{ m/s})D^{0.5}$,
Log. Std. Dev.:	$\beta = 0.28D^{-0.5} \leq 0.8$,
Truncation Point:	EP = 1 %,

where EP denotes exceedance probability. The rationale for defining a truncation point is explained in Appendix C. These equations provide a parametric representation of the lognormal distribution. The first equation defines the PGV value with a 50 percent probability that the damage will be greater than a given value, D. The second equation defines the logarithmic standard deviation about the median value for PGV.

A comparison of the lognormal distribution at PGV of 2.44 m/s and 5.35 m/s with the uniform distribution in Section 6.5.1 identifies values of D (in the units of percent damaged area) where the uniform distribution underestimates exceedance probability with respect to the lognormal distribution[11]. For a PGV of 5.35 m/s, the uniform distribution for damage provides a good approximation for D less than about 1.67 percent. Above this damage level, the estimate of exceedance probability from the uniform distribution for damage is significantly less than from the lognormal distribution. For PGV of 2.44 m/s, the uniform distribution for damage significantly overestimates exceedance probability (i.e., is conservative) for damage between 0.06 percent and 0.56 percent. However, a more significant issue is that the uniform distribution for damage significantly underestimates exceedance probability for damage greater than 0.60 percent.

Both the uniform distribution and the lognormal distribution provide acceptable representations of the damaged areas on the waste package, as shown in Section 6.5.1 and in Appendix C. In effect, these distributions are two alternative conceptual models for the damaged areas on the waste package from vibratory ground motion. Rather than sample from two alternative conceptual models, it was decided to modify Equation 6.5-2 so as to slightly increase the linear upper bound for damage, D_{ub}. This modification, shown in Equation 6.5-3, eliminates the underestimate in exceedance probability for the uniform distribution relative to the lognormal distribution. In effect, Equation 6.5-3 provides an upper bound for the two alternate conceptual models.

$$\begin{aligned} D_{ub} &= 0.436 \times PGV - 0.305 && \text{for PGV} > 0.700 \text{ m/s}, \\ &= 0 && \text{otherwise.} \end{aligned} \qquad \text{(Eq. 6.5-3)}$$

[11] A distribution that underestimates exceedance probability is less conservative for a given damage level. For example, a distribution that predicts a probability of 15 percent for the damage area being 1 percent or greater predicts less damage than a distribution that predicts a probability of 90 percent for the damaged area being 1 percent or greater.

D_{ub} has the units of percent damage, so that a PGV of 5.35 m/s results in damaged area of 2.0 percent. Details of the comparison between the lognormal distribution and the uniform distribution are presented in Appendix C. Figure 6.5-6 compares the modified upper bound (Equation 6.5-3) to the original upper bound (Equation 6.5-2) for the uniform distribution.

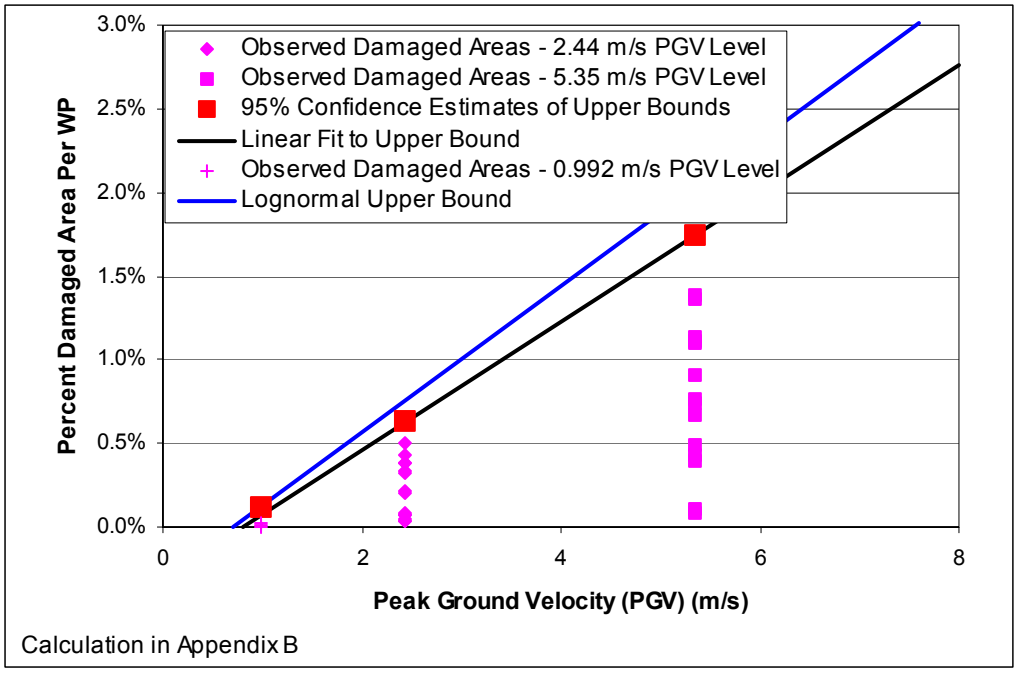

Figure 6.5-6. Comparison of Upper Bounds Based on a Lognormal Distribution (Blue Curve) with the Bayesian Estimate of the Uniform Distribution's Upper Bound (Black Curve)

6.5.3 Final Abstraction for Waste Package Damage from Ground Motion

The discussion in Sections 6.5.1 and 6.5.2 presented the calculations and damage areas on the waste package from vibratory ground motion. The results from these sections indicate that, without additional damage data for PGV values below 2.44 m/s, it is prudent to choose the more conservative fit (Equation 6.5-3) for the upper bound of the uniform distribution for waste package damage for TSPA-LA. Structural response calculations at a PGV near 1 m/s provide additional insight into the appropriateness of a uniform versus a lognormal distribution for the damage to the waste package. The distribution for the maximum value of PGV has an upper bound of 5 m/s, as discussed in Section 6.4.4. With this upper bound, there is little utility to performing structural response calculations for PGV values greater than 5.35 m/s.

As explained in Sections 6.3.4 and 6.3.5, TSPA-LA requires the effective area for flow and transport through the waste package, rather than the damaged area that exceeds the residual stress threshold for Alloy 22. The effective area is determined by the density of stress corrosion cracks and the area of individual cracks in the regions where the residual stress exceeds the residual stress threshold. The product of the crack density per unit surface area, ρ_{SCC}, and the area per crack, A_{SCC} defines the effective area of the stress corrosion cracking (SCC) network per unit area of damaged surface. This product ranges from 0.00328 to 0.0131 at room temperature (DTN: MO0403SPASCRKD.000 [DIRS 168105]). Stated differently, the effective area of a

crack network is a factor of 76 to 305 less than the damaged surface area that exceeds the residual stress threshold.

For TSPA-LA, the crack network on the waste package provides a pathway for diffusive transport of radionuclides out of the waste package. The factor defining the effective area for diffusive transport is sampled from a uniform distribution with a lower bound of 0.00328 and an upper bound of 0.0131. The sampled value for the factor is then multiplied by the sampled value for the damaged area, based on a uniform distribution with upper bound given by Equation 6.5-3. This procedure directly incorporates the uncertainty in the distribution of damaged areas and the uncertainty in the factor defining the effective area of a crack network into TSPA-LA.

Advective flow through the network of stress corrosion cracks on the waste package is not included in TSPA, as discussed in Section 6.3.5. The network of stress corrosion cracks on the waste package has high tortuosity and surface roughness, and narrow to very small apertures at the crack tip(s) (see Figure 6.3-2). This physical morphology will eliminate advective flux through the cracks because of infilling of small apertures with corrosion products, because of high surface tension when a narrow aperture is bridged by a single droplet, and because there is minimal head gradient or pressure gradient driving liquid flow through the narrow apertures. Evaporation-induced precipitation of calcite and other minerals in the groundwater may also occur within the cracks on the waste package. The morphology of the crack network, the lack of a driving gradient, and the potential for plugging with precipitates provide the basis for eliminating advective flow through the crack networks.

6.5.4 Drip Shield Damage from Ground Motion

The mechanical response of the drip shield to vibratory ground motions has the potential to damage the drip shield as a barrier to flow. This loss of integrity could occur because of damaged areas on the drip shield (i.e., those areas that exceed the residual stress threshold for Titanium Grade 7) from impacts between the drip shield and the waste package, emplacement pallet, invert, and drift wall. Loss of integrity as a barrier to flow could also occur because of separation between two adjacent drip shields. Separation is an important consideration because it neutralizes the drip shield as a flow barrier and rockfall barrier.

Structural response calculations determine the damaged areas on the drip shield under vibratory ground motions. However, the presence of damaged areas and the associated network of stress corrosion cracks are excluded from TSPA-LA because the advective flux of liquid through the drip shield is predicted to be negligible (see discussion in Section 6.3.6). The crack network has high tortuosity and surface roughness, and the cracks narrow to very small apertures at the crack tip(s). It is likely that this physical morphology will eliminate advective flux through the cracks because of infilling of narrow apertures with corrosion products, because of high surface tension when a narrow aperture is bridged by a single droplet, because there will be minimal head gradient or pressure gradient driving flow through the narrow apertures with high tortuosity and surface roughness, and because the cracks are predicted to plug from evaporation-induced precipitation of calcite and other minerals in the seepage.

The same structural response calculations also determine the onset and degree of drip shield separation. However, as discussed in Section 6.5.5, drip shield separation is excluded from TSPA-LA because the ground motion amplitudes that are sufficient to separate the drip shields are also large enough to partially or completely collapse drifts in the lithophysal or nonlithophysal zones of the repository. The presence of rockfall, either as larger rock blocks or small fragments, around the drip shield causes frictional loads on the sides of the drip shield. Rockfall can also cause gravitational loads on top of the drip shield if the rockfall completely covers the drip shield. The presence of even small frictional or gravitational loads has been shown to restrain the relative motion between adjacent drip shields, thereby preventing drip shield separation.

Although the presence of rockfall makes drip shield separation extremely unlikely, testing and validation of the TSPA-LA model includes consideration of drip shield separation because the technical basis for excluding separation was established after the start of model validation activities. Appendix D documents the abstraction for drip shield separation that is included in the TSPA-LA model validation studies.

In summary, damage to the drip shield from vibratory ground motion is not included in the TSPA-LA. The structural response calculations for the drip shield are briefly summarized in the next two subsections, followed by a summary of the analysis that excludes drip shield separation from TSPA-LA.

6.5.4.1 Structural Response Calculations

Damage to the drip shield from vibratory ground motion is determined by structural response calculations (BSC 2003 [DIRS 163425]). A set of 15 calculations for the dynamic response of the drip shield was performed for a set of 15 ground motions with a PGV of 2.44 m/s. A similar set of calculations was also performed for a PGV of 5.35 m/s. The stochastic (uncertain) input parameters for the 15 calculations are the 15 sets of three-component ground-motion time histories, the metal-to-metal friction coefficient, and the metal-to-rock friction coefficient. A Monte Carlo sampling scheme defines the appropriate combinations of ground-motion time histories and friction coefficients (BSC 2004 [DIRS 169059], Section 6.4). The set of 15 ground-motion time histories for these analyses is identical with that for the analyses of rockfall induced by vibratory ground motion and for waste package structural response. The drift is unfilled at the time of the seismic event and the potential coupling between rockfall and the dynamic motion of the EBS components during the event is not included in the analyses.

These calculations incorporate the potential for corrosion to degrade the drip shield over the first 20,000 years after repository closure by reducing the thickness of the drip shield plates by 2 mm. These calculations evaluate mechanical properties at 150°C to represent the potential degradation in mechanical strength if a seismic hazard occurs during the initial thermal pulse after repository closure (Assumption 5.5). The objectivity of the finite-element mesh was also demonstrated (BSC 2003 [DIRS 163425], Appendix C).

The damage to the drip shield is determined by comparing the residual first principal stress on the drip-shield plates to the failure criterion for Titanium Grade 7, which is defined in Section 6.3.3. The results from each structural response calculation are evaluated to determine

the elements in the plates whose residual stress exceeds 50 percent of the yield strength of Titanium Grade 7; the failed elements are then converted into a damaged surface area. This conversion considered that if a single element on the surface of the waste package fails, then all elements beneath this element also fail.

The structural response calculations do not represent the dynamic response of the invert to the ground motion. The invert is represented as an elastic body whose surface responds instantaneously and uniformly to the given ground motion. In other words, the ground motion time histories for the three components of motion are applied directly to the surface of the invert. This is a reasonable approach for small amplitude ground motions because the invert is compacted under the weight of the waste packages and drip shield and because any remaining steel framework in the invert will tend to provide structural integrity and rigidity. These effects result in an invert that tends to move as a single unit. For high amplitude ground motions, the invert ballast has the potential to be thrown up and redistributed, allowing the heavy EBS components to settle on the bottom of the drift, directly in contact with the rock floor. In this case, applying the ground motions directly to the surface of the invert is again a reasonable approach.

6.5.4.2 Drip Shield Damage

The results of the structural response calculations for ground motions at the 0.19 m/s, 2.44 m/s, and 5.35 m/s PGV levels are summarized as follows:

- One simulation performed at the 0.19 m/s PGV level indicates that there is no damage to the drip shield (BSC 2004 [DIRS 169220], Calculation Results I). This simulation is based on the single (three component) ground motion that was developed for preclosure design purposes at the 0.19 m/s PGV level. More specifically, the drip shields do not separate and no area of the drip shield exceeds the residual stress threshold of 50 percent of the yield strength of Titanium Grade 7.

- Fourteen simulations were performed to completion at the 2.44 m/s PGV level. The results of these calculations do not indicate any separation of drip shields. The data for damaged area on the drip shield (BSC 2004 [DIRS 169220], Table 4) indicates that the mean percent damaged area is 0.70 percent and the maximum percent damaged area is 2.13 percent. As with the waste package calculations for the 2.44 m/s PGV level, ground motion #16 was substituted for ground motion #15 because of its anomalous response spectrum (see footnote to Table 6.5-1 for additional details).

  The suite of ground motions for computing drip shield response at the 2.44 m/s PGV level do not include intercomponent variability (see Section 6.4.2). In this situation, it is possible that some realizations might experience drip shield separation with the second suite of ground motions. The damage abstraction for TSPA-LA is based on the results with the first suite of ground motions, which indicate no separation. This is a reasonable approach because the damage areas for the 2.44 m/s PGV level are generally small, indicating limited potential for the large relative displacements in the vertical direction that are required to separate adjacent drip shields. This is also a reasonable approach because the sensitivity study for waste package damage with intercomponent variability at the 2.44 m/s PGV level (Section 6.5.1.5) found that the original set of calculations

(without intercomponent variability) spanned a broad range that included the revised damage data with intercomponent variability.

- Five simulations performed at the 5.35 m/s PGV level indicate separation of adjacent drip shields in each calculation (BSC 2004 [DIRS 169220], Calculation Results I). The ground motions become very intense at 5.35 m/s, resulting in large displacements and high-speed impacts for the unanchored repository components.

  Separation occurs between adjacent drip shields because of plastic deformation of the drip shield and because of the large magnitude of the ground motions. In fact, each of the five simulations demonstrates that a drip shield rides over its adjacent neighbor, implying that a separation must occur somewhere in the emplacement drift. The degree to which the drip shield rides over its neighbor is substantial, on the order of 10 to 25 percent of the length of the drip shield (BSC 2003 [DIRS 163425], Figures IV-3 through IV-7). These separations represent a lower bound because four of the five numerical simulations terminated before the end of the ground-motion time history.

  The prediction of drip shield separation for the 5.35 m/s PGV level is very idealized for two reasons. First, the finite-element representation has rigid boundaries (that move with the invert) at the axial ends of the computational space, and the presence of rigid boundaries amplifies the interaction between adjacent drip shields. The ground motions are expected to be synchronous over the length scale of the drip shield. Synchronous ground motions will generally lead to synchronous motions of the drip shield, all other factors being equal. However, synchronous motion of adjacent drip shields is destroyed once a drip shield impacts either rigid boundary at the ends of the computational model. The resulting asynchronicity increases the relative motion and impacts between adjacent drip shields, decreasing the onset time for and increasing the degree of drip shield separation. The second reason is that the presence of rockfall is not included in the structural response calculations for the drip shields, as explained in the next section. The ground motion amplitudes at the 5.35 m/s PGV level are large enough to cause rockfall in both the lithophysal and nonlithophysal zones (BSC 2004 [DIRS 166107], Sections 6.4.2.2.2 and 6.3.1.6.4). The presence of rubblized backfill and larger rock blocks around the drip shields restricts the relative vertical displacement between adjacent drip shields, reducing the potential for separation at extreme ground motions.

6.5.5 Rockfall Prevents Drip Shield Separation

Drip shield separation is excluded from TSPA-LA because (1) ground motion amplitudes that are sufficient to cause drip shield separation are also large enough to partially or completely collapse drifts in the repository, and (2) rockfall occurs within the first second or two of the arrival of these large amplitude ground motions. In this situation, rockfall provides restraints on the motion of the drip shields, preventing differential motion that could lead to separation.

Ground motion amplitudes near and above the 2.44 m/s PGV level are large enough to cause rockfall in both the lithophysal and nonlithophysal zones. In the lithophysal zones, drift collapse is observed at and above the 2 m/s PGV level (BSC 2004 [DIRS 166107], Section 6.4.2.2.2, fourth bullet under subheading ‘Discussion’). Figure 6.5-7 presents an example of rockfall in lithophysal rock for the case of a peak ground velocity of 3.33 m/sec for three rock quality levels

that span the expected strength range. Collapse of the drifts occurs for all rock types in Figure 6.5-7, covering of the drip shield with rubble. Partial collapse of drifts occurs for peak ground velocities below 2 m/sec, resulting in rubble constraint to the sidewalls of drip shield. In the nonlithophysal zones, significant (but not complete) collapse is observed at 2.44 m/s and at 5.35 m/s (BSC 2004 [DIRS 166107], Section 6.3.1.6.4).

The collapse in the lithophysal rock is coincident with the arrival of the first strong ground motion – i.e., collapse occurs within seconds of the arrival of the first pulse of the accelerogram (BSC 2004 [DIRS 166107], Section 6.4.2.2.2). Large blocks also start to fall from the drift walls in the nonlithophysal zones shortly after the arrival of the ground motion (BSC 2004 [DIRS 166107], Section 6.3.1.6.1).

In either the lithophysal or nonlithophysal zones, rockfall occurs at PGV levels substantially lower than the 5.35 m/s PGV level that results in drip shield separation (Section 6.5.4.2). It follows that the drip shield is partly surrounded by rockfall whenever separation could potentially occur, and this rockfall can occur near the start of the ground motion. The larger rock blocks or the smaller rock fragments provide normal and shear confinement to the sidewalls and possibly the crown of the drip shield. The horizontal acceleration imparted to the drip shield by the ground motion will be resisted by the frictional forces between the rock and the drip shield plates and between the footings and the invert. The exterior bulkhead structure of the drip shield (Figure 6.5-8) provides an additional physical restraint or "locking" mechanism between the drip shield and rubble that makes lateral movement unlikely. Thus, the presence of rockfall around the drip shields will restrict the relative displacements that are required to separate adjacent drip shields, making separation very unlikely even for extreme ground motions.

It is important to note that smaller, more frequent seismic events will also provide rockfall around the drip shield. Smaller events are much more probable during a 10,000-year period. For a Poisson process (Assumption 5.4), smaller seismic events with a rate of 10^{-5} per year are about 100 times more probable than extreme events with a rate of 10^{-7} per year. These smaller events can contribute to the buildup of rockfall around the drip shield before an extreme event occurs. For example, ground motions at the 1.5 m/s PGV level (near a 10^{-5} per year annual exceedance frequency) generate rockfall from partial collapse of the drifts in the lithophysal zones (BSC 2004 [DIRS 166107], Section 6.4.2.2.2). Since higher probability (e.g., 10^{-5}) events are much more likely than lower probability (e.g., 10^{-7}) events, it is reasonable to expect that significant rubble would exist in the drift and provide some confinement for the drip shield prior to the high amplitude, low probability ground motion that could result in drip shield separation.

A kinematic study of drip shield motion (BSC 2004 [DIRS 169753], Section 5.3) has confirmed that a relatively small amount of rockfall can constrain the asynchronous motion of the drip shields and prevent drip shield separation. This study considers the kinematic response of multiple drip shields in a single emplacement drift under vibratory ground motion. Analyses were conducted for emplacement drifts that are open, partly filled with collapsed rock, and completely filled with collapsed rock. The drip shields remain connected for almost all cases, even for open drifts with extreme ground motions at the 5.35 m/s PGV level. Separation is only observed in the very unrealistic case that there is no metal-to-metal friction, an open drift, and the 5.35 m/s PGV ground motion. However, the kinematic calculations demonstrate that a small amount of friction force is sufficient to stabilize the motion of the drip shields and prevent drip

shield separation. Since rockfall in the lithophysal or nonlithophysal zones occurs at PGV levels substantially lower than the 5.35 m/s PGV level that results in drip shield separation (Section 6.5.4.2), and since smaller, more frequent seismic events may also provide rockfall around the drip shield, the friction forces will be present that prevent drip shield separation.

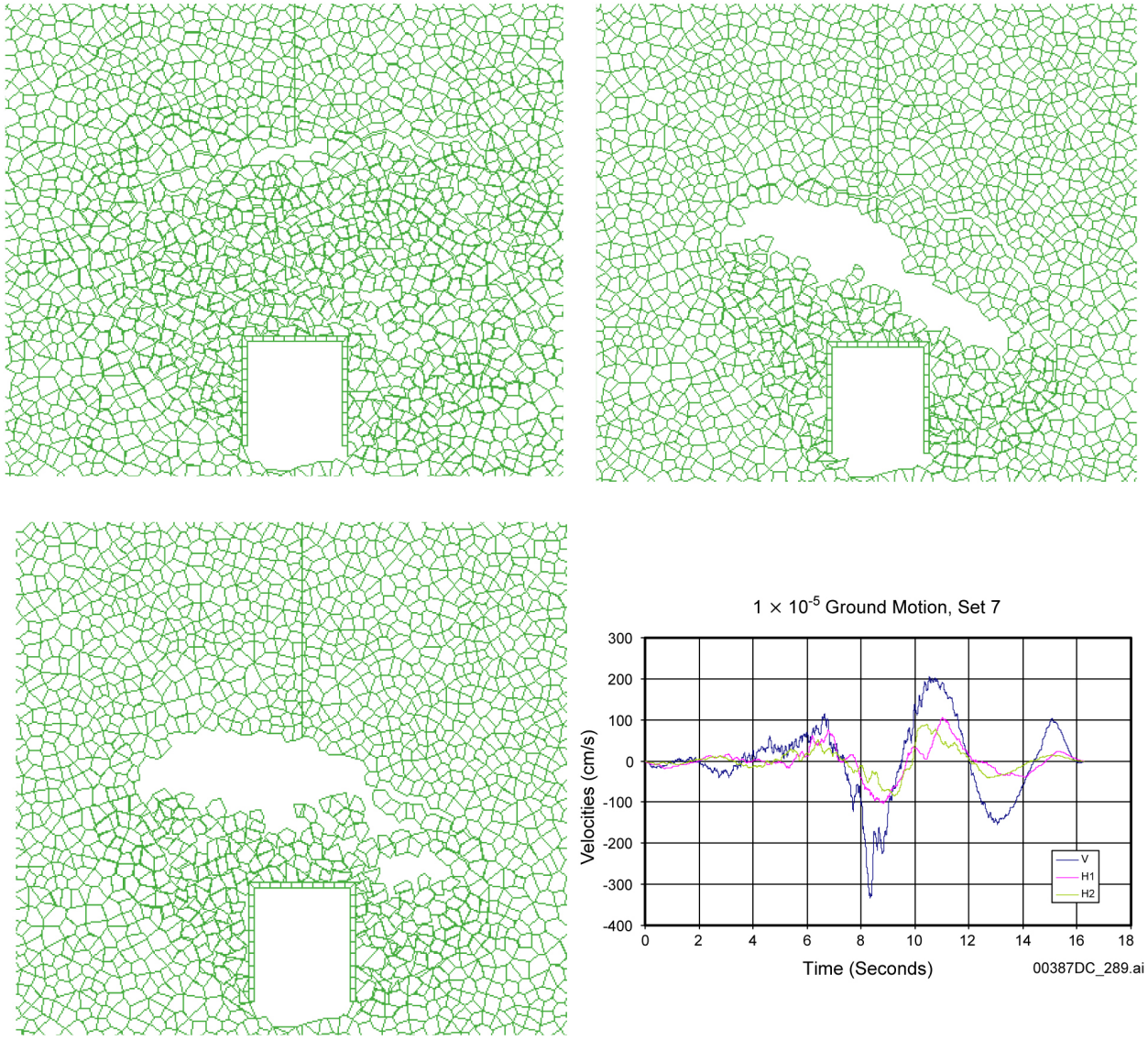

Source: BSC 2004 [DIRS 166107], Figure 6-127.

NOTE: (upper left) Rock Strength Category 1 (40.6 m^2/m drift length), (upper right) Category 5 (19.7 m^2/m), (lower left) Category 3 (15.4 m^2/m), and (lower right) Ground Motion History 7, PGV=333 cm/sec.

Figure 6.5-7. Collapse of Emplacement Drifts in all Rock Qualities of Lithophysal Rock for Peak Ground Velocity of 333 cm/sec

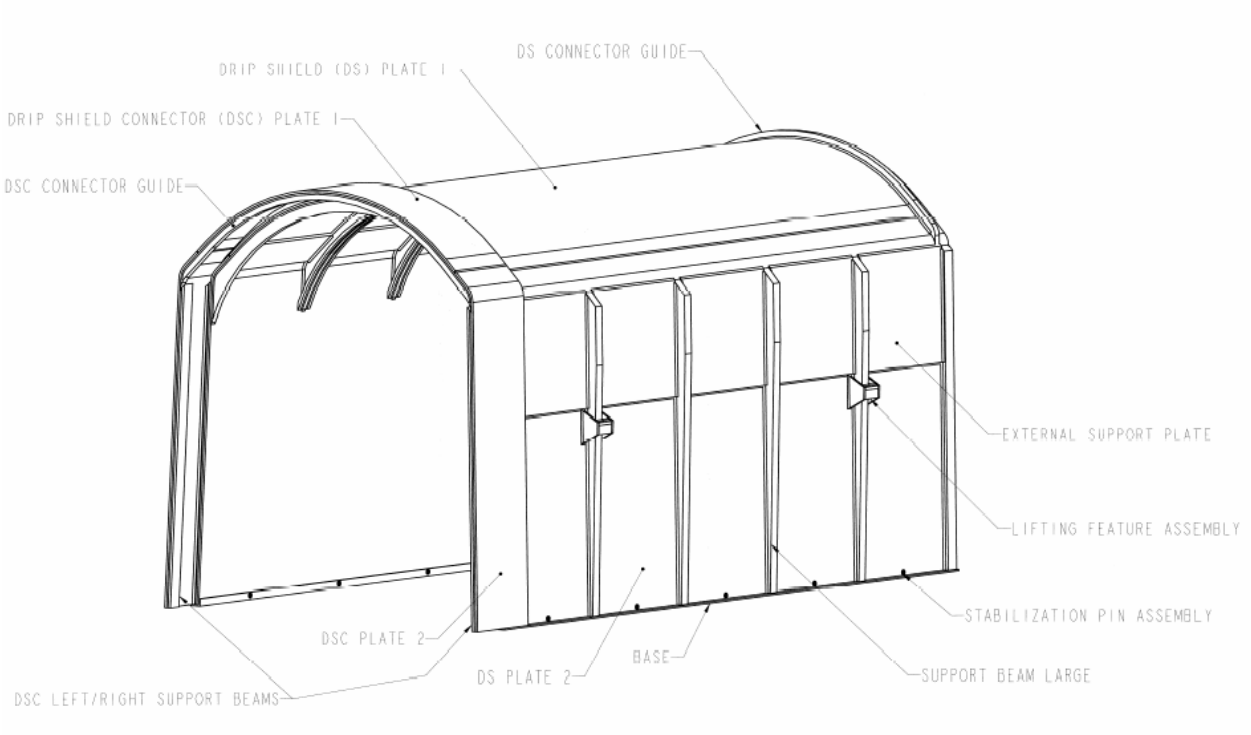

Source: BSC 2004 [DIRS 168275].

Figure 6.5-8. Geometry of the Drip Shield – Side View

6.5.6 Failure Abstraction for the Cladding from Ground Motion

The mechanical response of the waste package to vibratory ground motion can produce dynamic impacts between adjacent waste packages, between the waste package and its emplacement pallet, and between the waste package and the drip shield. During each of these impacts, the waste package may experience very high acceleration in the axial and lateral directions. These accelerations can be "transmitted" to the fuel rod assemblies and fuel rods. The assemblies and fuel rods may impact the lid of a waste package due to the end-on (axial) impact of adjacent waste packages, or be pushed sideways, toward the sidewall of the waste package, during impact with the emplacement pallet or drip shield. Either of these impacts has the potential to fail the fuel rod cladding.

As noted in the notes for Tables 6.5-1 and 6.5-2 in Section 6.5.1.3, the end-on impact between two adjacent waste packages accounts for 89.7 percent of the mean damage to the waste package at the 2.44 m/s PGV level and 76.0 percent of the mean damage to the waste package at the 5.35 m/s PGV level, based on a residual stress threshold of 80 percent of yield strength. These results imply that the end-on impact of adjacent waste packages produces more severe forces and accelerations than the side-on impact between a waste package and the emplacement pallet or drip shield. These results are consistent with the approach to the end-on impact calculations, which are based on a waste package impacting an almost rigid plane of symmetry located midway between two adjacent waste packages (see discussion of conservatism in Section 6.5.1.2).

6.5.6.1 Structural Response Calculations

The maximum waste package velocities from end-on impacts with the 15 ground motions at the 2.44 m/s PGV level vary between 1.4 to 4.5 m/s (BSC 2004 [DIRS 167083], Tables 6.1.2-1 through 6.1.2-15). In other words, realizations with ground motions with 2.44 m/s PGV have an impact velocity of at least 1.4 m/s. Similarly, the maximum waste package velocities for end-on impacts at the 5.35 m/s PGV level vary between 1.3 m/s and 6.5 m/s (BSC 2004 [DIRS 167083], Tables 6.2.2-1 through 6.2.2-15). That is, realizations for ground motions with 5.35 m/s PGV have an impact velocity of at least 1.3 m/s (The minimum value for the 5.35 m/s PGV level is less than that for the 2.44 m/s PGV level because substantial stochastic variability in the 15 ground motions leads to substantial variability in waste package response.).

The resulting fuel assembly accelerations due to this range of impact velocities have been analyzed using a finite-element representation of the fuel assemblies. The maximum peak acceleration and the average peak acceleration for the assemblies in a waste package have been determined through detailed structural response calculations for a waste package with internal fuel rod assemblies impacting a rigid wall (BSC 2004 [DIRS 167369], Tables 14 and 15). The peak and average accelerations from the structural response calculations have been evaluated for cutoff frequencies of 450 Hertz, 600 Hertz, and 1,000 Hertz. The accelerations for a cutoff frequency of 450 Hertz are repeated in Table 6.5-5.

Table 6.5-5. Fuel Assembly Accelerations from Waste Package-to-Waste Package Impact Calculations for a 450 Hertz Cutoff Frequency

Parameter	Initial Impact Velocity (m/s)				
	0.5	1	2	4	6
Maximum Peak Acceleration (*g*'s)	75	144	263	323	506
Average Peak Acceleration (*g*'s)	35	72	115	155	194

Source: BSC 2004 [DIRS 167369], Tables 14 and 15.

The finite-element calculations for the fuel assembly accelerations do not include any damping. Impact calculations with no damping often produce acceleration time histories with peak values that are influenced by the spatial and temporal discretization of the calculations. In this situation, the output is typically filtered through a low-pass filter to determine a more realistic acceleration time history. The cutoff frequency for the filter is a compromise between damping the extraneous numerical noise while leaving the fundamental modes of the structure intact. Filtering the output below 400 Hertz dampens the fundamental modes of waste package and fuel assembly, potentially leading to erroneous results. Filtering the output at greater than 1,000 Hertz preserves computational noise and can also lead to misleading results. A cutoff frequency of 450 Hertz dampens the numerical noise but has minimal impact on the fundamental modes of fuel assembly and waste package (BSC 2003 [DIRS 162602], Appendix D).

6.5.6.2 Cladding Damage

The minimum impact velocity for the 2.44 m/s and 5.35 m/s PGV ground motions is 1.3 m/s, as noted above. Interpolating on the results in Table 6.5-5 for the known accelerations from impact calculations for velocities of 1 m/s and 2 m/s, the maximum peak acceleration is 180 *g*'s[12] and the average peak acceleration is 85 *g*'s[13] for an impact at 1.3 m/s with a 450 Hertz cutoff frequency. With a cutoff frequency of 600 Hertz, the average peak accelerations for 1 m/s and 2 m/s are 99 *g*'s and 147 *g*'s, respectively (BSC 2004 [DIRS 167369], Table 15). The interpolated value for the average peak acceleration at 1.3 m/s impact velocity is then 113 *g*'s[14] for the 600 Hertz cutoff.

The integrity of fuel rod cladding during cask drop or tip over incidents has been extensively studied for zircalloy-clad light water reactor spent fuel assemblies (Chun et al. 1987 [DIRS 144357]; Sanders et al. 1992 [DIRS 102072]. The work by Chun et al. (1987 [DIRS 144357]) is more useful here because it explicitly calculates *g*-loads for axial buckling and for yielding due to side drops. The range of *g*-loads for failure due to axial buckling varies between 82 *g*'s for the Westinghouse 17×17 fuel assembly to 252 *g*'s for the Combustion Engineering 16×16 fuel assembly (Chun et al. 1987 [DIRS 144357], Table 4]). The range of *g*-loads for yielding due to side drops varies between 63 *g*'s for a Westinghouse 17×17 fuel assembly to 211 *g*'s for a Combustion Engineering 16×16 fuel assembly (Chun et al. 1987 [DIRS 144357], Table 4). The actual *g*-loads for failure may be lower because: (1) the weight of the fuel pellets is not transferred to the cladding (Chun et al. 1987 [DIRS 144357], page 2]), and (2) the potential effects of cladding defects or existing failures are not included in the analysis. These effects increase the inertial mass or weaken the clad, possibly causing failure at lower *g*-loads.

Based on Table 6.5-5, end-on impacts of adjacent waste packages result in average fuel assembly accelerations of 85 *g*'s at the lowest impact velocity, and often much greater values for higher impact velocities. The use of a 600 Hertz cutoff filter increases this minimum value to 113 *g*'s. Simple fuel rod failure criteria indicate that clad failure occurs between 82 *g*'s and 252 *g*'s, depending on the type of fuel rod (Chun et al. 1987 [DIRS 144357], Table 4). In this situation, 100 percent perforation of the cladding is reasonable when a ground motion event occurs with a PGV of 2.44 m/s or greater.

One calculation is available for the structural response of the waste package to a ground motion with PGV values of 0.19 m/s and 0.384 m/s (BSC 2004 [DIRS 167083], Sections 6.3 and 6.4). There is no damage to the cladding for these ground motions because there is no appreciable motion of the waste package and no impact between adjacent waste packages. However, the potential exists for more significant displacements and impacts at the 1.05 m/s PGV level.

[12] Maximum peak acceleration at 1.3 m/s = 144 *g*'s + (263 *g*'s – 144 *g*'s)/(2 m/s–1m/s)(1.3m/s – 1m/s) = 179.7 *g*'s.

[13] Average peak acceleration at 1.3 m/s = 72 *g*'s + (115 *g*'s – 72 *g*'s)/(2m/s – 1m/s)(1.3m/s – 1m/s) = 84.9 *g*'s.

[14] Average peak acceleration at
1.3 m/s for the 600 Hertz low pass filter = 99 *g*'s + (147 *g*'s – 99 *g*'s)/(2m/s – 1m/s)(1.3m/s – 1 m/s) = 113.4 *g*'s.

6.5.6.3 Abstraction for Cladding Failure

The cladding damage for ground motion at the 1.05 m/s PGV level is conservatively set to 100 percent. In addition, the cladding damage goes to zero at the 0.55 m/s PGV level. This approach is consistent with Assumption 5.1, whereby damage from vibratory ground motion first begins between the 0.384 m/s PGV level, corresponding to an exceedance frequency of 10^{-4} per year, and the 1.05 m/s PGV level, corresponding to an exceedance frequency of 10^{-5} per year. The PGV value of 0.55 m/s is an intermediate value, corresponding to an exceedance frequency of 5×10^{-5} per year (Table 6.4-1). In other words, ground motions greater than those at the 0.384 m/s PGV level are required to damage the cladding.

The abstraction for damage to the cladding is then a simple look-up table with a linear interpolation between the four points in Table 6.5-6, as illustrated in Figure 6.5-9. There is no uncertainty in this abstraction because the abstraction represents a conservative, bounding estimate for cladding response at all values of PGV. Damage to the cladding occurs within all waste packages for TSPA—there is no spatial variability in the damage.

Table 6.5-6. Abstraction for Damage to the Cladding from Vibratory Ground Motion

PGV Value (m/s)	Damage to Cladding (%)
0.0	0
0.55	0
1.05	100
> 1.05	100

6.6 RESPONSE TO ROCKFALL

Rockfall induced by vibratory ground motion has the potential to damage the drip shield and waste package as barriers to flow and transport. Rockfall refers to the large rock blocks that may be ejected from the nonlithophysal zones of the repository during vibratory ground motion. Rockfall also refers to the rubblized material that may surround the drip shield and fill the drifts during catastrophic collapse of drifts in lithophysal zones of the repository. Detailed rockfall analyses have been performed for both of these failure mechanisms under vibratory ground motions (BSC 2004 [DIRS 166107]).

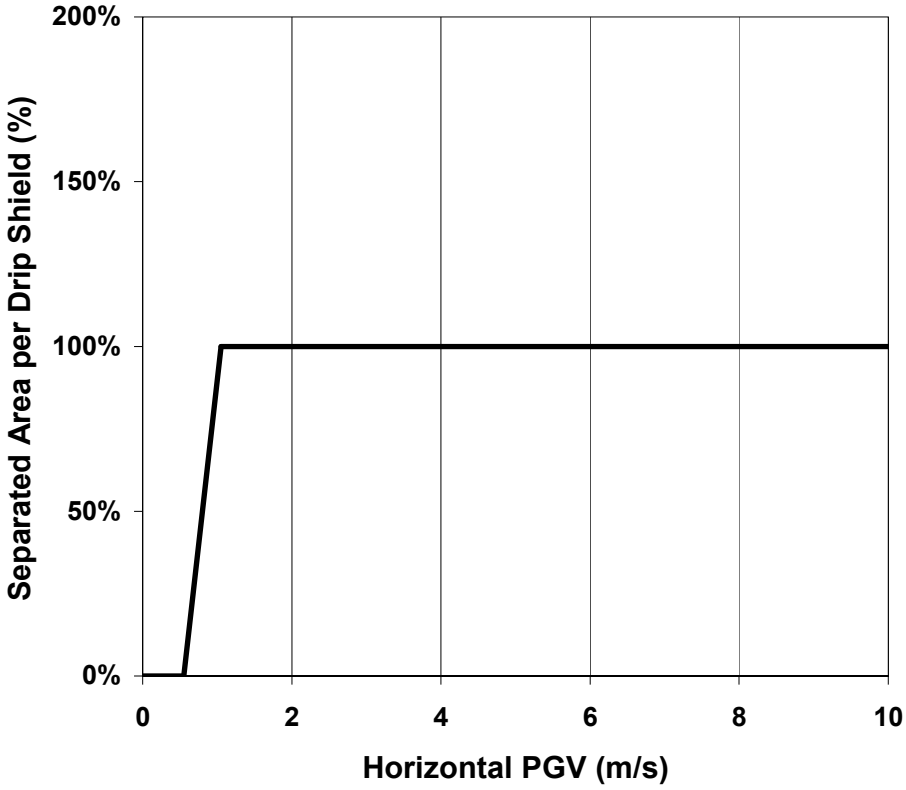

Figure 6.5-9. Damage Abstraction for Cladding Failure Via Perforation

The mechanical response of the drip shield has been analyzed for the impacts from large rock blocks and under the static load from rubblized backfill. Drip shield damage due to rock impact and waste package damage after drip shield separation have been considered to determine the damage to the drip shield and waste package from rockfall.

Damage to EBS components from rockfall has not been included in TSPA-LA. Table 6.6-1 summarizes the relevant analyses and key results that support excluding damage from rockfall from the seismic scenario class for TSPA-LA. As an example, consider the impact from a large rock block on the drip shield (first row in Table 6.6-1). This impact may result in deformation and residual stress that exceed the residual stress threshold for accelerated stress corrosion cracking. However, the resulting network of stress corrosion cracks are not a pathway for advective flow (Section 6.3.6) because of infilling of narrow apertures with corrosion products, because of high surface tension when a narrow aperture is bridged by a single droplet, because of insignificant head gradient or pressure gradient driving flow through the narrow apertures with high tortuosity and surface roughness, and because the cracks on the drip shield are predicted to plug from evaporation-induced precipitation of calcite and other minerals in the seepage over a few hundred years. The rockfall and structural response calculations for this analysis are discussed in Sections 6.6.1.1 and 6.6.1.2, respectively. The drip shield therefore remains intact as a long-term flow barrier, so rockfall-related damage is excluded from the seismic scenario.

6.6.1 Drip Shield Damage from Rockfall in the Nonlithophysal Zone

The potential source of damage to the drip shield in the nonlithophysal zones arises from the large rock blocks that may be shaken loose from the drift walls and fall onto the drip shield in response to vibratory ground motion (BSC 2004 [DIRS 166107], Section 6.3). Large rock blocks have the potential to deform the drip shield, resulting in accelerated stress corrosion cracking in areas that exceed the residual stress threshold for Titanium Grade 7. Large rock blocks also have the potential to collapse the drip shield. However, damage to the drip shield from large rock blocks in the nonlithophysal zones is not included in TSPA-LA because the associated crack network is not a pathway for advective flow (Section 6.3.6) and because impact by the largest rock block does not collapse the drip shield onto the waste package, as explained in Section 6.6.1.2. The drip shield therefore remains intact as a mechanical barrier and a flow barrier.

Table 6.6-1. Summary of Rockfall Damage to EBS Component

Damage Mechanism	Relevant Analyses (Section Ref.)	Key Results (Section Ref.)	Status in TSPA (Section Ref.)
Impact of rock blocks in nonlithophysal zones	• Rockfall calculations with 3DEC (6.6.1.1) • Drip shield structural response calculations for representative rock blocks (6.6.1.2)	• Drip shield does not buckle or collapse, even from impact of the largest rock block (6.6.1.2) • Drip shield does not contact the waste package, even for impact of the largest rock block (6.6.1.2)	• Drip shield remains intact as a mechanical barrier (6.6.1.2) • Drip shield remains intact as a flow barrier (6.3.6) • Drip shield damage from rock blocks excluded from TSPA
Damage from drift collapse in lithophysal zones	• Rockfall calculations for static loads from drift collapse (6.6.2.1) • Drip shield structural response calculations under static load (6.6.2.2)	• Drift collapse produces small rock fragments with little capacity to damage drip shield (6.6.2.1) • Drip shield does not buckle or collapse under static loads (6.6.2.2)	• Drip shield remains intact as a mechanical barrier (6.6.2.2) • Drip shield damage under static load excluded from TSPA
Damage to the waste package and cladding	• Drip shield structural response calculations for degree of separation (6.5.4 through 6.5.6) • Rockfall calculations in lithophysal zones (6.6.2.1)	• Drip shields do not separate below the 2.44 m/s PGV level (6.5.6) • Rock fragments in lithophysal zone (85 percent of repository) have little capacity to damage waste package (6.6.3) • Maximum degree of separation is 50 percent (6.5.6)	• Drip shield does not separate, remaining intact as a mechanical barrier except for extremely low frequency seismic events (6.5.6) • Waste packages will not be damaged in 85 percent of the repository even if drip shields separate (6.6.2) • Separated drip shields still provide partial protection for waste package (6.5.6) • Damage to waste package and cladding from rockfall excluded from TSPA

6.6.1.1 Nonlithophysal Rockfall Calculations

Geologic structure and rock strength define the failure mode in the nonlithophysal rock. The failure mode in these rocks results from stress-induced yield in the intact rock or along joint surfaces, followed by gravity-induced drop of discrete rock blocks that are ejected from the walls of the drift. Analysis of rockfall in the nonlithophysal zone requires ground motion time histories, fracture geometries, and fracture properties as input parameters or boundary conditions for the calculations. To ensure adequate representation of uncertainty and variability, individual rockfall calculations use 15 ground motions at a PGV level of 2.44 m/s and at a PGV level of 5.35 m/s, combined with 105 synthetic fracture patterns. The *Drift Degradation Analysis* model report (BSC 2004 [DIRS 166107], Section 6.3) provides a detailed description of the nonlithophysal rockfall calculations with the 3DEC computer program.

Based on the results of these calculations, a set of six representative blocks and three representative impact locations was selected to span the range of block impacts from the 3DEC analyses. The idea behind this approach is to perform a limited set of calculations that span the range of rock sizes, rock velocities, and rock impact points on the drip shield. This limited set of calculations then provides the basis for determining the structural response of the drip shield (1) to the maximum rock blocks in the nonlithophysal zone, and (2) to the smaller blocks that can be ejected during drift collapse in the lithophysal zone.

6.6.1.2 Structural Response Calculations

Damage to the drip shield from impact of individual rock blocks is determined by structural response calculations (BSC 2004 [DIRS 168993]). The objective of these calculations is to determine the areas on the drip shield where the residual stress exceeds the threshold value (50 percent of yield strength) for Titanium Grade 7 and to determine the potential for buckling and collapse, particularly for rock blocks with the greatest kinetic energy. The six representative rock sizes impact the drip shield from three different angles: vertically downward onto the top of the drip shield, at a 60° angle (with the horizontal) onto the transition region between the top and side of the drip shield, and horizontally into the side wall. The block impacts the drip shield edge-on to maximize damage. These calculations incorporate the potential for corrosion to degrade the drip shield over the first 20,000 years after repository closure by reducing the thickness of the drip shield plates by 2 mm. The 20,000-year period is selected to demonstrate that repository performance remains robust well after the 10,000-year regulatory period has ended. These calculations also evaluate mechanical properties at 150°C to represent the potential degradation in mechanical strength if a seismic hazard occurs during the initial thermal pulse after repository closure.

A key result from this suite of calculations is that the maximum vertical displacement in the drip shield components takes place in the longitudinal stiffener during the vertical impact of the 11.5 metric tons (MT) rock block, which has the highest kinetic energy (BSC 2004 [DIRS 168993], Section 6). The maximum peak dynamic displacement is 25.4 cm (254 mm) (BSC 2004 [DIRS 168993], Figure II-5). The drip shield does not buckle or collapse from this impact. In addition, this maximum displacement is less than the minimum clearance, 367.1 mm, between the interior height of the drip shield and the top of any waste package (BSC 2004 [DIRS 168489], Figure 1). It follows that the drip shield does not contact any waste package

even for an impact by the largest rock block, thereby providing a mechanical barrier against rockfall for the waste package and cladding.

Table 6.6-2 shows the damage results for the rock blocks generated by ground motions with PGV between 2.44 m/s and 5.35 m/s (BSC 2004 [DIRS 169220], Tables 2 and 3). The information in Table 6.6-2 provides data on the potential for smaller rock blocks to damage the drip shield, and is useful for the analysis of damage in the lithophysal zones in the next section.

Table 6.6-2. Damaged Area from Individual Rock Blocks Impacting the Drip Shield

Rock Mass and Kinetic Energy (MT and Joules)	Damaged area (m^2; and as a % of Total Drip Shield Surface Area)		
	Rockfall Onto Top Of Drip Shield (90° from horizontal)	Rockfall Onto Drip Shield Corner (60° from horizontal)	Rockfall Onto Drip Shield Side-Wall (40° from horizontal)
0.25 MT Rock (~0 J)	0.0 (0.00%)	0.0 (0.00%)	0.0 (0.00%)
0.11 MT Rock (42 J)	0.0 (0.00%)	0.0 (0.00%)	0.0 (0.00%)
0.15 MT Rock (902 J)	0.0015 (0.00%)	0.0091 (0.02%)	0.0 (0.00%)
3.3 MT Rock (24712 J)	0.548 (1.43%)	0.416 (1.09%)	0.0 (0.00%)
14.5 MT Rock (163083 J)	3.508 (9.17%)	0.612 (1.60%)	0.079 (0.21%)
11.5 MT Rock (348174 J)	4.304 (11.25%)	2.835 (7.41%)	1.126 (2.94%)

Source: BSC 2004 [DIRS 169220], Tables 2 and 3.

MT = metric ton

6.6.2 Drip Shield Damage from Rockfall in the Lithophysal Zone

Two potential sources of damage to the drip shield have been considered in the lithophysal zone: damage from the individual rock fragments that fall onto the drip shield and the static load on the drip shield from drift collapse. The individual rock fragments are too small to do significant damage to the drip shield and the mean static loads from a collapsed drift are not predicted to collapse the drip shield. Damage to the drip shield from rockfall in the lithophysal zone is not included in the drip shield damage abstraction for TSPA-LA, but is discussed here for completeness.

6.6.2.1 Lithophysal Rockfall Calculations

In the lithophysal zones, the rock mass has very low compressive strength and is permeated with void spaces of varying size. Average joint spacing is less than 1 meter, and at certain locations this spacing is much smaller, on the order of 0.1 meters (BSC 2004 [DIRS 166107], Section 6.1.4.1). The drifts in the lithophysal zone are predicted to collapse into small fragments with particle sizes of centimeters to decimeters (BSC 2004 [DIRS 166107], Section 8.1) under the loads imposed by vibratory ground motions with a PGV of 2.0 m/s or greater. The *Drift*

Degradation Analysis model report (BSC 2004 [DIRS 166107] Section 6.4) provides a detailed description of the lithophysal rockfall calculations.

The small fragments from lithophysal failure have little capability to damage the drip shield because the small mass and energy of the individual fragments cannot cause significant permanent deformation of the drip shield, as shown by the top rows of Table 6.6-2. As an example, consider a fragment that is a cube 0.1-meter (4-inches) on a side. The volume of this fragment is 0.001 m^3 and its mass is 2.3 kg (0.0023 MT), assuming a tuff density of 2,300 kg/m^3. The velocity of this fragment is approximated as 7.7 m/s for a 3-meter drop under gravitational acceleration, and the associated kinetic energy is 59 Joules. A comparison of the mass and kinetic energy of the 0.1 meter fragment with the second row in Table 6.6-2 indicates that there should be no damage from the impact of this fragment on the drip shield.

The probability of large coherent (key) blocks being generated by the collapse process in the lithophysal zones is very low (BSC 2004 [DIRS 166107], Section 6.4.3), so their presence is not considered in this analysis.

6.6.2.2 Structural Response to Static Loads

Drift collapse in the lithophysal zones can impose a static load on the drip shield from the weight of the natural backfill that fills the drifts as a result of the collapse. The structural response of the drip shield to the static load from a hypothetical engineered backfill and fallen host rock generated by tunnel collapse has been evaluated with structural response calculations (BSC 2003 [DIRS 162601]). The hypothetical engineered backfill is not representative of the current repository design, and only provides a load on the structure. The layer of engineered backfill in these calculations is taken to be 0.9 meters thick or 1.1 meters thick. The fallen host rock is 5.5 meters thick. The applied pressure from these materials is 143 kPa if the hypothetical engineered backfill is 0.9 meters thick and 146 kPa if the engineered backfill is 1.1 meters thick. The calculations are performed using material properties at room temperature and at 150°C. The calculations also consider a uniform thinning of the drip shield plates by 1 mm on both sides and by 1.5 mm on both sides (BSC 2003 [DIRS 162601], Table 5.2-1 and Section 5.2).

The maximum stress in any component of the drip shield is always less than the yield strength for this combined load (BSC 2003 [DIRS 162601], Section 6 and Table 6.2). At room temperature, the highest stress in the drip shield is 43 percent of the yield strength for Titanium Grade 7. At 150°C, the highest stress in the drip shield is 68 percent of the yield strength for Titanium Grade 7. In addition, the average stress in the large support beams (the peripheral bulkheads) of the drip shield is far enough below the yield strength of Titanium Grade 24 to alleviate any concern of buckling. (The drip shield plates are fabricated from Grade 7, while the supporting structure is fabricated from Grade 24.)

A failure criterion based on yield strength is appropriate for evaluating the stability of the drip shield under static load. For static loading, the failure of the drip shield is determined by mechanical collapse or buckling of the drip shield. In this situation, a local stress of 68 percent of the yield strength of Titanium Grade 7 does not imply structural failure of the drip shield as a mechanical barrier.

The potential rock loads in the lithophysal zones after complete collapse of the emplacement drift have also been analyzed for 6 cases using a discontinuum representation of the host rock (BSC 2004 [DIRS 166107], Section 6.4.2.5 and Figure 6-174). The average pressures on the top, left side, and right side of the drip shield for the 6 cases are 128 kPa, 42 kPa, and 62 kPa, respectively. The maximum mean pressures on the top, left side, and right side are 155 kPa, 70 kPa, and 129 kPa, respectively. These mean pressures are an average over the individual elements of the finite-element model on the top, left side, or right side of the structure. The peak local pressure on an individual element is 700 kPa (all data from BSC 2004 [DIRS 166107], Section 6.4.2.5). The drip shield is stable under these loads. To estimate a factor-of-safety for structural stability of the drip shield under quasi-static load, the density of the rubble was progressively increased by 2.5, 3, and 4 times. This approach is appropriate because it increases the vertical and lateral pressures in tandem, without additional assumptions about extreme vertical or lateral loads. The drip shield is stable at density multiplication factors of 2.5 and 3. The drip shield undergoes severe plastic deformation in its support beams at a density multiplication factor of 4. The conclusion from this discontinuum rockfall analysis is that there is a factor of safety of approximately 3 for the drip shield under static loading (BSC 2004 [DIRS 166107], Section 6.4.2.5).

6.6.3 Damage to the Waste Package and Cladding from Rockfall

Damage to the waste package and cladding from rockfall has not been included in the abstractions for TSPA-LA. The waste package and cladding are not damaged because the drip shield remains structurally intact for seismic events with a PGV up to 5.35 m/s, deflecting even the largest rock blocks away from the waste package. The drip shield also does not separate for ground motions with a PGV up to 5.35 m/s (see Section 6.5.5). It is therefore reasonable to screen out damage to the waste package and cladding from rockfall because the drip shield remains intact as a mechanical barrier up to the 5 m/s PGV level that is considered in the TSPA-LA.

6.7 RESPONSE TO FAULT DISPLACEMENT

In addition to inducing severe ground motion/acceleration as discussed in the previous sections, seismic events can also result in fault displacements within the emplacement drifts. Fault displacement could impact key EBS components in two ways:

- Separation between adjacent drip shields could allow a pathway for seepage to contact the waste packages, thereby potentially accelerating corrosion-induced waste package failure.

- Mechanical damage to the waste packages, drip shields, and fuel rod cladding caused directly by the fault displacement.

Potential faulting within the emplacement drifts that has a reasonable likelihood of slipping during the 10,000-year regulatory period generally results in very small displacements associated with the faults. With the exception of the Solitario Canyon fault and the Ghost Dance fault, which are immediately outside the western and eastern boundaries of the emplacement drifts, a fault displacement of greater than 0.1 cm requires a mean annual exceedance frequency of less than 10^{-5} per year. For such low-frequency events, there is significant uncertainty and variability

in the expected magnitude of the fault displacement developed by the PSHA. Given the lack of precision in the estimated fault displacement magnitudes for very low frequency events, a highly detailed calculation of drip shield and waste package response to such events is not warranted. Rather, the focus is on the potential for the waste package to be pinned when fault displacement is greater than the available clearance around the waste package for unfilled and filled drifts. Thus, the response calculations presented herein are intentionally simplistic and conservative.

For a fault displacement that occurs along an emplacement drift, a sudden discontinuity in the floor and roof of the tunnel may occur. This would result in one portion of the tunnel being displaced vertically relative to the adjacent section. Such a discontinuity in the tunnel axis could cause separation of adjacent drip shields, and if severe enough, could cause shearing of a waste package at that location. The discussion in this section identifies the conditions under which these damage mechanisms could occur.

6.7.1 Clearance Between EBS Components and the Drift

To determine the response of the drip shield, waste package and cladding to a fault displacement, consider the layout within the emplacement drift, shown schematically in Figure 6.7-1. The tunnel itself is nominally 5500 mm in diameter. Within the tunnel, the steel support beams and associated ballast form a level invert whose top surface is 863.6 mm above the lowest part of the tunnel floor (BSC 2004 [DIRS 170074]). Sitting on this invert floor is the waste package emplacement pallet, which raises the waste package off the invert floor. While the actual elevation difference between the invert floor and the bottom of the waste package varies depending on the specific diameter of the waste package, the exact value is not important for this analysis. As indicated in the discussion that follows, this elevation difference is not actually used in the analysis.

The drip shield is also sitting on the invert floor. The drip shield has an external height of 2885.62 mm (BSC 2004 [DIRS 169220], Table 1), rounded up to 2886 mm for this analysis. The internal height of the drip shield, defined as the distance from the invert floor to the lowest point on the underside of the top of the drip shield, is 2716 mm (BSC 2004 [DIRS 168489], Figure 1). There is then a clearance of 1751 mm between the top of the drip shield and the tunnel roof. A summary of these parameters, which are independent of waste package design, along with the source of the values, is provided in Table 6.7-1.

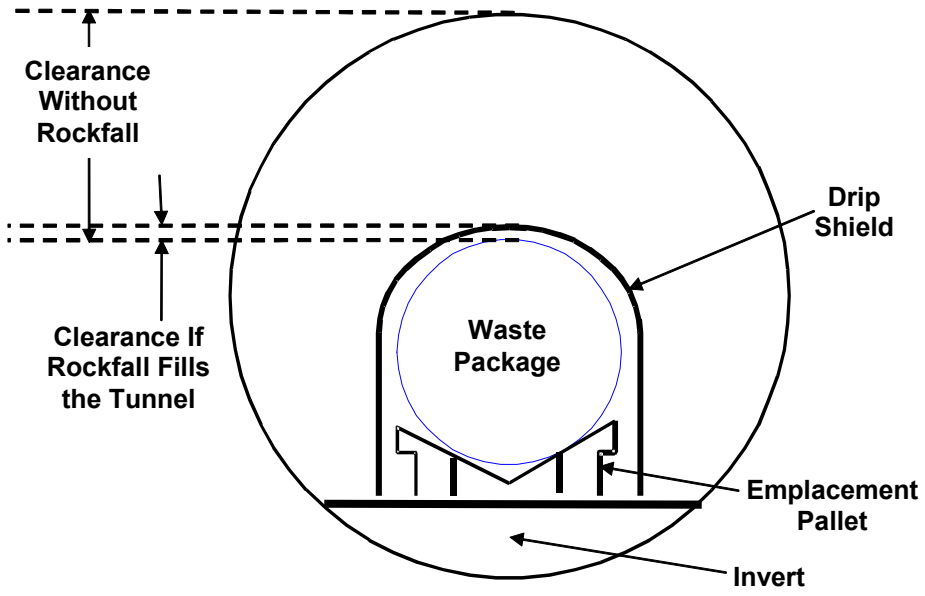

Figure 6.7-1. Schematic Diagram of EBS Components Illustrating the Clearances for Fault Displacement

Table 6.7-1. Emplacement Drift Configuration Dimensions that are Independent of the Waste Package

Description	Value	Source
Drift Diameter	5.5 m	BSC 2004 [DIRS 169058], Figure 1
Invert Thickness (maximum)	863.6 mm	BSC 2004 [DIRS 170074]
Drip Shield Height - Exterior	2885.62 mm	BSC 2004 [DIRS 169220], Table 1
Drip Shield Height - Interior	2716 mm	BSC 2004 [DIRS 168489], Figure 1
Clearance from Top of Drip Shield to Roof of Tunnel	1751 mm	Calculated: (5500 – 863.6 – 2885.62 = 1750.78)

Table 6.7-2 summarizes the exterior dimensions of the various waste package designs (BSC 2004 [DIRS 169472], Table 1), rounded to five significant figures. The most important parameter for the analyses presented herein is the outside diameter of the waste package outer barrier, which is seen to vary between 1,294 mm and 2,045 mm. Also shown in Table 6.7-2 is the calculated clearance between the top of the waste package and the underside of the drip shield in the undisturbed state, without the pallet. This clearance is defined as the interior height of the drip shield less the outside diameter of the waste package outer barrier. The elevation of the package above the invert is ignored in calculating the clearance, as explained below. This clearance varies between 671 mm and 1422 mm, depending on waste package type. Table 6.7-2 also shows the clearance between the top of the waste package and underside of the drip shield for selected packages with the pallet in place. The presence of the pallet reduces the clearance by 270.9 mm to 303.9 mm.

Table 6.7-2. Waste Package Dimensions and Clearance Between Drip Shield and Waste Package

Package Type	Outside Diameter of WP Outer Barrier (mm)	Nominal Length (mm)	Clearance Without Pallet (mm)	Clearance With Pallet (mm)	Difference in Clearances (mm)
44-BWR	1675.1	5024.4	1041	765.2	275.8
24-BWR	1294.1	5024.4	1422	—	—
21-PWR	1637.0	5024.4	1079	806.2	272.8
12-PWR	1313.2	5560.4	1403	1132.1	270.9
Naval-Long	1863.7	5837.4	852	562.1	289.9
Naval-Short	1863.7	5202.2	852	562.1	289.9
5 DHLW/DOE SNF -Short	2044.7	3452.8	671	367.1	303.9
5 DHLW/DOE SNF -Long	2044.7	5059.4	671	367.1	303.9
2-MCO/2-DHLW	1749.4	5059.4	967	—	—

Source: BSC 2004 [DIRS 169472], Table 1 for nominal length; outside diameter of outer barrier defined by drawings identified in BSC 2004 [DIRS 169472], Table 1; clearance with pallet based on BSC 2004 [DIRS 170074].

NOTE: Clearance without pallet is calculated as the interior height of the drip shield minus the outside diameter of the waste package outer barrier, rounded to 4 significant digits.
Difference in Clearances = Clearance Without Pallet – Clearance With Pallet.

WP = waste package; BWR = boiling water reactor; DHLW = defense high-level radioactive waste; PWR = pressurized water reactor; SNF = spent nuclear fuel; MCO = multicanister overpack.

The clearance between the top of the drip shield and the roof of the tunnel (Table 6.7-1) and the clearance between the top of the waste package and the bottom of the drip shield (Table 6.7-2) are measures of how much fault displacement could occur before the waste packages are potentially degraded through a shearing mechanism. At the start of a large seismic event, the clearance above the drip shield will be unimpeded because the drifts are expected to be unfilled before the seismic event and because a fault displacement can occur in a very short time in comparison to the ground motion. If a drift collapses from a large seismic event, the available clearance above the drip shield will be a function of the rubble filling a collapsed drift. Once a drift collapses, the space surrounding the drip shield will be partly or completely filled with loosely packed rock fragments. This loosely packed material still allows significant motion of the drip shield during the fault displacement, as explained below. For those tunnels in the lower lithophysal zone of the repository, tunnel collapse is calculated to occur for ground motions with PGV values greater than or equal to 2.0 m/s (BSC 2004 [DIRS 166107], Section 6.4.2.2.2).

The actual response of the EBS components to a fault displacement scenario is complicated. As a conservative simplification, the fault displacement is analyzed considering:

- The fault is perpendicular to the tunnel axis with the displacement being purely vertical
- The fault displacement occurs at a discrete plane, creating a “knife-edge” discontinuity.

Vertical faulting is consistent with the faults investigated at the site. As part of the exploratory studies of the site, the Enhanced Characterization of the Repository Block (ECRB) Cross-Drift was dug through a representative part of the repository footprint to obtain visual evidence of both rock stratigraphy and faulting. The results of this investigation (Mongano et al. 1999

[DIRS 149850], pp. 51 to 59) found evidence for four faults along the length of the ECRB Cross-Drift between the Ghost Dance and Solitario Canyon faults that bound the location of the emplacement drifts. One of these was the Sundance fault, the other three are unnamed faults that showed between one and a few meters of cumulative faulting. In each of these cases, the measured displacements were characterized as vertical, which is consistent with the assumption made herein. By treating the faults as perpendicular to the tunnel axis, no credit is taken for sideways movement of the waste packages that could lessen the degree to which fault displacement could cause damage.

An actual fault zone has a finite width over which the displacement could occur. However, based on the observations reported in the investigation of the ECRB Cross-Drift (Mongano et al. 1999 [DIRS 149850], pp. 51 to 59), the width of the fault disturbed zone varied between just under a meter to a little over 2 meters. Thus, the width of the zone is less than the length of any waste package type. If during a single seismic faulting event, the total displacement were to be distributed over a sufficiently wide zone, a single waste package could potentially see less than the total fault displacement, resulting in a decreased probability of failure. By treating fault displacement as a sharp discontinuity in the tunnel floor/roof, the likelihood of damage to the waste package is increased. Thus, the overall treatment is conservative.

A sudden discontinuity in the tunnel floor would tend to raise one end of a drip shield and waste package. However, the other EBS components, specifically the invert and emplacement pallet, would also be affected. A significant amount of the invert (ballast) from the elevated portion of the tunnel is expected to fall into the lower tunnel segment. In addition, the steel supports in the invert and the emplacement pallet are likely to collapse at the plane of displacement, further degrading the integrity of the invert. Movement along a sudden discontinuity will also affect the rubble surrounding the drip shield after tunnel collapse. The rubble is a loosely packed material with a typical porosity in the 20 percent to 30 percent range. With this free space, the rubble has substantial movement in the plane of discontinuity and longitudinally along the tunnel axis during the fault displacement. The movement of the rubble will allow the drip shield to move with the fault displacement, rather than being rigidly pinned to the invert. In this situation, the effective clearance around the drip shield is expected to be significantly larger than space between the top of the waste package and bottom of the drip shield.

The exact details of these events are difficult to predict. For example, the timing of the fault displacement versus drift collapse is highly uncertain, so the full clearance between the top of the drip shield and the roof of the tunnel may not be available. On the other hand, the potential for substantial movement of rubble after drift collapse has been confirmed in ground motion calculations at the 2.44 m/s PGV level (BSC 2004 [DIRS 166107], Section 6.4.2.5.3). These simulations demonstrate that the rubble particles undergo large dynamic motion in response to displacements of the tunnel walls, similar to what would occur during a vertical fault displacement. It follows that the clearance between the top of the drip shield and the roof of the tunnel will be partly available, but the exact value is difficult to quantify.

As a simplification, the approximation is made that the clearance between the top of the waste package and the bottom of the drip shield is determined without the pallet. This is a reasonable approximation because the clearance between the top of the drip shield and the roof of the tunnel, 1751 mm (see Table 6.7-1), is more than five times greater than the differences in clearance with or without the pallet, 270.9 mm to 303.9 mm (Table 6.7-2). In other words, the height of rubble above the drip shield is much greater than the difference in clearance due to the pallet. Since the porosity and dynamic motion of the rubble allows the drip shield to displace horizontally and vertically during the ground motion, the difference in clearance due to the pallet can be accommodated by drip shield displacements that are a small percentage of the height of the rubble. It follows that the potential for upward displacements of the drip shield into the large rubble-filled space between the top of drip shield and roof of the tunnel allows for vertical motions that can exceed the maximum difference (303.9-mm) in clearance due to the pallet. It is then reasonable to neglect the presence of the pallet in defining clearances between components because of the potential for upward displacement of the drip shield. No credit is taken for any shifting of the ballast in the invert.

The maximum allowable displacement of the waste package before it is pinned also depends on the condition and dynamic response of the drift after the seismic event. In those cases where drift collapse does not occur from the ground motion or from gradual degradation of the host rock, then the allowable waste package displacement without damage is much greater than the free height under the drip shield. For example, upward displacement of the waste package could cause the drip shield to lift since there is no tunnel debris to hold it in place. In those cases where the drift collapses, the loosely packed rubble can still allow substantial dynamic movement of the drip shield. The maximum allowable fault displacement prior to waste package damage is determined by ignoring the presence of the pallet, as explained above. The calculated clearances are summarized in Table 6.7-3.

Table 6.7-3. Maximum Allowable Displacement Before Waste Package is Pinned

Package Type	Maximum Allowable Displacement With Tunnel Collapse (mm)	Maximum Allowable Displacement Without Tunnel Collapse (mm)
44-BWR	1041	2792
24-BWR	1422	3173
21-PWR	1079	2830
12-PWR	1403	3154
Naval-Long	852	2603
Naval-Short	852	2603
5 DHLW/DOE SNF -Short	671	2422
5 DHLW/DOE SNF -Long	671	2422
2-MCO/2-DHLW	967	2717

NOTES: Maximum allowable displacement with tunnel collapse = clearance without pallet in Table 6.7-2. Maximum allowable displacement without tunnel collapse is given by the interior height of the drip shield (2716 mm) minus the outer diameter of the waste package (Table 6.7-2) plus 1750.78 mm, rounded to 4 significant digits.

BWR = boiling water reactor; DHLW = defense high-level radioactive waste; PWR = pressurized water reactor; SNF = spent nuclear fuel; MCO = multicanister overpack

The values in Table 6.7-3 represent the failure criteria for waste packages and drip shields under fault displacement. Fault displacement in excess of these values is conservatively considered to fail the waste package, the overlying drip shield, and the internal cladding through direct shearing.

Failure of the drip shields could also occur without direct waste package damage. One mechanism for this is lifting of one drip shield relative to its neighbor, thereby creating a pathway for ingress of seepage water onto the waste package. However, drip shield failure without waste package damage will generally have low consequence for performance assessment, so it will be screened out from TSPA-LA based on low consequence and is not considered further herein.

6.7.2 Faults Intersecting Emplacement Drifts

The location, frequency, and magnitude of potential fault displacements within the emplacement drift footprint must be analyzed to determine the potential impacts of fault displacement on the Yucca Mountain repository. Such fault displacements could occur at known faults that intersect the emplacement drifts (based on surface mapping), or at other locations within the repository.

6.7.2.1 Location of Known Faults

Information on known faults intersecting the emplacement drifts is obtained from three sources. The traces for the Sever Wash fault, Drill Hole Wash fault, Pagany Wash fault, and the western splay off the main Ghost Dance fault relative to the repository are provided in (BSC 2004 [DIRS 168180], Figure 4). The intersection of these traces with individual emplacement drifts is defined in (BSC 2004 [DIRS 168180], Table 9); the western splay off the main Ghost Dance is denoted as the West Ghost Dance fault in Figure 4 and Table 9 of BSC 2004 [DIRS 168180]. The trace of the Sundance fault relative to the emplacement drifts is provided in the Geologic Framework Model (DTN: MO0012MWDGFM02.002 [DIRS 153777]). Lastly, the location of emplacement drifts relative to the geologic units is defined in by the Geologic Framework Model (DTN: MO0012MWDGFM02.002 [DIRS 153777]). From these three sources of information, the intersections of known faults with specific tunnels and the local rock type (lithophysal or nonlithophysal) can be determined.

This information is summarized in Figure 6.7-2 and in Table 6.7-4, where tunnels are identified by panel number and tunnel number, plus a designation for east or west when appropriate (see BSC 2004 [DIRS 164519], Figure 1, for the drift nomenclature). As can be seen from Table 6.7-4, there are 22 locations in the lithophysal zones where a known fault intersects an emplacement drift, plus another eight locations where such an intersection occurs in the nonlithophysal zones. Intersections where two rock types occur at an intersection are conservatively assigned to the lithophysal category because this is most restrictive in terms of clearance for the waste package. This information, along with the frequency of a fault displacement of sufficient magnitude to cause waste package failure at these locations, can be used to determine the frequency and consequence of waste package failure.

The potential tunnel intersections with the western splay off the main Ghost Dance fault are not included in Table 6.7-4 and are not included in the fault displacement model for TSPA-LA. The western splay off the main Ghost Dance fault intersects drifts 2-17 through 2-27, at the southernmost end of panel 2 (BSC 2004 [DIRS 168180], Figure 4 and Table 9, denoted as the West Ghost Dance fault). Drifts 2-18 through 2-27 lie in a contingency area for repository development (BSC 2004 [DIRS 168370], Figure 2). This area has been designated as a contingency area because it is in the vicinity of the intensely fractured zone between Stations 42+00 and 51+50 of the ECRB Main Drift (Albin et al. 1997 [DIRS 101367], discussion of the Third Domain on pages 69-72). Special mining procedures may be required for tunnel excavation and ground support in this area because of the ground conditions, and the utility of this emplacement area will be determined during repository development. Given the uncertainties in the use of the contingency area at this time, it is reasonable to exclude it from consideration in TSPA-LA.

6.7.2.2 Faulting Other Than at Known Faults

During a major seismic event, faulting could occur not only coincident with the location of well characterized, known faults, but also elsewhere in the repository. In characterizing the potential magnitude of fault displacement elsewhere in the repository (see Section 6.7.3), rock conditions ranging from intact rock to the presence of existing small faults with about 2 meters of cumulative offset are considered. As is discussed in Section 6.7.3, the frequency of significant fault displacement (>10 cm) is low, even for the most extreme events with exceedance frequency of 10^{-8} per year, except where an existing fault is located with cumulative offset of about 2 meters. However, the exact location and number of such small faults is not known because they are not readily identified through surface mapping. Thus, it is necessary to estimate the density of such small faults based on either existing site data or natural analogues.

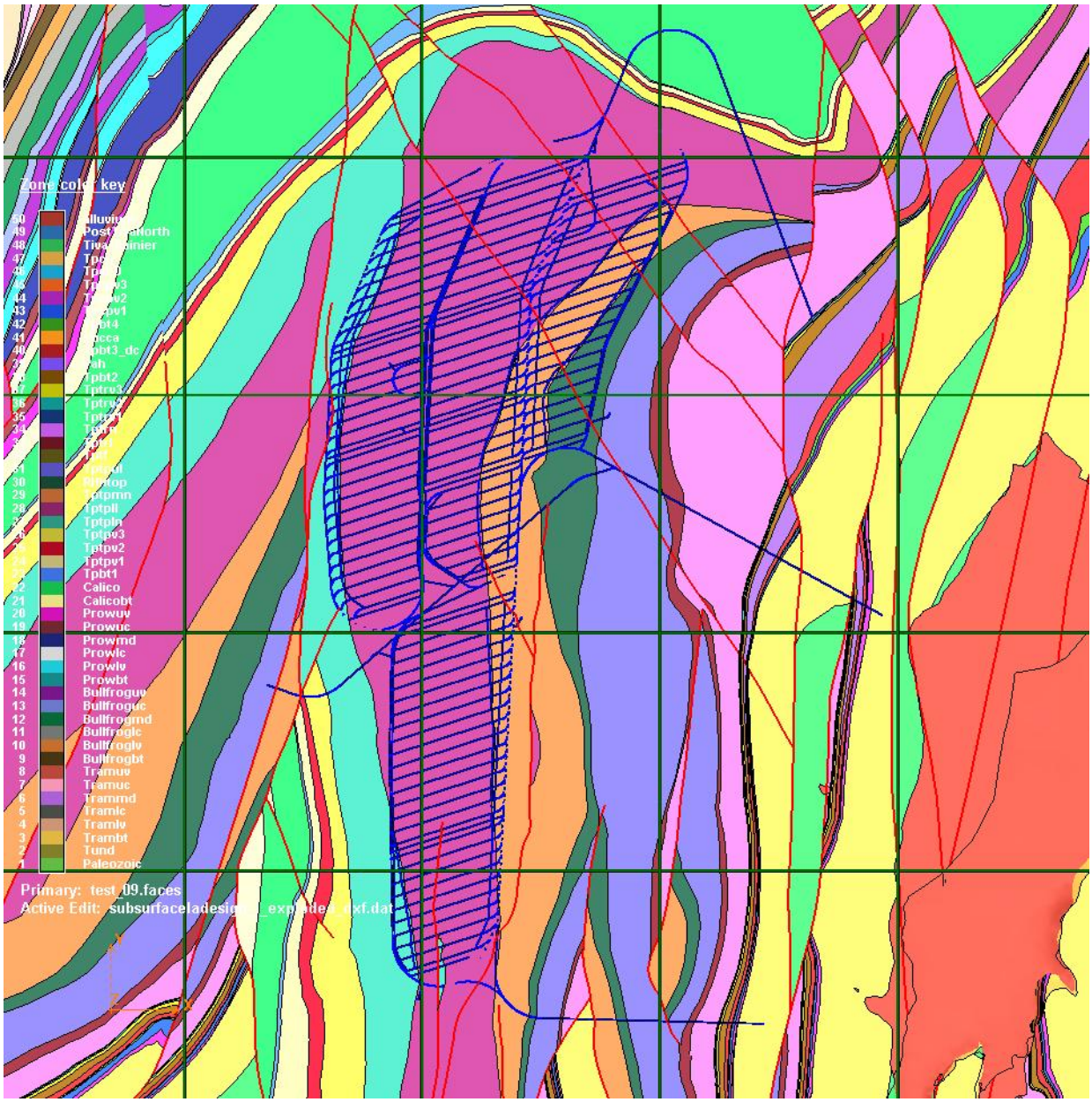

Source: DTN: MO0012MWDGFM02.002 [DIRS 153777].

Figure 6.7-2. Overlay of Known Fault Traces with Emplacement Drifts and Rock Type

Table 6.7-4. Intersections of Known Faults with Emplacement Drifts

Fault Designator	Tunnel Intersections in Lithophysal† Zones	Tunnel Intersections in Nonlithophysal[a] Zones
Sundance fault	1-6	1-8
	1-7	2-1
Drill Hole Wash fault	4-1	3-10 E
	4-2	3-11 E
	3-4 W	3-12 E
	3-5 W	-
	3-6 W	-
	3-7 W	-
	3-8 W	-
	3-9 W	-
	3-13E	
	3-14 E	-
	3-15 E	-
	3-16 E	-
	3-17 E	-
Pagany Wash fault	3-1 W	3-5 E
	3-1 E	3-6 E
	3-2 E	3-7 E
	3-3 E	-
	3-4 E	-
Sever Wash fault	3-2 E	-
	3-3 E	-

[a] Lithophysal zones are the RHHtop (top of Tptpul) and Tptpll strata in (BSC 2004 [DIRS 168370], Table 8); Nonlithophysal zones are the Tptpmn and Tptpln strata in (BSC 2004 [DIRS 168370], Table 8).

Sources: BSC 2004 [DIRS 168180], Table 9 for drift intersections with Sever Wash, Drill Hole Wash, and Pagany Wash faults.

DTN: 0012MWDGFM02.002 [DIRS 153777] for drift intersections with Sundance fault and for locations of geologic units relative to fault traces and emplacement drifts. See Table 4-1 for the relevant Earthvision files.

BSC 2004 [DIRS 164519], Figure 1 for panel and drift nomenclature.

One means of quantifying the likelihood of such smaller faults is through use of the data obtained from the characterization of the ECRB Cross-Drift (Mongano et al. 1999 [DIRS 149850], pp. 51 to 59). The ECRB Cross-Drift extends through the repository footprint near its north/south midpoint and spans the approximate east/west extent of the repository. Over the length of this tunnel, three small faults were identified with cumulative displacement of between about one meter and a few meters. This is thought to be generally representative of the density of small faults throughout the repository, so one can make an estimate of the number of such small faults that might intersect the emplacement drifts. In reviewing the repository layout (BSC 2004 [DIRS 164519], Figure 1), it can be seen that there are 57 emplacement drifts that span the entire north to south extent of the repository (designated 3-1 W through 3-22 W, 1-1 through 1-8, and 2-1 through 2-27). While in several cases these tunnels are much shorter than the ECRB Cross-Drift, for abstraction purposes the three unknown small faults intersect the

repository footprint along its entire north to south extent. Emplacement drifts 2-18 through 2-27 lie in the contingency area (BSC 2004 [DIRS 168370], Figure 2), in the vicinity of an intensely fractured zone (Albin et al. 1997 [DIRS 101367], discussion of the Third Domain on pages 69-2), and their development and use in the repository is uncertain at this time. Without drifts 2-18 through 2-27, there are a total of 47 tunnels and 141 locations (47 times 3) where small faults intersect the emplacement drifts.

Since the exact location of these potential faults is unknown, one cannot determine with certainty whether they would intersect the emplacement drifts in the lithophysal zones or not. To estimate the fraction of intersections corresponding to lithophysal zones, we use the fact that the estimated fraction of the overall repository in the lithophysal zone is 0.85, based on the emplacement areas in the upper lithophysal zone, Tptpul, and in the lower lithophysal zone, Tptpll[15]. This fractional area is applied to the 141 small fault intersections to get a probability-weighted distribution of fault intersections versus rock stratigraphy. The result is 119.85 small fault intersections with drifts in lithophysal zones and 21.15 small fault intersections with drifts in nonlithophysal zones.

6.7.3 Fault Displacement Hazards

Magnitudes of fault displacement along two of the known faults (Sundance and Drill Hole Wash) as a function of probability are obtained from *Probabilistic Seismic Hazard Analyses for Fault Displacement and Vibratory Ground Motion at Yucca Mountain, Nevada* (CRWMS M&O 1998 [DIRS 103731]; DTN: MO0401MWDRPSHA.000 [DIRS 166962]). In Section 8 of that document, the DOE has developed fault displacement hazard curves for fifteen faulting conditions mapped within the immediate vicinity of Yucca Mountain. Mean fault displacement hazard curves are used in all the following analyses. The faulting conditions relevant to this abstraction are as follows:

- Site 2 - Solitario Canyon fault
- Site 3 - Drill Hole Wash fault
- Site 4 - Ghost Dance fault
- Site 5 - Sundance fault
- Site 7 - A generic location within the repository, approximately 100 meters east of the Solitario Canyon fault. The ground conditions at the generic location include intact rock (7d), a hypothetical fracture with no cumulative displacement (7c), a hypothetical shear with 10 cm of offset (7b), and a hypothetical small fault with 2 meter offset (7a).
- Site 8 - A generic location within the repository, midway between the Solitario Canyon fault and the Ghost Dance fault. The ground conditions at the generic location include intact rock (8d), a hypothetical fracture with no cumulative displacement (8c), a hypothetical shear with 10 cm of offset (8b), and a hypothetical small fault with 2 meter offset (8a).

[15] The fraction of the repository in the Tptpul and Tptpll = (224,398 m^2 + 4,013,268 m^2)/(4,983,152 m^2) = 0.85, based on the data in (BSC 2004 [DIRS 168370], Table 8).

Four known faults intersect the emplacement areas of the repository. These four faults are the Drill Hole Wash fault, the Sundance fault, the Pagany Wash fault, and the Sever Wash fault. It is assumed that displacements on the Pagany Wash and Sever Wash faults are identical to those on the Drill Hole Wash fault (Assumption 5.2).

Generic locations identified as Site 7 and Site 8 apply throughout the repository. Locations 7a and/or 8a correspond to small hypothetical faults with about 2 meter offset. There are 141 intersections of these small faults with the emplacement drifts, based on the estimate in Section 6.7.2.2.

Table 6.7-5 provides the displacement values from the mean hazard curves as a function of the mean annual exceedance frequency (or probability) (DTN: MO0401MWDRPSHA.000 [DIRS 166962], data files associated with sites 3, 5, 7a-7d and 8a-8d are identified in Table 4-1 of this report). The first and third faults (Solitario Canyon and Ghost Dance, with fault displacement hazards defined by CRWMS M&O 1998 [DIRS 103731], Figures 8-3 and 8-5) in Table 6.7-58 are adjacent to the repository block and are not considered further because no waste packages lie on these faults. Locations 7 and 8 have essentially the same estimated hazard curves and fault displacements relative to the accuracy of the results in *Probabilistic Seismic Hazard Analyses for Fault Displacement and Vibratory Ground Motion at Yucca Mountain, Nevada* (CRWMS M&O 1998 [DIRS 103731]; DTN: MO0401MWDRPSHA.000 [DIRS 166962]). Thus, this analysis does not distinguish between Sites 7a and 8a for estimating the consequences to waste packages that lie on these faults.

6.7.4 Consequence for the Waste Packages

A comparison of Table 6.7-5 with Table 6.7-3 shows that no waste package would be damaged by even the most extreme events with exceedance frequency of 10^{-8} per year at locations 7a, 7b, 7c, 8a, 8b, and 8c. The waste packages will survive these events because the maximum displacement at these sites, 9 cm = 90 mm, is less than the available clearances in Table 6.7-3. However, several of the waste package designs could potentially fail due to fault displacement for hazards near the 10^{-8} per year level if they are directly over one of the four known faults (Drill Hole Wash, Sundance, Pagany Wash, and Sever Wash) intersecting the emplacement drifts. Further, the defense high-level radioactive waste (DHLW) waste packages could potentially fail when placed over the small hypothetical faults at Sites 7a and 8a. Thus, the frequency of waste package failure at a given fault location is a function of the clearance for the specific type of waste package emplaced there.

Waste package distribution by type is available in the design basis inventory (BSC 2004 [DIRS 169472], Table 11). This inventory is repeated in Table 6.7-6, along with the waste package dimensions. *D&E/PA/C IED Typical Waste Package Components Assembly* (BSC 2004 [DIRS 169472], Table 1), the source document for the waste package dimensions, does not provide information for the 5 DHLW Long/1 DOE SNF Short or the 5 DHLW Long Only waste package configurations. This is because these two configurations use the same waste package as the 5 DHLW Long/1 DOE SNF Long configuration with different assemblies loaded. Thus, the waste package exterior dimensions are the same for all three configurations.

Table 6.7-5. Fault Displacement from Mean Hazard Curves

	Mean Annual Exceedance Frequency (1/yr)				
	10^{-4} [b]	10^{-5} [b]	10^{-6} [c]	10^{-7} [c]	10^{-8} [c]
Site Number and Fault Name	**Displacement (cm)**				
2 - Solitario Canyon	<0.1	32.0	190	500	>1000
3 - Drill Hole Wash [a]	<0.1	<0.1	17	80	240
4 - Ghost Dance	<0.1	<0.1	13	58	160
5 - Sundance	<0.1	<0.1	6	42	~145
7a - small fault with 2-m offset	<0.1	<0.1	2	20	~75
7b - shear with 10-cm offset	<0.1	<0.1	1	6	9
7c - fracture with no displacement	<0.1	<0.1	0.1	<1	<1
7d - intact rock [c]	<0.1	<0.1	<0.1	<0.1	<0.1
8a - small fault with 2-m offset	<0.1	<0.1	2	20	~75
8b - shear with 10-cm offset	<0.1	<0.1	1	6	9
8c - fracture with no displacement	<0.1	<0.1	0.1	<1	<1
8d - intact rock [c]	<0.1	<0.1	<0.1	<0.1	<0.1

DTN: MO0401MWDRPSHA.000 [DIRS 166962]; data files associated with sites 3, 5, 7a-7d and 8a-8d are listed in Table 4-1 of this report; data for sites 2 and 4 located in CRWMS M&O 1998 [DIRS 103731], Figures 8-3 and 8-5, respectively.

[a] Also representative of Pagany Wash and Sever Wash faults.

[b] See DTN: MO0401MWDRPSHA.000 [DIRS 166962] for displacement hazards at Sites 3, 5, 7a-c and 8a-c for the 10-4 and 10-5 per year annual exceedance frequencies. See also CRWMS M&O 1998 [DIRS 103731], Table 8-1 for displacement hazards at 10-4 and 10-5 annual exceedance frequencies.

[c] See DTN: MO0401MWDRPSHA.000 [DIRS 166962] data files associated with Sites 3, 5, 7a-c and 8a-c are listed in Table 4-1 of this report; data for Sites 2 and 4 located in CRWMS M&O 1998 [DIRS 103731], Figures 8-3 and 8-5, respectively. Data for Sites 7d and 8d are inferred from (CRWMS M&O 1998 [DIRS 103731] Section 8.2.1, first paragraph), which indicates that displacements at Sites 7d and 8d are below 0.1 cm down to 10-8 per year annual exceedance frequency.

Table 6.7-6. Design Basis Waste Package Dimensions and Inventory

Waste Package Configuration	Waste Package Length (m)	Waste Package Diameter (m)	Nominal Quantity
21-PWR with Absorber Plates	5.0244	1.6370	4299
21-PWR with Control Rods	5.0244	1.6370	95
12-PWR with Absorber Plates - Long	5.5604	1.3132	163
44-BWR with Absorber Plates	5.0244	1.6751	2831
24-BWR with Absorber Plates	5.0244	1.2941	84
5 DHLW Short/1 DOE SNF - Short	3.4528	2.0447	1147
5 DHLW Long/1 DOE SNF - Long	5.0594	2.0447	1406
5 DHLW Long/1 DOE SNF - Short	5.0594	2.0447	31
5 HLW Long Only	5.0594	2.0447	679

Table 6.7-6. Design Basis Waste Package Dimensions and Inventory (Continued)

Waste Package Configuration	Waste Package Length (m)	Waste Package Diameter (m)	Nominal Quantity
2-MCO/2-HLW	5.0594	1.7494	149
Naval-Short	5.2022	1.8637	144
Naval-Long	5.8374	1.8637	156

Sources: BSC 2004 [DIRS 169472], Table 1 for nominal length; outside diameter of outer barrier defined by drawings referenced in BSC 2004 [DIRS 169472], Table 1.

BSC 2004 [DIRS 169472], Table 11 for nominal quantity.

NOTES: The diameter of the HLW packages is taken to be that of the DHLW packages in Table 6.7-3.

The length of the DHLW Short package is taken to be that of the 5 DHLW/DOE SNF - Short package in Table 6.7-3.

The length of the DHLW Long and HLW Long packages is taken to be that of the 5 DHLW/DOE SNF - Long package in Table 6.7-3.

BWR = boiling water reactor; DHLW = defense high-level radioactive waste; PWR = pressurized water reactor; SNF = spent nuclear fuel; MCO = multicanister overpack

To simplify the analysis, the inventory of waste packages is split into four groups. Waste packages of similar design (similar waste type) are grouped together, and the maximum diameter for the waste package types in each group is conservatively assigned to the group. These groupings are chosen to facilitate consequence assessment for the waste package groupings in TSPA-LA. The four groupings are as follows.

- PWR: includes 21-PWR with absorber plates, 21-PWR with control rods, and the 12-PWR Long with absorber plates.
- BWR: includes 44-BWR with absorber plates and 24-BWR with absorber plates.
- Naval: includes Naval-Long and Naval-Short.
- HLW: includes 5 DHLW/1 DOE SNF – Short, 5 DHLW/1 DOE SNF – Long, and all other high-level radioactive waste (HLW) designs.

The waste package designs in bold letters are the ones with the largest diameter in the group, and thus are chosen to represent the diameter for all packages in that group. While the inclusion of the 12-PWR design with the PWR group, the 24-BWR design with the BWR group, and the 2-multicanister overpack/2-DHLW design with the HLW group conservatively accounts for the likelihood of failure for those waste package designs (by overestimating diameter), the impact of this approximation is small because in each case the number of such packages is small relative to the total number of packages in the group.

The percentage of the inventory of the waste packages for each group is calculated based on the total length of that waste package type versus the total length of all emplaced waste packages. Length is the appropriate parameter here because it more accurately represents the probability that a waste package is directly on a fault. These results are shown in Table 6.7-7. The average length per package type is shown for information only. It is used to calculate the fraction of waste packages by waste package type.

Table 6.7-7. Parameters for Simplified Groups of Waste Packages

Waste Package Group	Effective Waste Package Length[c], L_{eff} (m)	Maximum Waste Package Diameter, D_{max} (m)	Waste Package Surface Area [a] (m^2)	Nominal Quantity (-)	Total Waste Package Length for Group [b] (m)	Fraction of Waste Packages (% of Total Length)
PWR	5.0436	1.6370	30.15	4557	22984	42.0
BWR	5.0244	1.6751	30.85	2915	14646	26.8
Naval	5.5325	1.8637	37.85	300	1660	3.0
HLW	4.5193	2.0447	35.60	3412	15420	28.2

NOTE: (-)=dimensionless.

[a] Surface Area = $(\pi/2)(D_{max})^2 + \pi D_{max} L_{eff}$.

[b] Total Waste Package Length for Group= $\Sigma(\text{Length})_i \times (\text{Nominal Quantity})_i$ summed over the package types in each group, based on the lengths and nominal quantities in Table 6.7-6.

[c] Effective Waste Package Length = L_{eff} = Total Length / Nominal Quantity.

PWR = pressurized water reactor, BWR = boiling water reactor

Using the maximum waste package diameter in Table 6.7-7 and the calculated maximum fault displacements before the waste package is pinned in Table 6.7-3, the following maximum fault displacement values (to cause waste package damage) are used in the analysis.

A determination of waste package failure is made by comparing the maximum allowable displacements in Table 6.7-8 with the fault displacement hazard curve in Table 6.7-5. As a reminder, the Solitario Canyon and main Ghost Dance faults are not included in this analysis because these faults lie outside the emplacement areas of the repository, and the western splay off the main Ghost Dance fault is not included in this analysis because its development and use in the vicinity of an intensely fractured zone is uncertain at this time.

Consider the case where tunnel collapse has not occurred. As can be seen from Table 6.7-8, the HLW waste package group is subject to potential failure when the fault displacement exceeds the maximum allowable displacement of 2,479 mm. However, as can be seen from Table 6.7-5, the maximum fault displacement for any of the faults that intersect the emplacement drifts is 240 cm = 2,400 mm, which corresponds to a 10^{-8} fault displacement along the Drill Hole Wash fault (the Solitario Canyon fault has larger displacements, but no drifts in the current repository layout intersect this known fault). Thus, since the maximum fault displacement is less than the allowable displacement of 2,479 mm, no damage to EBS components would be predicted without tunnel collapse. The same conclusion is valid for the other waste package designs, with even greater margin.

Table 6.7-8. Maximum Allowable Fault Displacements Before a Waste Package Group Is Pinned

Waste Package Group	Maximum Allowable Displacement With Tunnel Collapse (mm)	Maximum Allowable Displacement Without Tunnel Collapse (mm)
PWR	1079	2887
BWR	1041	2849
Naval	852	2660
HLW	671	2479

BWR = boiling water reactor; PWR = pressurized water reactor, HLW = high-level radioactive waste.

Now consider the case where tunnel collapse has occurred, as is expected in the lower lithophysal zones for seismic hazards with an annual exceedance frequency of 10^{-6} or less. First, it is evident from a comparison of Tables 6.7-8 and 6.7-5 that all BWR, PWR, and Naval waste packages are predicted to survive a fault displacement event for Sites 7a and 8a, even in the lower lithophysal zones. The maximum fault displacement in Table 6.7-5 for Sites 7 and 8 is 75 cm = 750 mm, less than the allowable fault displacement of 852 mm for the Naval group with drift collapse in the lower lithophysal units. Again, the same conclusion is valid for the BWR and PWR waste package designs, with even greater margin.

However, at mean annual exceedance frequencies between 10^{-7} per year and 10^{-8} per year, waste package failure may occur for any of the waste packages placed directly over the four known faults intersecting the emplacement drifts, as well as for the HLW waste package group placed over faults characterized by location 7a and 8a. In those cases, the fault displacement values in Table 6.7-5 exceed the maximum allowable displacements summarized in Table 6.7-8 for the case of drift collapse.

The probability of a fault displacement event severe enough to cause waste package failure is a function of both the specific fault (different fault displacements for a given probability) as well as the specific waste package design (different allowable displacements). The exceedance frequency is equal to the exceedance probability for values much less than one per year. To determine the probability associated with a fault displacement event severe enough to cause waste package damage, the fault displacement hazard curves from the *Probabilistic Seismic Hazard Analyses for Fault Displacement and Vibratory Ground Motion at Yucca Mountain, Nevada* (MO0401MWDRPSHA.000 [DIRS 166962]) are used. The relevant information is provided in file: *./displ/tot-haz/s3.frac_mean.gz* of the DTN for the Drill Hole Wash fault, in file: *./displ/tot_haz/s5.frac_mean.gz* for the Sundance fault, and in files: *./displ/tot-haz/s7a.frac_mean.gz* and *./displ/tot-haz/s8a.frac_mean.gz* of the DTN for locations 7a and 8a. These curves show the predicted fault displacement as a function of probability of the event (a graphical presentation of the results in Table 6.7-5). Using the maximum allowable displacements from Table 6.7-8 (for each waste package group), the associated event probabilities are determined from the hazard curves in DTN: MO0401MWDRPSHA.000 [DIRS 166962]. The resulting fault exceedance probabilities that would cause waste package failure are summarized in Table 6.7-9. As previously stated, the Pagany Wash and Sever Wash faults are represented by the Drill Hole Wash fault (Assumption 5.2). Again, these results only apply to the lower lithophysal zone, which is predicted to collapse from seismic hazards at these annual exceedance frequencies.

As expected, the highest frequency fault displacement events leading to waste package failure are associated with the HLW waste packages, which have the largest diameter.

Table 6.7-9. Fault Exceedance Frequencies (per year) That Cause Failure in the Lower Lithophysal Zone[a]

Fault	PWR	BWR	Naval	HLW
Sundance	$< 2\times10^{-8}$	$< 2\times10^{-8}$	$< 3\times10^{-8}$	$< 5\times10^{-8}$
Drill Hole Wash	$< 5\times10^{-8}$	$< 5\times10^{-8}$	$< 1\times10^{-7}$	$< 2\times10^{-7}$
Pagany Wash	$< 5\times10^{-8}$	$< 5\times10^{-8}$	$< 1\times10^{-7}$	$< 2\times10^{-7}$
Sever Wash	$< 5\times10^{-8}$	$< 5\times10^{-8}$	$< 1\times10^{-7}$	$< 2\times10^{-7}$
7a/8a[b]	N/A	N/A	N/A	$< 2\times10^{-8}$

[a] Tunnels in the lithophysal zones are predicted to collapse from ground motions at these mean annual exceedance frequencies, so the maximum allowable displacement is based on Table 6.7-8 with tunnel collapse and Table 6.7-5 for fault displacement as a function of exceedance frequency.

[b] The value of 2×10^{-8} is conservative for the hazard curve at sites 7a/8a. The plotted hazard curves at Sites 7a/8a (CRWMS M&O 1998 [DIRS 103731], Figures 8-8 and 8-11) indicate exceedance frequency values of about 1.2×10^{-8} and 1.4×10^{-8} corresponding to the allowable displacement of 671 mm for the HLW group. These exceedance frequencies are almost at the low probability cutoff for the scenario. The value entered in Table 6.7-9 has been conservatively rounded up to 2×10^{-8}.

BWR = boiling water reactor, PWR = pressurized water reactor, HLW = high-level radioactive waste.

There are two locations where the Sundance fault intersects the emplacement drifts in the lower lithophysal zone (from Table 6.7-4), 20 locations where either the Drill Hole Wash, Pagany Wash, or Sever Wash faults intersect the emplacement drifts in the lower or upper lithophysal zones (Table 6.7-4), and 119.85 locations (probability-weighted) where additional small faults intersect the emplacement drifts in the lower lithophysal zone (Section 6.7.2.2). Combining this information with the probability of finding a particular waste package group at a given point in the repository (Table 6.7-7), an estimate can be made of the expected number of each type of waste package at the four known faults. This result is shown in Table 6.7-10. Note that the number of waste packages is not an integral number because it represents an average expectation of finding a particular waste package along a particular fault. The Pagany Wash, Sever Wash and Drill Hole Wash faults have been combined in Table 6.7-10 because they have the same fault displacement hazard curves.

Table 6.7-10. Expected Number of Waste Packages Emplaced on Faults in Lithophysal Zones

	PWR Group	BWR Group	Naval Group	HLW Group	Total
Sundance	0.84	0.54	0.06	0.56	2
Drill Hole Wash, etc.	8.40	5.35	0.61	5.64	20
7a/8a	50.3	32.1	3.64	33.8	119.85

NOTE: Total values are based on the spreadsheet in Appendix E. Sums of the contributions by fault are not exact because of round off.

BWR = boiling water reactor, PWR = pressurized water reactor, HLW = high-level radioactive waste.

6.7.5 Damage Abstraction for Fault Displacement

The expected number of waste package failures as a function of annual exceedance frequency is calculated by combining the results in Tables 6.7-9 and 6.7-10. These results are shown in Table 6.7-11. A spreadsheet with the details of this calculation is provided as Appendix E.

When a waste package fails by fault displacement, the damaged area on the waste package is determined by sampling a uniform distribution with a lower bound of 0 m^2 and an upper bound equal to the area of the waste package lid, as explained below. The area of the lid for the PWR, BWR, Naval, and HLW groups is 2.105 m^2, 2.204 m^2, 2.728 m^2 and 3.284 m^2, respectively, based on maximum waste package diameters of 1.637 m, 1.6751 m, 1.8637 m, and 2.0447 m in Table 6.7-7. For example, PWR group has a maximum diameter of 1.637 m, corresponding to a lid area of $\pi(1.637\ m)^2/4 = 2.105\ m^2$; similar calculations are performed for the other waste package groups. The total damaged area from a faulting event is based on the weighted sum of the damage to each type of waste package.

Table 6.7-11. Expected Waste Package Failures versus Annual Exceedance Frequency

Annual Exceedance Frequency (1/yr)	Expected Number of Waste Package Failures				
	PWR	BWR	Naval	HLW	Total
$> 2 \times 10^{-7}$	0	0	0	0	0
1×10^{-7} to 2×10^{-7}	0	0	0	5.64	5.64
5×10^{-8} to 1×10^{-7}	0	0	0.61	5.64	6.24
3×10^{-8} to 5×10^{-8}	8.40	5.35	0.61	6.20	20.56
2×10^{-8} to 3×10^{-8}	8.40	5.35	0.67	6.20	20.62
1×10^{-8} to 2×10^{-8}	9.24	5.89	0.67	39.98	55.78

NOTE: Total values are based on the spreadsheet in Appendix E. Sums of the contributions by waste package type are not exact because of round off.

BWR = boiling water reactor; PWR = pressurized water reactor, HLW = high-level radioactive waste.

The lower bound is appropriate for annual exceedance frequencies near 10^{-7} per year because a waste package that is minimally pinned from fault displacement should only have minor crimping with a very small damaged area. The upper bound is appropriate for a fault that shears a waste package near its lid. In this case, the lid welds have the potential to fracture, separating the lid from the package and potentially exposing the entire waste form to seepage and release. The use of a uniform distribution is appropriate here because reasonable upper and lower bounds can be defined and because the use of this type of distribution maintains the uncertainty in the damaged area for this abstraction.

When a waste package fails from fault displacement, the associated drip shield and fuel rod cladding also fail as barriers to flow and transport. A sheared drip shield will allow all seepage to pass through it for TSPA; that is, the damaged area is taken as the total surface area of the drip shield so there is no flux splitting (diversion of seepage) on the drip shield. Similarly, cladding becomes 100 percent perforated in response to a fault displacement that can shear a waste package. These damage abstractions for the drip shield and cladding represent conservative, bounding approximations, particularly for annual exceedance frequencies near 10^{-7} per year.

6.7.6 An Alternate Conceptual Model for Damage from Fault Displacement

The analysis of waste package failure due to fault displacement presented herein provides a basis for estimating the number of potentially damage-inducing faults that intersect the emplacement drifts. This analysis uses the known location of larger faults (e.g., Sundance fault, Drill Hole Wash fault, etc.) relative to the planned location of the emplacement drifts, as well as an estimate of the density of smaller-displacement faults based on the observed fault density along the exploratory tunnel. The maximum allowable fault displacement before waste package damage occurs was shown to vary between 671 mm and 1079 mm depending on waste package design (Table 6.7-8). Using this site-specific information, it is shown that there are 30 locations where known faults intersected the planned emplacement drifts (Table 6.7-4) plus an estimated 141 locations where unmapped faults could intersect the drifts (Section 6.7.2.2) for a total of 171 fault intersections. Of these, there are a maximum of 55.8 locations (probability weighted by waste package type and location within the repository footprint) that are calculated to cause waste package damage (Table 6.7-11) with an occurrence frequency between 2×10^{-7} per year and 10^{-8} per year.

As an alternate conceptual model, we consider work published in "Methodologies for the Evaluation of Faulting at Yucca Mountain, Nevada" (Waiting et al. 2003 [DIRS 164449]). This paper presents an assessment of the consequences of fault displacement at Yucca Mountain based on historical earthquake activity in the Western United States. Four historic rupture events were considered to arrive at a median value for fault rupture density (length of faulting per unit area of surface). A conservative median value of 20 km/km^2 was obtained from this analysis of the four events considered. Using this value, along with a representative angle of 50 degrees between the typical tunnel orientation and the orientation of the faults and an 80 meter drift spacing, the authors determined that there would be 191 waste package locations where a fault would intersect an emplacement drift at Yucca Mountain. This result compares favorably to the 171 fault intersections calculated in this report.

The specific analog event considered by Waiting et al. (2003 [DIRS 164449]), for purposes of quantification, was the Borah Peak earthquake from 1983. Prior analysis of this event had shown that the maximum displacement for the Borah Peak earthquake was 2.7 meters, with an average displacement of approximately 1 meter. Given the fact that the mean annual exceedance frequency for 1 meter of displacement at Yucca Mountain ranges from approximately 10^{-6}/yr for the Solitario Canyon fault to approximately 10^{-8}/yr for the Sundance fault, the probability-weighted number of waste package failures is calculated to be between 1.91×10^{-4} to 1.91×10^{-6}. It should be noted that the upper end of this range applies only to the Solitario Canyon fault. As discussed in Section 6.7.3, no drifts intersect the Solitario Canyon fault or the main Ghost Dance fault for the current repository footprint. The largest fault displacement would be expected to correspond to the Drill Hole Wash fault. The mean annual exceedance frequency for one meter of displacement for this fault is on the order of 10^{-7}/yr. Thus, the probability-weighted number of waste package failures would be between 1.91×10^{-5} to 1.91×10^{-6}.

The results presented in Table 6.7-11 are not stated in terms of probability-weighted number of waste package failures. Thus, a direct comparison with the results of the alternate model is not possible. However, it is straightforward to recast the Table 6.7-11 results in a compatible form. Considering the number of incremental waste packages that are calculated to fail within each probability range, the product of the annual exceedance frequency (using the upper end of the range) and the number of incremental waste packages calculated to fail represents the probability-weighted number of waste package failures for that exceedance interval. The sum of this result for all exceedance frequency ranges gives the equivalent total number of probability-weighted waste package failures. Table 6.7-12 presents the details of this calculation.

So the probability-weighted number of waste package failures for the model in this report is 2.61×10^{-6}. This value is within the range of results provided by the alternate conceptual model, 1.91×10^{-5} to 1.91×10^{-6}. Thus, the alternate conceptual model based on the use of analog data provides results that are consistent with the results of the model presented in this report for both the probability-weighted number of waste package failures and the number of fault intersections with the emplacement drifts. This comparison provides added confidence in the validity of the results presented herein.

Table 6.7-12. Calculation of Probability Weighted Waste Package Failures

Exceedance Frequency (Per Year)	# Incremental WP Failures	Probability Weighted WP Failures
2×10^{-7}	5.64	1.13×10^{-6}
1×10^{-7}	0.60	0.06×10^{-6}
5×10^{-8}	14.32	0.72×10^{-6}
3×10^{-8}	0.06	0.002×10^{-6}
2×10^{-8}	35.16	0.70×10^{-6}
Totals	**55.78**	**2.61×10^{-6}**

WP = waste package.

6.7.7 Final Abstraction for Damage from Fault Displacement

The seismic scenario class for TSPA-LA will use the abstraction described in Section 6.7.5 as the basis for damage to EBS components from fault displacement.

6.7.8 Failure by Waste Package Type for Criticality Studies

As noted in Section 6.7.4, the inventory of waste packages for the fault damage abstraction is divided into four groups: PWR, BWR, Naval, and HLW. While this grouping is convenient for TSPA, criticality analyses require a more detailed analysis of the potential for waste package failure by individual waste package type. This section applies the same methodology that is used for the fault damage abstraction to individual waste package types in support of criticality studies. This information is not used in TSPA-LA. Appendix E provides details of the calculations for Tables 6.7-13 through 6.7-17.

Tables 6.7-1 through 6.7-6 remain unchanged for the criticality analysis by waste package type. Table 6.7-7 is modified for 10 individual waste package types, as shown in Table 6.7-13.

Table 6.7-13. Parameters for Simplified Inventory for Criticality

Waste Package Group	Nominal Length (m)	Nominal Quantity (-)	Total Length for Package Type[a] (m)	Fraction of Waste Packages (% of Total Length)
21-PWR with Absorber Plates	5.0244	4299	21600.	39.48
21-PWR with Control Rods	5.0244	95	477.32	0.87
12-PWR with Absorber Plates - Long	5.5604	163	906.35	1.66
44-BWR with Absorber Plates	5.0244	2831	14224.	26.00
24-BWR with Absorber Plates	5.0244	84	422.05	0.77
5 DHLW Short/1 DOE SNF - Short	3.4528	1147	3960.4	7.24
5 DHLW/DOE – Long[b]	5.0594	2116	10706.	19.57
2-MCO/2-HLW	5.0594	149	753.85	1.38
Naval-Short	5.2022	144	749.12	1.37
Naval-Long	5.8374	156	910.63	1.66
TOTALS		11,184	54709.	100.00

Sources: BSC 2004 [DIRS 169472], Table 1 for nominal length; BSC 2004 [DIRS 169472], Table 11 for nominal quantity.

NOTE: (-)=dimensionless.

[a] Total Length for Package Type = (Nominal Length) × (Nominal Quantity), rounded to 5 significant figures.
[b] 5 DHLW-DOE Long Package represents three package types: 5 DHLW Long/1 DOE SNF – Long, 5 DHLW Long/1 DOE SNF – Short, the 5 HLW Long Only Package Types. The clearances for these three package types are identical because they have the same nominal length and outer diameter of outer shell (Table 6.7-7), so their damage from fault displacement is also identical.

BWR = boiling water reactor; DHLW = defense high-level radioactive waste; PWR = pressurized water reactor; SNF = spent nuclear fuel; MCO = multicanister overpack, DHLW = defense high-level radioactive waste, HLW = high-level radioactive waste, DOE = U.S. Department of Energy.

Table 6.7-14 presents the calculated maximum fault displacements before each waste package is pinned. This table is essentially identical with Table 6.7-3, although the 21-PWR waste package type has two entries, with absorber plates and with control rods, in Table 6.7-14, versus one entry in Table 6.7-3. The maximum allowable fault displacements in Table 6.7-14 are based on a collapsed tunnel because the fault displacements for the most severe event considered by TSPA are insufficient to pin a waste package when the emplacement drift does not collapse.

Table 6.7-14. Maximum Allowable Displacement With Tunnel Collapse Before Waste Package is Pinned

Package Type	Maximum Allowable Displacement With Tunnel Collapse (mm)
21-PWR with Absorber Plates	1079
21-PWR with Control Rods	1079
12-PWR with Absorber Plates - Long	1403
44-BWR with Absorber Plates	1041
24-BWR with Absorber Plates	1422
5 DHLW Short/1 DOE SNF - Short	671
5 DHLW/DOE - Long	671
2-MCO/2-HLW	967
Naval-Short	852
Naval-Long	852

NOTE: Maximum allowable displacement with tunnel collapse is the clearance without pallet in Table 6.7-2. Clearance without pallet is calculated in Table 6.7-1 as the interior height of the drip shield minus the outside diameter of the package outer barrier, rounded to 4 significant figures.

BWR = boiling water reactor; PWR = pressurized water reactor; MCO = multicanister overpack, HLW = high-level radioactive waste, SNF = spent nuclear fuel.

A comparison of the maximum allowable displacements in Table 6.7-14 with the fault displacement hazard curves provides a basis for determining failure of the different waste package types for the faults within the repository block. The Solitario Canyon and main Ghost Dance faults are not included in this analysis because these faults lie outside the emplacement areas of the repository, and the western splay off the main Ghost Dance fault is not included in this analysis because its development in the vicinity of an intensely fractured zone is uncertain at this time.

Waste package failure may occur for any of the waste packages placed directly over the four known faults intersecting the emplacement drifts, as well as for the HLW waste package group placed over faults characterized by location 7a and 8a. The frequency of a fault displacement event severe enough to cause waste package failure is a function of both the specific fault (different fault displacements for a given exceedance frequency) as well as the specific waste package type (different allowable displacements). The fault displacement hazard curves from the *Probabilistic Seismic Hazard Analyses for Fault Displacement and Vibratory Ground Motion at Yucca Mountain, Nevada* (MO0401MWDRPSHA.000 [DIRS 166962]) are used to determine the annual exceedance frequency associated with a displacement severe enough to cause damage (see calculations in Appendix E). The fault displacement hazard curves are provided in file: *./displ/tot-haz/s3.frac_mean.gz* for the Drill Hole Wash fault, in file: *./displ/tot_haz/s5.frac_mean.gz* for the Sundance fault, and in files: *./displ/tot_haz/s7a.frac_mean.gz* and *./displ/tot-haz/s8a.frac_mean.gz* for locations 7a and 8a. These curves show the predicted fault displacement as a function of exceedance frequency. Using the maximum allowable displacements from Table 6.7-14, the resulting fault exceedance probabilities that would cause waste package failure are summarized in Table 6.7-15. The Pagany Wash and Sever Wash faults are represented by the Drill Hole Wash fault (Assumption 5.2).

Table 6.7-15. Fault Exceedance Frequencies (Per Year) That Cause Failure in Lithophysal Zones[a]

Package Type	Sundance	Drill Hole Wash, Pagany Wash, & Sever Wash	7a/8a[b]
21-PWR with Absorber Plates	$< 1.8\times10^{-8}$	$< 5.2\times10^{-8}$	N/A[b]
21-PWR with Control Rods	$< 1.8\times10^{-8}$	$< 5.2\times10^{-8}$	N/A
12-PWR with Absorber Plates - Long	$< 1.1\times10^{-8}$	$< 3.1\times10^{-8}$	N/A
44-BWR with Absorber Plates	$< 2.0\times10^{-8}$	$< 5.5\times10^{-8}$	N/A
24-BWR with Absorber Plates	$< 1.1\times10^{-8}$	$< 3.1\times10^{-8}$	N/A
5 DHLW Short/1 DOE SNF - Short	$< 4.3\times10^{-8}$	$< 1.3\times10^{-8}$	$< 1.4\text{x}10^{-8}$
5 DHLW/DOE - Long	$< 4.3\times10^{-8}$	$< 1.3\times10^{-8}$	$< 1.4\text{x}10^{-8}$
2-MCO/2-HLW	$< 2.3\times10^{-8}$	$< 6.4\times10^{-8}$	N/A
Naval-Short	$< 2.8\times10^{-8}$	$< 7.9\times10^{-8}$	N/A
Naval-Long	$< 2.8\times10^{-8}$	$< 7.9\times10^{-8}$	N/A

[a] Tunnels in lithophysal zones are predicted to collapse from ground motions at these mean annual exceedance frequencies, so the maximum allowable displacement is based on Table 6.7-14 with tunnel collapse. All exceedance frequencies are rounded up from the exact interpolated values in Appendix E.

[b] Exceedance frequency based on the maximum value for Sites 7a and 8a. N/A indicates that the interpolated values for exceedance frequency are less than 1×10^{-8} per year and are excluded from the analysis.

BWR = boiling water reactor; DHLW = defense high-level radioactive waste; PWR = pressurized water reactor; MCO = multicanister overpack; DOE = U.S. Department of Energy; HLW = high-level radioactive waste.

There are two locations where the Sundance fault intersects the emplacement drifts in the lithophysal zones (from Table 6.7-4), 20 locations where either the Drill Hole Wash, Pagany Wash, or Sever Wash faults intersect the emplacement drifts in the lithophysal zones (Table 6.7-4), and 119.85 locations (probability-weighted) where additional small faults intersect the emplacement drifts in the lower lithophysal zone (Section 6.7.2.2). Combining this information with the probability of finding a particular waste package group at a given point in the repository (see last column of Table 6.7-13), the expected number of each type of waste package found at the four known faults is shown in Table 6.7-16. The number of intersections for locations 7a and 8a has been rounded up to 120 in Table 6.7-16.

The expected number of waste package failures as a function of annual exceedance frequency can be calculated by combining the results in Tables 6.7-15 and 6.7-16. These results are shown in Table 6.7-17.

Table 6.7-16. Expected Number of Waste Package Types Emplaced on Faults

Package Type	Sundance	Drill Hole Wash, Pagany Wash, & Sever Wash	7a/8a
21-PWR with Absorber Plates	0.7896	7.8962	47.3774
21-PWR with Control Rods	0.0174	0.1745	1.0470
12-PWR with Absorber Plates - Long	0.0331	0.3313	1.9880
44-BWR with Absorber Plates	0.5200	5.1999	31.1992
24-BWR with Absorber Plates	0.0154	0.1543	0.9257

Table 6.7-16. Expected Number of Waste Package Types Emplaced on Faults (Continued)

Package Type	Sundance	Drill Hole Wash, Pagany Wash, & Sever Wash	7a/8a
5 DHLW Short/1 DOE SNF - Short	0.1448	1.4478	8.6867
5 DHLW/DOE - Long	0.3914	3.9137	23.4820
2-MCO/2-HLW	0.0276	0.2756	1.6535
Naval-Short	0.0274	0.2739	1.6431
Naval-Long	0.0333	0.3329	1.9974
TOTALS	2.0000	20.0000	120.00

Table 6.7-17. Failure of Waste Package Types by Annual Exceedance Probability

Package Type	Exceedance Frequency Range (Per Year)					
	$> 2\times10^{-7}$	1×10^{-7} - 2×10^{-7}	6×10^{-8} - 1×10^{-7}	4×10^{-7} - 6×10^{-8}	2×10^{-8} - 4×10^{-8}	1×10^{-8} - 2×10^{-8}
21-PWR with Absorber Plates	0	0	0	7.90	7.90	8.69
21-PWR with Control Rods	0	0	0	0.17	0.17	0.19
12-PWR with Absorber Plates - Long	0	0	0	0	0.33	0.36
44-BWR with Absorber Plates	0	0	0	5.20	5.20	5.72
24-BWR with Absorber Plates	0	0	0	0	0.15	0.17
5 DHLW Short/1 DOE SNF - Short	0	1.45	1.45	1.59	1.59	10.28
5 DHLW/DOE - Long	0	3.91	3.91	4.31	4.31	27.79
2-MCO/2-HLW	0	0	0.28	0.28	0.30	0.30
Naval-Short	0	0	0.27	0.27	0.30	0.30
Naval-Long	0	0	0.33	0.33	0.37	0.37
TOTALS	0	5.36	6.24	20.05	20.62	54.17

DHLW = defense high-level radioactive waste; MCO = multicanister overpack, DOE = U.S. Department of Energy, HLW = high-level radioactive waste.

6.8 POST-SEISMIC CHANGES IN THE LOCAL ENVIRONMENT

A large seismic event, involving both vibratory ground motion and/or fault displacement, has the potential to change the local environment around the emplacement drifts. The most obvious physical change is that the emplacement drifts in the lithophysal zone are predicted to collapse at the 2.0 m/s PGV ground motion level (BSC 2004 [DIRS 166107], Section 6.4.2.2.2), and by

inference at greater ground motion levels. Drift collapse alters the shape of the drift and fills it with a natural backfill, resulting in the following potential process-level changes in and around the engineered barrier system:

- Seepage may increase because an irregular drift shape reduces the effectiveness of the drift wall as a capillary barrier and because of a loosening of the fractures around the drift.

- Temperature of the drip shield and waste package may increase relative to an unfilled drift because the backfill provides an insulating blanket on top of the drip shield.

- Localized corrosion may increase because of increased temperature and because of rock and water contact with the drip shield or waste package.

- The dissolution rates of CSNF and HLW glass increase with temperature.

6.8.1 Change in Seepage Flux into the Drifts

A change in the seepage flux into the emplacement drifts in the lithophysal zones is being incorporated into the seismic abstractions for TSPA-LA. The seepage into the emplacement drifts in the lithophysal zones is determined in an analogous manner as ambient seepage by using the seepage table for collapsed drifts as provided in DTN: LB0307SEEPDRCL.002 [DIRS 164337], file: *ResponseSurfaceSMPACollapsedDrift.dat*. This table is invoked after a seismic event occurs, provided the PGV amplitude is large enough to collapse the drifts. The seepage fluxes provided in this table are considered conservative but not unrealistic.

In addition to switching to the seepage table for collapsed drifts, a temperature constraint is also applied to the seepage flux after drift collapse in the lithophysal zones. Specifically, the seepage onto the waste package is set to zero for the period of above-boiling temperatures by using a 100ºC threshold temperature at the waste package surface. This constraint implies that seepage can enter the drift and be diverted through the rubble to the invert beneath the waste package, but cannot contact the waste package surface until the waste package surface temperature drops below 100ºC. This threshold temperature is based on a sensitivity study of seepage arrival times at the drip shield crown for a collapsed drift that is filled with rubble (BSC 2004 [DIRS 169565], Section 6.3.7.3 and Table 6.3-44). This study considers rubble with high and low values of thermal conductivity and seepage magnitudes that vary between 100 liters/year/waste package and 10,000 liters/year/waste package. The temperature threshold of 100°C is a reasonable upper bound to the ranges of waste package temperature that significantly delay the arrival of seepage at the drip shield crown. A 100°C temperature is therefore an appropriate threshold to limit the presence of liquid seepage in a rubble-filled drift.

For TSPA-LA, all ground motions with PGV equal to or greater than 0.384 m/s will be considered large enough to collapse the drifts in the lithophysal zones. This threshold for change is consistent with the fact that tunnels in the lithophysal zone do not collapse for the 0.19 m/s PGV level of ground motion (BSC 2004 [DIRS 166107], Section 6.4.2.2.1). Recent rockfall calculations have determined that a PGV of 2 m/s is a more reasonable threshold for drift

collapse in the lithophysal zones (BSC 2004 [DIRS 166107] Section 6.4.2.2.2, 4th bullet under subheading 'Discussion'). The seismic scenario class continues to use the conservative value of 0.384 m/s because the technical basis for the 2.0 m/s threshold level was established after the start of TSPA-LA model development.

There is no change in the seepage flux into the emplacement drifts in the nonlithophysal zones after a seismic event. This is appropriate for two reasons. First, the seepage abstraction already includes an enhancement factor for limited collapse of the emplacement drifts, such as when large rock blocks are ejected without catastrophic tunnel collapse. Second, complete drift collapse is not observed for ground motion amplitudes at the 5.35 m/s PGV level in the nonlithophysal rock (BSC 2004 [DIRS 166107], Section 6.3.1.6.4). Since the 5.35 m/s PGV level is beyond the bounding PGV values of 1.5 m/s to 5 m/s that are expected at the repository level (Section 6.4.4), complete collapse of drifts in the nonlithophysal rock is a very improbable event. In this situation, the temperature constraint on seepage in the nonlithophysal zones is the same as that used for intact drifts, wherein seepage does not enter the emplacement drifts until the drift wall temperature drops below 100ºC.

6.8.2 Changes for Localized Corrosion

Accelerated localized corrosion can has the potential to occur on the waste package if the package is exposed to condensation within the drift and if the thermal and aqueous environment results in aggressive chemical conditions on the waste package. If a seismic event occurs when the conditions for accelerated localized corrosion of Alloy 22 are satisfied, then any seepage that falls onto the waste package will flow into the waste package without diversion. This is a reasonable change because enhanced localized corrosion on the waste package generates corroded areas directly beneath the seeps. Once these corroded areas penetrate the outer and inner shells of the waste package, the seeps fall directly onto the waste package internals, without diversion by the surface of the waste package.

6.8.3 Changes for a Collapsed Drift

The presence of rubble around the drip shield may cause changes in the temperature and relative humidity of EBS components. A parameter study was conducted to examine the impact of drift collapse on in-drift thermohydrologic parameters (BSC 2004 [DIRS 169565], Section 6.3.7). The Multiscale Thermohydrologic Model (MSTHM) was used to examine the effect of a rubble filled drift on waste package and invert temperature and relative humidity at the waste package and invert. The drift collapses (instantaneously) to twice its initial diameter (i.e., 11 m collapsed diameter), and is filled with rubble with a bulking factor of 0.231. The thermal conductivity of the rubble (K_{th}) is defined as the intact rock thermal conductivity of the Tptpll multiplied by the factor (1/(1 + BF)) where BF is the bulking factor. Two thermal conductivity values (a "high" case based on a bulking factor of 0.231, and a "low" case which is taken to be one-half the "high" case value) of the dry and wet rubble thermal conductivity were used in the analyses, as shown in Table 6.8-1. The appropriate range for the bulking factor, 0.2 to 0.4, is discussed in (BSC 2004 [DIRS 166107], Section 6.4.2.5.2 under Bulking).

Table 6.8-1. Thermal Conductivity of Rubble

Property	Intact Host-Rock Property Value	Host-Rock Rubble Property Value	Basis for Rubble Property Value
Bulk dry thermal conductivity	1.28 W/m-K	1.0 W/m-K (High-K_{th} case) 0.5 W/m-K (Low-K_{th} case)	Intact Value x 1/(1 + BF) (High-K_{th} rubble value)/2
Bulk wet thermal conductivity	1.89 W/m-K	1.515 W/m-K (High-K_{th} case) 0.7575 W/m-K (Low-K_{th} case)	Intact Value x 1/(1 + BF) (High-K_{th} rubble value)/2

Source: BSC 2004 [DIRS 169565], Table 6.2-3.

Figure 6.8-1 shows the in-drift thermohydrologic parameters as functions of time from repository closure for the case of the "hottest" waste package, which is the 21-PWR absorber plate commercial spent nuclear fuel (CSNF). These plots show three cases: a) an open, noncollapsed drift, b) a collapsed, rubble-filled drift with high-K_{th} for the rubble, and c) a collapsed, rubble-filled drift with low-K_{th}. The temperature or any of the other environmental parameters follow the intact drift curve until the time of collapse. At that point, the temperature and other parameters translate vertically to one of the other curves, depending on the thermal conductivity of the rubble.

Examination of the waste package temperature curve (Figure 6.8-1) shows that significant impact to peak waste package temperature results only if drift collapse occurs within the first 100 to 200 years after closure. After that time, the waste package temperature remains below the peak temperature for the intact drift case that occurs within about 20 to 30 years after closure. The total time during which the waste package surface remains above boiling for the "hottest" waste package case is approximately 1,000 years for the intact drift, 1,500 years for the high-K_{th} case and 2,000 years for the low K_{th} case. The relative humidity at the waste package decreases significantly for collapsed drift because of the increase in local temperature.

When a TSPA model can accept temperature and relative humidity time histories from these eight representative waste package emplacement configurations, then the data should be directly used for all waste packages in lithophysal zones after drift collapse. When a TSPA model can only accept input for the CSNF or the codisposal waste package types, than a choice must be made among these eight time histories.

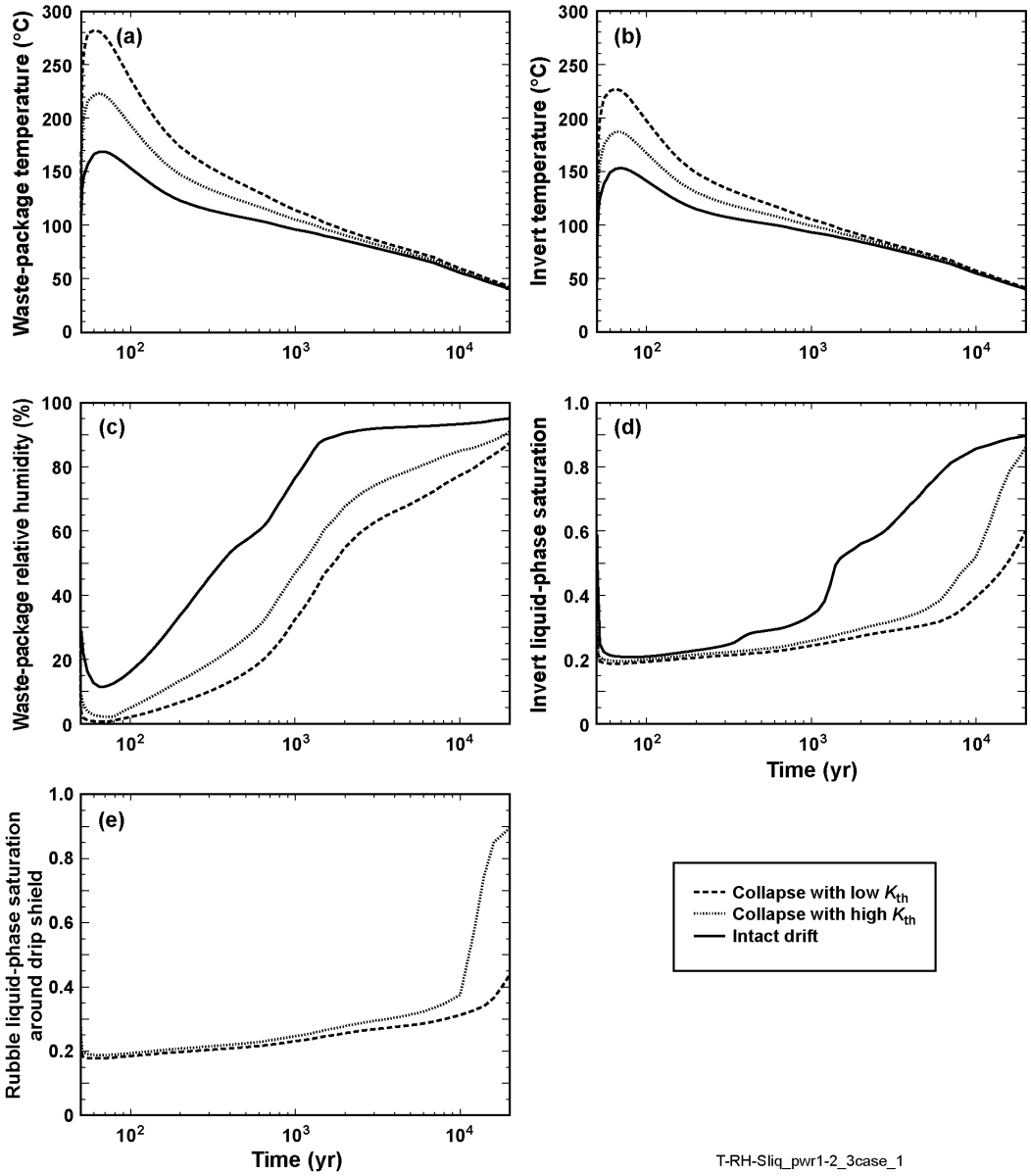

Source: BSC 2004 [DIRS 169565] Figure 6.3-54.

NOTES: Thermohydrologic response for the mean infiltration flux at the P2WR5C10 location, which is in the Tptpll (tsw35) unit (see BSC 2004 [DIRS 169565], Figure 6.3-1 and Figure 6.3-54 for location). The cases are: (1) intact-drift (nominal) case, (2) low-probability-seismic collapsed drift with high- K_{th} host-rock rubble, and (3) low-probability-seismic collapsed drift with low-K_{th} rubble. The plotted variables are (a) waste-package temperature, (b) invert temperature, (c) waste-package relative humidity, (d) invert liquid-phase saturation, and (e) matrix liquid-phase saturation of the rubble surrounding the drip shield.

The digital results for the temperature time histories are defined in (DTN: LL040310323122.044 [DIRS 168769], files: *Twp_dhlw-l1_3case.dat*, *Twp_dhlw-s1_3case.dat*, *Twp_bwr1-1_3case.dat*, *Twp_bwr1-2_3case.dat*, *Twp_bwr2-1_3case.dat*, *Twp_pwr1-1_3case.dat, Twp_pwr1-2_3case.dat*, and *Twp_pwr2-1_3case.dat*). The digital results for the relative humidity time histories are defined in (DTN: LL040310323122.044 [DIRS 168769], files: *RHwp_dhlw-l1_3case.dat*, *RHwp_dhlw-s1_3case.dat*, *RHwp_bwr1-1_3case.dat, RHwp_bwr1-2_3case.dat, RHwp_bwr2-1_3case.dat, RHwp_pwr1-1_3case.dat, RHwp_pwr1-2_3case.dat,* and *RHwp_pwr2-1_3case.dat*).

Figure 6.8-1. Thermohydrologic Response for the 21-PWR Absorber Plate CSNF (PWR 1-2) Waste Package

The recommended choice for the CSNF waste package groups is based on the BWR or PWR configuration in the MSTHM that produces a temperature history closest to the mean response for these types of packages. The mean response is a reasonable approach here because there are substantial uncertainties in predictions of the thermal conductivity of the rubble and backfill around the drip shield. The calculations with high and low values for thermal conductivity are designed to represent this uncertainty, and waste package configuration with the mean thermal response captures this effect. The recommended choice for the co-disposal waste package groups cannot be based on the mean because there are only two DHLW configurations, so the recommended choice is to use the configuration with the maximum temperature change.

Table 6.8-2 summarizes the maximum temperature change for the six PWR/BWR configurations from the MSTHM calculations with the lower bound for thermal conductivity.

The maximum temperature change for the PWR 2-1 package is 111.75°C, which is closest to the mean of these six cases. The recommended choice is to use the PWR 2-1 time histories for temperature and relative humidity, files: *Twp_pwr2-1_3case.dat* and *RHwp_pwr2-1_3case.dat*, respectively, for the TSPA models based on CSNF waste package groupings.

The maximum temperature changes for the DHLW-l1 and DHLW-s1 waste package emplacement configurations are 99.85°C and 122.98°C, respectively. The recommended choice is to use the DHLW-s1 time histories for temperature and relative humidity, files: *Twp_dhlw-s1_3case.dat* and *RHwp_dhlw-s1_3case.dat*, respectively, for the TSPA models based on co-disposal waste package groupings.

Table 6.8-2. Maximum Temperature Change for MSTHM Configurations with Low Thermal Conductivity

MSTHM Waste Package Configuration	Maximum Temperature Change (°C)[a]
BWR 1-2	126.77
BWR 1-1	119.88
BWR 2-1	118.76
PWR 1-1	90.01
PWR 2-1	111.75
PWR 1-2	121.81
Mean Value	114.83

[a] Each file in DTN: LL040310323122.044 [DIRS 168769] defines time dependent temperatures for the following cases: (i) no backfill, denoted by T0, (ii) backfill with low thermal conductivity, denoted by T_l, and (iii) backfill for high thermal conductivity, denoted by T_h. The files also define the temperature change between the low thermal conductivity and no backfill cases, denoted by T_l – T0, and the temperature change between the high thermal conductivity and no backfill cases, denoted by T_h – T0. The data for maximum temperature change are based on the maximum value in the T_l – T0 case.

BWR = boiling water reactor; MSTHM = Multiscale Thermohydrological Model.

For TSPA-LA, all ground motions with PGV equal to or greater than 0.384 m/s will be considered large enough to collapse the drifts. This threshold for change is consistent with the fact that tunnels in the lithophysal zones do not collapse for the 0.19 m/s PGV level of ground motion (BSC 2004 [DIRS 166107], Section 6.4.2.2.1). Recent rockfall calculations have determined that a PGV of 2 m/s is a more reasonable threshold for drift collapse in the lithophysal zones (BSC 2004 [DIRS 166107] Section 6.4.2.2.2, 4th bullet under subheading 'Discussion'). The seismic scenario class continues to use the conservative value of 0.384 m/s for TSPA-LA because the technical basis for the 2.0 m/s threshold was established after the start of TSPA-LA model development.

There is no change in temperature or relative humidity for the emplacement drifts in the nonlithophysal zones because the drifts are not expected to be completely filled with rock blocks in the nonlithophysal zones (BSC 2004 [DIRS 166107], Section 6.3.1.6.4). In this situation, the top and sides of the drip shield will not be completely covered with rock blocks and rubble, so the nominal temperature and nominal relative humidity time histories are more appropriate for this case.

6.9 SEISMIC SCENARIO CLASS

The impact of seismic hazards on repository performance is being represented in a separate scenario, called the seismic scenario, for TSPA-LA. The rationale for defining a separate scenario is based on several key observations:

- Seismic events with annual frequencies down to 10^{-8} per year must be considered by TSPA-LA.

  10 CFR 63.114 [DIRS 156605], Requirements for Performance Assessment, states that:

  > Any performance assessment used to demonstrate compliance with §63.113 must: (d) Consider only events that have at least one chance in 10,000 of occurring over 10,000 years.

  Seismic events with very large ground motion amplitudes/fault displacements, corresponding to annual exceedance frequencies down to 10^{-8} per year, must be considered by TSPA-LA, even though their probability is very low during the 10,000-year regulatory period.

- The nominal scenario class cannot determine the impact of low frequency seismic events in a computationally efficient manner. A separate scenario for seismic hazards is desirable.

Events with very small annual frequencies of occurrence cannot be represented in the nominal scenario class in a computationally efficient fashion. Accurate representation of events with annual frequency of occurrence down to 10^{-8} per year would require millions of realizations in the nominal scenario class, which is not computationally feasible. The alternative is to define a separate scenario for seismic hazards that determines dose in a probability-weighted manner, as explained below.

- The mean dose time history is the main parameter for compliance determinations.

  Radionuclide release limits for the repository are expressed in terms of the mean of the distribution of projected doses to the reasonably maximally exposed individual, per 10 CFR 63.303 and 63.311 [DIRS 156605]. Calculation of releases from the seismic scenario class must generate mean dose for consistency with the nominal scenario class.

- Damage from seismic events is represented as a network of stress corrosion cracks for the damaged areas wherein the residual tensile stress exceeds a given threshold for Alloy 22 on the surfaces of the waste package or for Titanium Grade 7 on the surfaces of the drip shield.

  The damage from seismic events is represented as a network of stress corrosion cracks for the damaged areas on the waste package and drip shield. The probability distributions for these damaged areas are a function of the amplitude of the seismic event. For example, the amplitude of a ground motion is defined through the horizontal PGV, and the upper bound of the uniform distribution for damaged area on the waste package is given as a linear function of PGV (see Section 6.5.3). The individual damage abstractions for the waste package, the drip shield, and the cladding are based on the results from structural response calculations and rockfall calculations, as discussed in Sections 6.5 through 6.8.

The seismic scenario class is based on a single seismic event that occurs at a randomly chosen time in each realization of the TSPA-LA. That is, the conditional probability of a seismic event is one for each realization, even though the exceedance frequency range for these events varies from 10^{-4} per year down to 10^{-8} per year. The damage from this single event is based on the damage abstractions for the drip shield, the waste package and the cladding. The damaged areas on the waste package define a network of stress corrosion cracks that are potential pathways for transport through the EBS. The damage to the drip shield is expressed as the degree of separation between adjacent drip shields for TSPA-LA model validation testing; drip shield separation has been screened out of TSPA-LA otherwise. The damage to the cladding is expressed as a percentage of perforated fuel rods. The seepage flux for the emplacement drifts in the lithophysal zones changes after a seismic event occurs, and there is no flux splitting on the waste package (i.e., the fraction of the liquid flux onto the outer surface of the package that can flow inside the waste package and contact the waste form) if the seismic event occurs when conditions for accelerated localized corrosion are satisfied. Once radionuclides are released from the EBS, flow and transport in the unsaturated zone and the saturated zone are based on the same models and algorithms as for the nominal scenario class. Biosphere calculations and biosphere parameters for the seismic scenario class are also unchanged from the nominal scenario class.

Each realization of the seismic scenario class determines an annual dose time history for a single seismic event with a specific value for PGV_i and its corresponding mean annual exceedance frequency λ_i. These dose time histories do not represent the mean dose, as called for in 10 CFR 63.303 [DIRS 156605], because a single hazard always occurs in each realization. A mean dose time history is calculated using a probability-weighted sum and average of all the realizations for the seismic scenario class. The weighting factor for each realization corrects for the actual expected number of seismic events and for importance sampling based on the use of log-uniform distributions for annual exceedance frequency and event time.

6.9.1 Computational Approach

The mean dose for the seismic scenario class is calculated using a two-step approach: (1) in the first step, TSPA-LA generates a set of R realizations that have robust sampling of all levels of seismic events (PGV level and fault displacement amplitudes) with the potential to generate releases from the EBS, and (2) in the second step, the mean or expected dose time history is calculated using a weighted sum and average of the dose time histories from the R realizations evaluated during the first step. Additional postprocessing can present results as cumulative distribution functions, as complementary cumulative distribution functions, or can evaluate the variability of the dose time histories, if necessary.

The mathematical basis for calculating the mean dose as a weighted sum and average of the individual dose time histories is presented in Appendix F. The following discussion explains how these two steps are implemented in a Monte Carlo computational procedure.

6.9.1.1 Description of the First Step

The first step generates R realizations of future performance with the TSPA-LA model for the seismic scenario class for the seismic hazards of ground motion and fault displacement. This suite of R realizations represents the combined epistemic and aleatory uncertainty in the TSPA-LA model for the seismic scenario class. Epistemic uncertainty is captured by those stochastic parameters that represent the "lack of knowledge" uncertainty in various processes. Aleatory uncertainty is captured by the stochastic parameters that represent the randomness of processes, such as the uncertainty in the timing and amplitude of seismic hazards.

The TSPA-LA model for the seismic scenario class is very similar to the TSPA-LA model for the nominal scenario class, with the following major exceptions: (1) damaged area on the waste package is determined by sampling stochastic parameters in an abstraction for waste package damage, rather than by the waste package degradation model for corrosion processes; (2) the damaged area on the waste package is represented as a network of stress corrosion cracks, rather than as large breaches on the package, (3) the failure of cladding is represented as a percent of fuel rods perforated at the time of the seismic event, and (4) a single seismic event occurs at a random time during each realization. The primary output from each of these R realizations is a time history of dose to the reasonably maximally exposed individual.

For each realization, the value of $PGV_{hazard,i}$, its associated annual exceedance frequency, λ_i, and the time of occurrence of the seismic hazard, t_i, are determined by a Monte Carlo process that samples appropriate distributions for these parameters. Since PGV_{hazard} and λ are functionally

related, it is sufficient to sample one parameter or the other; λ is sampled for TSPA-LA. Each realization has a single seismic event that occurs at a randomly selected time during the calculation. The type of distribution for λ_i and t_i is discussed next.

The sampling for the annual exceedance frequency uses a logarithmic scale, rather than a linear scale to ensure robust sampling throughout the relevant frequency range. This approach ensures adequate representation of very low frequency events with high PGV levels that may result in large doses. More specifically, λ_i is determined by sampling a log-uniform distribution with lower bound λ_{min} and upper bound λ_{max}. The use of a log-uniform distribution is a computational device for accelerating convergence to the mean or expected values in a Monte Carlo scheme; it does not represent the physical response of the site. The bounds must be chosen to encompass the seismic exceedance frequencies with the potential to release significant radionuclides from the EBS. Typical values of λ_{max} and λ_{min} for the seismic scenario class are 10^{-4} per year and 10^{-8} per year, respectively, because this range spans the response of the system, from no damage at 10^{-4} per year (Assumption 5.1) to the regulatory limit at 10^{-8} per year.

The timing of seismic events is assumed to follow a Poisson process (see Assumption 5.4). The probability of a Poisson process with frequency λ_i producing a single event in a time interval, T, is given approximately by $\lambda_i T$ when $\lambda_i T$ is much less than one. In other words, the probability of an event occurring increases linearly with time. In spite of this uniform distribution for events with time, it is useful to sample the event time in TSPA, t_i, from a log-uniform distribution between T_{min} and T_{max}. This approach, sometimes called importance sampling, ensures adequate representation of early-time events that might result in larger doses from longer travel times during the 10,000-year regulatory period. The importance sampling has no physical meaning, but does help to accelerate convergence of the Monte Carlo technique in TSPA. Typical values of T_{max} will be 10,000 years, the regulatory period, or 20,000 years. As noted in Section 1.2, the 20,000-year duration for the seismic analyses is designed to demonstrate that repository performance remains robust well after the 10,000-year regulatory period. The value for T_{min} is a TSPA-determined parameter.

Once the value of the annual exceedance frequency (λ_i) is determined for the i^{th} realization, the corresponding value of the peak ground velocity ($PGV_{hazard,i}$) is calculated. The relationship between PGV and λ is the hazard curve, and is site- and location-specific (see Section 6.4).

The hazard curves for vibratory ground motion and for fault displacements are central to the seismic scenario. These hazard curves represent both aleatory and epistemic uncertainties in the hazards (see Sections 6.4.1 and 6.4.2). The seismic scenario class is based on the mean hazard, considering the range of epistemic uncertainty for a given value of PGV. This is a reasonable approach because the mean (epistemic) estimate of the (aleatory) mean dose is linear in the exceedance frequency, λ, for a given value of PGV. The use of the mean hazard implies that the aleatory variance of dose is represented in TSPA, but the epistemic variance of dose is not captured in the seismic scenario class.

The TSPA-LA requires a mean hazard curve at Point B, corresponding to the emplacement drifts. The derivation of the PGV hazard curve at Point B is explained in Section 6.4.3, with the calculations documented in Appendix A. Figure 6.4-2 in Section 6.4.3 illustrates the scaled

hazard curve for Point B. The hazard curve in Figure 6.4-2 is unbounded, in the sense that PGV continues to increase, leading to very large PGV values that may not be physically realizable for the seismic sources and geologic conditions in and around Yucca Mountain. Analysis of the geologic conditions and other corroborating evidence provides a basis for estimating the maximum feasible or bounding value of PGV at the emplacement drifts. This bound is represented as a distribution because of uncertainty in estimating seismic sources, ground motion attenuation, and limits on future behavior. The bounding PGV distribution for TSPA-LA has a lower bound of 1.5 m/s, an upper bound of 5 m/s, and the distribution type is uniform (Section 6.4.4). This bounding distribution limits the sampled value of $PGV_{hazard,i}$ from the hazard curve: PGV_i is the minimum of the sampled values for $PGV_{hazard,i}$ and $PGV_{bound,i}$ in the i^{th} realization.

Once the final value for PGV_i is known, the distributions for the damaged area on the waste package (see Section 6.5.3), the degree of separation of the drip shield (only for validation testing of the TSPA-LA model; see Sections 6.5.5 and D1 through D3), and perforation of the cladding (see Section 6.5.6) are sampled. For example, the damaged area on the waste package is represented as a uniform distribution whose upper bound is a function of the value of PGV for the i^{th} realization. Once the value of PGV_i is known, the upper bound is calculated and the uniform distribution sampled to determine the damaged area on the waste package for this realization. This approach explicitly includes the variability from the structural response calculations in the TSPA-LA model through sampling.

Damage from fault displacement occurs simultaneously with damage from vibratory ground motion. The sampled value of λ_i determines the number of damaged waste packages by type, based on the abstraction in Table 6.7-11 (see Section 6.7). The damaged area from fault displacement is determined by sampling a distribution with a lower bound of 0 and an upper bound based on the lid area for each type of waste package.

Simultaneous damage from fault displacement and vibratory ground motion is a reasonable approach for the seismic scenario class. Damage from fault displacement only occurs for the largest seismic hazards, with an annual exceedance frequency of 2×10^{-7} per year or less (see Table 6.7-11). Such a large seismic hazard is always accompanied by vibratory ground motion, so fault displacement and ground motion are not considered independent processes for the TSPA-LA. On the other hand, the known faults and small hypothetical faults with a 2 meter cumulative offset (Sites 7a/8a in the PSHA) move simultaneously in the abstraction for TSPA-LA. The potential correlations among fault displacement hazard curves in the PSHA was not considered during the expert elicitation, and little information is available to support development of correlations for dependent or independent displacement along the known faults.

6.9.1.2 Description of the Second Step

Each of the R realizations generates a time history of dose to the reasonably maximally exposed individual, conditional upon the occurrence of a single seismic event. However, "compliance is based upon the mean of the distribution of projected doses of DOE's performance assessments which project the performance of the Yucca Mountain disposal system for 10,000 years after disposal," as noted in 10 CFR 63.303 [DIRS 156605].

The mean annual dose is calculated using a weighted sum and average of the R realizations performed during the first step. The weighting factors for each realization are derived in Appendix F. The weighting factors for each realization correct for the number of expected seismic events in each realization (t_i λ_i), for the log-uniform distribution for the annual frequency of occurrence ($ln(\lambda_{max}/\lambda_{min})$, and for the log-uniform distribution for the event time ($ln(T_{max}/T_{min})$. The mean dose, as derived in Section 2 of Appendix F for the ground motion hazard, is given by Equation F-12. This equation can be extended to include the fault displacement hazards because each realization has a common exceedance frequency for both ground motion and fault displacement. The extension of Equation F-12 becomes:

$$\overline{D}(t) = \frac{1}{R}\ln\left(\frac{\lambda_{\max}}{\lambda_{\min}}\right)\ln\left(\frac{T_{\max}}{T_{\min}}\right)\sum_{i=1}^{R} t_i \lambda_i D_i\{t \mid t_i, PGV_i, \vec{d}_i, \vec{e}_i\} \qquad \text{(Eq. 6.9-1)}$$

where

$D_i\{t \mid t_i, PGV_i\}$ is the dose at time t for the i^{th} realization, which has a seismic event of magnitudes PGV_i and $\vec{d}_i$ occurring at time t_i

$\overline{D}(t)$ is the mean dose for the scenario at time t

R is the number of realizations in the scenario

λ_{max} is the maximum value for the occurrence frequency

λ_{min} is the minimum value for the occurrence frequency

T_{max} is the maximum time (duration) of the scenario

T_{min} is the minimum time in the log-uniform sampling for the event time

λ_i is the exceedance frequency associated with PGV_i on the ground motion hazard curve

$\vec{d}_i$ is the vector of fault displacements corresponding to λ_i on the fault displacement hazard curves

$\vec{e}_i$ is a vector representing all the epistemically uncertain parameters that are sampled for the i^{th} realization of the seismic scenario class.

6.9.2 Computational Algorithm

The first step in the computational algorithm for the seismic scenario class, as described in Section 6.9.1.1, generates R realizations of future performance with the TSPA-LA model. The computational algorithm has been split into 14 simple operations to document the procedure for this scenario class. The first 10 operations define the constant parameters, stochastic parameters, and formulas that represent the epistemic and aleatory uncertainty for the TSPA-LA model. Each realization of the TSPA-LA model is based on a single sampling of the stochastic parameters from the first 10 operations. Repeated samplings of the stochastic parameters generate a full suite of R realizations of the TSPA-LA model. The second step in the computational algorithm (see Section 6.9.1.2) evaluates the mean dose from these R realizations, using the formula and parameters defined in the eleventh operation.

The modifications for post-seismic event response are summarized in Operations 12, 13, and 14. While these operations are part of the TSPA-LA model calculations in the first step, the parameter values are defined by reference rather than by analysis in this model report. These modifications are listed last in the procedure to emphasize this difference.

A list of the 14 operations in the computational procedure follows. The parameters for the computational procedure are listed in Table 6.9-1.

1. Determine the mean annual exceedance frequency, λ_i, for the i^{th} realization.

   The value of λ is sampled from a log-uniform distribution between λ_{min} and λ_{max}. A log-uniform distribution ensures robust sampling in each decade of the distribution. The values of λ_{min}, λ_{max}, and λ_i are represented by the parameters LAMBDA_MIN, LAMBDA_MAX, and LAMBDA, respectively, in Table 6.9-1.

2. Determine the corresponding value of PGV_i through the hazard curve, $\lambda = \lambda(PGV)$.

   The value of $PGV_{hazard,i}$ is determined by a table lookup, using the scaled PGV hazard curve for Point B. The interpolation between points in this table is based on a linear interpolation using the value of $\log(\lambda)$ at individual points. This is referred to as a log-linear interpolation scheme in the lookup table for PGV as a function of λ. The value of $PGV_{hazard,i}$ is the parameter PGV_h in Table 6.9-1.

   A second value of PGV, $PGV_{bound,i}$, is sampled from a uniform distribution between 1.5 m/s and 5 m/s (Section 6.4.4). This distribution represents the (epistemic) uncertainties associated with the sources and attenuation of extreme ground motions in and around Yucca Mountain. The distribution for PGV_{bound} is independent of exceedance frequency because this distribution represents epistemic uncertainty, which is independent of the aleatory uncertainty represented by the scaled hazard curve at Point B. The value of $PGV_{bound,i}$ is the maximum value of PGV at Point B identified in Table 4-1. The value of $PGV_{bound,i}$ is the parameter PGV_b in Table 6.9-1.

   The final value of PGV_i for this realization is defined as:

   $$PGV_i = MIN(PGV_h, PGV_b). \quad \text{(Eq. 6.9-2)}$$

   The value of PGV_i is denoted as PGV in Table 6.9-1. The subscript *i* has been dropped from PGV and from all other parameters in Table 6.9-1 because all values in Table 6.9-1 are on a per realization basis.

3. Determine the fraction of damaged waste package surface area due to vibratory ground motion for each realization.

   The percent of damaged waste package surface area is a random variable with distribution parameters that are functions of PGV_i. This damage abstraction is defined by a uniform distribution with a lower bound of 0 percent damaged area

and an upper bound that is a linear function of PGV_i (see Sections 6.5.3 through 6.5.6). The fraction of damaged surface area is applied to all waste packages in the repository (i.e., there is no spatial variability).

- The upper bound of the uniform distribution is defined by:

$$\text{MAX}\ (0.0,\ 0.436*PGV_i - 0.305), \qquad \text{(Eq. 6.9-3)}$$

in the units of percentage of damaged surface area. The value of this function is represented in Table 6.9-1 by the parameter WP_DAMAGE_MAX.

- The lower bound of the uniform distribution is 0 percent. This value is represented by the parameter WP_DAMAGE_MIN in Table 6.9-1.

- The sampled value of the uniform distribution (for each realization) is denoted as WP_DAMAGE%.

- The fraction of damaged surface area is denoted as WP_DAMAGE and calculated as:

$$\text{WP\_DAMAGE} = \text{WP\_DAMAGE\%}/100 \qquad \text{(Eq. 6.9-4)}$$

This damaged area must then be converted into an effective area for flow and transport, as discussed in Operation 4.

4. Determine the effective flow/transport area through the damaged area on the waste package. The effective transport area is based on the geometry and gap widths for a network of tight SCCs (Section 6.3.5). The scaling factor that determines the effective flow/transport area is a stochastic parameter because there is uncertainty in the geometry, orientation, and gap width for the SCC network. The scaling factor is sampled from a uniform distribution whose lower and upper bounds span the full range of SCC geometries considered (Sections 6.3.5 and 6.3.6). The scaling factor is applied to all waste packages in the repository (i.e., there is no spatial variability).

   - The upper bound of the uniform distribution is 0.0131, and represented in Table 6.9-1 by the parameter SCALE_FACTOR_MAX.

   - The lower bound of the uniform distribution is 0.00328. This value is represented by the parameter SCALE_FACTOR_MIN in Table 6.9-1.

   - The sampled value of the scaling factor is denoted as SCALE_FACTOR in Table 6.9-1.

   - The effective flow/transport area for any type of waste package, as a fraction of the total surface area, is denoted as WP_TRANS_AREA and calculated as:

$$\text{WP\_TRANS\_AREA} = \text{WP\_DAMAGE} * \text{SCALING\_FACTOR}. \qquad \text{(Eq. 6.9-5)}$$

5. Significant advective flow through the network of tight SCCs on the waste package is not expected to occur in the post-seismic environment. The SCC network allows diffusive transport but prevents advective flow into or out of the waste package (Sections 6.3.4 and 6.3.5). The crack network has high tortuosity and surface roughness, narrowing to very small apertures at the crack tip(s). This physical morphology limits advective flux through the cracks to insignificant levels because of infilling of narrow apertures with corrosion products, because of high surface tension when a narrow aperture is bridged by a droplet, because the head gradient or pressure gradient driving flow through narrow apertures with high tortuosity and surface roughness will be small, and because some plugging of cracks from evaporation-induced precipitation may occur over a few hundred years.

6. Direct, structural deformation of the drip shield from vibratory ground motion and from rockfall induced by vibratory ground motion is not included in the seismic scenario for TSPA-LA. Local deformation of the drip shield may result from ground motion and rockfall, but the associated SCCs are expected to limit advective flow to insignificant levels, based on the same reasoning as for the waste package (see Operation (5) above and Section 6.3.6). In this situation, direct damage to the drip shield from vibratory ground motion and from rockfall induced by vibratory ground motion is not incorporated into the seismic scenario for TSPA-LA.

7. Drip shield separation has been screened out of TSPA, although the validation testing for the TSPA-LA model retains a drip shield separation model because the technical basis for separation was established after the start of model validation activities. Drip shield separation is excluded from TSPA-LA because (1) ground motion amplitudes that are sufficient to cause drip shield separation are also large enough to partially or completely collapse drifts in the repository, and (2) rockfall occurs within the first second or two of the arrival of large amplitude ground motion (see discussion in Section 6.5.5).

   The basis for the drip shield separation model is described in Appendix D. The potential for drip shield separation is represented by a uniform distribution that is zero at a PGV of 2.44 m/s and has a range of 10 percent to 50 percent of the drip shield surface area at a PGV of 5.35 m/s. The details are as follows:

   - The upper bound of the uniform distribution, DS_DAMAGE_MAX, is a function of PGV and defined in Table 6.9-1 with a linear interpolation between the points.

   - The lower bound of the uniform distribution, DS_DAMAGE_MIN, is a function of PGV and defined in Table 6.9-1 with a linear interpolation/extrapolation between the points.

- The sampled value of the uniform distribution is denoted as DS_DAMAGE%.

- The fraction of separated surface area is denoted as DS_DAMAGE and calculated as:

$$DS\_DAMAGE = (DS\_DAMAGE\%\_GM)/100 \quad \text{(Eq. 6.9-6)}$$

This separated area allows advective flow through all the drip shields in the repository (i.e., there is no spatial variability). There is no correction for the effective flow area because this is a physical separation, not a damaged area with high residual stress.

8. Cladding does not fail for a ground motion with a PGV level of 0.55 m/s or less (see Assumption 5.1). Cladding experiences complete failure (i.e., 100 percent of the cladding is perforated) at the time of the seismic event for ground motions with PGV amplitude of 1.05 m/s or greater (Section 6.5.6).

   The abstraction for cladding failure is defined in Table 6.9-1 with a linear interpolation for the percent damage to the cladding between the appropriate values of PGV. In other words, cladding damage is (1) zero for PGV values less than 0.55 m/s, (2) 100 percent for PGV values greater than 1.05 m/s, and (3) based on a linear interpolation for intermediate values of PGV. The linear interpolation has 0 percent damage at 0.55 m/s PGV and 100 percent damage at 1.05 m/s PGV. This damage abstraction applies to the fraction of cladding that is not initially damaged.

   This parameter is denoted by CLAD_DAMAGE_GM in Table 6.9-1. There is no uncertainty in this damage abstraction because it is a bounding estimate for cladding failure. The percent of failed cladding is applied to all fuel assemblies in the repository (i.e., there is no spatial variability), except for any assemblies with initial cladding failures.

9. Determine the percent failed area on the waste package due to fault displacement. The expected number of waste packages that fail, as a function of annual exceedance frequency, is defined in Table 6.9-1.

   - The expected number of waste packages that fail from fault displacement is a small fraction of the total packages in the repository because few waste packages are located on known faults. In addition, these failures only occur for a small fraction of the realizations in the seismic scenario class because there are no failures from fault displacement for a displacement less than 671 mm (Table 6.7-3). Displacements greater than 671 mm first occur on the Drill Hole Wash fault, the Pagany Wash fault, and the Sever Wash fault at an annual frequency of occurrence less than or equal to 2×10^{-7} per year (Table 6.7-9). In this situation, damage from fault displacement only occurs for exceedance frequencies between 1×10^{-8} per year and 2×10^{-7} per year,

and a special waste package group(s) or bin(s) should be used to represent the waste package failures from fault displacement.

- The thermohydraulic and seepage environment for the special group(s) or bin(s) should be chosen independently and randomly. For example, if the fault-failed packages are binned into two groups for CSNF and codisposal (CDSP) packages, then two randomly chosen environments should be used for each of the two groups.

- When a waste package fails by fault displacement, the failed area on each waste package is determined by sampling a uniform distribution with a lower bound of 0 m^2 and an upper bound equal to the area of the waste package lid. These sampled distributions are denoted by FAILED_AREA_PWR, FAILED_AREA_BWR, FAILED_AREA_NAVAL, and FAILED_AREA_HLW in Table 6.9-1.

- The area of the lid for the PWR, BWR, Naval, and HLW groups is 2.105 m^2, 2.204 m^2, 2.728 m^2, and 3.2836 m^2, respectively. These areas are denoted as LID_AREA_PWR, LID_AREA_BWR, LID_AREA_NAVAL, and LID_AREA_HLW in Table 6.9-1.

- The surface area of a package in the PWR, BWR, Naval, and HLW groups is 30.15 m^2, 30.85 m^2, 37.85 m^2, and 35.60 m^2, respectively. These areas are denoted as SURF_AREA_PWR, SURF_AREA_BWR, SURF_AREA_NAVAL, and SURF_AREA_HLW in Table 6.9-1.

- The fraction of failed area for the PWR waste package type is calculated as:

$$FRACTION\_FAILED\_PWR = FAILED\_AREA\_PWR/SURF\_AREA\_PWR \quad \text{(Eq. 6.9-7)}$$

with similar equations for the BWR, Naval, and HLW waste package types. This failed area allows advective flow and advective and diffusive transport.

- The expected number of package failures for the three waste package types are denoted by NO_PWR_FAILURES, NO_BWR_FAILURES, NO_NAVAL_FAILURES, and NO_HLW_FAILURES in Table 6.9-1.

- If a waste package is damaged by fault displacement, the associated drip shield is taken to be 100 percent damaged. The number of impacted drip shields is then identical to the total number of waste packages that will be damaged by the fault displacement. The parameters NO_DRIP_SHIELD_FD and DRIP_SHIELD_DAMAGE_FD in Table 6.9-1 define the number and amount of damage to the drip shields from fault displacement.

- Cladding in waste packages that are damaged by a fault displacement is taken to be 100 percent perforated. The 100 percent perforation applies to all the fuel assemblies in the number of waste packages that are damaged by the fault displacement. The parameters NO_CLAD_FD and CLAD_DAMAGE_FD in

Table 6.9-1 define the number and amount of damage to the drip shields from fault displacement.

10. Determine the time of the seismic event for each realization.

    The time of the event, EVENT_TIME, is determined by sampling a log-uniform distribution with a lower bound denoted by TIME_MIN and an upper bound denoted by TIME_MAX in Table 6.9-1. A typical value of TIME_MAX is 10,000 or 20,000 years. The appropriate value for TIME_MIN will be determined by the TSPA staff.

11. Calculate the mean dose for all realizations, i = 1, 2, …, *R*.

    The weighting factor for each realization corrects for the expected number of seismic events in each realization, for the log-uniform sampling for the exceedance frequency, λ_i. and for the log-uniform sampling for event time, t_i. The appropriate formula (Eq. 6.9-1) for calculating the mean or expected dose with log-uniform sampling for the event time and log-uniform sampling for the annual exceedance frequency, λ_i, is:

$$\begin{aligned}\overline{D}(t) &= \frac{1}{R}\ln\left(\frac{\lambda_{\max}}{\lambda_{\min}}\right)\ln\left(\frac{T_{\max}}{T_{\min}}\right)\sum_{i=1}^{R} t_i \lambda_i D_i\{t \mid t_i, PGV_i, \vec{d}_i, \vec{e}_i\}, \\ &= \frac{1}{R}\sum_{1}^{R} WEIGHTED\_DOSE_i, \\ &= Mean(WEIGHTED\_DOSE),\end{aligned} \qquad \text{(Eq. 6.9-8)}$$

    where $\overline{D}(t)$ is the expected (mean) dose, $D_i\{t|t_i,PGV_i\}$ is the dose from the i^{th} realization with seismic hazards of amplitude PGV_i and $\vec{d}_i$ occurring at time t_i, and *R* is the total number of realizations. The term $t_i\ \lambda_i$ is denoted by EVENT_WEIGHT in Table 6.9-1. The term $ln\left(\frac{T_{max}}{T_{min}}\right)ln\left(\frac{\lambda_{max}}{\lambda_{min}}\right)$ is represented as the parameter SAMPLE_WEIGHT in Table 6.9-1. The term WEIGHTED_DOSE is the product of EVENT_WEIGHT, SAMPLE_WEIGHT, and the DOSE at any given time.

12. Modify the seepage in the lithophysal zones after the seismic event.

    The seepage into the emplacement drifts in the lithophysal zones is determined by using the seepage table for collapsed drifts, as provided in LB0307SEEPDRCL.002 [DIRS 164337], file: *ResponseSurfaceSMPACollapsedDrift.dat* (Section 6.8.1). This seepage table is invoked after a seismic hazard occurs, provided the hazard is large enough to collapse the drifts. For TSPA-LA, all ground motions with a PGV greater than

0.384 m/s will be considered large enough to collapse drifts in the lithophysal zones (Section 6.8.1). The parameter COLLAPSE_THRESH_LITH in Table 6.9-1 defines the PGV threshold (0.384 m/s) for collapse in lithophysal zones.

There is no change in the seepage flux into nonlithophysal zones after a seismic hazard occurs (Section 6.8.1). The parameter COLLAPSE_THRESH_NONLITH in Table 6.9-1 defines the PGV threshold for collapse in nonlithophysal zones. COLLAPSE_THRESH_NONLITH is set to 5.35 m/s (Section 6.8.1). There is no collapse in nonlithophysal zones with this value because PGV_b is always less than 5 m/s for TSPA-LA (see Operation 2 above).

13. Modify the flux through the drip shield and into the waste package after the seismic event if conditions are satisfied for accelerated localized corrosion to occur.

    The flux splitting algorithm for the seismic scenario is identical to the flux splitting algorithm for the nominal scenario, with one exception (Sections 6.8.2 and D4). If the seismic hazard occurs at a time when the conditions for the existence of accelerated localized corrosion of Alloy 22 are satisfied, then any seepage that falls onto the waste package will flow into the package without diversion or flux splitting. If localized corrosion occurs under deliquescent salt conditions, then the area for transport out of the waste package is conservatively bounded by the surface area exposed to dust deposition, which is the entire waste package surface area (BSC 2004 [DIRS 169984], Section 8.3.1).

    If drip shield separation is activated for validation testing and if the seismic hazard has a PGV level greater than 2.44 m/s (so drip shield separation occurs), then the percent seepage that passes through the drip shield will be equal to the percent drip shield separation. For example, if the drip shields are separated by 25 percent of their axial length, then 25 percent of the seepage onto the drip shield will fall directly onto the waste package. In addition, any resulting seepage that falls onto the waste package will flow into the package without diversion or flux splitting. If these conditions are not satisfied, then the flux splitting algorithm for the nominal scenario class will be unchanged after a seismic event.

    Once localized corrosion is initiated after drip shield separation, the area for diffusive and advective transport out of the waste package is the total area of the waste package that is directly exposed to seepage (BSC 2004 [DIRS 169984], Section 8.3.1). Again, if the drip shields have separated by 25 percent of their axial length, then the transport area on the waste package is 25 percent of its surface area. This approach is an upper bound because all the exposed surface material is lost to localized corrosion, even if seepage never contacts exposed areas of the waste package.

14. Modify the temperature and relative humidity on the waste after drift collapse in the lithophysal zones.

The temperature and relative humidity of the waste package after drift collapse will be defined by the data in (DTN: LL040310323122.044 [DIRS 168769], temperature time histories defined in files: *Twp_dhlw-l1_3case.dat*, *Twp_dhlw-s1_3case.dat, Twp_bwr1-1_3case.dat, Twp_bwr1-2_3case.dat*, *Twp_bwr2-1_3case.dat, Twp_pwr1-1_3case.dat, Twp_pwr1-2_3case.dat,* and *Twp_pwr2-1_3case.dat*; relative humidity time histories defined in files: *RHwp_dhlw-l1_3case.dat, RHwp_dhlw-s1_3case.dat, RHwp_bwr1-1_3case.dat, RHwp_bwr1-2_3case.dat, RHwp_bwr2-1_3case.dat, RHwp_pwr1-_3case.dat, RHwp_pwr1-2_3case.dat,* and *RHwp_pwr2-1 3case.dat*). If a TSPA-LA model cannot accept eight waste package emplacement configurations in this DTN, then the PWR 2-1 and DHLW-s1 configurations are recommended for defining the temperature and relative humidity changes for CSNF and co-disposal waste package groups in TSPA-LA. These new histories are used for seismic hazards with a PGV level greater than 0.384 m/s. There is no change in the temperature and relative humidity for the nonlithophysal zones because the drifts do not collapse in the nonlithophysal zones (Section 6.8.3), and the amount of rubble is generally expected to be insufficient to completely cover the top and sides of the drip shield.

Table 6.9-1. Definition of Parameters for the Seismic Scenario Class

Parameter Name	Description, Units, and Type	Definition
EVENT_TIME	Distribution for the time when the seismic event occurs in this realization Units: {yr} Type: Distribution sampled once per realization	Log-Uniform Distribution: Minimum Value: TIME_MIN Maximum Value: TIME_MAX
TIME_MAX	Duration of the seismic scenario class Units: {yr} Type: Data	Typical values are 10,000 years or 20,000 years.
TIME_MIN	Minimum value of the log-uniform distribution for event time Units: {yr} Type: Data	The appropriate value for TIME_MIN will be determined by the TSPA staff.
LAMBDA	Distribution of annual exceedance frequency for the seismic scenario class Units: {1/yr} Type: Distribution sampled once per realization	Log-Uniform Distribution: Minimum Value: LAMBDA_MIN Maximum Value: LAMBDA_MAX
LAMBDA_MIN	Minimum annual exceedance frequency Units: {1/yr} Type: Data	1×10^{-8} per year
LAMBDA_MAX	Maximum annual exceedance frequency Units: {1/yr} Type: Data	1×10^{-4} per year

Table 6.9-1. Definition of Parameters for the Seismic Scenario Class (Continued)

Parameter Name	Description, Units, and Type	Definition
PGV_h	Hazard curve for horizontal PGV as a function of LAMBDA Units: {m/s} Type: Table, function of LAMBDA	Table lookup as a function of the value of LAMBDA for this realization. Use log-linear interpolation between λ values: λ (1/yr) — PGV (m/s) 6.26×10^{-4} — 0.159 2.78×10^{-4} — 0.239 9.30×10^{-5} — 0.398 1.84×10^{-5} — 0.796 3.07×10^{-6} — 1.59 2.28×10^{-7} — 3.98 8.15×10^{-8} — 5.57 2.60×10^{-8} — 7.96 6.56×10^{-9} — 11.9
PGV_b	Distribution of the bounding value for PGV. Units: {m/s} Type: Distribution sampled once per realization	Uniform distribution: Minimum value = 1.5 m/s Maximum value = 5 m/s
PGV	Value of PGV for this realization. Units: {m/s} Type: Function	$PGV = MIN(PGV_h, PGV_b)$
WP_DAMAGE_MAX	Maximum value of % damaged area on the waste package for this realization. Units: {%} Type: Function of PGV	MAX(0.0, 0.436*(PGV) – 0.305)
WP_DAMAGE_MIN	Minimum value of % damaged surface area on the waste package for this realization. Units: {%} Type: Constant	0%
WP_DAMAGE%	Distribution of % damaged surface area on the waste package. Units: {%} Type: Distribution sampled once per realization	Uniform Distribution: Minimum Value: WP_DAMAGE_MIN Maximum Value: WP_DAMAGE_MAX
WP_DAMAGE	Fraction of damaged surface area on the waste package. Units: {-} Type: Function	WP_DAMAGE%/100 (-)=dimensionless
SCALE_FACTOR_MIN	Minimum value of scale factor for defining the transport area of a network of SCCs on the waste package. Units: {-} Type: Constant	0.00328 (-) (-)=dimensionless
SCALE_FACTOR_MAX	Maximum value of scale factor for defining the area of a network of SCCs on the waste package. Units: {-} Type: Constant	0.0131 (-)

Table 6.9-1. Definition of Parameters for the Seismic Scenario Class (Continued)

Parameter Name	Description, Units, and Type	Definition
SCALE_FACTOR	Scale factor distribution for the area of a network of SCCs on the waste package for this realization. Units: {-} Type: Distribution sampled once per realization	Uniform Distribution: Minimum Value: SCALE_FACTOR_MIN Maximum Value: SCALE_FACTOR_MAX
WP_TRANS_AREA	Effective fractional area for transport through a network of SCCs on the waste package. Units: {-} Type: Function	WP_DAMAGE * SCALE_FACTOR
DS_DAMAGE_MAX	Maximum value of % separated area on the drip shield for this realization. Units: {%} Type: Table Look-up as function of PGV with linear interpolation between points	Table lookup as a function of the value of PGV for this realization. PGV (m/s) — Damage (%) 0 — 0 2.44 — 0 5.35 — 50 20[a] — 50 [a]The value of 20 m/s provides the mathematical extension of the abstraction for values of PGV greater than 5.35 m/s, consistent with Table D-2. Such extreme values will not be sampled in TSPA-LA because PGV_b is always less than 5 m/s.
DS_DAMAGE_MIN	Minimum value of % separated area on the drip shield. Units: {%} Type: Table Look-up as a function of PGV, with linear interpolation between points and linear extrapolation for PGV > 5.35 m/s.	Table lookup as a function of the value of PGV for this realization. PGV (m/s) — Damage (%) 0 — 0 2.44 — 0 5.35 — 10
DS_DAMAGE%	Distribution of % separated area on the drip shield. Units: {%} Type: Distribution sampled once per realization	Uniform Distribution: Minimum Value: DS_DAMAGE_MIN Maximum Value: DS_DAMAGE_MAX
DS_DAMAGE	Fraction of separated surface area on the drip shield. Units: {-} Type: Function A separated drip shield allows advective flow onto the waste package.	DS_DAMAGE%/100
CLAD_DAMAGE_GM	Percent perforated cladding from vibratory ground motion. Units: {%} Type: Table look-up as function of PGV This damage is applied to all fuel assemblies, except for assemblies with initial clad damage or initial clad failures.	Table lookup as a function of the value of PGV for this realization. PGV {m/s} — Damage {%} 0 — 0 0.55 — 0 1.05 — 100 20[b] — 100 [b]The value of 20 m/s provides the mathematical extension of the abstraction for values of PGV greater than 1.05 m/s, consistent with Table 6.5-6. Such extreme values of PGV will not be sampled in TSPA-LA because PGV_b is always less than 5 m/s.

Table 6.9-1. Definition of Parameters for the Seismic Scenario Class (Continued)

Parameter Name	Description, Units, and Type	Definition
LID_AREA_PWR	Lid area of the PWR waste package group for fault displacement. Units: {m^2} Type: Data	2.105 m^2
LID_AREA_BWR	Lid area of the BWR waste package group for fault displacement. Units: {m^2} Type: Data	2.204 m^2
LID_AREA_NAVAL	Lid area of the Naval waste package group for fault displacement. Units: {m^2} Type: Data	2.728 m^2
LID_AREA_HLW	Lid area of the HLW waste package group for fault displacement. Units: {m^2} Type: Data	3.284 m^2
FAILED_AREA_PWR	Distribution of failed area on the PWR waste package group for fault displacement. Units: {m^2} Type: Distribution sampled once per realization	Uniform Distribution: Minimum Value: 0.0 Maximum Value: LID_AREA_PWR
FAILED_AREA_BWR	Distribution of failed area on the BWR waste package group for fault displacement. Units: {m^2} Type: Distribution sampled once per realization	Uniform Distribution: Minimum Value: 0.0 Maximum Value: LID_AREA_BWR
FAILED_AREA_ NAVAL	Distribution of failed area on the Naval waste package group for fault displacement. Units: {m^2} Type: Distribution sampled once per realization	Uniform Distribution: Minimum Value: 0.0 Maximum Value: LID_AREA_NAVAL
FAILED_AREA_HLW	Distribution of failed area on the HLW waste package group for fault displacement. Units: {m^2} Type: Distribution sampled once per realization	Uniform Distribution: Minimum Value: 0.0 Maximum Value: LID_AREA_HLW
SURF_AREA_PWR	Surface area for a waste package in the PWR group for fault displacement. Units: {m^2} Type: Data	30.15 m^2
SURF_AREA_BWR	Surface area for a waste package in the BWR group for fault displacement. Units: {m^2} Type: Data	30.85 m^2

Table 6.9-1. Definition of Parameters for the Seismic Scenario Class (Continued)

Parameter Name	Description, Units, and Type	Definition
SURF_AREA_ NAVAL	Surface area for a waste package in the Naval group for fault displacement. Units: {m^2} Type: Data	37.85 m^2
SURF_AREA_HLW	Surface area for a waste package in the HLW group for fault displacement. Units: {m^2} Type: Data	35.60 m^2
FRACTION_FAILED_ AREA_PWR	Fraction of failed surface area on PWR waste package group from fault displacement. Units: {-} Type: Function	FAILED_AREA_PWR/SURF_AREA_PWR
FRACTION_FAILED_ AREA_BWR	Fraction of failed surface area on BWR waste package group from fault displacement. Units: {-} Type: Function	FAILED_AREA_BWR/SURF_AREA_BWR
FRACTION_FAILED_ AREA_NAVAL	Fraction of failed surface area on Naval waste package group from fault displacement. Units: {-} Type: Function	FAILED_AREA_NAVAL/SURF_AREA_ NAVAL
FRACTION_FAILED_ AREA_HLW	Fraction of failed surface area on HLW waste package group from fault displacement. Units: {-} Type: Function	FAILED_AREA_HLW/SURF_AREA_HLW
NO_PWR_ FAILURES	Number of failed PWR waste packages from fault displacement. Units: {-} Type: Step function of annual exceedance frequency, λ All fault-failed PWR packages are located in a single, randomly chosen thermohydraulic and seepage environment for CSNF packages in each realization.	Table lookup as a function of the value of λ for this realization. λ (1/yr) — # Failures (-) $> 5 \times 10^{-8}$ — 0 3×10^{-8} to 5×10^{-8} — 8.40 2×10^{-8} to 3×10^{-8} — 8.40 1×10^{-8} to 2×10^{-8} — 9.24
NO_BWR_ FAILURES	Number of failed BWR waste packages from fault displacement. Units: {-} Type: Step function of annual exceedance frequency, λ All fault-failed BWR packages are located in a single, randomly chosen thermohydraulic and seepage environment for CSNF packages in each realization.	Table lookup as a function of the value of λ for this realization. λ (1/yr) — # Failures (-) $> 5 \times 10^{-8}$ — 0 3×10^{-8} to 5×10^{-8} — 5.35 2×10^{-8} to 3×10^{-8} — 5.35 1×10^{-8} to 2×10^{-8} — 5.89

Table 6.9-1. Definition of Parameters for the Seismic Scenario Class (Continued)

Parameter Name	Description, Units, and Type	Definition
NO_NAVAL_ FAILURES	Number of failed Naval waste packages from fault displacement. Units: {-} Type: Step function of annual exceedance frequency, λ All fault-failed Naval packages are located in a single, randomly chosen thermohydraulic and seepage environment for CDSP packages in each realization. The environments for CSNF and CDSP packages should be chosen independently.	Table lookup as a function of the value of λ for this realization. λ (1/yr) — # Failures (-) $> 1 \times 10^{-7}$ — 0 5×10^{-8} to 1×10^{-7} — 0.61 3×10^{-8} to 5×10^{-8} — 0.61 2×10^{-8} to 3×10^{-8} — 0.67 1×10^{-8} to 2×10^{-8} — 0.67
NO_HLW_FAILURES	Number of failed HLW packages from fault displacement. Units: {-} Type: Step function of annual exceedance frequency, λ All fault-failed HLW packages are located in a single, randomly chosen thermohydraulic and seepage environment for CDSP packages in each realization. The environments for CSNF and CDSP packages should be chosen independently.	Table lookup as a function of the value of λ for this realization. λ (1/yr) — # Failures (-) $> 2 \times 10^{-7}$ — 0 1×10^{-7} to 2×10^{-7} — 5.64 5×10^{-8} to 1×10^{-7} — 5.64 3×10^{-8} to 5×10^{-8} — 6.20 2×10^{-8} to 3×10^{-8} — 6.20 1×10^{-8} to 2×10^{-8} — 39.98
NO_DRIP_SHIELD_ FD	Number of drip shields damaged by fault displacement (Step 9). Units: {-} Type: Function	NO_PWR_FAILURES + NO_BWR_FAILURES + NO_NAVAL_FAILURES + NO_HLW_FAILURES
DRIP_SHIELD_DAM AGE_FD	Magnitude of drip shield damage for all waste packages failed by fault displacement (Step 9). Units: {%} Type: Constant	100%
NO_CLAD_FD	Number of waste packages with cladding damaged by fault displacement (Step 9). Units: {-} Type: Function	NO_PWR_FAILURES + NO_BWR_FAILURES + NO_NAVAL_FAILURES + NO_HLW_FAILURES
CLAD_DAMAGE_FD	Magnitude of clad damage in all waste packages failed by fault displacement (Step 9). Units: {%} Type: Constant	100%
COLLAPSE_ THRESH_LITH	The minimum value of PGV that results in complete collapse of emplacement drifts in the lithophysal zones of the repository (Step 12). Units: {m/s} Type: Constant	0.384 m/s

Table 6.9-1. Definition of Parameters for the Seismic Scenario Class (Continued)

Parameter Name	Description, Units, and Type	Definition
COLLAPSE_ THRESH_NONLITH	The minimum value of PGV that results in complete collapse of emplacement drifts in the nonlithophysal zones of the repository. Units: {m/s} Type: Constant	5.35 m/s[c] [c]There is no collapse in the nonlithophysal zones with this value because the value of PGV_b is always less than 5 m/s.
EVENT_WEIGHT	Expected number of events in this realization. Units: {-} Type: Function	LAMBDA × EVENT_TIME
SAMPLE_WEIGHT	Correction for sampling of log-uniform distributions for time of the event and for annual exceedance frequency. Units: {-} Type: Function	LN(TIME_MAX/TIME_MIN) × LN(LAMBDA_MAX/LAMBDA_MIN)
WEIGHTED_DOSE	The probability-weighted dose for this realization. Units: {mrem/yr} Type: Function	EVENT_WEIGHT × SAMPLE_WEIGHT × DOSE, where DOSE is the time dependent (unweighted) dose for this realization.

NOTE: The symbol "-" denotes a dimensionless parameter.

CSNF = commercial spent nuclear fuel; PWR = pressurized water reactor; CDSP = codisposal; PGV = peak ground velocity; HLW = high-level radioactive waste; SCC = stress corrosion crack.

6.9.3 Limitations

There are three important limitations for the seismic scenario class for TSPA-LA: the duration of the calculations, the possibility of rockfall in the drifts before the seismic event, and the range of validity of the model abstraction for waste package damage.

The seismic scenario class for TSPA-LA is designed for a duration of 20,000 years. This design limitation arises from two factors. The first factor relates to the parameters for the structural response calculations, namely structural thicknesses and mechanical properties for the drip shield and waste package. The thicknesses of the drip shield and waste package have been reduced to represent the potential degradation of these structures by general corrosion over the first 10,000 years to 20,000 years after repository closure. The mechanical properties of Alloy 22 and of Titanium Grade 7 have been evaluated at an elevated temperature, 150ºC, which provides conservative values for over 98.5 percent of the 10,000-year regulatory period for the high temperature operating model and for 100 percent of the time for the low temperature operating mode. This approach is highly conservative from a risk assessment viewpoint because materials will be stronger than represented in the structural response calculations for about 98.5 percent of the realizations in the TSPA-LA. The definition of structural thickness and material properties should be reevaluated and new abstractions developed if the duration of the seismic scenario class is extended beyond 20,000 years.

The second factor for the design limitation related to the duration of the seismic scenario class is that coupled effects from multiple seismic events are not considered because seismic hazards with the potential to have a significant impact on engineered barriers are anticipated to occur

very rarely during the 20,000 year period. This is a reasonable approach for events that occur with an annual frequency of 10^{-5} per year or less over a 10,000 year or 20,000 year period. This is also a reasonable approach for annual exceedance frequencies between 10^{-4} and 10^{-5} per year if the corresponding ground motions and fault displacements produce small damage to EBS components (as is true for these abstractions).

The second limitation is related to the condition of the drifts at the time of the seismic event. Structural response calculations for the drip shield and waste package do not include backfill around the drip shield at the time of the seismic event. This representation is consistent with the present design that does not include engineered backfill but may become invalid if long-term fatigue of the tuff rock causes drift degradation and substantial collapse before a second seismic event with the potential to damage EBS components occurs.

6.10 VERIFICATION OF SCIENTIFIC ANALYSES

The abstractions for cladding damage from vibratory ground motions and for the EBS damage from fault displacement are stochastic distributions whose parameters are a function of the amplitude or the exceedance frequency of the ground motion. These abstractions are considered scientific analyses because they are based on standard statistical techniques that bound the component response. Since these abstractions are not models, they are not validated per AP-SIII.10Q, *Models*. Verification that these abstractions are an accurate representation of the variability and uncertainty in damage to the EBS components is discussed below.

- Damage to Cladding from Vibratory Ground Motion

  The abstraction for damage to the cladding has 100 percent of the cladding perforated after a ground motion with PGV of 1.05 m/s or larger occurs. This is a conservative, bounding approach (see discussion in Section 6.5.6) that does not require further verification.

- Damage to EBS Components from Fault Displacement

  The abstraction for damage to the waste package and drip shield from fault displacement is based on the mean hazard curves for displacement of known faults in the repository block and on the available clearances between EBS components. The analysis of damage from fault displacement demonstrates that there is no damage from faulting until an annual exceedance frequency less than 2×10^{-7} per year is reached. In other words, only the largest fault displacements have the potential to damage the EBS components.

  If a package is damaged by fault displacement, the damaged area on the waste package is defined as a uniform distribution with a lower bound of 0 and an upper bound given by the lid area. The lower bound represents a situation with minor crimping of the waste package; the upper bound represents a situation in which the welds fail and the lid completely separates from the waste package. These damage states are intended to be bounding conditions because there is high uncertainty in the state of the drift, the invert, and the EBS components after a major fault displacement.

If a package is damaged by fault displacement, the damaged area on the drip shield surrounding that package is 100 percent. This total damage state is a bounding condition because some fault displacements produce minimal crimping between the waste package and drip shield. Similarly, the cladding is 100 percent perforated for a fault displacement that damages the waste package.

The damage abstraction for fault displacement has been compared to an alternate conceptual model proposed by (Waiting et al. 2003 [DIRS 164449]). There is reasonable agreement between the damage abstraction in this report and the alternate conceptual model, considering that the alternate model is based on historical data for fault displacement in the western United States and that the damage abstraction is based on hazard curves specific to Yucca Mountain. For example, the number of fault intersections predicted by the damage abstraction is 171, versus 191 for the alternate conceptual model. Similarly, the probability weighted number of waste package failures is predicted to be 2.3×10^{-6} for the damage abstraction, within the range of 1.9×10^{-6} to 1.9×10^{-5} for the alternate conceptual model. This agreement provides added confidence in the damage abstraction for fault displacement.

The abstractions for diversion of seepage (also called flux splitting) by the drip shield and waste package after a seismic event are simple scientific analyses of flow patterns through stress corrosion cracks or through the area exposed by drip shield separation (only applicable to validation testing of the TSPA-LA model). Verification that these abstractions are an accurate representation of the variability and uncertainty in damage to the EBS components is discussed below.

- Flow Through a Network of Stress Corrosion Cracks

  Sections 6.3.4 through 6.3.6 summarize the morphology of stress corrosion crack networks on the waste package and drip shield. The network of stress corrosion cracks on the waste package and drip shield have high tortuosity and high surface roughness, and narrow to very small apertures at the crack tip(s) (Figure 6.3-2). This physical morphology will eliminate significant advective flux through the crack geometry because there is minimal head gradient or pressure gradient driving flow through the narrow apertures and because narrow cracks will infill with corrosion products and evaporation-induced precipitation of minerals over time. *Engineered Barrier System Features, Events, and Processes* (BSC 2004 [DIRS 169898], Sections 6.2.63 and 6.2.64) provides more detailed technical arguments that screen advective flow through stress corrosion cracks on the waste package and drip shield out of TSPA-LA.

- Flow Through Separated Drip Shields (only for validation testing of TSPA-LA)

  Separated drip shields provide a direct pathway for seepage from the roof of the drift to fall directly onto the exposed portion of a waste package. The abstraction for flow diversion with separated drip shields is based on the percent of axial separation between adjacent shields. This approach conservatively maximizes the potential seepage onto the waste package because all seepage from the roof, even the seepage falling beyond the footprint of the package, contacts the crown of the package. This bounding approach to the flow diversion abstraction does not require further verification.

7. VALIDATION

The Seismic Consequence Abstraction report develops abstractions for the response of EBS components to seismic hazards at a geologic repository in Yucca Mountain, Nevada. It also defines the methodology for using these abstractions in a seismic scenario class for the TSPA-LA. The seismic hazards addressed are vibratory ground motion, fault displacement, and rockfall induced by ground motion. The EBS components are the drip shield, waste package, and the fuel rod cladding. Consistent with the intended use, the *Technical Work Plan For: Regulatory Integration Modeling of Drift Degradation, Waste Package and Drip Shield Vibratory Motion and Seismic Consequences* (BSC 2004 [DIRS 171520]) specifies model validation level of confidence III for the waste package consequence abstraction and model validation level of confidence II for the drip shield consequence abstraction.

Confidence Building During Model Development to Establish Scientific Basis and Accuracy for Intended Use

The applicable TWP (BSC 2004 [DIRS 171520], Section 2.2.2) specifies criteria for *Confidence Building During Model Development*. Additionally, the development of the model should be documented in accordance with the requirements of Section 5.3.2(b) of AP-SIII.10Q. The development of the Seismic Consequences Abstraction has been conducted according to these criteria, as follows:

1. *Selection of input parameters and/or input data, and a discussion of how the selection process builds confidence in the model. [AP-SIII.10 Q 5.3.2(b) (1) and AP-2.27Q Attachment 3 Level I (a)]*

   The types and quality of the data selected as input builds confidence in the model. The inputs to the Seismic Consequences Abstraction have all been obtained from controlled sources. Section 4.1 provides a discussion of the inputs and Table 4-1 identifies the data and design parameters used. Additional information that corroborates Table 4-1 and therefore builds additional confidence is discussed in Section 6.1.4. Discussions of parameter ranges and uncertainties are covered throughout Section 6. Model assumptions have been described in Section 5. Thus, this requirement can be considered satisfied.

2. *Description of calibration activities, and/or initial boundary condition runs, and/or run convergences, simulation conditions set up to span the range of intended use and avoid inconsistent outputs, and a discussion of how the activity or activities build confidence in the model. Inclusion of a discussion of impacts of any non-convergence runs [(AP-SIII.10Q 5.3.2(b)(2) and AP-2.27Q Attachment 3 Level I (e)].*

   The Seismic Consequences Abstractions for waste package and drip shield damage are functional relationships based on structural response calculations documented elsewhere, therefore detailed discussions regarding initial and boundary conditions, run convergences and non-convergences associated with the structural response calculations are not included in this report. The Seismic Consequences Abstraction spans the range of intended use by covering the full range of peak ground velocities that are applicable; by defining the failure mechanisms, residual stress thresholds, and failure morphology for

the waste package and drip shield; by consideration of responses to rockfall; and by responses to fault displacement.

The seismic failure criteria for Alloy 22 and Titanium Grade 7 have been selected in a conservative manner. The failure criteria are based on considerations of accelerated corrosion due to residual stress, rather than the ultimate tensile stress of Alloy 22 or Titanium Grade 7. In fact, none of the structures reached ultimate tensile failure in the structural calculations. The rationale for selection of the residual stress thresholds for failure is documented in Sections 6.3.2 and 6.3.3, based on information in *Stress Corrosion Cracking of the Drip Shield, the Waste Package Outer Barrier, and the Stainless Steel Structural Material* (BSC 2004 [DIRS 169985], page 6-7 in Section 6.2.1). The conservative approach to defining the residual stress thresholds for failure provides a safety margin that helps to enhance confidence in the seismic failure criteria. The failure criteria are considered appropriate for their intended use because they are a conservative interpretation of the experimental data for the corrosion of Alloy 22 and Titanium Grade 7 under conditions relevant to Yucca Mountain and are consistent with current scientific understanding.

This requirement can be considered satisfied.

3. *Discussion of the impacts of uncertainties to the model results including how the model results represent the range of possible outcomes consistent with important uncertainties.[(AP-SIII.10 Q 5.3.2(b)(3) and AP-2.27Q Attachment 3 Level 1 (d) and (f)]*.

   The calculations of damaged areas on the waste package and drip shield due to vibratory ground motions and rockfall induced by vibratory ground motions exhibit substantial variability induced by the uncertainties in seismic ground motions and other input parameters. This variability has been directly propagated into the TSPA-LA by defining stochastic parameters that are sampled during each realization of the seismic scenario class. A more detailed discussion can be found in Section 8.2 under Acceptance Criterion 3: **Data Uncertainty Is Characterized and Propagated Through the Model Abstraction.** Treatment of model uncertainty is discussed in Section 8.2 under Acceptance Criterion 4: **Model Uncertainty Is Characterized and Propagated Through the Model Abstraction.**

4. *Formulation of defensible assumptions and simplifications. [AP-2.27Q Attachment 3 Level I (b)]*.

   Discussion of assumptions is provided in Sections 5. The basis for the simplifications in the seismic damage abstractions is provided in Sections 6.5.1 through 6.5.6.

5. *Consistency with physical principles, such as conservation of mass, energy, and momentum. [AP-2.27Q Attachment 3 Level I (c)]*

   Consistency with physical principles, such as conservation of mass, energy, and momentum, is maintained because the abstractions are based on detailed structural response calculations. Structural calculations for the response of large engineered components (e.g., waste package, drip shield, or cladding) due to impact and vibration is

a well-established technology. The deformation of these types of structures can be evaluated with standard, commercially available finite-element programs. As a result, there is high confidence in the results from the computational process because of the extensive testing of commercial software on a wide variety of problems, including impact calculations. In addition, each computational study is based on a mesh refinement analysis and other supporting calculations that provide additional confidence in the results. No changes to the finite-element software are needed for these calculations. These engineering codes have been qualified for their intended use under LP-SI.11Q-BSC and the engineering calculations are performed under AP-3.12Q.

The abstractions for waste package response to vibratory ground motions and for drip shield response to vibratory ground motions are stochastic distributions whose parameters (i.e., the upper and lower bounds for a uniform distribution) are a function of the amplitude of the ground motion. These distributions, also called damage abstractions, are based on information from detailed structural response calculations. These distributions are model abstractions because they represent this detailed computational information in a simplified manner for TSPA-LA. The underlying information for the model abstractions are created by models that have been validated under AP-SIII.10Q and by engineering calculations with software qualified under LP-SI.11Q-BSC. The status of the engineering calculations for structural response, of the rockfall models and analyses, and of the failure criteria are discussed next, followed by a discussion of the validation of the individual model abstractions.

The results from the engineering calculations are considered appropriate for their intended use for several reasons. First, the calculations are based on standard, commercially available software that has demonstrated the capability to accurately analyze impact processes. Second, the finite-element representation of EBS components is designed (via mesh refinement studies) to accurately represent the potential damage from the impact processes. And lastly, the ground motions for the calculations are based on state-of-the-art techniques for representing seismic phenomena. On the other hand, two features of the boundary conditions for these engineering calculations are notable for their conservatism. First, the structural response calculations for the waste package have a rigid boundary (that moves with the invert) at the axial ends of the computational space. This is conservative for end-to-end impacts of adjacent waste packages because adjacent packages are likely to be moving synchronously during part of the ground motion, rather than with equal and opposite velocities as implied by a rigid wall. In addition, a rigid boundary is always stiffer than the adjacent structure. Both of these features lead to higher end-to-end damage for a rigid boundary than for an adjacent waste package in an emplacement drift. Similarly, the presence of a rigid boundary for the drip shield simulations amplifies any tendency toward drip shield separation because impacts with neighboring drip shields are always with equal and opposite velocities, as implied by the rigid wall, rather than synchronously. The second feature of the boundary conditions is that the very low frequency ground motions at the 5.35 m/s PGV level may be physically unrealizable, as discussed in Section 6.4.4.

The rockfall calculations are also performed with commercially available software, although it is necessary to modify the software for computational efficiency, for the representation of fractures with short or intermittent trace lengths, and for constitutive models for tuff. Because of these modifications, the rock mechanics codes are qualified and the models validated for their intended

application to lithophysal and nonlithophysal tuffs in accordance with AP-SIII.10Q. This model validation is documented in Section 7 of *Drift Degradation Analysis* (BSC 2004 [DIRS 166107]).

Confidence Building After Model Development to Support the Scientific Basis of the Model

The model abstraction for waste package response to vibratory ground is a simple numerical fit to the percent failed surface area as a function of PGV. The fit involves selecting the most appropriate distribution to represent the variability of damage as a function of PGV. The appropriate distributions and functional fits for the waste package has been developed and documented in Microsoft Excel spreadsheets. The numerical values in this spreadsheet has been verified during the checking process for this model report. This spreadsheet is found in Appendix B of this report, as well as electronically on a CD-ROM (Appendix H). Details of the validation process for the model abstractions are as follows:

- **Abstraction for Damage to the Waste Package from Ground Motion**

  The abstraction for damage to the waste package is based on a uniform distribution. The selection of a uniform distribution is justified by the comparisons shown in Figures 6.5-1 and 6.5-2 of Section 6.5.1. Figure 6.5-4 (also in Section 6.5.1) compares the upper bound of this uniform distribution with the calculated damage from ground motions with PGVs of 0.992 m/s, 2.44 m/s, and 5.35 m/s. The lower bound of this distribution is zero. Figure 6.5-6 provides an alternate upper bound, based on a lognormal distribution. The discussion in Section 6.5.2 and Appendix C explains how the calculated damage to the waste package is bounded by the upper and lower limits of the uniform distribution, providing objective evidence of its adequacy.

  The level of confidence required for validation of the damage abstraction for the waste package under vibratory ground motion is high (Level III) because damage to the waste package is a significant factor in determining dose in TSPA calculations. The abstraction for damage to the waste package has been validated by (1) corroboration of the abstraction results with damage data from structural response calculations, and by (2) an independent technical review that also includes corroboration of results with an alternative conceptual model. The model validation review criteria are (BSC 2004 [DIRS 171520], Section 2.2.2.2):

  1. Is the model abstraction reasonable and appropriate for its intended use?
  2. For given inputs, are the outputs of the model abstraction reasonable?
  3. Are limitations of the model abstraction adequately described?

  Corroboration of Abstraction Model. The input data for development of the waste package damage abstraction are documented in *D&E / PA/C IED Typical Waste Package Components Assembly* (BSC 2004 [DIRS 169990], Tables 16 and 17) and *Additional Structural Calculations of Waste Package Exposed to Vibratory Ground Motion* (BSC 2004 [DIRS 171717] for Realization 11 at the 5.35 m/s PGV level). Corroborating information for the damage abstraction are defined in *Structural Calculations of Waste*

Package Exposed to Vibratory Ground Motion (BSC 2004 [DIRS 167083], Section 6.3, last paragraph; Section 6.4, last paragraph; and Attachment XI-2).

The technical approach for this model abstraction is that a simple distribution is fit to the available information for the damaged area. In this regard, a uniform distribution provides an excellent representation of the damaged areas at the 2.44 m/s and 5.35 m/s PGV levels, as shown by Figures 6.5-1 and 6.5-2. The R^2 correlation of the damaged area data at the 5.35 m/s PGV level with a straight line is 0.9818, as shown in Figure 6.5-1. Similarly, the R^2 correlation of the damaged area data at 2.44 m/s PGV level with a straight line is 0.946, as shown in Figure 6.5-2. These correlations are relevant because a uniform distribution corresponds to a straight line for the cumulative probability distribution plots in Figures 6.5-1 and 6.5-2. Clearly, there is an excellent fit of these data with a uniform distribution.

The upper bound of the uniform distribution is conservatively set at the 95^{th} percent confidence level, as illustrated in Figure 6.5-3. This upper bound is also reasonable for the preliminary damage assessment at the 1 m/s PGV level, corresponding to the 10^{-5} annual exceedance frequency (Figure 6.5-4). Finally, the upper bound has been increased to provide results that are conservative relative to an alternate conceptual model based on a log normal distribution of the data developed during the independent technical review (see below and Figure 6.5-6). Further details are provided in the discussion in Sections 6.5.1 through 6.5.3.

Independent Technical Review and Alternate Conceptual Model. The independent technical review of the waste package damage abstraction is documented in Appendix C. This independent technical review is based on a log normal distribution as an alternate conceptual model for the damage abstraction, rather than the uniform distribution proposed in Section 6.5.1. The recommendation of the independent technical review has been incorporated into the waste package damage abstraction, as discussed in Section 6.5.3 and shown in Figure 6.5-6. This recommendation increased the upper bound on the uniform distribution for the damage abstraction so that it is conservative relative to both distributions types throughout the range of PGV values for the damaged area data.

These results fulfill the requirements in (BSC 2004 [DIRS 171520], Section 2.2.2.2) as follows:

1. Is the model abstraction reasonable and appropriate for its intended use?
   The uniform distribution for the model abstraction provides an excellent representation of the damage data from structural response calculations, judging by the fact that the R^2 values for the correlations, 0.9818 and 0.946, are very close to unity. An R^2 value of 1 indicates perfect correlation between data and a straight line and an R^2 value of 0 indicates no correlation between the data and a straight line.

2. For given inputs, are the outputs of the model abstraction reasonable?
   The outputs from the model abstraction are consistent with the input data from structural response calculations, as shown in Figures 6.5-1, 6.5-2, and 6.5-3, and

Figure 6.5-6. The upper bound of the uniform distribution provides a conservative representation of damage for a log-normal distribution or for a uniform distribution at the 95th percentile confidence level, as discussed in Appendix C.

3. Are limitations of the model abstraction adequately described?
   For TSPA-LA, the abstraction for damage to the waste package is being used over a range of PGV values for which structural response calculations have been performed. Structural response calculations have been performed at the 1 m/s, 2.44 m/s, and 5.35 m/s PGV levels. The maximum value of PGV is 5 m/s for TSPA-LA (Section 6.4.4), a value that lies within the range of the structural response data. The minimum value of PGV that causes damage to the waste package is 0.7 m/s, based on Equation (6.5-3). This value is close to the 1 m/s PGV level for structural response calculations and consistent with Assumption 5.1. In addition, the independent technical review confirmed that the damage abstraction provides a more than adequate representation of the damage surface between 1.5 m/s and 6 m/s (Section C3.2). The structural response calculations are performed for an open drift, without backfill or rockfall, as discussed in Sections 1.2 and 6.9.3.

- **Abstraction for Damage to the Drip Shield from Direct Ground Motion**

Damage to the drip shield from vibratory ground motion and from rockfall induced by vibratory ground motion has been screened out of TSPA-LA (Section 6.5.5). However, a drip shield separation model has been retained for validation testing of the TSPA-LA model. The abstraction for damage to the drip shield from ground motion is based on a uniform distribution. Sections D1 through D3 in Appendix D define the upper bound of this uniform distribution with the calculated damage from ground motions with a PGV of 2.44 m/s and 5.35 m/s. The lower bound of this distribution is zero. The calculated damage to the drip shield is bounded by the upper and lower bounds of this uniform distribution for a PGV value of 5.35 m/s. The 50 percent upper bound at a PGV of 5.35 m/s is based on the maximum estimate, as explained in Section 6.5.4. In this situation, there is objective evidence of the adequacy of the abstraction, based on the fact that the calculated damage is bounded by the upper and lower limits of the uniform distribution.

The level of confidence required for validation of the abstractions for the drip shield is moderate (Level II). An intact drip shield can deflect seepage and rockfall away from the waste package, thereby reducing advective releases from the waste package. The abstraction for damage to the drip shield from ground motion has been validated by (1) corroboration of the abstraction results with computational data from structural response calculations, and by (2) an independent technical review. The model validation review criteria (BSC 2004 [DIRS 171520], Section 2.2.2.2) are:

1. Is the model abstraction reasonable and appropriate for its intended use?
2. For given inputs, are the outputs of the model abstraction reasonable?
3. Are limitations of the model abstraction adequately described?

Corroboration of Abstraction Model. The input data for development of the drip shield separation abstraction are documented in (BSC 2004 [DIRS 169220], Calculation Results I, Calculation Results III, and Table 2). The technical approach for this model abstraction is identical to that for the other model abstractions for seismic damage. Namely, a simple distribution is fit to the available information for structural damage. However, this model abstraction is unique in the sense that separation is not observed at 2.44 m/s PGV level, so the only nonzero data points are at a PGV level of 5.35 m/s. In particular, the damaged area at a PGV of 5.35 m/s is conservatively bounded by 50 percent, based on the discussion in Section D.1 of Appendix D. The technical approach here is consistent with the methodology for the waste package damage abstraction, although this model abstraction is essentially a bounding analysis for low frequency, high amplitude seismic events. The corroboration of the drip shield separation abstraction results with data from the structural response calculations is demonstrated by conservatism of the 50 percent upper bound for separation in comparison with the structural response data. The basis for the abstraction for drip shield separation is discussed in more detail in Sections D1 through D3 of Appendix D.

Independent Technical Review. The independent technical review of the drip shield damage abstraction is documented in Appendix D, Sections D5 through D8. The recommendations of the review have been appropriately incorporated into the drip shield damage abstraction, as discussed in Section 6.5.6.

These results fulfill the requirements in (BSC 2004 [DIRS 171520], Section 2.2.2.2) as follows:

1. Is the model abstraction reasonable and appropriate for its intended use?
   A uniform distribution provides a bounding representation of the data for drip shield separation. The upper bound of 50 percent and lower bound of 10 percent maximize damage in comparison with the structural response data at the 5.35 m/s PGV level.

2. For given inputs, are the outputs of the model abstraction reasonable?
   The outputs from the model abstraction are consistent with the structural response calculations at the 2.44 m/s PGV level, which show no drip shield separation, and with the structural response calculations at the 5.35 m/s level, which do show drip shield separation. However, the degree of drip shield separation at 5.35 m/s PGV level is probably strongly influenced by the boundary conditions for the finite-element representation. Kinematic calculations with multiple drip shields in an emplacement drift demonstrate that drip shield separation is an extremely low probability occurrence for an open drift. In addition, small frictional forces from rockfall maintain synchronous response of the drip shields, without separation. Drip shield separation has therefore been screened out of TSPA-LA, as explained in Section 6.5.5.

3. Are limitations of the model abstraction adequately described?
   The use of the abstraction for drip shield separation is limited to validation testing of the TSPA-LA model, as explained throughout this document.

As discussed in Section 6.10, the abstractions for cladding damage from vibratory ground motions and for EBS damage from fault displacement are considered scientific analyses because they are based on standard statistical techniques that bound the component response. Since these abstractions are not models, they are not validated per AP-SIII.10Q.

The level of confidence required for validation of the abstraction for EBS damage from fault displacement is low. Damage to EBS components from fault displacement is a low probability event that occurs only for seismic hazards with annual exceedance frequencies of 2×10^{-7} per year or less (see Table 6.7-11 in Section 6.7.5). In addition, the maximum number of waste packages that are impacted by fault displacement is less than 60 because only packages located directly on certain faults can be damaged (see Table 6.7-11 in Section 6.7.5). Given the low probability of fault displacements that are large enough to damage the waste package and given the small number of packages involved, it follows that fault displacement will have only a small impact on dose in the seismic scenario.

The abstraction for damage to the cladding from vibratory ground motion results in 100 percent of the cladding perforated in response to a ground motion with PGV of 1.05 m/s or larger (Table 6.5-7). This is a bounding approach, as discussed in Section 6.5.6, which does not require further verification and is consistent with the available information and scientific understanding.

Similarly, the abstractions for flow diversion (also called flux splitting) on the drip shield and waste package after a seismic event are also simple scientific analyses of potential flow patterns through stress corrosion cracks or through the area exposed by drip shield separation. Since these abstractions are not models, they are not validated per AP-SIII.10Q. The verification of the post-seismic event flow diversion abstractions is discussed in Section 6.10.

Validation Summary

The Seismic Consequences Abstraction and its components have been validated by applying acceptance criteria based on an evaluation of the model's relative importance to the potential performance of the repository system. All validation requirements defined in the applicable TWP (BSC 2004 [DIRS 171520], Section 2.2.2) have been fulfilled. For the damage abstraction of the waste package under vibratory ground motion, this included corroboration of abstraction results with computational data, and independent technical review that includes corroboration of results with an alternative mathematical model (Appendix C). For the damage abstraction of the drip shield, this included corroboration of results with computational data from structural response calculations and an independent technical review (Appendix D). Requirements for confidence building during model development have also been satisfied. The model development activities and post development validation activities described establish the scientific bases for the Seismic Consequences Abstraction. Based on this, the Seismic Consequences Abstraction and its components are considered to be sufficiently accurate and adequate for the intended purpose and to the level of confidence required by each abstraction component's relative importance to the potential performance of the repository system.

8. CONCLUSIONS

8.1 SUMMARY

The purpose of this work is to develop abstractions for the response of EBS components to seismic hazards at a geologic repository at Yucca Mountain, Nevada, and to define the methodology for using these abstractions in a seismic scenario class for the TSPA-LA. The seismic hazards are vibratory ground motion, fault displacement, and rockfall due to ground motion. The EBS components are the drip shield, the waste package, and the fuel cladding. The following abstractions for seismically-induced damage have been developed:

- Damage to the waste package from vibratory ground motions
- Damage to the drip shield from vibratory ground motions
- Damage to the cladding from end-to-end impacts of adjacent waste packages
- Damage to the waste package, drip shield and cladding from fault displacement.

The recommended implementation of these abstractions and their associated input parameters for TSPA-LA is defined in Section 6.9.2 and Table 6.9-1. This computational algorithm can also be referenced through DTN: MO0409SPACALSS.005. The recommended implementation of damage from fault displacement for criticality analyses is defined in Section 6.7.8. The results in Section 6.7.8 can also be referenced through DTN: MO0409SPACALSS.005. The scaling factor for estimating ground motion time histories near the 1 m/s PGV level is discussed in Section 6.5.1.4 and calculated in Appendix A, bottom of page A-6. The numerical value of this scaling factor, 0.4066, can be referenced through DTN: MO0305SPASFEGM.000.

Damage to the drip shield from rockfall in the lithophysal zones is not abstracted for TSPA-LA because the lithophysal zone is expected to shatter into small fragments that cannot produce damaged areas on the drip shield.

The seismic scenario class is designed to efficiently determine the mean dose for seismic events with annual frequencies down to 10^{-8} per year. The seismic scenario class is based on a single seismic hazard occurring at a randomly chosen time in each realization of the TSPA-LA. That is, the conditional probability of a seismic event is 1 for each realization. The damage from this single event is based on the abstractions for the drip shield, the waste package and the cladding. The damaged areas on the EBS components define pathways for flow and transport through the EBS. Once radionuclides are released from the EBS, flow and transport in the unsaturated zone and the saturated zone are based on the same models and algorithms as for the nominal scenario class. Biosphere calculations and parameters for the seismic scenario class are also unchanged from the nominal scenario class.

Each realization of the seismic scenario class determines an annual dose time history for a single seismic hazard with known value of PGV and fault displacement. These dose time histories do not represent the mean dose, as called for in 10 CFR 63.303 [DIRS 156605], because a single hazard always occurs in each realization. However, a mean dose time history can be calculated using a probability-weighted sum and average of all the realizations for the seismic scenario class. The weighting factor for each realization corrects for the expected number of seismic

events in each realization and for the logarithmic sampling of the hazard curve for PGV and of the time of the seismic event.

The major limitations of the postclosure abstractions for the seismic scenario class are as follows:

- The structural response calculations include degradation of the waste package and drip shield over a 20,000-year time frame, which includes the initial 10,000-year regulatory period.

- Coupled effects from multiple seismic events are not considered because seismic hazards with the potential to have a significant impact on engineered barriers are anticipated to occur very rarely during the 10,000-year regulatory period. More specifically, seismic hazards with the greatest potential to damage the engineered barriers correspond to large disruptive events with annual exceedance frequencies much less than 10^{-4} per year (see Section 6.5 of this report), so there is only a very small probability that multiple events with the potential to induce significant damage will occur over a 10,000-year or 20,000-year period.

- Spatial variability has not been represented in the damage abstractions for EBS components under ground motion.

- Structural response calculations for the drip shield and waste package do not include backfill around the drip shield at the time of the seismic event. This representation is consistent with the present design that does not include an engineered backfill, is consistent with the results from drift degradation analyses under nominal repository conditions, and is consistent with rockfall analyses that indicate complete drift collapse does not occur until peak ground velocity exceeds a threshold of 2 m/s in the lithophysal regions of the repository.

- Structural response calculations are based on the 21-PWR waste package (Section 6.5.1.1). The design for the 21-PWR package is very similar to the design of the 44-BWR package, and these two package types account for almost 65 percent of the packages in the inventory for TSPA-LA (BSC 2004 [DIRS 169472], Table 11, for the 21-PWR AP, 21-PWR control rod, and 44-BWR absorber plate). It is reasonable to base damage estimates on the 21-PWR waste package because it is the dominant package design in the repository.

- The hazard curve for peak ground velocity at the emplacement drifts (defined in Section 6.4.3) has PGV values that exceed 5 m/s for annual exceedance frequencies below 10^{-7} per year (see Table 6.4-1 in Section 6.4.3). These PGV values are extremely large and may not be physically realizable for the seismic sources and geologic conditions in and around Yucca Mountain. A distribution for the maximum feasible or bounding values for PGV has been developed and included in TSPA-LA, based on an analysis of geologic conditions and other corroborating evidence at the repository site (Section 6.4.4).

- The ground motions for structural response calculations were created using different approaches for intercomponent variability and for spectral conditioning. Section 6.4.2 provides a discussion on the methodology for defining the suites of ground motions that are used in the structural response calculations, and Section 6.5.1.5 presents the result of a study of the sensitivity of damaged area to intercomponent variability.

8.2 HOW THE ACCEPTANCE CRITERIA ARE ADDRESSED

Acceptance Criterion 1: System Description and Model Integration Are Adequate.

(1): Total system performance assessment adequately incorporates important design features, physical phenomena, and couplings, and uses consistent and appropriate assumptions throughout the mechanical disruption of engineered barrier abstraction process;

Response: Section 6 explains the basis for the damage abstractions for the waste package (Sections 6.5.1 through 6.5.3), drip shield (Sections 6.5.4 and 6.5.5) and cladding (Section 6.5.6) in response to vibratory ground motion and fault displacement. The structural response calculations in Section 6.5.1 through 6.5.6 include the mechanical coupling between the EBS components in defining damaged areas on the drip shield and waste package or percent failed cladding. Section 6.6 considers the potential damage to the EBS components from rockfall induced by vibratory ground motion. Finally, Section 6.8 defines the thermal and hydrological changes to the in-drift environment after a seismic event. These sections collectively address the methodology for incorporating design features, seismic response, and mechanical/thermal/hydrologic coupling within the damage abstractions for the seismic scenario class. Specific aspects of the methodology are as follows:

- The abstractions for damaged areas on the waste package, drip shield, and cladding are based on a statistically robust sampling of uncertain parameters, including the ground motion time histories, rock fracture patterns, rock compressive strength, and friction coefficients (see Sections 6.5.1 through 6.5.7). The abstractions are based on rockfall and structural response calculations that use consistent assumptions and consistent material properties.

- All abstractions are based on the mean hazard curves for ground motion and fault displacement, as discussed in Section 6.4. This is consistent with Brocoum (2001 [DIRS 159576], enclosure).

- Degradation of the drip shield and waste package is addressed for the first 10,000 years to 20,000 years after repository closure by reducing the thickness of the outer shell of the waste package and the thickness of the drip shield plates by 2 mm, as discussed in Assumption 5.5.

- Material properties for structural response calculations are based on a temperature of 150°C, resulting in conservative values for 98.5 percent of the first 10,000 years after closure for the high temperature operating mode, as discussed in

Assumption 5.5. This choice is even more conservative over the first 20,000 years after repository closure.

- Drip shield damage from rockfall induced by vibratory ground motion in the lithophysal and nonlithophysal zones is analyzed but not included in the damage abstractions (Section 6.6). Rockfall is analyzed with state-of-the-art computer codes that are used for other drift degradation calculations.

- All relevant seismic-related FEPs are considered in Section 6.2. The seismic-related FEPs in Table 6.2-1 are directly included in these abstractions. The seismic-related FEPs for damage to EBS components from seismic-induced rockfall and from seismic-induced drift collapse are screened out of TSPA-LA, based on the arguments summarized in Table 6.2-2.

(3): The abstraction of mechanical disruption of engineered barriers uses assumptions, technical bases, data, and models that are appropriate and consistent with other related U.S. Department of Energy abstractions. For example, assumptions used for mechanical disruption of engineered barriers are consistent with the abstraction of degradation of engineered barriers (Section 2.2.1.3.1 of the *Yucca Mountain Review Plan*). The descriptions and technical bases provide transparent and traceable support for the abstraction of mechanical disruption of engineered barriers;

Response: The seismic scenario class is represented as a separate scenario class in TSPA. The rationale for this approach is explained in Section 6.9. The seismic scenario class generally uses the same assumptions, technical bases, data and models as the nominal scenario. Major exceptions are: (1) the failure mechanisms for the waste package and drip shield and cladding, as discussed in Section 6.3, (2) changes to the in-drift seepage, temperature, and relative humidity after a seismic event (Section 6.8), and (3) alternate flow diversion (also called flux splitting) for the drip shield and waste package in the post-seismic environment (Section 6.8). Specific aspects of the seismic scenario class are as follows:

- All abstractions are based on the mean hazard curves for ground motion and fault displacement, as discussed in Section 6.4. This is consistent with Brocoum (2001 [DIRS 159576], enclosure).

- The analysis of rockfall for the seismic scenario and for the nominal scenario is based on the same set of computer codes (Section 6.6 and BSC 2004 [DIRS 166107]). Similarly, the LS-DYNA code is used for both design calculations and structural response calculations for the seismic scenario (Section 6.5).

- The residual stress threshold for failure of Alloy 22 is also used as the threshold for initiation of stress corrosion cracking in the representation of corrosion processes on the waste package, as discussed in Sections 6.3.2 and 6.3.3.

(4): Boundary and initial conditions used in the total system performance assessment abstraction of mechanical disruption of engineered barriers are propagated throughout its abstraction approaches;

Response: The rockfall and structural response calculations use the same sets of ground motions at the 2.44 m/s PGV level and the 5.35 m/s PGV level. Other boundary and initial conditions that ensure consistency are as follows:

- The abstractions for damaged areas on the waste package, drip shield, and cladding are based on a statistically robust sampling of uncertain parameters, including the ground motion time histories, rock fracture patterns, rock compressive strength, and friction coefficients (see Sections 6.5.1 through 6.5.7). The abstractions are based on rockfall and structural response calculations that use consistent boundary conditions and initial conditions.

- All abstractions are based on the mean hazard curves for ground motion and fault displacement, as discussed in Section 6.4. This is consistent with Brocoum (2001 [DIRS 159576], enclosure).

- Degradation of the drip shield and waste package is addressed for the first 10,000 years to 20,000 years after repository closure by reducing the thickness of the outer shell of the waste package and the thickness of the drip shield plates by 2 mm, as discussed in Assumption 5.5.

- Material properties for structural response calculations are based on a temperature of 150°C, resulting in conservative values for 98.5 percent of the first 10,000 years after closure for the high temperature operating mode, as discussed in Assumption 5.5.

(5): Sufficient data and technical bases to assess the degree to which features, events, and processes have been included in this abstraction are provided.

Response: The seismic-related FEPs in Table 6.2-1 are directly included in these abstractions. The seismic-related FEPs for damage to EBS components from seismic-induced rockfall and from seismic-induced drift collapse are screened out of TSPA-LA, based on the arguments summarized in Table 6.2-2. Damage to EBS components from ground motion, rockfall, drift collapse, and shear due to fault displacement have been considered in the abstractions for the seismic scenario class or in the structural response calculations that support the abstractions.

Acceptance Criterion 2: Data Are Sufficient for Model Justification.

(1): Geological and engineering values, used in the license application to evaluate mechanical disruption of engineered barriers, are adequately justified. Adequate descriptions of how the data were used, interpreted, and appropriately synthesized into the parameters are provided.

Response: The underlying data for the seismic scenario are based on experimental data for stress corrosion cracking, on handbook values and manufacturer's literature for the elastic and inelastic properties of EBS component materials, and on expert elicitation. Specific source documents that support development of the seismic scenario class are as follows:

- The residual stress failure criteria are based on experimental data for the initiation of stress corrosion cracking in Alloy 22 and Titanium Grade 7 (BSC 2004 [DIRS 169985], Section 6.2.1).

- The constitutive models for Alloy 22 and for Titanium Grade 7 are based on material properties in the published literature. More specifically, the Young's modulus, Poisson's ratio, yield strength, and fraction factors are based on data in published literature (BSC 2004 [DIRS 167083] Section 5).

- Hazard curves are based on the results of an expert elicitation (CRWMS M&O 1998 [DIRS 103731]; DTN: MO0401MWDRPSHA.000 [DIRS 166962], with files listed in Table 4-1). The ground motion time histories for the rockfall and structural response calculations have been developed in a manner that is consistent with and builds upon the results of this expert elicitation.

(3): Data on geology of the natural system, engineering materials, and initial manufacturing defects, used in the total system performance assessment abstraction, are based on appropriate techniques. These techniques may include laboratory experiments, site-specific field measurements, natural analog research, and process-level modeling studies. As appropriate, sensitivity or uncertainty analyses used to support the U.S. Department of Energy total system performance assessment abstraction are adequate to determine the possible need for additional data.

Response: The underlying data for the seismic scenario are based on experimental data for stress corrosion cracking, on handbook values and manufacturer's literature for the elastic and inelastic properties of EBS component materials, and on expert elicitation. Specific sources that support development of the seismic scenario class are as follows:

- The residual stress failure criteria are based on experimental data for the initiation of stress corrosion cracking in Alloy 22 and Titanium Grade 7 (BSC 2004 [DIRS 169985], Section 6.2.1).

- The constitutive models for Alloy 22 and for Titanium Grade 7 are based on material properties in the published literature. More specifically, the Young's modulus, Poisson's ratio, yield strength, and fraction factors are based on data in published literature (BSC 2004 [DIRS 167083] Section 5).

- Hazard curves are based on the results of an expert elicitation (CRWMS M&O 1998 [DIRS 103731]; DTN: MO0401MWDRPSHA.000 [DIRS 166962], with files listed in Table 4-1). The ground motion time histories for the rockfall and structural response calculations have been developed in a manner that is consistent with and builds upon the results of this expert elicitation.

(4): Engineered barrier mechanical failure models for disruption events are adequate. For example, these models may consider effects of prolonged exposure to the expected emplacement drift environment, material test results not specifically designed or performed for the Yucca Mountain site, and engineered barrier component fabrication flaws.

Response: The potential failure modes of EBS components are analyzed in Section 6.3.1. Based on this discussion, accelerated stress corrosion cracking is the most likely failure mechanism for EBS components during a seismic event, rather than puncture or tearing at the ultimate tensile strain. The constitutive models for Alloy 22 and for Titanium Grade 7 are based on material properties in the published literature. More specifically, the Young's modulus, Poisson's ratio, yield strength, and fraction factors are based on data in published literature, as summarized in (BSC 2004 [DIRS 167083] Section 5).

Acceptance Criterion 3: Data Uncertainty Is Characterized and Propagated Through the Model Abstraction.

Data uncertainty is explicitly included in the seismic abstractions for TSPA-LA. Parameter uncertainty has been directly incorporated into the hazard curves that are direct inputs to the fault displacement model and the computational methodology for the seismic scenario. Parameter uncertainty is also included in the ground motion time histories that are direct inputs to the rockfall and structural response calculations that provide the basis for the damage abstractions. Uncertainty in the input parameters for the structural response and rockfall calculations is described next, followed by information on Subcriteria (1), (2), and (3) for this acceptance criterion.

Uncertainty in Input Parameters for Structural Response Calculations

The structural response calculations for the waste package response and drip shield under vibratory ground motions include three major sources of uncertainty: (1) the ground motion time histories (aleatory uncertainty), (2) the metal-to-metal friction coefficient (epistemic uncertainty), and (3) the metal-to-rock friction coefficient (epistemic uncertainty):

- Fifteen sets of three-component ground motion time histories are used to represent the uncertainty in the seismic hazard at PGV levels of 2.44 m/s and 5.35 m/s. One horizontal component of each of the fifteen sets of ground motions is scaled to have the same horizontal PGV because its uncertainty has been incorporated into the hazard curves during the PSHA. The peak ground acceleration and the duration of the time histories span a wide range of response. For example, the peak ground acceleration for the first horizontal ground motion component at the 2.44 m/s PGV level ranges from about 1.5 *g* to 7 *g*.

- The metal-to-metal friction coefficient between the waste package and emplacement pallet varies from 0.2 to 0.8 to represent the uncertainty in its value. The friction coefficient affects the onset of sliding and dissipation of energy for the EBS components as a function of the amplitude of the ground motion. However, the importance of

friction is anticipated to diminish with increasing ground motion level because the EBS components begin to slide almost immediately for high amplitude ground motions.

- The metal-to-rock friction coefficient between the emplacement pallet and the invert or between the drip shield and the invert varies from 0.2 to 0.8 to represent the uncertainty in its value. Again, the friction coefficient affects the onset of sliding and dissipation of energy for the unanchored EBS components as a function of the amplitude of the ground motion. However, the importance of friction is anticipated to diminish with increasing amplitude of the ground motions.

The selection of friction coefficients as major sources of uncertainty, in addition to the ground motions, is based on the potential for frictional forces to influence the kinematics of EBS components. Variability in ground motions is often the most significant uncertainty in structural response calculations for nuclear plant components. Variability of friction coefficients may be important if damage varies significantly with the relative motions or impacts between adjacent structures.

The variations of these uncertain input parameters are simultaneously included in the fifteen structural response calculations at each seismic hazard level. This is accomplished by a Monte Carlo procedure that ensures robust sampling of the uncertain parameters over their full ranges (Sections 6.5.1 and 6.5.4). The Monte Carlo procedure and the sampled values of the three uncertain input parameters are described and documented in *Sampling of Stochastic Input Parameters for Rockfall and Structural Response Calculations Under Vibratory Ground Motion* (BSC 2004 [DIRS 169059]).

The results from the structural response calculations are post processed to determine the damaged areas on the drip shield or waste package. The seismic damage abstractions for the waste package and drip shield make use of a residual stress threshold as a failure criterion (Sections 6.3.2 and 6.3.3). If the residual stress from mechanical damage exceeds the stress threshold for the barrier, then the affected area(s) are represented as a network of stress corrosion cracks. The residual stress threshold for the waste package is based on a uniform distribution between 80 and 90 percent of the yield strength for Alloy 22 (Section 6.3.2 and 6.3.3). Post processing of the output from waste package calculations has determined the damaged areas corresponding to both 80 and 90 percent of the yield strength of Alloy 22 (BSC 2004 [DIRS 167083], Tables 6.4.1-2 and 6.4.2-2). The residual stress threshold for titanium is (very) conservatively set to a constant value of 50 percent of the yield strength of Titanium Grade 7, so no uncertainty is propagated into TSPA-LA for damaged area on the drip shield from vibratory ground motion.

Uncertainty in Input Parameters for Rockfall Calculations

All rockfall calculations include the ground motion time histories as a major source of uncertainty (Section 6.6). Fifteen ground motions again represent the uncertainty in the seismic hazard at each annual exceedance frequency. In the lithophysal units, the rock compressive strength is an uncertain input parameter that is represented as five discrete levels of rock strength, ranging from low (5 MPa) to high (30 MPa). In the nonlithophysal units, the synthetic fracture pattern is an uncertain input parameter. The synthetic fracture pattern is a representation

of the fracture system geometry in three dimensions. More than 30 synthetic fracture patterns are used in the rockfall calculations for the nonlithophysal units. The variations in these uncertain parameters are simultaneously included in the rockfall analyses at each seismic hazard level (BSC 2004 [DIRS 166107]).

The stochastic input parameters for the rockfall calculations are based on engineering judgment. For example, the rock compressive strength is a key parameter for tunnel failure in a continuum material, while the fracture geometry is a key parameter for identifying the size and location of rock blocks that can be shaken loose from the walls of a tunnel. Fracture properties can also be important in the nonlithophysal units, but are conservatively represented rather than being incorporated into the stochastic sampling scheme.

The results from the rockfall calculations are not direct inputs to TSPA-LA. Rockfall calculations for lithophysal units predict drift collapse at PGV levels of 2 m/s and greater; however, the strong seismic waves are predicted to shatter the lithophysal rock into small fragments that cannot damage the drip shield or waste package as a flow barrier.

Rockfall calculations for the nonlithophysal units predict a wide range of block sizes and velocities that can be ejected from the tunnel walls and impact the drip shield. More specifically, each rockfall calculation for the nonlithophysal unit predicts a complex, time-dependent sequence of rock blocks that impact the drip shield at varying locations and velocities. These impacts can cause damage to the drip shield if the block has enough mass and kinetic energy.

Propagation of Uncertainty Into TSPA

The calculations of damaged area on the waste package and drip shield due to vibratory ground motions exhibit substantial variability induced by the uncertainties in seismic ground motions and other input parameters. This variability has been directly represented in TSPA-LA by defining stochastic parameters that are sampled during each realization of the seismic scenario class. For example:

- For a given value of PGV, damage to the waste package from vibratory ground motion is represented as a uniform distribution that is sampled for each realization of the seismic scenario class. The lower bound of this distribution is zero damage for all values of PGV. The upper bound of this distribution is a linear function of PGV. This function represents the maximum damage with a 95 percent confidence limit, based on the damage results for the 2.44 m/s and 5.35 m/s PGV hazard levels. The upper range of this uniform distribution is illustrated in Figures 6.5-3, 6.5-4, and 6.5-5.

- The uncertainty in the residual stress threshold for Alloy 22 has not been propagated into the abstraction for TSPA-LA. The damage states for the waste packages are based on an average of the damage areas using the 80 and 90 percent Alloy 22 failure criteria. This is an accurate representation for the mean damage area due to the variability in the uniformly distributed residual stress threshold. This approach is reasonable because the variability in damaged area due to the uncertainty in failure criterion is approximately a factor of 2, while the variability in damaged area due to the ground motions at a given value of PGV is more than an order of magnitude (Tables 6.5-1 and 6.5-2). In this

situation, it is reasonable to ignore the variability in damaged area due to failure criterion because the variability from ground motions is the dominant effect on uncertainty.

- For a given value of PGV, damage to the drip shield from vibratory ground motion is represented as a uniform distribution for PGV values of 2.44 m/s and greater. The lower bound of this distribution is a linear function pf PGV that rises from zero damage to 10 percent for PGV values of 2.44 m/s and 5.35 m/s, respectively. The upper bound of this distribution is a linear function of PGV that rises from zero damage to 50 percent damage between 2.44 m/s and 5.35 m/s, respectively, and then remains constant at 50 percent for PGV values greater than 5.35 m/s.

The abstraction for cladding does not propagate uncertainty into TSPA-LA because it is based on a simplified response that is bounded with two damage states: zero damage below PGV of 0.55 m/s and 100 percent damage for PGV values of 1.05 m/s and greater.

Discussion for Subcriteria (1), (2), and (3)

(1): Models use parameter values, assumed ranges, probability distributions, and bounding assumptions that are technically defensible, reasonably account for uncertainties and variabilities, and do not result in an under-representation of the risk estimate;

Response: The above discussion directly addresses the technical defensibility, uncertainty, and variabilities in parameter values. Specific examples include:

- Rockfall models and structural response calculations use parameter values and parameter ranges that are defensible and account for variabilities in rock properties and fracture patterns and uncertainties in ground motion time histories and friction coefficients.

- A major uncertainty in the response of the lithophysal zone is the rock compressive strength. This parameter is sampled from 5 levels for the rockfall calculations.

- Material properties for structural response calculations are based on a temperature of 150°C, which is conservative over 98.5 percent of the time for the first 10,000 years after closure. This choice is even more conservative for the first 20,000 years after repository closure (Assumption 5.5).

(2): Process-level models used to represent mechanically disruptive events, within the emplacement drifts at the proposed Yucca Mountain repository, are adequate. Parameter values are adequately constrained by Yucca Mountain site data, such that the effects of mechanically disruptive events on engineered barrier integrity are not underestimated. Parameters within conceptual models for mechanically disruptive events are consistent with the range of characteristics observed at Yucca Mountain.

Response: The LS-DYNA code is used to determine the mechanical response of EBS components to vibratory ground motion. LS-DYNA is used for both design calculations and for the structural response calculations for the seismic scenario (Section 6.5). The analysis of rockfall for the seismic scenario and for the nominal scenario is based on state-of-the-art

computer codes that can represent continuum and discontinuous response of rock in the lithophysal and nonlithophysal units of the repository (Section 6.6 and BSC 2004 [DIRS 166107]). The appropriateness of the parameters within LS-DYNA and for the rockfall calculations are discussed in underlying documents, such as *Drift Degradation Analysis* (BSC 2004 [DIRS 166107]), and are beyond the scope of this document.

(3): Uncertainty is adequately represented in parameter development for conceptual models, process-level models, and alternative conceptual models considered in developing the assessment abstraction of mechanical disruption of engineered barriers. This may be done either through sensitivity analyses or use of conservative limits; and Review Plan for Safety Analysis Report 2.2-33.

Response: The discussion preceding Subcriterion (1) directly addresses the incorporation of parameter uncertainty into the abstraction process. Specific examples include:

- A major uncertainty in the response of the lithophysal zone is the rock compressive strength. This parameter is sampled from 5 levels for the rockfall calculations.

- A major uncertainty in the response of the nonlithophysal zone is the fracture geometry and fracture properties. These uncertainties are represented by the use of numerous synthetic joint fracture patterns that are generated in a statistically sound manner and incorporated into the rockfall calculations for the nonlithophysal zones.

- Material properties for structural response calculations are based on a temperature of 150°C, which is conservative over 98.5 percent of the time for the first 10,000 years after closure. This choice is even more conservative for the first 20,000 years after repository closure (Assumption 5.5).

- Thicknesses of the waste package outer shell and drip shield plates have been reduced by 2 mm to conservatively account for general corrosion over the first 10,000 years to 20,000 years after closure (Assumption 5.5).

- Uncertainty and variability in damaged areas of the waste package and drip shield are represented in the abstractions as a sampled distribution (Sections 6.5.3 and 6.5.6). This uncertainty is directly incorporated into the abstractions for TSPA-LA.

Acceptance Criterion 4: Model Uncertainty Is Characterized and Propagated Through the Model Abstraction.

The seismic consequence abstractions have considered alternate conceptual models, primarily through different representations of the mean damage and the distribution of damage about the mean. Model uncertainty has been directly incorporated into the hazard curves that are direct inputs to the fault displacement model and the computational methodology for the seismic scenario. Model uncertainty is also included in generating the ground motion time histories that are input to the rockfall and structural response calculations that provide the basis for the damage abstractions.

In Section 6.5, the maximum damage to the waste package is represented as a linear function of PGV. This is equivalent to a linear function for the mean because damage is represented as a uniform distribution from zero to its maximum value. This linear function is consistent with Assumption 5.1 because it results in zero damage at the 0.7 m/s PGV level. An alternate formulation is to represent the mean damage as a power law function of PGV. However, this alternate formulation has been eliminated because it results in substantially greater damage than calculated for the 1.05 m/s PGV ground motions, while the linear function is an excellent fit to the damage data at this ground motion level.

The distribution of damaged areas on the waste package has been analyzed for the 2.44 m/s, 5.35 m/s and 1.05 m/s PGV levels. At the 5.35 m/s PGV level, the damage values can be represented by either a normal distribution or a uniform distribution. At the 2.44 m/s PGV level, the damage becomes bimodal. These points can be represented with a normal distribution that is truncated at a small, nonzero damage value, or again with a uniform distribution. The uniform distribution is selected for the abstraction for several reasons. First, it is conservative relative to a normal distribution for high values of damage because it will be sampled uniformly across its range, rather than being skewed towards sampling around the mean. Second, the normal distribution at 2.44 m/s PGV produces negative damage values because its mean and standard deviation are approximately equal. Extrapolating this behavior to lower ground motions, say at the 1.05 m/s PGV level, is highly uncertain without additional calculations. Third, a uniform distribution is a reasonable representation for the computational results for damage.

The damage to the drip shield from vibratory ground motion is based on similar considerations. The damage to the drip shield at 2.44 m/s PGV level is zero because there is no damage from rockfall and no drip shield separation. The damage to the drip shield at the 5.35 m/s PGV level is substantial because adjacent drip shields can separate. A uniform distribution is a reasonable representation of the limited computational data for the 5.35 m/s PGV level.

The damage abstraction for fault displacement has been compared to an alternate conceptual model proposed by Waiting et al. (2003 [DIRS 164449]). There is reasonable agreement between the damage abstraction in this report and the alternate conceptual model, considering that the alternate model is based on historical data for fault displacement in the western United States and that the damage abstraction is based on hazard curves specific to Yucca Mountain. For example, the number of fault intersections predicted by the damage abstraction is 171, versus 191 for the alternate conceptual model. Similarly, the probability weighted number of waste package failures is predicted to be 2.3×10^{-6} for the damage abstraction, within the range of 1.9×10^{-6} to 1.9×10^{-5} for the alternate conceptual model. This agreement provides added confidence in the damage abstraction for fault displacement.

Discussion for Subcriteria (2) and (3)

(2): Consideration of conceptual model uncertainty is consistent with available site characterization data, laboratory experiments, field measurements, natural analog information and process-level modeling studies; and the treatment of conceptual model uncertainty does not result in an under-representation of the risk estimate;

Response: The above discussion directly addresses how conceptual model uncertainty has been incorporated into the abstractions for the seismic scenario class. Specific examples include:

- The hazard curves for vibratory ground motion and fault displacement were developed from an expert elicitation (CRWMS M&O 1998 [DIRS 103731). This elicitation process explicitly considered conceptual model uncertainty during its development of the hazard curves.

- Grid convergence studies and alternate finite element representations have been evaluated for the rockfall models (BSC 2004 [DIRS 166107]) and for the structural response calculations (BSC 2004 [DIRS 167083], Attachments VI, VII, and XI) (BSC 2004 [DIRS 170844]). An alternate damaged area interpolation scheme has also been investigated (BSC 2004 [DIRS 170843]). Calculations have been performed with the most appropriate numerical representations, so this particular source of model uncertainty is not propagated through the damage abstractions for TSPA-LA.

(3): Appropriate alternative modeling approaches are investigated that are consistent with available data and current scientific knowledge, and appropriately consider their results and limitations using tests and analyses that are sensitive to the processes modeled.

Response: The discussion before Subcriterion (2) directly addresses how alternate modeling approaches were addressed. Specific examples include:

- The hazard curves for vibratory ground motion and fault displacement were developed from a expert elicitation (CRWMS M&O 1998 [DIRS 103731). The individual groupings of experts developed alternate conceptual models for defining the seismic hazards at Yucca Mountain.

- Grid convergence studies and alternate finite element representations have been evaluated for the rockfall models (BSC 2004 [DIRS 166107]) and for the structural response calculations (BSC 2004 [DIRS 167083], Attachments VI, VII, and XI; and BSC 2004 [DIRS 170844]). An alternate damaged area interpolation scheme has also been investigated (BSC 2004 [DIRS 170843]). Calculations have been performed with the most appropriate numerical representations, so this particular source of model uncertainty is not propagated through the damage abstractions for TSPA-LA.
- Alternative modeling approaches have been evaluated for the conceptual and computational models of lithophysal and nonlithophysal rock (BSC 2004 [DIRS 166107]), but are beyond the scope of this document.
- Alternate distributions for damage abstractions have been considered in abstracting the damage results for the waste package (see Sections 6.5.1 through 6.5.3).
- The damage abstraction for fault displacement has been compared to an alternate conceptual model proposed by Waiting et al. (2003 [DIRS 164449]).

Acceptance Criterion 5: Model Abstraction Output Is Supported by Objective Comparisons.

(1): Models implemented in this total system performance assessment abstraction provide results consistent with output from detailed process-level models and/or empirical observations (laboratory and field testings and/or natural analogs).

The consistency of the abstractions, with the detailed output from structural response calculations, are summarized in Table 8.2-1.

Table 8.2-1. Comparison of Seismic Abstractions with Objective Evidence

Abstraction	Objective Comparison
Damage to Waste Package from Ground Motion	The abstraction for damage to the waste package is based on a uniform distribution. Figures 6.5-3 and 6.5-4 compare the upper bound of this uniform distribution with the calculated damage from ground motions with a PGV of 1.067 m/s, 2.44 m/s, and 5.35 m/s. The lower bound of this distribution is zero. Figures 6.5-3 and 6.5-4 demonstrate that the calculated damage to the waste package is bounded by the upper and lower bounds of this uniform distribution, providing objective evidence of its adequacy. An independent technical review has also been performed for this damage abstraction to provide increased confidence in the model abstraction.
Damage to Drip Shield from Ground Motion (only for validation testing of the TSPA-LA model)	The abstraction for drip shield separation from ground motion is based on a uniform distribution. The upper limit of this uniform distribution provides an upper bound for the separation at a PGV of 5.35 m/s, providing objective evidence of its adequacy.
Damage to Cladding from Ground Motion	The abstraction for damage to the cladding has that 100 percent of the cladding perforated after a ground motion with PGV of 1.05 m/s or larger occurs. This scientific analysis is based on a conservative, bounding approach.
Damage to Waste Package, Drip Shield, and Cladding from Fault Displacement	The abstraction for damage to the waste package and drip shield from fault displacement is based on the hazard curves for displacement of known faults in the repository block and available clearances for EBS components. The analysis of fault displacement demonstrates that there is only damage from fault displacement with a 2×10^{-7} per year annual exceedance frequency, or less (see Table 6.7-11). In this situation, damage from fault displacement is a very low probability occurrence. In addition, a maximum of 56 packages is affected by fault displacement (see Table 6.7-11). In this situation, it is appropriate to verify this scientific analysis through the normal checking process for model reports.

EBS = engineered barrier system; PGV = peak ground velocity; TSPA-LA = total system performance assessment – license application.

(2): Outputs of mechanical disruption of engineered barrier abstractions reasonably produce or bound the results of corresponding process-level models, empirical observations, or both.

Response: Objective comparisons between the calculated damage to EBS components and the corresponding abstractions for TSPA-LA are summarized in Table 8.2-1.

(3): Well-documented procedures, that have been accepted by the scientific community to construct and test the mathematical and numerical models, are used to simulate mechanical disruption of engineered barriers.

Response: The objective comparisons in Table 8.2-1 are an accepted method for comparing abstractions with the underlying data from structural response calculations or for defining the bounding response of EBS components.

INTENTIONALLY LEFT BLANK

9. INPUTS AND REFERENCES

The following is a list of the references cited in this document. Column 2 represents the unique six digit numerical identifier (the Document Input Reference System number), which is placed in the text following the reference callout (e.g., BSC 2003 [DIRS 166274]). The purpose of these numbers is to assist in locating a specific reference. Within the reference list, multiple sources by the same author (e.g., BSC 2003) are sorted alphabetically by title.

9.1 DOCUMENTS CITED

Albin, A.L.; Singleton, W.L.; Moyer, T.C.; Lee, A.C.; Lung; R.C.; Eatman, G.L.; and Barr, D.L. 1997. Geology of the Main Drift - Station 28+00 to 55+00, Exploratory Studies Facility, Yucca Mountain Project, Yucca Mountain, Nevada. Bureau of Reclamation and US Geological Survey Denver, Colorado. Denver, Colorado: U.S. Geological Survey. ACC: MOL.19970625.0096. 101367

Andresen, P.L.; Emigh, P.W.; Young, L.M.; and Gordon, G.M. 2001. "Stress Corrosion Cracking of Annealed and Cold Worked Titanium Grade 7 and Alloy 22 in 110°C Concentrated Salt Environments." Corrosion/2001, 56th Annual Conference & Exposition, March 11-16, 2001, Houston, Texas, USA, Paper No. 01130, Houston, Texas: NACE International. TIC: 255671. 167840

Brocoum, S. 2001. "Transmittal of Report Addressing Key Technical Issues (KTI) Structural Deformation and Seismicity (SDS)." Letter from S. Brocoum (DOE/YMSCO) to C.W. Reamer (NRC), October 25, 2001, OL&RC: TCG-0140, with enclosure. ACC: MOL.20020304.0297; MOL.20030714.0094. 159576

BSC (Bechtel SAIC Company) 2001. *Plugging of Stress Corrosion Cracks by Precipitates*. CAL-EBS-MD-000017 REV 00. Las Vegas, Nevada: Bechtel SAIC Company. ACC: MOL.20011010.0168. 156807

BSC 2001. *Environment on the Surfaces of the Drip Shield and Waste Package Outer Barrier.* ANL-EBS-MD-000001 REV 00 ICN 02. Las Vegas, Nevada: Bechtel SAIC Company. ACC: MOL.20010724.0082. 155640

BSC 2003. *21-PWR Waste Package Side and End Impacts.* 000-00C-DSU0-01000-000-00B. Las Vegas, Nevada: Bechtel SAIC Company. ACC: ENG.20030227.0067. 162293

BSC 2003. *Development of Earthquake Ground Motion Input for Preclosure Seismic Design and Postclosure Performance Assessment of a Geologic Repository at Yucca Mountain, NV.* MDL-MGR-GS-000003 REV 00. Las Vegas, Nevada: Bechtel SAIC Company. ACC: DOC.20031201.0001. 166274

BSC 2003. *Drip Shield Statically Loaded by Backfill and Loose Rock Mass.* 000-00C-TED0-00300-000-00A. Las Vegas, Nevada: Bechtel SAIC Company. ACC: ENG.20030224.0004. 162601

BSC 2003. *Drop of Waste Package on Emplacement Pallet – A Mesh Study.* 000-00C-DSU0-02200-000-00A. Las Vegas, Nevada: Bechtel SAIC Company. ACC: ENG.20030915.0001. 165497

BSC 2003. *Maximum Accelerations on the Fuel Assemblies of a 21-PWR Waste Package During End Impacts.* 000-00C-DSU0-01100-000-00A. Las Vegas, Nevada: Bechtel SAIC Company. ACC: ENG.20030327.0002. 162602

BSC 2003. *Seismic Consequence Abstraction.* MDL -WIS-PA-000003 REV 00. Las Vegas, Nevada: Bechtel SAIC Company. ACC: DOC.20030818.0006. 161812

BSC 2003. *Structural Calculations of Drip Shield Exposed to Vibratory Ground Motion.* 000-00C-PEC0-00100-000-00A. Las Vegas, Nevada: Bechtel SAIC Company. ACC: ENG.20030618.0009. 163425

BSC 2004. *21-PWR Waste Package End Impacts - A Mesh Study.* 000-00C-WIS0-02100-000-00A. Las Vegas, Nevada: Bechtel SAIC Company. ACC: ENG.20040617.0005. 170844

BSC 2004. *Additional Structural Calculations of Waste Package Exposed to Vibratory Ground Motion.* 000-00C-WIS0-01700-000-00B. Las Vegas, Nevada: Bechtel SAIC Company. 171717

BSC 2004. *Alternative Damaged Area Evaluation for Waste Package Exposed to Vibratory Ground Motion.* 000-00C-WIS0-01900-000-00A. Las Vegas, Nevada: Bechtel SAIC Company. ACC: ENG.20040420.0010. 170843

BSC 2004. *Characterize Framework for Seismicity and Structural Deformation at Yucca Mountain, Nevada.* ANL-CRW-GS-000003 REV 00, with errata. Las Vegas, Nevada: CRWMS M&O. ACC: MOL.20000510.0175; DOC.20040223.0007. 168030

BSC 2004. *D&E / PA/C IED Emplacement Drift Configuration and Environment.* 800-IED-MGR0-00201-000-00B. Las Vegas, Nevada: Bechtel SAIC Company. ACC: ENG.20040326.0001. 168489

BSC 2004. *D&E / PA/C IED Interlocking Drip Shield and Emplacement Pallet.* 800-IED-WIS0-00401-000-00D. Las Vegas, Nevada: Bechtel SAIC Company. ACC: ENG.20040503.0018. 169220

BSC 2004. *D&E / PA/C IED Subsurface Facilities Committed Materials.* 800-IED-WIS0-00302-000-00B. Las Vegas, Nevada: Bechtel SAIC Company. ACC: ENG.20040318.0031. 169058

BSC 2004. *D&E / PA/C IED Subsurface Facilities.* 800-IED-WIS0-00104-000-00A. Las Vegas, Nevada: Bechtel SAIC Company. ACC: ENG.20040309.0029. 168180

BSC 2004. *D&E / PA/C IED Subsurface Facilities.* 800-IED-WIS0-00103-000-00A. Las Vegas, Nevada: Bechtel SAIC Company. ACC: ENG.20040309.0028. 168370

BSC 2004. *D&E / PA/C IED Subsurface Facilities.* 800-IED-WIS0-00101-000-00A. Las Vegas, Nevada: Bechtel SAIC Company. ACC: ENG.20040309.0026. 164519

BSC 2004. *D&E / PA/C IED Typical Waste Package Components Assembly.* 800-IED-WIS0-00204-000-00B. Las Vegas, Nevada: Bechtel SAIC Company. ACC: ENG.20040202.0012. 167369

BSC 2004. *D&E / PA/C IED Typical Waste Package Components Assembly.* 800-IED-WIS0-00202-000-00C. Las Vegas, Nevada: Bechtel SAIC Company. ACC: ENG.20040517.0008. 169472

BSC 2004. *D&E / PA/C IED Typical Waste Package Components Assembly.* 800-IED-WIS0-00205-000-00D. Las Vegas, Nevada: Bechtel SAIC Company. ACC: ENG.20040518.0001. 169990

BSC 2004. *Design and Engineering, Interlocking Drip Shield Configuration.* 000-M00-SSE0-00101-000-00B. Las Vegas, Nevada: Bechtel SAIC Company. ACC: ENG.20040305.0020. 168275

BSC 2004. *Drift Cross Section Showing Emplaced Waste Package and Drip Shield.* 800-M00-WIS0-00101-000-00A. Las Vegas, Nevada: Bechtel SAIC Company. ACC: ENG.20040420.0013. 170074

BSC 2004. *Drift Degradation Analysis.* ANL-EBS-MD-000027 REV 03. Las Vegas, Nevada: Bechtel SAIC Company. 166107

BSC 2004. *Drip Shield Structural Response to Rock Fall.* 000-00C-SSE0-00300-000-00A. Las Vegas, Nevada: Bechtel SAIC Company. ACC: ENG.20040405.0019. 168993

BSC 2004. *Engineered Barrier System Features, Events, and Processes.* ANL-WIS-PA-000002 REV 03. Las Vegas, Nevada: Bechtel SAIC Company. 169898

BSC 2004. *Features, Events, and Processes: Disruptive Events.* ANL-WIS-MD-000005 REV 001, with errata. Las Vegas, Nevada: Bechtel SAIC Company. ACC: DOC.20031212.0005; DOC.20040209.0001; DOC.20040401.0006. 168789

BSC 2004. *General Corrosion and Localized Corrosion of Waste Package Outer Barrier.* NL-EBS-MD-000003 REV 02. Las Vegas, Nevada: Bechtel SAIC Company. 169984

BSC 2004. *Mechanical Assessment of the Drip Shield Subject to the Vibratory Motion of the Dynamic and Static Rock.* CAL-WIS-AC-000002 REV00. Las Vegas, Nevada: Bechtel SAIC Company. 169753

BSC 2004. *Multiscale Thermohydrologic Model.* ANL-EBS-MD-000049 REV 02. Las Vegas, Nevada: Bechtel SAIC Company. 169565

BSC 2004. *Peak Ground Velocities for Seismic Events at Yucca Mountain, Nevada.* ANL-MGR-GS-000004 REV 000A. Las Vegas, Nevada: Bechtel SAIC Company. 170137

BSC 2004. *Q-List.* 000-30R-MGR0-00500-000-000 REV 00. Las Vegas, Nevada: Bechtel SAIC Company. ACC: ENG.20040721.0007. 168361

BSC 2004. *Sampling of Stochastic Input Parameters for Rockfall and Structural Response Calculations Under Vibratory Ground Motion.* ANL-EBS-PA-000009 REV 0 Errata 1. Las Vegas, Nevada: Bechtel SAIC Company. ACC: DOC.20040312.0003. 169059

BSC 2004. *Seismic Consequence Abstraction.* MDL-WIS-PA-000003 REV 0, Errata 1. Las Vegas, Nevada: Bechtel SAIC Company. ACC: DOC.20030818.0006; DOC.20040218.0002. 167780

BSC 2004. *Stress Corrosion Cracking of the Drip Shield, the Waste Package Outer Barrier, and the Stainless Steel Structural Material*. ANL-EBS-MD-000005 REV 02. Las Vegas, Nevada: Bechtel SAIC Company. 169985

BSC 2004. *Structural Calculations of Waste Package Exposed to Vibratory Ground Motion.* 000-00C-WIS0-01400-000-00A. Las Vegas, Nevada: Bechtel SAIC Company. ACC: ENG.20040217.0008. 167083

BSC 2004. *Technical Work Plan For: Regulatory Integration Modeling of Drift Degradation, Waste Package and Drip Shield Vibratory Motion and Seismic Consequences* TWP-MGR-GS-000003 REV 00 ICN 01. Las Vegas, Nevada: Bechtel SAIC Company. ACC: DOC.20040810.0003 171520

Budnitz, R.J.; Apostolakis, G.; Boore, D.M.; Cluff, L.S.; Coppersmith, K.J.; Cornell, C.A.; and Morris, P.A. 1997. *Recommendations for Probabilistic Seismic Hazard Analysis: Guidance on the Uncertainty and Use of Experts.* NUREG/CR-6372. Two volumes. Washington, D.C.: U.S. Nuclear Regulatory Commission. TIC: 235076; 235074. 103635

Canori, G.F. and Leitner, M.M. 2003. *Project Requirements Document.* TER-MGR-MD-000001 REV 02. Las Vegas, Nevada: Bechtel SAIC Company. ACC: DOC.20031112.0006. 166275

Chun, R.; Witte, M.; and Schwartz, M. 1987. *Dynamic Impact Effects on Spent Fuel Assemblies.* UCID-21246. Livermore, California: Lawrence Livermore National Laboratory. ACC: HQX.19881020.0031. 144357

CRWMS M&O (Civilian Radioactive Waste Management System Management and Operating Contractor) 1998. *Probabilistic Seismic Hazard Analyses for Fault Displacement and Vibratory Ground Motion at Yucca Mountain, Nevada.* Milestone SP32IM3, September 23, 1998. Three volumes. Las Vegas, Nevada: CRWMS M&O. ACC: MOL.19981207.0393. 103731

Gardner, D. 2000. "Meeting Summary, NRC/DOC Technical Exchange on Structural Deformation and Seismicity KTI, October 11-12, 2000." E-mail from D. Gardner to C. Hanlon, October 13, 2002, with attachment. ACC: MOL.20001102.0041; MOL.20001102.0042. 154287

Hahn, G.J. and Shapiro, S.S. 1967. *Statistical Models in Engineering*. New York, New York: John Wiley & Sons. TIC: 247729. 146529

Helton, J.C. 1994. "Treatment of Uncertainty in Performance Assessments for Complex Systems." Risk Analysis, 14, (4), 483-511. New York, New York: Plenum Press. TIC: 245848. 107739

Helton, J.C. 1997. "Uncertainty and Sensitivity Analysis in the Presence of Stochastic and Subjective Uncertainty." Journal of Statistical Computation and Simulation, 57, (1-4), 3-76. New York, New York: Gordon and Breach Science Publishers. TIC: 245958. 107496

Helton, J.C. and Davis, F.J. 2000. *Sampling-Based Methods for Uncertainty and Sensitivity Analysis.* SAND99-2240. Albuquerque, New Mexico: Sandia National Laboratories. TIC: 251256. 156572

Helton, J.C. and Davis, F.J. 2002. *Latin Hypercube Sampling and the Propagation of Uncertainty in Analyses of Complex System.* SAND2001-0417. Albuquerque, New Mexico: Sandia National Laboratories. TIC: 254367. 163475

Herrera, M.L. 2004. *Evaluation of the Potential Impact of Seismic Induced Deformation on the Stress Corrosion Cracking of the YMP Waste Packages.* SIR-04-015 Revision No. 1. San Jose, California: Structural Integrity Associates, Inc. 168133

Kaplan, S. and Garrick, B.J. 1981. "On the Quantitative Definition of Risk." Risk Analysis, 1, (1), 11-27. New York, New York: Plenum Press. TIC: 241205. 100557

McGarr, A. 1984. "Some Applications of Seismic Source Mechanism Studies to Assessing Underground Hazard." Proceedings of the 1st International Congress on Rockbursts and Seismicity in Mines, Johannesburg, 1982. Gay, N.C. and Wainwright, E.H., eds. Pages 199-208. Johannesburg, South Africa: South African Institute of Mining and Metallurgy. TIC: 254652. 163996

McGuire, R.K.; Silva, W.J.; and Costantino, C.J. 2001. *Technical Basis for Revision of Regulatory Guidance on Design Ground Motions: Hazard- and Risk-Consistent Ground Motion Spectra Guidelines.* NUREG/CR-6728. Washington, D.C.: U.S. Nuclear Regulatory Commission. TIC: 251294. 157510

McKay, M.D.; Beckman, R.J.; and Conover, W.J. 1979. "A Comparison of Three Methods for Selecting Values of Input Variables in the Analysis of Output from a Computer Code." Technometrics, 21, (2), 239-245. Alexandria, Virginia: American Statistical Association. TIC: 221741. 127905

Menges, C.M. and Whitney, J.W. 1996. "Distribution of Quaternary Faults in the Site Area." Chapter 4.2 of Seismotectonic Framework and Characterization of Faulting at Yucca Mountain, Nevada. Whitney, J.W., ed. Milestone 3GSH100M. Denver, Colorado: U.S. Geological Survey. TIC: 237980. ACC: MOL.19970129.0041. 106342

Mongano, G.S.; Singleton, W.L.; Moyer, T.C.; Beason, S.C.; Eatman, G.L.W.; Albin, A.L.; and Lung, R.C. 1999. *Geology of the ECRB Cross Drift - Exploratory Studies Facility, Yucca Mountain Project, Yucca Mountain, Nevada.* Deliverable SPG42GM3. Denver, Colorado: U.S. Geological Survey. ACC: MOL.20000324.0614. 149850

Newmark, N.M. and Rosenblueth, E. 1971. *Fundamentals of Earthquake Engineering. Civil Engineering and Engineering Mechanics Series.* Englewood Cliffs, New Jersey: Prentice-Hall. TIC: 248548. 151246

NRC (U.S. Nuclear Regulatory Commission) 2003. *Yucca Mountain Review Plan, Final Report.* NUREG-1804, Rev. 2. Washington, D.C.: U.S. Nuclear Regulatory Commission, Office of Nuclear Material Safety and Safeguards. TIC: 254568. 163274

Paté-Cornell, M.E. 1996. "Uncertainties in Risk Analysis: Six Levels of Treatment." Reliability Engineering and System Safety, 54, 95-111. New York, New York: ElSever. TIC: 245961. 107499

Rossman, A.J.; Short, T.H.; and Parks, M.T. 1998. "Bayes Estimators for the Continuous Uniform Distribution." Journal of Statistic Education. Alexandria, Virginia: American Statistical Association. Accessed April 7, 2003. TIC: 254033. http://www.amstat.org/publications/jse/v6n3/rossman.html 162631

Rubinstein, R.Y. 1981. *Simulation and the Monte Carlo Method.* New York, New York: John Wiley & Sons. TIC: 254563. 163476

Sanders, T.L.; Seager, K.D.; Rashid, Y.R.; Barrett, P.R.; Malinauskas, A.P.; Einziger, R.E.; Jordan, H.; Duffey, T.A.; Sutherland, S.H.; and Reardon, P.C. 1992. *A Method for Determining the Spent-Fuel Contribution to Transport Cask Containment Requirements.* SAND90-2406. Albuquerque, New Mexico: Sandia National Laboratories. ACC: MOV.19960802.0116. 102072

Sawyer, D.A.; Fleck, R.J.; Lamphere, M.A.; Warren, R.G.; Broxton, D.E.; and Hudson, M.R. 1994. "Episodic Caldera Volcanism in the Miocene Southwestern Nevada Volcanic Field: Revised Stratigraphic Framework, $^{40}Ar/^{39}$ AR Geochronology, and Implications for Magmatism and Extension." Geological Society of America Bulletin, 106, (10), 1304-1318. Boulder, Colorado: Geological Society of America. TIC: 222523. 100075

Waiting, D.J.; Stamatakos, J.A.; Ferrill, D.A.; Sims, D.W.; Morris, A.P.; Justus, P.S.; and Ibrahim, A.K. 2003. "Methodologies for the Evaluation of Faulting at Yucca Mountain, Nevada." Proceedings of the 10th International High-Level Radioactive Waste Management Conference (IHLRWM), March 30-April 2, 2003, Las Vegas, Nevada. Pages 377-387. La Grange Park, Illinois: American Nuclear Society. TIC: 254559. 164449

9.2 CODES, STANDARDS, AND REGULATIONS

10 CFR Part 63. Energy: Disposal of High-Level Radioactive Wastes in a Geologic Repository at Yucca Mountain, Nevada. 156605

AP-2.14Q, Rev. 3, ICN 0. *Document Review*. Washington, D.C.: U.S. Department of Energy, Office of Civilian Radioactive Waste Management. ACC: DOC.20030827.0018.

AP-2.22Q, Rev. 1, ICN 1. *Classification Analyses and Maintenance of the Q-List*. Washington, D.C.: U.S. Department of Energy, Office of Civilian Radioactive Waste Management. ACC: DOC.20040714.0002.

AP-2.27Q, Rev. 1, ICN 4. *Planning for Science Activities*. Washington, D.C.: U.S. Department of Energy, Office of Civilian Radioactive Waste Management. ACC: DOC.20040610.0006.

AP-3.12Q, Rev. 2, ICN 2. *Design Calculations and Analyses*. Washington, D.C.: U.S. Department of Energy, Office of Civilian Radioactive Waste Management. ACC: DOC.20040318.0002.

AP-3.15Q, Rev. 4, ICN 5. *Managing Technical Product Inputs*. Washington, D.C.: U.S. Department of Energy, Office of Civilian Radioactive Waste Management. ACC: DOC.20040812.0004.

AP-SIII.10Q, Rev. 2, ICN 7. *Models*. Washington, D.C.: U.S. Department of Energy, Office of Civilian Radioactive Waste Management. ACC: DOC. 20040920.0002.

AP-SV.1Q, Rev. 1, ICN 1. *Control of the Electronic Management of Information*. Washington, D.C.: U.S. Department of Energy, Office of Civilian Radioactive Waste Management. ACC: DOC.20040308.0001.

LP-SI.11Q-BSC, Rev. 0, ICN 1. *Software Management.* Washington, D.C.: U.S. Department of Energy, Office of Civilian Radioactive Waste Management. ACC: DOC.20041005.0008.

9.3 SOURCE DATA, LISTED BY DATA TRACKING NUMBER

LB0307SEEPDRCL.002. Seepage Into Collapsed Drift: Data Summary. Submittal date: 07/21/2003.	164337
LL040310323122.044. Input and Output Files of the MSTHM Micro-Abstractions for the Collapsed-Drift Cases for the TSPA-LA Low-Probability Seismic Scenario. Submittal date: 03/26/2004.	168769
MO0012MWDGFM02.002. Geologic Framework Model (GFM2000). Submittal date: 12/18/2000.	153777
MO0210PGVPB107.000. Design Peak Ground Velocity for the Repository Level (Point B) at 10^{-7} Annual Exceedance Probability. Submittal date: 10/17/2002.	162713
MO0303DPGVB106.002. Design Peak Ground Velocity for the Repository Level (Point B) at 10^{-6} Annual Exceedance Probability. Submittal date: 03/10/2003.	162712
MO03061E9PSHA1.000. Spectral Acceleration and Velocity Hazard Curves Extended to 1E-9 Based on the Results of the PSHA for Yucca Mountain. Submittal date: 06/09/2003.	163721
MO0401MWDRPSHA.000. Results of the Yucca Mountain Probabilistic Seismic Hazard Analysis (PSHA). Submittal date: 01/21/2004.	166962
MO0401SEPPGVRL.022. Peak Ground Velocity for the Repository Level (Point B) at 10^{-5} Annual Exceedance Frequency. Submittal date: 01/26/2004.	169099
MO0403SPASCRKD.000. Seismic Crack Density Model Outputs for LA. Submittal date: 03/09/2004.	168105
MO0407SEPFEPLA.000. LA FEP List. Submittal date: 07/20/2004.	170760
MO0404BPVELEMP.000. Bounding Peak Horizontal Ground Velocity at the Emplacement Level, Yucca Mountain, Nevada. Submittal date: 04/01/2004.	171052

9.4 PRODUCT OUTPUT, LISTED BY DATA TRACKING NUMBER

MO0305SPASFEGM.000. Scaling Factor for Estimating the 10^{-5} Per Year Ground Motions. Submittal date: 05/07/2003.

MO0409SPACALSS.005. Computational Algorithm of the Seismic Scenario for TSPA. Submittal date: 09/22/2004.

INTENTIONALLY LEFT BLANK

APPENDIX A

SPREADSHEET FOR SCALED HAZARD CURVE AT POINT B AND FOR COMBINED HAZARD AT POINT B WITH UNIFORM DISTRIBUTION FOR BOUNDING VALUE OF PGV

List of Inputs

MO03061E9PSHA1.000. Spectral Acceleration and Velocity Hazard Curves Extended to 1E-9 Based on the Results of the PSHA for Yucca Mountain. Submittal date: 06/09/2003. [DIRS 163721]

MO0303DPGVB106.002. Design Peak Ground Velocity for the Repository Level (Point B) at 10 6 Annual Exceedance Probability. Submittal date: 03/10/2003. [DIRS 162712]

MO0210PGVPB107.000. Design Peak Ground Velocity for the Repository Level (Point B) at 10-7 Annual Exceedance Probability. Submittal date: 10/17/2002. [DIRS 162713]

MO0401SEPPGVRL.022. Peak Ground Velocity for the Repository Level (Point B) at 10-5 Annual Exceedance Frequency. Submittal date: 01/26/2004. [DIRS 169099]

Relevant Formulas

The PGV hazard curve at Point A is defined by the points ($PGV_{Point\ A,i}$, $\lambda_{Point\ A,i}$) for $i = 1, 2, \ldots, n$, where PGV is the peak ground velocity and λ is the annual exceedance frequency. The scaled hazard curve for point B is defined by the following formulas:

$$PGV_{Point\ B,i} = a(PGV_{Point\ A,i})$$
$$\lambda_{Point\ B,i} = \lambda_{Point\ A,i}, \qquad \text{(Eq. A-1)}$$

for $i = 1, 2, \ldots, n$. The values of the exceedance frequency remain unchanged in Equation 1, and can be denoted more simply as λ_i. The quantity a is a constant, 0.7959, that minimizes the error with the known PGV values at Point B for the 10^{-5} per year, 10^{-6} per year, and 10^{-7} per year annual exceedance frequencies. The value of a is determined by trial and error, using a spreadsheet to calculate the error with the known values at Point B for varying values of a.

The values of PGV between the n points defined by Equation (A-1) are calculated with a log-linear interpolation scheme. For a given value of λ such that $\lambda_k < \lambda < \lambda_{k+1}$, the interpolation is given by[16]:

$$PGV = PGV_{Point\ B,k} + \frac{PGV_{Point\ B,k+1} - PGV_{Point\ B,k}}{\log(\lambda_{k+1}) - \log(\lambda_k)}(\log(\lambda) - \log(\lambda_k)) \qquad \text{(Eq. A-2)}$$

Output Information

Table A-1 defines the points for the scaled PGV hazard curve at Point B. The numerical values in Table A-1 are rounded off from more exact calculations in the spreadsheet.

[16] A log-log interpolation scheme can also be used to determine intermediate values on the hazard curve. The difference between a log-linear and log-log interpolation scheme is generally on the order of a few percent and not significant for total system performance assessment (TSPA) applications. For example, the value of 0.796 in Table A-1 becomes 0.818 with a log-log interpolation scheme, an increase of less than 3 percent.

Table A-1. Scaled Points for the PGV Hazard Curve at Point B

Scaled PGV At Point B (cm/s)	Annual Exceedance Frequency (1/yr)
15.9	6.26×10^{-4}
23.9	2.78×10^{-4}
39.8	9.30×10^{-5}
79.6	1.84×10^{-5}
159	3.07×10^{-6}
398	2.28×10^{-7}
557	8.15×10^{-8}
796	2.60×10^{-8}
1190	6.56×10^{-9}

The interpolated values of PGV for various values of the annual exceedance frequency are given in Table A-2. The numerical values in Table A-2 are rounded off from more exact calculations in the spreadsheet. The errors of the scaled hazard curve with the known values at Point B for the 10^{-5} per year, 10^{-6} per year, and 10^{-7} per year annual exceedance frequencies are +1.6 percent, +7.5 percent, and -1.8 percent, respectively.

Table A-2. Interpolated Values on the Scaled PGV Hazard Curve for Point B

Annual Exceedance Frequency (1/yr)	Interpolated PGV at Point B (cm/s)	Comments
5×10^{-4}	18.1	
10^{-4}	38.7	
5×10^{-5}	55.0	
10^{-5}	106.6	Error of +1.6 percent relative to the exact value of 105 cm/s
10^{-6}	262.3	Error of +7.5 percent relative to the exact value of 244 cm/s
10^{-7}	525.5	Error of –1.8 percent relative to the exact value of 535 cm/s
1×10^{-8}	1072	

Finally, the ratio of the PGV values at Point B for annual exceedance frequencies of 10^{-5} per year to 10^{-6} per year is given by:

$$\frac{PGV\ at\ 10^{-5}}{PGV\ at\ 10^{-6}} = \frac{106.6\,cm/s}{262.3 cm/s} = 0.4066. \qquad \text{(Eq. A-3)}$$

This ratio has been used to generate approximate ground motions for the 10^{-5} per year hazard level. It is available as a product output in DTN: MO0305SPASFEGM.000.

The spreadsheet defining the values in Tables A-1 and A-2 follows.

DEFINE THE MEAN HORIZONTAL PGV HAZARD CURVE AT POINT B (THE EMPLACEMENT		
DRIFTS) AND USE THIS CURVE TO ESTIMATE THE HORIZONTAL PGV VALUES AT		
ANNUAL EXCEEDANCE FREQUENCIES BETWEEN 5E-04 PER YEAR AND 1E-08 PER YEAR.		
ALSO CALCULATE THE MEAN HAZARD IF HORIZONTAL PEAK GROUND VELOCITY		
IS LIMITED BY A UNIFORM DISTRIBUTION BETWEEN 1.5 M/S AND 5 M/S.		
This calculation estimates the mean hazard curve for horizontal PGV at Point B (the emplacement		
drifts), based on the mean hazard curve for PGV at Point A (a reference rock outcrop at the		
repository elevation) and three known PGV values at Point B. More specifically, the known PGV		
values at point B are the basis for defining a scaling factor that minimizes the squared differences		
between the scaled hazard curve and the three known values of PGV at Point B. This approach		
preserves the shape of the Point A hazard curve.		
The scaling factor, 0.7959, minimizes the sum of the squared errors, providing a least squares fit.		
The small magnitude of the errors between the scaled Point A hazard curve and the known values		
at Point B, +1.57, +7.49 percent, and -1.77 percent, confirms that this is a reasonable approach.		
PGV values at Point B for various annual exceedance probabilities are then calculated using an		
interpolation that is linear in PGV and in the log of the annual exceedance frequency. A final		
analysis calculates the mean hazard curve at Point B if the maximum value of PGV is capped or		
limited by a uniform distribution between 1.5 m/s and 5 m/s.		
Input Data for the mean horizontal PGV hazard curve at Point A:		
DTN: MO03061E9PSHA1.000 [DIRS 163721]. PGV values are in cm/sec.		
Input Data for mean horizontal PGV values at Point B:		
Horizontal PGV value at Point B for the 10^{-5} mean annual exceedance probability, 1.05 m/s, is		
from DTN: MO0401SEPPGVRL.022 [DIRS 169099].		
Horizontal PGV value at Point B for the 10^{-6} mean annual exceedance probability, 2.44 m/s,		
is from DTN: MO0303DPGVB106.002 [DIRS 162712].		
Horizontal PGV value at Point B for the 10^{-7} mean annual exceedance probability, 5.35 m/s,		
is from DTN: MO0210PGVPB107.000 [DIRS 162713].		
Interpolate to find PGV values for 10^{-5}, 10^{-6}, and 10^{-7} annual exceedance probabilities at Point		
A, using a log-linear interpolation scheme. First, interpolate for 10^{-5} per year:		
Annual	**Point A**	**Interpolated**
Exceedance	**Horizontal**	**Value For 10^{-5}**
Frequency	**PGV**	**At Point A**
(1/yr)	**(cm/sec)**	**(cm/sec)**
1.83594E-05	100	134.0
3.07391E-06	200	

Interpolate for 10-06 per year:		
Annual	**Point A**	**Interpolated**
Exceedance	**Horizontal**	**Value At 10^{-6}**
Frequency	**PGV**	**At Point A**
(1/yr)	**(cm/sec)**	**(cm/sec)**
3.07391E-06	200	329.5
2.28195E-07	500	

Interpolate for 10-07 per year:		
Annual	**Point A**	**Interpolated**
Exceedance	**Horizontal**	**Value At 10^{-7}**
Frequency	**PGV**	**For C22Point A**
(1/yr)	**(cm/sec)**	**(cm/sec)**
2.28195E-07	500	660.3
8.15299E-08	700	

Now use trial and error to find the value of a Scale Factor that minimizes the sum of the square of the residuals for PGV with the known values at Point B.

	Scale Factor:	**0.79589**

	Known	**Scaled Value**	**Known**		
Annual	**Point A**	**for**	**Point B**	**Square**	
Exceedance	**Horizontal**	**Horizontal**	**Horizontal**	**of the**	**Percent**
Frequency	**PGV**	**PGV**	**PGV**	**Residuals**	**Error**
(1/yr)	**(cm/sec)**	**(cm/sec)**	**(cm/sec)**	**(cm^2/sec^2)**	**(%)**
1.00E-05	134.0	106.645	105.0	2.7	1.57%
1.00E-06	329.5	262.3	244.0	334.2	7.49%
1.00E-07	660.3	525.5	535.0	89.5	-1.77%
		Sum of Residuals:		**426.40787**	

Using the Scale Factor, define the Scaled PGV Hazard Curve at Point B.
Data in first and third columns are based on DTN: MO03061E9PSHA1.000 [DIRS 163721], file: h_vel_extended.frac_mean.

Point A	**Scaled**	**Annual**
Horizontal	**Horiz. PGV**	**Exceedance**
PGV	**for Point B**	**Frequency**
(cm/sec)	**(cm/sec)**	**(1/yr)**
10	7.96	2.18808E-03
20	15.92	6.26181E-04
30	23.88	2.78161E-04
50	39.79	9.30240E-05

Using the Scale Factor, define the Scaled PGV Hazard Curve at Point B. Data in first and third columns are based on DTN: MO03061E9PSHA1.000 [DIRS 163721], file: h_vel_extended.frac_mean. (Continued)		
Point A Horizontal PGV (cm/sec)	**Scaled Horiz. PGV for Point B (cm/sec)**	**Annual Exceedance Frequency (1/yr)**
100	79.59	1.83594E-05
200	159.2	3.07391E-06
500	397.9	2.28195E-07
700	557.1	8.15299E-08
1000	795.9	2.59826E-08
1500	1193.8	6.56355E-09
Known Values at Point B:		
105	1.00E-05	
244	1.00E-06	
535	1.00E-07	
The following figure presents the original hazard curve at Point A, the scaled hazard curve at Point B, and the three known values at Point B.		

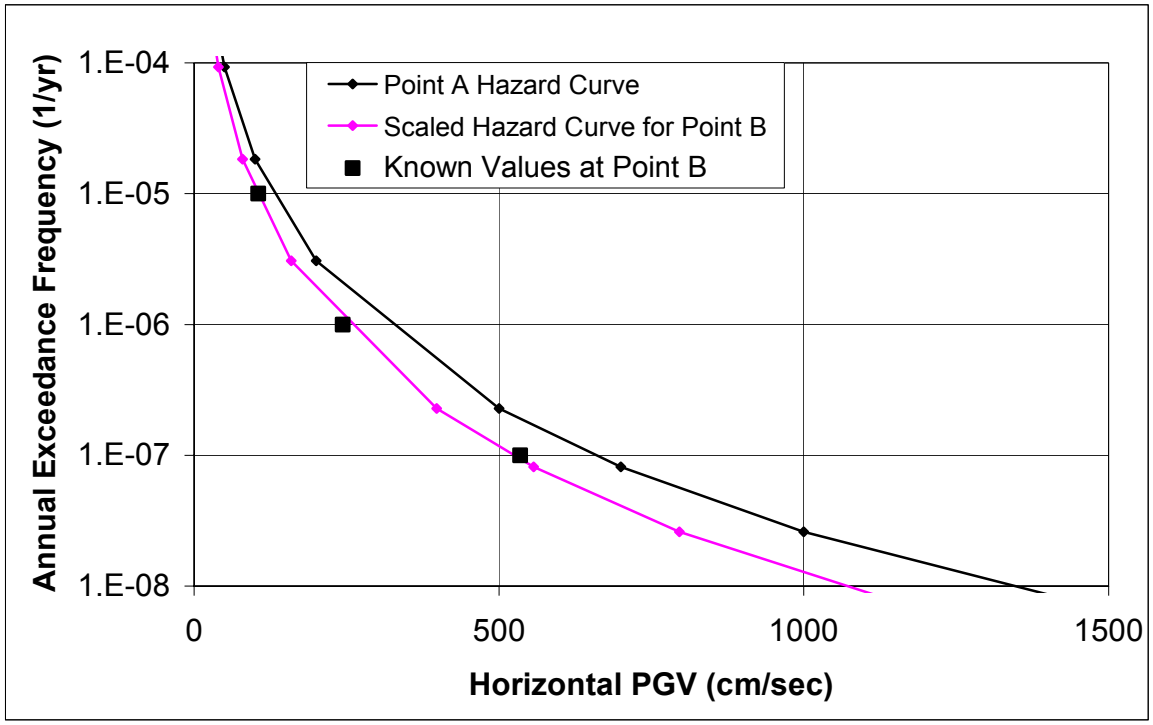

Figure A-1. Scaled Hazard Curve for Point B

Interpolate for horizontal PGV values at Point B at 5 x 10^{-04}, 10^{-04}, 5 x 10^{-05}, 10^{-05}, 10^{-06}, 10^{-07}, and 10^{-08}				
per year. The interpolation is linear in the log(λ), where λ is the annual exceedance probability.				
	Points on the Point B Curve			
Value of	**Bracketing This Value**			
Annual	**Annual**	**Scaled**		
Exceedance	**Exceedance**	**Horizontal PGV**	**Interpolated**	**% Error With**
Frequency	**Frequency**	**for Point B**	**Value of PGV**	**Known Values**
(1/yr)	**(1/yr)**	**(cm/sec)**	**(cm/sec)**	**At Point B**
5.00E-04	6.26181E-04	15.92	18.1	
	2.78161E-04	23.88		
1.00E-04	2.78161E-04	23.88	38.7	
	9.30240E-05	39.79		
5.00E-05	9.30240E-05	39.79	55.0	
	1.83594E-05	79.59		
1.00E-05	1.83594E-05	79.59	106.6	1.57%
	3.07391E-06	159.2		
1.00E-06	3.07391E-06	159.2	262.3	7.49%
	2.28195E-07	397.9		
1.00E-07	2.28195E-07	397.9	525.5	-1.77%
	8.15299E-08	557.1		
1.00E-08	2.59826E-08	795.9	1072.1	
	6.56355E-09	1193.8		
Ratio of PGV at 10^{-5} to PGV at 10^{-6} on scaled hazard curve:				0.4066

Calculate the combined mean hazard from the hazard curve at Point B and a uniform distribution for the maximum value of PGV between 1.5 m/s and 5 m/s. The mean combined hazard gives the probability that PGV is greater than a given value, X. This probability is the product of the probability that the hazard curve at Point B is greater than X and the probability that the uniform distribution is greater than X.

The values in this table are based on the results from the Microsoft Excel spreadsheet; independent calculations with these values may differ slightly from the spreadsheet calculations because of round off.

	Points on the Point B					
	Curve Bracketing the					
	The Value of X				**CCDF for**	
Given Value	**Scaled**	**Annual**	**Interpolated**	**CCDF for Prob PGV>X**	**Prob PGV>X for Uniform**	**Prob PGV > X**
of PGV	**Horiz. PGV**	**Exceedance**	**Exceedance**	**for Hazard**	**Distribution**	**Combined**
"X"	**for Point B**	**Frequency**	**Frequency**	**at Point B**	**PGV-MAX**	**PGV Hazard**
(cm/sec)	**(cm/sec)**	**(1/yr)**	**(1/yr)**	**(-)**	**(-)**	**(-)**
38.7	23.88	2.78E-04	1.00E-04	1.00E-04	1	1.00E-04
	39.79	9.30E-05				
55	39.79	9.30E-05	5.00E-05	5.00E-05	1	5.00E-05
	79.59	1.84E-05				
106.6	79.59	1.84E-05	1.00E-05	1.00E-05	1	1.00E-05
	159.2	3.07E-06				

	Points on the Point B					
	Curve Bracketing the					
	The Value of X				CCDF for	
Given Value	Scaled	Annual	Interpolated	CCDF for Prob PGV>X	Prob PGV>X for Uniform	Prob PGV > X
of PGV	Horiz. PGV	Exceedance	Exceedance	for Hazard	Distribution	Combined
"X"	for Point B	Frequency	Frequency	at Point B	PGV-MAX	PGV Hazard
(cm/sec)	(cm/sec)	(1/yr)	(1/yr)	(-)	(-)	(-)
150	79.59	1.84E-05	3.78E-06	3.78E-06	1	3.78E-06
	159.2	3.07E-06				
200	159.2	3.07E-06	1.97E-06	1.97E-06	0.86	1.69E-06
	397.9	2.28E-07				
250	159.2	3.07E-06	1.14E-06	1.14E-06	0.71	8.17E-07
	397.9	2.28E-07				
300	159.2	3.07E-06	6.63E-07	6.63E-07	0.57	3.79E-07
	397.9	2.28E-07				
350	159.2	3.07E-06	3.85E-07	3.85E-07	0.43	1.65E-07
	397.9	2.28E-07				
400	397.9	2.28E-07	2.25E-07	2.25E-07	0.29	6.43E-08
	557.1	8.15E-08				
450	397.9	2.28E-07	1.63E-07	1.63E-07	0.14	2.33E-08
	557.1	8.15E-08				
474	397.9	2.28E-07	1.40E-07	1.40E-07	0.07	1.04E-08
	557.1	8.15E-08				
Points for plotting the combined mean hazard curve:						
Given Value	Prob PGV > X					
of PGV	Combined					
"X"	PGV Hazard					
(cm/sec)	(-)					
38.7	1.00E-04					
55	5.00E-05					
106.6	1.00E-05					
150	3.78E-06					
200	1.69E-06					
250	8.17E-07					
300	3.79E-07					
350	1.65E-07					
400	6.43E-08					
450	2.33E-08					
474	1.04E-08					

CCDF = complementary cumulative distribution function.

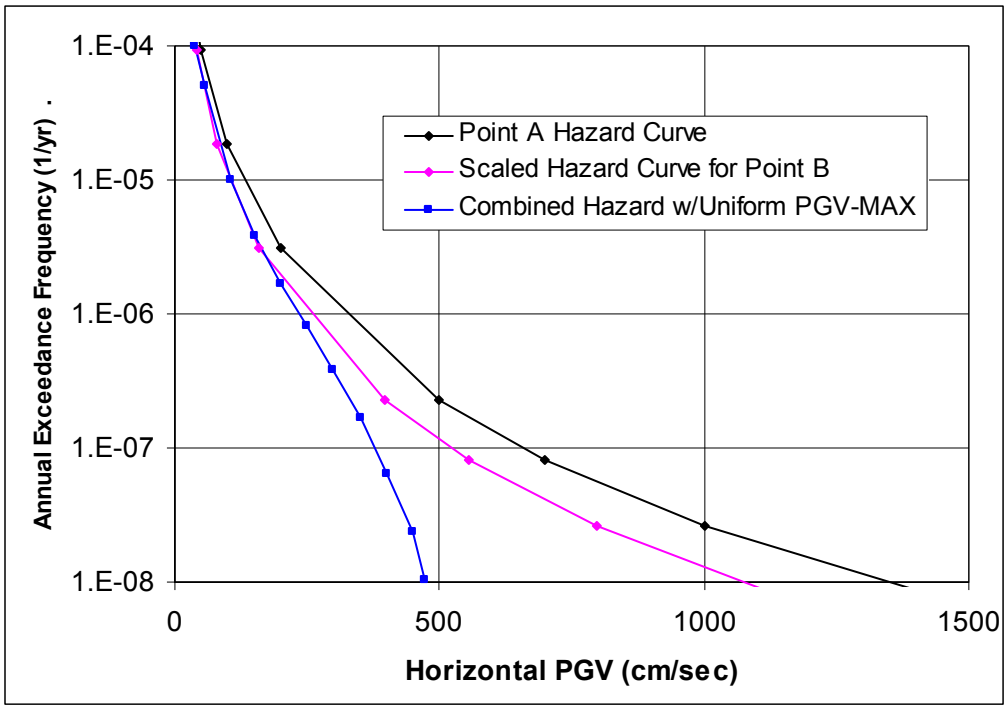

PGV = peak ground velocity.

Figure A-2. Scaled Hazard Curve at Point B and the Combined Hazard Curve with a Uniform Distribution for Bounding PGV

APPENDIX B

SPREADSHEET FOR WASTE PACKAGE DAMAGE ABSTRACTION

This spreadsheet contains the calculations that produce the
waste package damage abstraction described in Section 6.5.1.
The inputs, outputs, and formulas used in each worksheet are described below.
(1) Results_80 Yield Strength
This worksheet is a copy of the results presented in Tables 5 and 6 (see column labeled
Cumulative Damaged expressed as % of total area) for the damaged areas from
vibratory ground motion for the failure threshold of 80% of yield strength.
Minimum, maximum, mean, and standard deviation of the cumulative damaged area
are calculated for the data.
The PGV values are from DTN: MO0303DPGVB106.002 [DIRS 162712] and DTN: MO0210PGVPB107.000 [DIRS 162713].
The damage data are from BSC 2004 [DIRS 169990], Table 16.
(2) results_90% Yield Strength
This worksheet is a copy of the results presented in Tables 5 and 6 (see column labeled
Cumulative Damaged expressed as % of total area) for the damaged areas from
vibratory ground motion for the failure threshold of 90 percent of yield strength.
Minimum, maximum, mean, and standard deviation of the cumulative damaged area
are calculated for the data.
The PGV values are from DTN: MO0303DPGVB106.002 [DIRS 162712] and DTN: MO0210PGVPB107.000 [DIRS 162713].
The damage data are from BSC 2004 [DIRS 169990], Table 17 and BSC 2004 [DIRS 17171] for Realization 11.
(3) Avg_85%_vs_Uniform_Dist
In this worksheet, the cumulative % damage area is computed as the average
of the 80 percent Yield Strength and 90 percent Yield Strength results given in worksheets (1) and (2).
These average values are shown in column B.
The average values are then sorted in ascending order in column C.
The cumulative probability is computed for each point in column D.
Finally, the points are compared with a least squares fit to a straight line
determined by Microsoft Excel's fitting routine for PGV of 2.44 m/s and for PGV of 5.35 m/s.
The equation of the straight line and the r^2 value for the fit is also shown.
(4) Avg_85%_Upper_Bound
In this worksheet, the cumulative % damage area is computed as the average of the 80 percent
Yield Strength and 90 percent Yield Strength results given in worksheets (1) and (2). These average values are
shown in columns B and D. Then, the 95 percent upper confidence limit associated
with this value is computed using 95 percent upper confidence limitL = (alpha)^(-1/(n-1)) * max{observed value}
where alpha = 0.05 is the level of significance and UCL = upper confidence limit.
This is shown in Row 26 for PGV of 2.44 m/s and 5.35 m/s.
These formulas are taken from (Rossman et al. 1998 [DIRS 162631]).
Also shown in this worksheet are three graphs of percent failed area versus PGV.
The magenta squares and diamonds are the computed percent cumulative damage.
The red squares are the Bayesian 95 percent UCL in Row 26 of this worksheet.
Three graphs present (1) comparison of the Bayesian upper bound with the damaged
areas for PGV of 2.44 m/s and 5.35 m/s, (2) a comparison of the upper bound with the
results for PGV of 2.44 m/s, 5.35 m/s, and 1.037 m/s, and (3) a comparison of the
upper bound for the lognormal distribution, derived in Appendix C, with the upper
bound for the uniform distribution.
Preliminary damage statistics at the 0.992 m/s PGV level are from BSC 2004 [DIRS 167083], Table XI-2.

(1) Results_80% Yield Strength			
	Cumulative		**Cumulative**
	% Damage		**% Damage**
PGV (m/s)	**for 80% of Yield**	**PGV (m/s)**	**for 80% of Yield**
2.44	0.092%	5.35	1.28%
2.44	0.060%	5.35	1.84%
2.44	0.71%	5.35	0.82%
2.44	0.53%	5.35	0.96%
2.44	0.53%	5.35	1.67%
2.44	0.64%	5.35	1.28%
2.44	0.46%	5.35	1.49%
2.44	0.43%	5.35	0.14%
2.44	0.050%	5.35	1.74%
2.44	0.30%	5.35	0.70%
2.44	0.27%	5.35	0.57%
2.44	0.11%	5.35	0.53%
2.44	0.057%	5.35	0.099%
2.44	0.099%	5.35	1.03%
Minimum Value	0.050%		0.099%
Maximum Value	0.710%		1.840%
Mean Value	0.310%		1.011%
Standard Deviation	0.237%		0.567%
	Calculation of Bayesian Maximum:		
Confidence Level	95%		95%
Alpha	5%		5%
Upper Conf. Limit	0.894%		2.317%
Confidence Level	95%		95%
Ref: Rossman et al. 1998 [DIRS 162631]			
(2) Results_90% Yield Strength			
	Cumulative		**Cumulative**
	% Damage		**% Damage**
PGV (m/s)	**for 90% of Yield**	**PGV (m/s)**	**for 90% of Yield**
2.44	0.046%	5.35	0.92%
2.44	0.032%	5.35	0.89%
2.44	0.29%	5.35	0.53%
2.44	0.24%	5.35	0.53%
2.44	0.23%	5.35	0.60%
2.44	0.23%	5.35	0.53%
2.44	0.20%	5.35	0.74%
2.44	0.22%	5.35	0.074%
2.44	0.025%	5.35	1.03%
2.44	0.13%	5.35	0.28%
2.44	0.13%	5.35	0.30%
2.44	0.057%	5.35	0.25%
2.44	0.026%	5.35	0.07%
2.44	0.043%	5.35	0.50%
Minimum Value	0.025%		0.071%
Maximum Value	0.290%		1.030%
Mean Value	0.136%		0.518%
Standard Deviation	0.097%		0.303%
	Calculation of Bayesian Maximum:		
Confidence Level	95%		95%
Alpha	5%		5%
Upper Conf. Limit	0.365%		1.297%

Confidence Level	95%		95%
Ref: Rossman et al. 1998 [DIRS 162631]			
(3) Avg_85%_vs_Uniform_Dist			
	Cumulative		
	% Damage		**Cumulative**
PGV (m/s)	**for 85% of Yield**	**Sorted % Damage**	**Probability (-)**
2.44	0.069%	0.038%	0.036
2.44	0.046%	0.042%	0.107
2.44	0.500%	0.046%	0.179
2.44	0.385%	0.069%	0.250
2.44	0.380%	0.071%	0.321
2.44	0.435%	0.084%	0.393
2.44	0.330%	0.200%	0.464
2.44	0.325%	0.215%	0.536
2.44	0.038%	0.325%	0.607
2.44	0.215%	0.330%	0.679
2.44	0.200%	0.380%	0.750
2.44	0.084%	0.385%	0.821
2.44	0.042%	0.435%	0.893
2.44	0.071%	0.500%	0.964
	Cumulative		
	% Damage		**Cumulative**
PGV (m/s)	**for 85% of Yield**	**Sorted % Damage**	**Probability (-)**
5.35	1.100%	0.085%	0.036
5.35	1.365%	0.107%	0.107
5.35	0.675%	0.390%	0.179
5.35	0.745%	0.435%	0.250
5.35	1.135%	0.490%	0.321
5.35	0.905%	0.675%	0.393
5.35	1.115%	0.745%	0.464
5.35	0.107%	0.765%	0.536
5.35	1.385%	0.905%	0.607
5.35	0.490%	1.100%	0.679
5.35	0.435%	1.115%	0.750
5.35	0.390%	1.135%	0.821
5.35	0.085%	1.365%	0.893
5.35	0.765%	1.385%	0.964

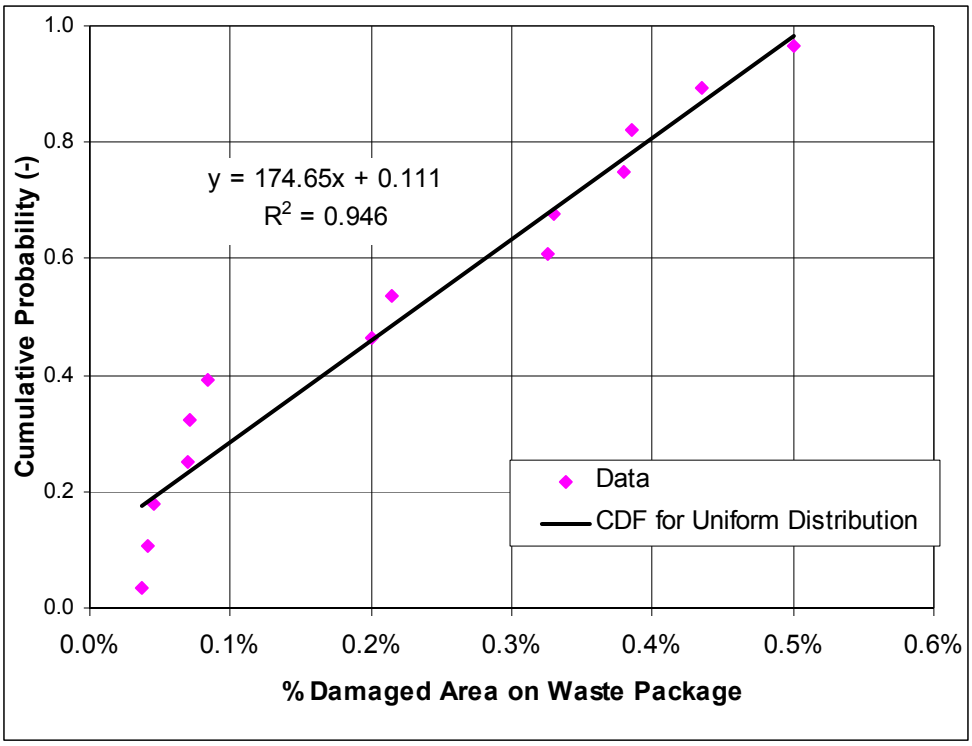

Figure B-1. Comparison of Damage Results for the 2.44 m/s PGV Level with a Uniform Distribution

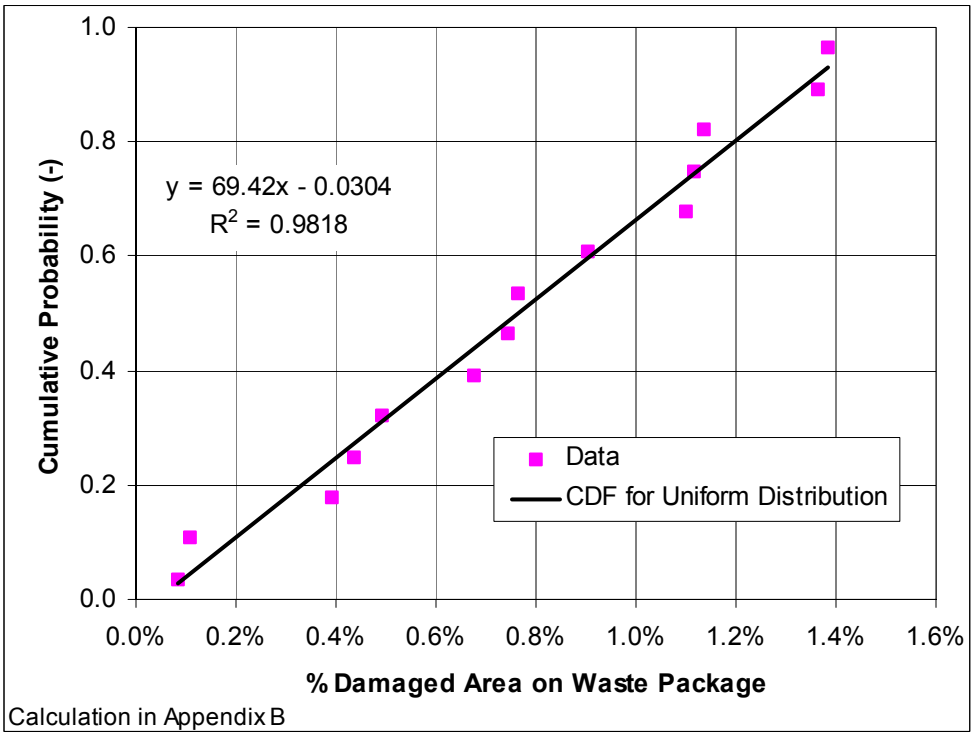

Figure B-2. Comparison of Damage Results for the 5.35 m/s PGV Level with a Uniform Distribution

(4) Avg_85%_Upper_Bound					
	Cumulative		Cumulative		Cumulative
	% Damage		% Damage		% Damage
PGV (m/s)	for 85% of Yield	PGV (m/s)	for 85% of Yield	PGV (m/s)	for 85% of Yield
2.44	0.069%	5.35	1.100%	0.992	0.0105%
2.44	0.046%	5.35	1.365%	0.992	0.0000%
2.44	0.500%	5.35	0.675%	0.992	0.0255%
2.44	0.385%	5.35	0.745%		
2.44	0.380%	5.35	1.135%		
2.44	0.435%	5.35	0.905%		
2.44	0.330%	5.35	1.115%		
2.44	0.325%	5.35	0.107%		
2.44	0.038%	5.35	1.385%		
2.44	0.215%	5.35	0.490%		
2.44	0.200%	5.35	0.435%		
2.44	0.084%	5.35	0.390%		
2.44	0.042%	5.35	0.085%		
2.44	0.071%	5.35	0.765%		
Minimum Value	0.038%		0.085%		0.000%
Maximum Value	0.500%		1.385%		0.026%
Mean Value	0.223%		0.764%		0.012%
Standard Deviation	0.166%		0.426%		0.013%
Calculation of Bayesian Maximum:					
Confidence Level	95%		95%		95%
Alpha	5%		5%		5%
Upper Conf. Limit	0.630%		1.744%	0.992	0.114%
Ref: Rossman et al. 1998 [DIRS 162631]					
Plot the Straight Line through the Bayesian Maxima:					
	Upper				
PGV (m/s)	**Limit (%)**				
2.44	0.630%				
5.35	1.744%	**Plot the Linear Fit:**			
Slope	0.3829%	**PGV**	**% Damage**		
y-intercept	-0.3048%	0.7959322	0		
x-intercept	0.795932203	8	0.02758718		
Plot Maximum of Lognormal Distribution (Appendix C, Eq. C-10):					
PGV	**Damage**				
0.7	0.0002%				
7.6	3.01%				

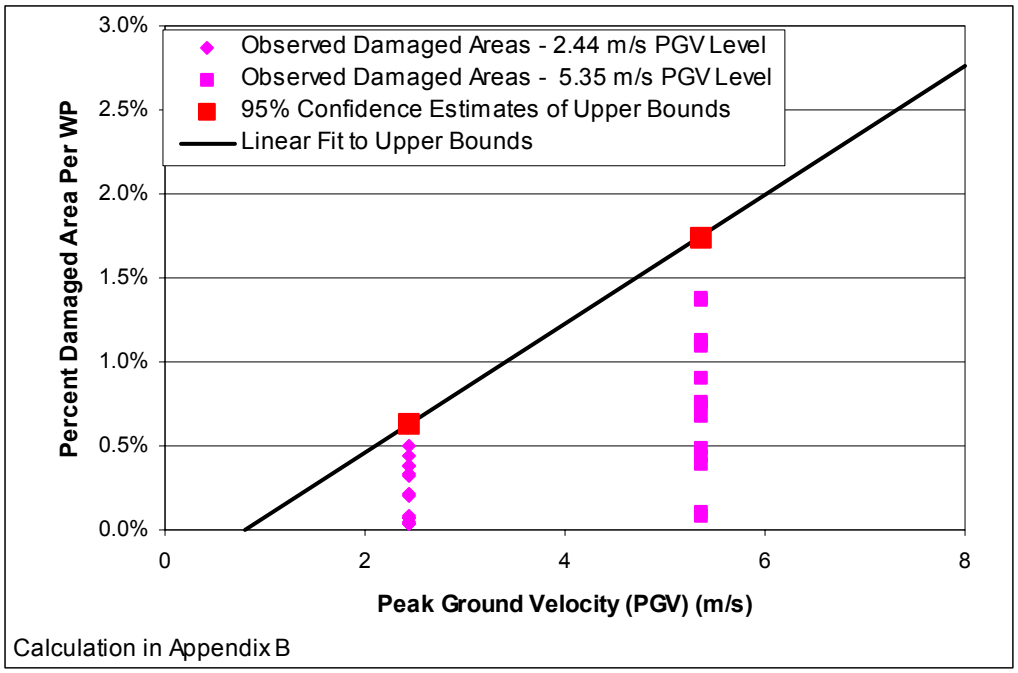

Figure B-3. Linear Fit to Bayesian Upper Bound of Damage Distribution

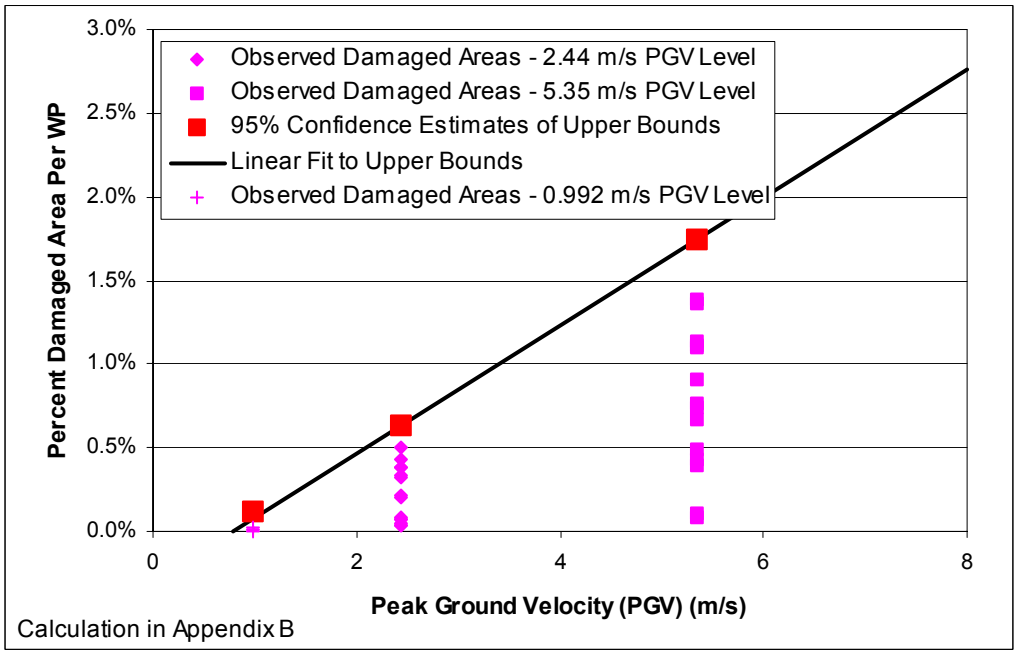

Figure B-4. Comparison of Linear Fit to Bayesian Upper Bound of Damage Distribution with the Damage Results for the 1.05 m/s PGV Level

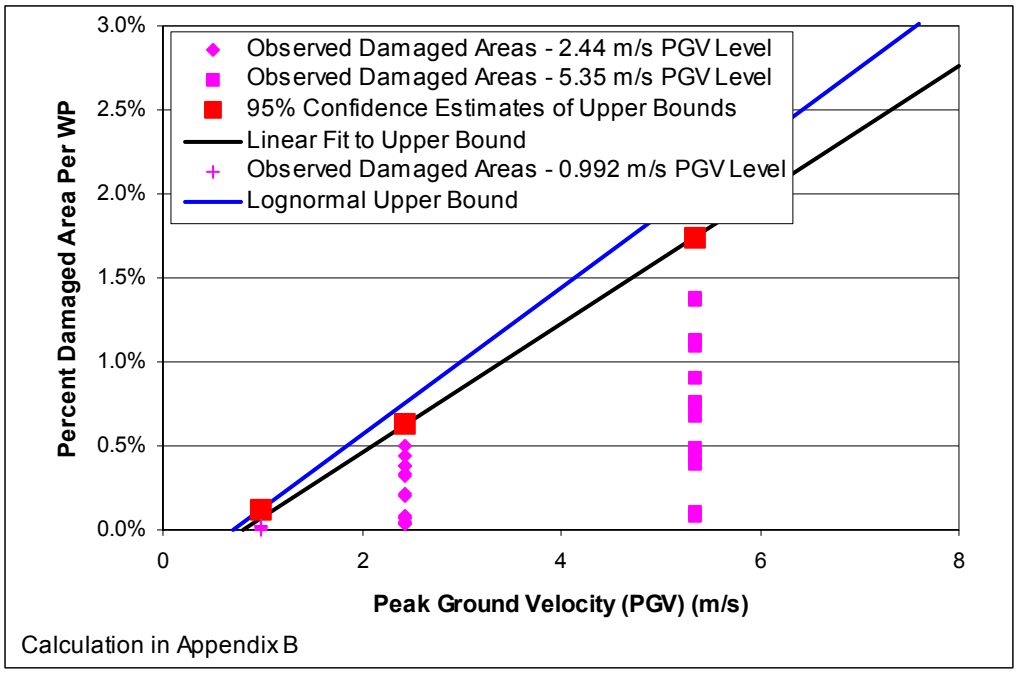

Figure B-5. Comparison of Upper Bounds Based on a Lognormal Distribution (Blue Curve) with the Bayesian Upper Bound

INTENTIONALLY LEFT BLANK

APPENDIX C

REVIEW COMMENTS ON ABSTRACTION FOR WASTE PACKAGE DAMAGE FROM VIBRATORY GROUND MOTION

Editor's Note: This appendix conducts an independent review of the *Seismic Consequence Abstraction* (BSC 2003 [DIRS 161812]) and *Seismic Consequence Abstraction* (BSC 2004 [DIRS 167780], errata) documents (identified as Ref. C1). Note that there have been no changes to damage data for the waste package since Dr. Kennedy performed his review in April 2004. Further note that any table references listed as "corresponding to tables in this report" refers to tables in REV 00 *Seismic Consequence Abstraction* (BSC 2004 [DIRS 167780], errata).

Review Comments on Abstraction for Waste Package Damage from Vibratory Ground Motion[17]

R.P. Kennedy
Original Dated June 2003; Revised April 2004

C1. INTRODUCTION

This report presents my review comments on the response surface for waste package damage from vibratory ground motion developed and presented in Section 6.5.1 of Ref. C1.

Damage is defined in terms of the percentage of damaged area D. The response surface defines the exceedance probability that the defined percentage of damaged area D might be exceeded as a function of the peak ground velocity (PGV).

C1.1 Symbols and Units Used Herein

D	=	Percentage of damaged area (%)
D_{UB}	=	Upper bound on D (%) as a function of PGV
D_{80}	=	Value of D obtained using 80 percent yield criteria
D_{90}	=	Value of D obtained using 90 percent yield criteria
EP	=	Exceedance probability (%)
NEP	=	Non-exceedance probability (%)
PGV	=	Peak ground velocity (m/sec)
U	=	Uniform damage surface defined by Equations (C-1) and (C-2)
LN	=	Lognormal damage surface defined by Equation (C-9)

C1.2 Response Surface Recommended in Ref. C1

Ref. C1 defines an upper bound D_{UB} (%) on D as a function of PGV (m/sec) by:

$$D_{UB} = 0.383(PGV) - 0.305 \qquad \text{(Eq. C-1)}$$

[17] Section numbers, table numbers, equation numbers, and reference numbers have been changed by adding a C to distinguish this appendix from the main body of the text. No significant changes have been made to the content of this independent review beyond editorial changes.

At any given PGV, Ref. C1 assumes the percentage of damaged area D(%) is uniformly distributed between zero and D_{UB}. Thus, the exceedance probability (%) for any specified D conditional on the given PGV is defined by:

$$EP = \left[1 - \frac{D}{D_{UB}}\right](100\%) \qquad \text{(Eq. C-2)}$$

Representation of the damage response surface by Equations (C-1) and (C-2) is attractive because it is very easy to use. However, several conservatisms and unconservatisms are embedded into the development of the damage surface represented by Equations (C-1) and (C-2). It is not intuitively obvious whether Equations (C-1) and (C-2) provide an adequate representation of the damage surface. It is also questionable as to how far this damage surface can be extrapolated beyond the limited database. Over what range of PGV values and what range of D values is it reasonable to express the damage surface by Equations (C-1) and (C-2)?

The damage surface defined by Equations (C-1) and (C-2) will hereinafter be called Uniform damage surface and will be represented in the attached tables by the symbol U.

C1.3 Scope of Review

Starting with the same database defined in Tables 6 and 7 of Ref. C1, I have developed in Section C2 a more complex description of the damage surface. This more complex damage surface attempts to correct the unconservatisms and conservatisms described subsequently associated with the U damage surface. This more complex damage surface is defined by log normally distributed exceedance probabilities exceedance probability as a function of both D and PGV, and will hereinafter be called Lognormal damage surface and will be represented in the attached tables by the symbol LN.

Exceedance probability results computed using this LN damage surface will be compared with those computed for the U damage surface. Recommendations concerning both the LN and U damage surface representations are presented in Section C3.

C1.4 Database Used to Develop Damage Surface Representations

Nonlinear time history analyses were performed for the following two ground motion levels:

$$\text{PGV} = 2.44 \text{ m/sec} \qquad \text{(Eq. C-3)}$$
$$\text{PGV} = 5.35 \text{ m/sec}$$

The results are reported in Tables 6 and 7 of Ref. C1 (corresponding to Tables 5 and 6 in this report). A total of 14 analyses for PGV = 2.44 m/sec are summarized in Table 6 of Ref. C1 (Table 5 of this report). A total of 14 analyses for PGV = 5.35 m/sec are summarized in Table 7 of Ref. C1 (Table 6 of this report). Two damage thresholds are used to compute the percentage of damaged area D for each analytical simulation. These two damage thresholds are:

- Damage occurs where the residual stress exceeds 80 percent of yield (called 80 percent yield criteria)
- Damage occurs where the residual stress exceeds 90 percent of yield (called 90 percent yield criteria).

It is outside of my expertise to comment on these damage threshold criteria. Furthermore, I have not reviewed any of the nonlinear analyses from which the percentage of damaged area D reported in Tables 6 and 7 of Ref. C1 were obtained.

The results presented in Tables 6 and 7 of Ref. C1 (Tables 5 and 6 of this report) are tabulated in Tables C-1 and C-2 where these results are ordered in the order of increasing percentage of damaged area D. Also shown in Tables C-1 and C-2 is the non-exceedance probability NEP corresponding to each of these ordered results as computed from:

$$\mathrm{NEP} = \frac{n - 0.5}{N}(100\%) \qquad \text{(Eq. C-4)}$$

where N is the total number of trials and n is the ordered trial number. The results shown in Tables C-1 and C-2 are the basis for both the U damage surface developed in Ref. C1 and the LN damage surface presented in Section C2.

Ref. C1 has assumed a uniform distribution of D between a lower bound value D90 based on the 90 percent yield criteria to an upper bound value D80 based on the 80 percent yield criteria. This assumption seems reasonable and will be made here as well.

C1.5 Comments on Development of U Damage Surface

As noted earlier, several conservatisms and unconservatisms are embedded into the development of the U damage surface developed in Ref. C1. These conservatisms and unconservatisms will be briefly discussed in the subsections of this section.

C1.5.1 Establishment of Upper Bound D_{UB}

Ref. C1 developed a mean estimate of $\overline{D}$ for each of the trials from:

$$\overline{D} = \frac{D_{90} + D_{80}}{2} \qquad \text{(Eq.C-5)}$$

which is the appropriate equation for the mean $\overline{D}$ for a uniform distribution. However, Ref. C1 ignored the scatter of D about $\overline{D}$. On average:

$$D_{80} \approx 2\ D_{90} \qquad \text{(Eq. C-6)}$$

This scatter of D about $\overline{D}$ should be considered when establishing D_{UB}. Since it was not considered, D_{UB} was unconservatively established.

Secondly, D_{UB} was established at the 95 percent upper confidence limit for the upper bound on $\overline{D}$. This upper bound D_{UB} cuts off the uniform distribution at the 5 percent exceedance probability, and assumes 0 percent exceedance probability beyond D_{UB}. In most seismic risk evaluations, the fragility curve or damage surface between about 1 percent exceedance probability and 5 percent exceedance probability significantly contributes to the mean computed annual risk when the fragility curve or damage surface is convolved with the hazard curve.

For both of the above reasons, D_{UB} has been unconservatively established. For example, Ref. C1 has established the following values of D_{UB}.

PGV (m/sec	D_{UB} (%)
2.44	0.630
5.35	1.744

Two of the 14 results reported in Table C-1 exceed D_{UB} = 0.630% for the 80 percent yield criteria case. Similarly two of the 14 results reported in Table C-2 are either at or exceed D_{UB} = 1.744 percent for the 80 percent yield criteria case.

C1.5.2 Use of Uniform Distribution From Zero to D_{UB}

For the U damage surface, Equation (C-2) is used to establish exceedance probability for any D corresponding to a specified PGV. This uniform distribution is very conservative for the distribution shown in Table C-1 for PGV = 2.44 m/sec. The trial results are not uniformly distributed, but are heavily skewed to low D. The distribution shown in Table C-2 for PGV = 5.35 m/sec is more nearly uniform and can be reasonably approximated by a uniform distribution.

C1.5.3 Linear Variation of D With PGV

Equations (C-1) and (C-2) assume that D_{UB} and D for any specified exceedance probability vary linear with PGV. My experience with sliding and impact problems is that the sliding displacements and impact velocities vary with PGV to a power greater than unity. If my past experience proves correct for the current problem, then this linear variation of D_{UB} and D with PGV may be increasingly unconservative for PGV values greater than 5.35 m/sec. Conversely, some conservatism may be introduced for PGV values between 2.44 m/sec and 5.35 m/sec. I am concerned about the extrapolation of Equation (C-1) beyond the range of PGV between about 1.5 m/sec and 6.0 m/sec.

The most important region of a fragility curve or damage surface is typically between exceedance probability values of 1 percent to 50 percent. Because of their shapes, either a log normally distributed or normally distributed fragility curve or damage surface will result in exceedance probability increasing faster than linear with PGV over this important range. Therefore, these distributions can generally be extrapolated further beyond the range of available data points. My preference is for the lognormal distribution because, within my experience, a lot of nonlinear computed fragility results reasonably fit this distribution. However, even this distribution should not be extrapolated too far. Extrapolation beyond the range of 1.5 m/sec to 8.0 m/sec is suspect even using a lognormal distribution.

C2. DEVELOPMENT OF IMPROVED DAMAGE SURFACE ESTIMATION

C2.1 Approach to Account for Variability of D between D_{80} and D_{90}

Assuming D varies uniformly between D80 and D90, the cumulative NEP for various D values can be estimated by the following procedure from the trial results presented in Tables C-1 and C-2 for PGV = 2.44 m/sec and 5.35 m/sec, respectively. First determine the NEPTH for the highest trial in Tables C-1 or C-2 for which D80 is less than the specified D. Next, determine all of the trials for which D is between D90 and D80. For each of these trials, find the percentage associated with being less than D assuming a uniform distribution. Then, the NEP associated with the specified D is given by:

$$NEP = NEP_{TH} + \frac{100\%}{N} \sum \left(\frac{D - D_{90}}{D_{80} - D_{90}} \right), \qquad \text{(Eq. C-7)}$$

where N is the total number of trials and the summation is performed only for the trials where D is between D_{90} and D_{80}. Lastly, the exceedance probability (EP) is given by:

$$EP = 100\% - NEP. \qquad \text{(Eq. C-8)}$$

The NEP or EP for D values less than the lowest D90 or greater than the highest D80 in Table C-1 for PGV = 2.44 m/sec or Table C-2 for PGV = 5.35 cannot be estimated by the above procedure. There are insufficient numbers of trials to cover these D values. The NEP for D below the lowest D90 is less than the lowest NEP in the tables, and the NEP for D higher than the highest D80 is greater than the highest NEP in the tables. Values of NEP for D in these regions are estimated by judgment.

Table C-3A presents the estimated exceedance probability values obtained for various D from the data in Tables C-1 and C-2 using the above procedure. Table C-3A becomes the database for establishing the damage surface.

C2.2 Improved Approximation of Damage Surface

A log normally distributed approximation of the damage surface was fit by trial and error to the exceedance probability (EP) data shown in Table C-3A. The following lognormal distribution was found to provide a good fit to Table C-3A:

Lognormal Distribution Parameters

Median :	$PGV_{50} = (5.7 \text{ m/sec})D^{0.5}$	
Log. Std. Dev.:	$\beta = 0.28D^{-0.5} \leq 0.8$	(Eq. C-9)
Truncation Point:	EP = 1%	

A practical problem associated with the use of the lognormal distribution is that it will predict small exceedance probability values even at very low PGV values. For sliding and impact problems, the extreme lower tail of the lognormal distribution should not be used because damage will not occur for low PGV values. A practical solution to this problem is to truncate the lognormal distribution at an exceedance probability of about 1.0 percent. Below this level, exceedance probability should be taken as zero. Nonlinear analyses performed for lower PGV levels would enable this truncation point to be better defined. However, the above recommendation has proven to be adequate for all risk assessments of which I am aware that have included sliding and impact fragilities.

Table C-3B shows the exceedance probability predicted by the lognormal LN damage surface defined by the parameters in Equation (C-9). Good agreement exists between Table C-3B and Table C-3A, except for the D = 0.03% and PGV = 2.44 m/sec case. The agreement for this case could be improved by use of a more complex equation for the logarithmic standard deviation β. However, this improvement was considered to be unnecessary because the computed risk is insensitive to exceedance probability when exceedance probability exceeds about 70 percent. Therefore, even for D = 0.03% and PGV = 2.44 m/sec, the fit is more than adequate.

C2.3 Comparison of Uniform U Damage Surface With Table 3A

Table C-3C shows the exceedance probability predicted by the uniform U damage surface used in Ref. C1 for the same cases shown in Table C-3A. The agreement is not as good as that obtained from the LN damage surface approximation.

For PGV = 5.35 m/sec, the U damage surface provides a good approximation to the Table C-3A results, except for D greater than about 1.67 percent where the U damage surface estimate of exceedance probability becomes seriously unconservative. This unconservatism could have significant unconservative consequences for estimating the annual probability of exceeding higher values of D.

For PGV = 2.44 m/sec, the U damage surface approximation significantly overestimates exceedance probability for D between 0.06 percent and 0.56 percent. However, a more significant issue is that the U damage surface significantly underestimates exceedance probability for D greater than 0.60 percent.

This unconservatism at higher D values can be easily corrected by changing Equation (C-1) to slightly increase D_{UB}. The unconservatism shown when comparing Table C-3C with Table C-3A is eliminated when:

$$D_{UB} = 0.436(PGV) - 0.305 \quad \text{(Eq. C-10)}$$

is used instead of Equation (C-1). The resulting D_{UB} values become:

PGV (m/sec	D_{UB} (%)
2.44	0.759
5.35	2.028

These D_{UB} values lie at about the EP = 1% level based upon the data presented in Table C-3A. They also adequately exceed the highest D_{80} values shown in Tables C-1 and C-2.

C2.4 Extension of Damage Surface to Other PGV Values

Nonlinear analyses have only been performed for PGV of 2.44 m/sec and 5.35 m/sec. However, it is necessary to extend the candidate damage surfaces over as broad a range of PGV values and D values as are credible. Table C-4 extends the estimated damage surface over the range of PGV from 1.5 m/sec to 8.0 m/sec, and D from 0.03 percent to 2.0 percent. This range is the maximum range over which I believe it is credible to extend the nonlinear results summarized in Tables C-1 and C-2.

Table C-4 shows the exceedance probabilities (EP) predicted by both the uniform U damage surface proposed in Ref. C1 and lognormal LN damage surface proposed in Section 2.2. Over the majority of the damage surface region covered by Table C-4, the U damage surface approximation provides a conservatively biased estimate of exceedance probability. In my judgment, the amount of conservative bias is not sufficient to seriously over predict the annual probability of exceeding any specified D when this damage surface is convolved with a seismic hazard curve.

However, there are a few regions where the U damage surface is significantly unconservative. These regions are identified by an underscore __ under the U predicted values. These under prediction regions could have an important unconservative effect on the predicted annual probability of exceeding a specified D because they all occur at low exceedance probability values within the range that generally significantly influences the annual probability of exceedance. These underlined under predictions of exceedance probability should be eliminated by the following suggestions.

First, the U damage surface proposed in Ref. C1 should not be extended to PGV values greater than about 6.0 m/sec. The extension to higher PGV values is likely to become seriously unconservative for the reason discussed in Section 1.5.3.

Second, the upper bound D_{UB} should be defined by Equation (C-10) instead of Equation (C-1). This change will resolve the issues discussed in Section 1.5.1.

C3. RECOMMENDATIONS

C3.1 Recommendations Concerning LN Damage Surface Representation

The LN damage surface representation defined by Equation (C-9) is judged to provide a good description of the damage surface over the entire range of PGV and D values covered by Table C-4. This range covers:

$$1.5\text{m/sec} \le \text{PGV} \le 8.0\ \text{m/sec}$$
$$0.03\% \le D \le 2.0\% \qquad \text{(Eq. C-11)}$$

Extension of this LN damage surface representation beyond the range of Equation (C-11) becomes questionable unless additional nonlinear analyses are performed.

An additional 15 nonlinear analyses conducted at a PGV of approximately 1.0 m/sec should be sufficient to enable a modified LN damage surface to be extended down to about 0.5 m/sec for D = 0.03% and larger. However, if percent damage areas less than 0.03 percent are also required, it will be necessary to perform nonlinear analyses at two PGV levels below 2.44 m/sec. The existing nonlinear analysis results are not helpful in defining the important region of the damage surface from EP = 1 percent to 70 percent for D less than 0.03 percent.

It is unlikely that the damage surface needs to be extended beyond PGV of 8.0 m/sec because such a high PGV is not very credible, at least in my judgment. However, it might be necessary to define the damage surface for percent damage area D greater than 2 percent. Nonlinear analyses would have to be conducted at a ground motion significantly above PGV of 5.35 m/sec to enable the damage surface to be extended above D = 2.0%. Ideally, the PGV for these additional analyses should be selected so that the nonlinear simulations produced D in the range of 1.5 percent to 10 percent if D needs to be extended beyond 2 percent.

C3.2 Recommendations Concerning U Damage Surface Representation

The primary advantage of the U damage surface representation presented in Ref. C1 is the ease with which it can be used. With one correction, this U damage surface representation is judged to provide a more than adequate representation of the damage surface over the following range:

$$1.5\text{m/sec} \le \text{PGV} \le 6.0\ \text{m/sec}$$
$$0.03\% \le D \le 2.0\% \qquad \text{(Eq. C-12)}$$

The one recommended correction is that D_{UB} used in Equation (C-2) should be computed by Equation (C-10), as opposed to Equation (C-1) recommended in Reference C1.

It is very questionable whether a linear equation such as Equation (C-1) or (C-10) can be extended to cover a range of PGV values larger than about a factor of four. Therefore, if the PGV range defined in Equation (C-12) must be extended, it is questionable whether the simplification of the U damage surface representation format can be maintained over a broader PGV range.

Reference

C1. *Seismic Consequence Abstraction* (BSC 2003 [DIRS 161812]) and *Seismic Consequence Abstraction* (BSC 2004 [DIRS 167780], Errata)

Table C-1. Percentage Damaged Area D Obtained from Nonlinear Analyses for PGV = 2.44 m/sec

NEP (%)	D(%)	
	80% Yield Criteria	90% Yield Criteria
3.57	.050	.025
10.71	.057068	.026
17.86	.060	.032
25.0	.092	.043
32.14	.066	.046
39.29	.11	.054
46.43	.27	.13
53.57	.30	.13
60.71	.43	.20
67.86	.46	.22
75.0	.53	.23
82.14	.53	.23
89.29	.64	.24
96.43	.71	.26

Table C-2. Percentage Damaged Area D Obtained from Nonlinear Analyses for PGV = 5.35 m/sec

NEP (%)	D(%)	
	80% Yield Criteria	90% Yield Criteria
3.57	.099	.071
10.71	.14	.074
17.86	.53	.25
25.0	.57	.30
32.14	.82	.39
39.29	.96	.50
46.43	1.03	.53
53.57	1.06	.53
60.71	1.28	.53
67.86	1.28	.60
75.0	1.49	.74
82.14	1.67	.89
89.29	1.74	.92
96.43	1.84	1.03

Table C-3. Exceedance Probabilities for Various Damage Area Percentages D and Peak Ground Velocities PGV

Table C-3A. Nonlinear Data Results from Tables C-1 and C-2

PGV	D(%)										
(m/sec)	.03	.06	.12	.25	.50	.75	1.00	1.25	1.5	1.75	2.0
2.44	97.6	77.4	60.7	46.0	11.1	1.5	X	X	X	X	X
5.35	X	98.5	91.5	89.3	75.6	58.5	40.7	19.8	10.2	4.4	2.0

Table C-3B. Lognormal LN Damage Surface Approximation

PGV	D(%)										
(m/sec)	.03	.06	.12	.25	.50	.75	1.00	1.25	1.5	1.75	2.0
2.44	87.1	75.7	60.4	39.1	10.2	1.5	0	0	0	0	0
5.35	98.3	95.3	89.4	87.0	76.3	59.8	41.0	24.2	12.9	5.2	1.9

Table C-3C. Uniform U Damage Surface Approximation

PGV	D(%)										
(m/sec)	.03	.06	.12	.25	.50	.75	1.00	1.25	1.5	1.75	2.0
2.44	95.2	90.5	80.9	60.3	20.6	0	0	0	0	0	0
5.35	98.3	96.6	93.1	85.7	71.3	57.0	42.7	28.3	14.0	0	0

Table C-4. Exceedance Probability Extended Over A Wide Range of PGV

PGV		Damage Area Percent D_P(%)										
(m/sec)		.03	.06	.12	.25	.5	.75	1.0	1.25	1.5	1.75	2.0
1.5	LN	69.9	53.6	36.6	12.6	0	0	0	0	0	0	0
	U	88.9	77.7	55.5	7.2	0	0	0	0	0	0	0
2.0	LN	81.1	67.3	50.6	26.4	3.8	0	0	0	0	0	0
	U	93.5	87.0	74.0	45.8	0	0	0	0	0	0	0
3.0	LN	91.7	83.0	69.9	53.6	22.8	6.2	1.1	0	0	0	0
	U	96.4	92.9	85.8	70.4	40.8	11.1	0	0	0	0	0
4.0	LN	95.9	90.6	81.1	72.8	49.2	25.8	10.3	3.1	0	0	0
	U	97.6	95.1	90.2	79.6	59.3	38.9	18.5	0	0	0	0
5.0	LN	97.9	94.5	87.7	84.2	70.7	51.6	32.0	16.6	7.4	2.6	0
	U	98.1	96.3	92.6	84.5	68.9	53.4	37.9	22.4	6.8	0	0
6.0	LN	98.8	96.6	91.8	90.8	84.2	72.7	57.3	40.5	25.4	14.0	6.8
	U	98.5	97.0	94.0	87.5	74.9	62.4	49.8	37.3	24.7	12.2	0
7.0	LN	99.3	97.8	94.3	94.6	91.8	86.0	76.8	64.6	50.5	36.3	23.8
	U	98.7	97.5	95.0	89.5	79.0	68.4	57.9	47.4	36.9	26.4	15.8
8.0	LN	99.6	98.5	96.0	96.0	95.8	93.2	88.7	81.8	72.4	61.0	48.5
	U	98.9	97.8	95.7	90.9	81.9	72.8	63.8	54.7	45.6	36.6	27.5

EP = exeedance probability

APPENDIX D

ABSTRACTION FOR DRIP SHIELD SEPARATION AND REVIEW COMMENTS ON ABSTRACTION FOR DRIP SHIELD DAMAGE FROM VIBRATORY GROUND MOTION

D1. INITIAL ABSTRACTION FOR DRIP SHIELD SEPARATION

Drip shield separation has been screened out of the seismic scenario class for TSPA-LA (Section 6.5.5), although a drip shield separation model is included in TSPA-LA model validation calculations because the technical basis for excluding separation was established after the start of model validation activities. Sections D1 through D4 describe the abstraction for drip shield separation that is included in the model validation calculations.

A uniform distribution has been selected to represent the degree of separation of drip shields from vibratory ground motion for TSPA-LA. The rationale for selection of a uniform distribution is that there are only five realizations for the 5.35 m/s PGV level, and a uniform distribution is a reasonable representation of the upper and lower bounds with a very limited number of data points.

The upper bound of the uniform distribution for degree of separation at a PGV value of 5.35 m/s or greater is 50 percent. The rationale for this value is as follows. The five structural response calculations at the 5.35 m/s PGV level (Section 6.5.4.2) demonstrate that a drip shield may cover or overlap its neighbor by a substantial amount. In an extreme case, each pair of drip shields in the emplacement drifts could be reduced to one-half their original length if one member of the pair completely covers the other member of the pair. In this situation, the total length of drip shield in a drift would be reduced by 50 percent. While more extreme situations are possible, such as a stack of three or four drip shields that cover one another, the probability of these situations is negligible. First, a tall pile of drip shields will probably be less stable than a 2-high stack under vibratory ground motions. Second, increasing structural deformations are required to add a third or fourth drip shield to a stack that is 2-high. Deformation must increase because the inner width of the third drip shield in a stack must be greater than the outer width of the second drip shield, and so on. The complex dynamics of the EBS components in response to ground motions make these arrangements highly improbable, especially given that ground motions are usually coherent over 10s of meters.

As discussed in Section 6.5.1.2, the uncertainty in damaged areas on the waste package is dominated by the uncertainty in the details of the ground motions at a given PGV level, rather than by the uncertainty in the residual stress threshold. It is anticipated that uncertainty in drip shield separation is also dominated by the uncertainty in the ground motions at the 5.35 m/s PGV level, particularly since the residual stress threshold for Titanium Grade 7 is set to a constant value. The use of a bounding argument to define an upper bound for drip shield separation is appropriate, in part, because of the limited number of realizations at the 5.35 m/s PGV level.

The lower bound of the uniform distribution for drip shield separation is initially defined as 0 percent at all PGV levels. In addition, the upper and lower bounds for drip shield separation are zero percent at all values of PGV less than or equal to 2.44 m/s. This is consistent with the structural response calculations, which indicate no drip shield separation at a PGV of 2.44 m/s for the 14 ground motions. The initial abstraction for damage from drip shield separation is defined by Table D-1.

Table D-1. Initial Abstraction for Drip Shield Separation from Vibratory Ground Motion, Based on a Uniform Distribution

PGV Value (m/s)	Lower Bound for Damaged Area	Upper Bound for Damaged Area
0.0	0	0
2.44	0	0
5.35	0	50%
> 5.35	0	50%

D2. INDEPENDENT TECHNICAL REVIEW OF SEPARATION ABSTRACTION

An independent technical review of this model abstraction has been performed by Dr. Robert P. Kennedy of RPK Structural Mechanics Consulting. The result of Dr. Kennedy's review is presented in Section D.4 of this appendix, and the portion that is relevant to the degree of drip shield separation is briefly summarized here.

Dr. Kennedy notes that there are only 5 data points for the damage from ground motions at the 10^{-7} per year level (PGV = 5.35 m/s). One knows that damage will be large, but it is difficult to estimate exceedance probability for various percent damage values. He also states that the upper bound of 50 percent for damage is probably reasonable for PGV = 5.35 m/s; however, the lower bound should probably be in excess of 10 percent at this level. Given limited data, his primary conclusion is that the drip shields are likely to be severely damaged at a PGV of 5.35 m/s.

D3. FINAL ABSTRACTION FOR DRIP SHIELD SEPARATION

The discussion in Sections 6.5.4.2, D1, and D2 presented the calculations and degree of separation of the drip shield from ground motion. The results and conclusions from these sections indicate that it is reasonable to choose the upper bound for degree of separation defined in Table D-1. The maximum damage of 50 percent for PGV values of 5.35 m/s is considered an upper bound. The rationale for this bound is twofold: (1) the five simulations for the PGV level of 5.35 m/s demonstrate that a drip shield rides over its adjacent neighbor by 10 percent to 25 percent of its axial length, well below the upper bound of 50 percent, and (2) the value of 50 percent corresponds to an extreme case in which each and every pair of drip shields through the repository is reduced to one-half of its original length.

However, Dr. Kennedy notes that using a lower bound of zero for the uniform distribution does not seem conservative for PGV values of 5.35 m/s. In this situation, it seems appropriate to define a lower bound that is a function of PGV. This lower bound is zero for all values of PGV that are less than or equal to 2.44 m/s because drip shield separation is not observed in the structural response calculations. For values of PGV between 2.44 m/s and 5.35 m/s, there is a linear interpolation between 0 percent damage and 10 percent damage, respectively. The value of 10 percent is selected because it is the minimum value for the 5 simulations at the PGV level of 5.35 m/s, and this minimum is appropriate for a uniform distribution. For values of PGV greater than 5.35 m/s, the lower bound is based on a linear extrapolation of the damage at 2.44 and 5.35 m/s. In other words, the minimum degree of separation continues to increase with PGV.

The abstraction is summarized in Table D-2 and illustrated in Figure D-1. The damage to the drip shield is applied to all drip shields throughout the repository. There is no spatial variability in the damage to the drip shield.

Table D-2. Final Abstraction for Degree of Drip Shield Separation from Vibratory Ground Motion, Based on a Uniform Distribution

PGV Value (m/s)	Lower Bound of Degree of Separation	Upper Bound of Degree of Separation
0.0	0	0
2.44	0	0
5.35	10%	50%
> 5.35	Linear extrapolation of values at 2.44 m/s and 5.35 m/s	50%

.

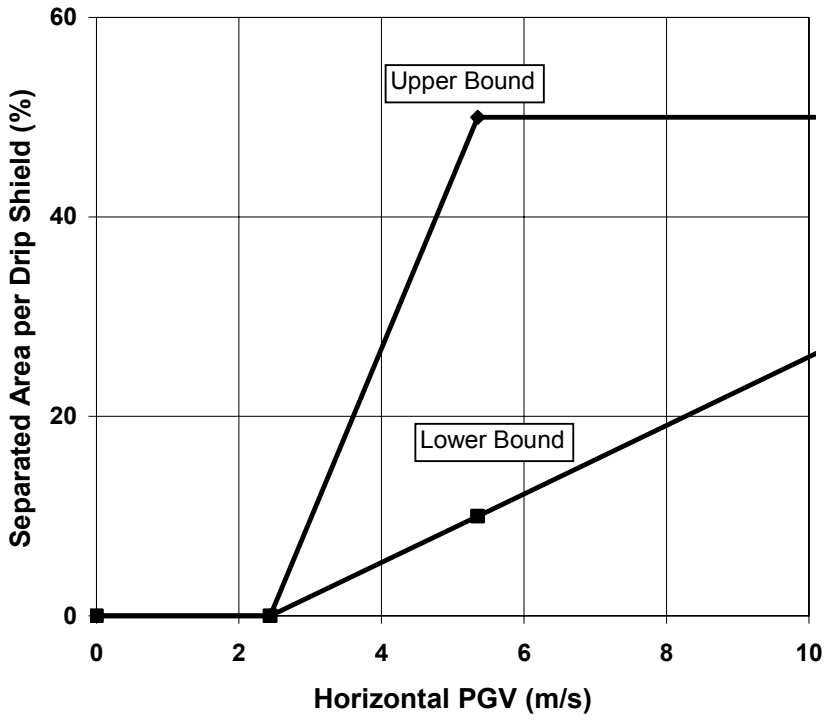

NOTE: Based on data in Table D-2.

Figure D-1. Upper and Lower Bounds of Uniform Distribution for Percent Separation of Drip Shields from Vibratory Ground Motion

D4. CHANGES FOR LOCALIZED CORROSION AFTER SEPARATION

Accelerated localized corrosion has the potential to occur on the waste package if the package is directly exposed to the seepage into the drift and if the thermal and aqueous environment results in aggressive chemical conditions on the waste package. Drip shield separation can occur for a ground motion with a PGV level greater than 2.44 m/s (Table D-2), allowing seepage to directly contact the waste package. This direct contact may lead to localized corrosion under certain chemical and thermal conditions.

If a seismic event with PGV greater than 2.44 m/s occurs when the conditions for the existence of accelerated localized corrosion of Alloy 22 are satisfied, then the flux splitting (i.e., the diversion of liquid seepage) on the drip shield is equal to the degree of separation of the drip shields. In other words, if the drip shields have separated by 25 percent of their axial length, then 25 percent of the seepage onto the drip shields falls directly on the waste package. This is a reasonable representation for the average seepage onto a waste package that is directly exposed to seepage from the crown of the drift. In addition, any seepage that falls onto the waste package flows into the waste package without diversion. This is a reasonable change because enhanced localized corrosion on the waste package generates corroded areas directly beneath the seeps. Once these corroded areas penetrate the outer and inner shells of the waste package, the seeps will fall directly onto the waste package internals, without diversion by the surface of the waste package.

Once localized corrosion is initiated, the area for diffusive and advective transport out of the waste package is equal to the total area of the waste package that is directly exposed to seepage. Again, if the drip shields have separated by 25 percent of their axial length, then the transport area on the waste package is taken to be 25 percent of its surface area. This approach is upper bound because all the exposed surface material is lost to localized corrosion, even if seepage never contacts exposed areas of the waste package.

Editor's Note: Sections D5 through D7 contain an independent review of the *Seismic Consequence Abstraction* (BSC 2003 [DIRS 161812]) and *Errata for Seismic Consequence Abstraction* (BSC 2004 [DIRS 167780]) documents (identified as Ref. D1). Note that there have been no changes to damage data for the drip shield since Dr. Kennedy performed his review in April 2004.

Review Comments on Abstraction for Drip Shield Damage from Vibratory Ground Motion[18]

R.P. Kennedy
Original Dated July 2003; Revised April 2004

D5. INTRODUCTION

This report presents my review comments on the response surface for drip shield damage from vibratory ground motion developed and presented in Section 6.5.4 of Ref. D1, and repeated in Sections 6.5.4.2 and D1 of this report.

Damage is defined in terms of the percentage of damaged area D. The response surface defines the exceedance probability (EP) that the defined percentage of damaged area D might be exceeded as a function of the peak ground velocity PGV.

D5.1 Symbols and Units Used Herein

D	=	Percentage of damaged area (%)
D_{UB}	=	Upper bound on D (%) as a function of PGV
EP	=	Exceedance probability (%)
NEP	=	Non-exceedance probability (%)
PGV	=	Peak ground velocity (m/sec)
U	=	Uniform damage surface defined by Equations (D-1) and (D-2)
LN	=	Lognormal damage surface defined by Equation (D-4)

D5.2 Response Surface Recommended in Section D1

Section D1 defines an upper bound D_{UB} (%) on D as a function of PGV (m/sec) by:

PGV Value (m/s)	D_{UB} %
0.0	0
0.55	0
2.44	2.68
5.35	50
20	50

(Eq. D-1)

[18] Section numbers, table numbers, equation numbers, and reference numbers have been changed by adding a D with an appropriate subsection number. No other changes have been made to the content of this independent review beyond editorial changes.

At any given PGV, Ref. D1 assumes the percentage of damaged area D (%) is uniformly distributed between zero and D_{UB}. Thus, the exceedance probability (%) for any specified D conditional on the given PGV is defined by:

$$EP = \left[1 - \frac{D}{D_{UB}}\right](100\%) \qquad \text{(Eq. D-2)}$$

The damage surface defined by Equations (D-1) and (D-2) will hereinafter be called Uniform damage surface and will be represented in the attached tables by the symbol U. In the following sections, I will present my review comments on this at each of the PGV values tabulated in Equation (D-1).

D6. DAMAGE SURFACE AT PGV = 2.44 M/SEC

D6.1 Comment on Drip Shield Damage Criteria Used at PGV = 2.44 m/sec

Ref. D1 assumes that the drip shield is damaged over any areas where the computed residual stress due to rockfall impact exceeds 50 percent of yield. Considering the large uncertainty on what residual stress level might ultimately lead to damage, I do not believe that a single deterministic percentage of yield residual stress value should be used to define the damage area. Instead, uncertainty bounds and a distribution function between these bounds should be estimated for the residual stress associated with damage. Based on the discussion in Ref. D1, the deterministic 50 percent of yield criteria appears to be very conservative.

D6.2 Comment on Uniform Damage Surface Equations At PGV = 2.44 m/sec

The percentage damage area D was computed in 14 simulations performed using PGV = 2.44 m/sec ground motion records. The results are presented in Table 14 of Ref. D1. These results are shown in Table D-3 and ordered from the lowest to highest D. Also shown in Table D-3 is the non-exceedance probability NEP corresponding to each of these ordered results as computed from:

$$NEP = \frac{n - 0.5}{N}(100\%) \qquad \text{(Eq. D-3)}$$

where N is the total number of trials and n is the ordered trial number.

Table D-4 compares these data results with percent damage areas predicted from the Uniform distribution U at PGV = 2.44 m/sec. It can be seen that the Uniform distribution defined in Ref. D1 is very conservative for percent damage areas D from about 0.50 percent and higher. It could lead to significant overestimation of the annual probability of exceeding D percentages greater than 0.50 percent.

A much better fit at PGV = 2.44 m/sec is provided by the following Lognormal distribution:

Lognormal LN		
Median:	$D_{50} = 0.55\%$	(Eq. D-4)
Log. Std. Dev.:	$\beta = 0.85$	

Table D-4 also shows the damage area percentage predicted by this Lognormal distribution LN. This Lognormal distribution predicts the simulation results well, although it also tends to overpredict the exceedance probability (EP) for D greater than about 1.25 percent. However, this overprediction is much less than that for the U distribution.

If the conservatism of the Uniform distribution U is unacceptable, one should consider using the Lognormal distribution at PGV = 2.44 m/sec.

D7. DAMAGE SURFACE AT PGV = 5.35 M/SEC AND HIGHER

Five simulations were performed for ground motions with PGV = 5.35 m/sec. Ref. D1 reports that large plastic deformations of the drip shield and separation between drip shields on the order of 10 to 25 percent of the length of the drip shield occurred in each of the simulations.

These limited data are not a very adequate basis for estimating the exceedance probability (EP) for various percent damage areas D at PGV = 5.35 m/sec. All that one can really say is that D will be large.

The upper bound D_{UB} = 50 percent in Table 15 of Ref. D1 is probably reasonable at PGV = 5.35 m/sec. However, a Uniform distribution with a lower bound of zero is not reasonable in my opinion. Considering increased corrosion rates due to high residual stresses, as well as drip shield separation, I would expect a lower bound on a Uniform distribution should be in excess of 10 percent at PGV = 5.35 m/sec. A more detailed review of the results of the five simulations might allow this lower bound to be better established.

Considering both increased corrosion rates and drip shield separations, I would expect both the upper bound and lower bound on a Uniform distribution for D to further increase as PGV is increased above 5.35 m/sec. I have no idea how to estimate this further increase. However, the percent damage areas at PGV = 5.35 m/sec for the drip shield might be sufficiently high since further increases in D may not have much impact on the overall risk assessment. The primary conclusion is that the drip shields are likely to be severely damaged at a PGV = 5.35 m/sec or higher.

D8. DAMAGE SURFACE AT PGV = 0.55 M/SEC

Ref. D1 assumes no damage occurs to the drip shield at a PGV of 0.55m/sec. This assumption should be validated by performing a few simulations using PGV = 0.55*g* ground motion.

Reference

D1 *Seismic Consequence Abstraction* (BSC 2003 [DIRS 161812]) and *Seismic Consequence Abstraction* (BSC 2004 [DIRS 167780], Errata).

Table D-3. Percentage Damaged Area Obtained from Nonlinear Analyses for PGV = 2.44 m/sec

NEP(%)	D(%)
3.57	0.12
10.71	0.14
17.86	0.26
25.0	0.26
32.14	0.27
39.29	0.30
46.43	0.50
53.57	0.65
60.71	0.67
67.86	0.98
75.0	1.12
82.14	1.19
89.29	1.25
96.43	2.13

Table D-4. Exceedance Probabilities for Various Damage Area Percentages D at PGV = 2.44 m/sec

	D%								
	0.12	0.25	0.50	0.75	1.00	1.25	1.50	1.75	2.00
Data	96.4	82.7	53.6	37.4	31.1	10.7	8.7	6.7	4.6
Uniform U	95.5	90.7	81.3	72.0	62.7	53.4	44.0	34.7	25.4
Lognormal LN	96.3	82.3	54.5	35.8	24.1	16.7	11.9	8.6	6.4

APPENDIX E

SPREADSHEET FOR FAULT DISPLACEMENT DAMAGE ABSTRACTION

Assessment of Waste Package Failure Due To Fault Displacement

This spreadsheet summarizes the supporting calculations for Section 6.7 of this report.

Table numbers correspond to the tables in Section 6.7 of this report.

Table 6.7-1 - Drip Shield Clearance Calculation (all units in mm)

			Reference/Formula
Drift diameter (Dd)		5500.0	BSC 2004 [DIRS 169058], Figure 1
Invert thickness (Ti)		863.6	BSC 2004 [DIRS 170074]
Drip shield height - exterior (Hdse)		2885.62	BSC 2004 [DIRS 169220], Table 1
Drip shield height - interior (Hdsi)		2716.0	BSC 2004 [DIRS 168489], Figure 1
Clearance above Drip Shield (Hdsc)		1750.78	= Dd - Hdse - Ti

Table 6.7-2 - Waste Package to Drip Shield Clearance

Nominal length from BSC (2004 [DIRS 169472], Table 1); Outer diameter of outer shell from drawings referenced in BSC (2004 [DIRS 169472], Table 1).

	Outer Diameter	Nominal Length	Clearance
Package	(mm)	(mm)	(mm)
44-BWR	1675.1	5024.4	1041
24-BWR	1294.1	5024.4	1422
21-PWR	1637.0	5024.4	1079
12-PWR	1313.2	5560.4	1403
Naval-Long	1863.7	5837.4	852
Naval-Short	1863.7	5202.2	852
5DHLW/DOE SNF - Short	2044.7	3452.8	671
5DHLW/DOE SNF - Long	2044.7	5059.4	671
2-MCO/2-DHLW	1749.4	5059.4	967

The formula for calculating the clearance is given by Hdsi - Outer Diameter of Waste Package.

Table 6.7-3 - Maximum Allowable Fault Displacement (in mm)

Two values are provided with and without drift collapse. In both cases, the behavior of the invert and pallet is approximated by treating the emplacement pallet as collapsed into the invert. No further collapse of the invert is accounted for.
With drift collapse, max allowable displacement = Hdsi – Outer Diameter of Waste Package.
Without drift collapse, max allowable displacement = Hdsi – Outer Diameter of Waste Package + Hdsc.

Package	with collapse	w/o collapse	
44-BWR	1041	2792	
24-BWR	1422	3173	
21-PWR	1079	2830	
12-PWR	1403	3154	
Naval-Long	852	2603	
Naval-Short	852	2603	
5DHLW/DOE SNF-Short	671	2422	
5DHLW/DOE SNF-Long	671	2422	
2-MCO/2-DHLW	967	2717	

Table 6.7-4 - Faults intersecting Drifts

BSC (2004 [DIRS 168180], Table 9) defines drift intersections with Sever Wash fault, Drill Hole Wash fault, Pagany Wash fault, and the western splay off the main Ghost Dance fault (denoted as the West Ghost Dance fault in Table 9).

DTN: MO0012MWDGFM02.002 [DIRS 153777] defines drift intersections with Sundance fault and the locations of geologic units relative to fault traces and emplacement drifts.

BSC (2004 [DIRS 164519], Figure 1) defines the numbering of drifts and panels.

Western splay off the main Ghost Dance fault (called the West Ghost Dance in the reference) intersects drifts 2-17 through 2-27. Drifts 2-18 through 2-27 are in the contingency area.

Development is uncertain because this area is in the vicinity of an intensely fractured zone (Albin et al. 1997 [DIRS 101367], discussion of Third Domain on pp. 69 to 72). The western splay off the main Ghost Dance fault has therefore, not been included in TSPA-LA.

Sundance Fault	***Lith Zones***	***Nonlith Zones***
	1-6	1-8
	1-7	2-1
Drill Hole Wash Fault	***Lith Zones***	***Nonlith Zones***
	4-1	3-10 E
	4-2	3-11 E
	3-4 W	3-12 E
	3-5 W	
	3-6 W	
	3-7 W	
	3-8 W	
	3-9 W	
	3-13 E	
	3-14 E	
	3-15 E	
	3-16 E	
	3-17 E	
Pagany Wash Fault	***Lith Zones***	***Nonlith Zones***
	3-1 W	3-5 E
	3-1 E	3-6 E
	3-2 E	3-7 E
	3-3 E	
	3-4 E	
Sevier Wash Fault	***Lith Zones***	***Nonlith Zones***
	3-2 E	
	3-3 E	

Table 6.7-5 - Fault Displacement Summary Information (in cm).

Based on Probabilistic Seismic Hazard Analysis (PSHA), CRWMS M&O 1998 [DIRS 103731], Figures 8-3 and 8-5 for sites 2 and 4, respectively, and on data in DTN: MO0401MWDRPSHA.000 [DIRS 166962] for the other sites listed below.

	Mean Annual Exceedance Frequency				
	1.00E-04	**1.00E-05**	**1.00E-06**	**1.00E-07**	**1.00E-08**
Site Number and Fault Name	**Displacement (cm)**				
2 – Solitario Canyon (60 m offset)	<0.1	32.0	190	500	>1000
3 – Drill Hole Wash	<0.1	<0.1	17	80	240
4 – Ghost Dance	<0.1	<0.1	13	58	160
5 – Sundance	<0.1	<0.1	6	42	~145
7a – small fault with 2 m offset	<0.1	<0.1	2	20	~75
7b – shear with 10 cm offset	<0.1	<0.1	1	6	9
7c – fracture with no displacement	<0.1	<0.1	0.1	<1	<1
7d – intact rock	<0.1	<0.1	<0.1	<0.1	<0.1
8a – small fault with 2 m offset	<0.1	<0.1	2	20	~75
8b – shear with 10 cm offset	<0.1	<0.1	1	6	9
8c – fracture with no displacement	<0.1	<0.1	0.1	<1	<1
8d – intact rock	<0.1	<0.1	<0.1	<0.1	<0.1

Table 6.7-6 – Waste Package Inventory

BSC 2004 [DIRS 169472], Table 11 for nominal length; outside diameter of outer barrier defined In drawings referenced in BSC 2004 [DIRS 169472], Table 1. Waste package nominal quantity from BSC 2004 [DIRS 169472], Table 11.

WP Configuration	WP Length (m)	WP Diam. (m)	Nominal Quantity		
21-PWR AP	5.0244	1.6370	4299		
21-PWR CR	5.0244	1.6370	95		
12-PWR AP Long	5.5604	1.3132	163		
44-BWR AP	5.0244	1.6751	2831		
24-BWR AP	5.0244	1.2941	84		
5 DHLW Short/1 DOE SNF – Short	3.4528	2.0447	1147		
5 DHLW Long/1 DOE SNF – Long	5.0594	2.0447	1406		
5 DHLW Long/1 DOE SNF – Short	5.0594	2.0447	31		
5 HLW Long Only	5.0594	2.0447	679		
2-MCO/2-HLW	5.0594	1.7494	149		
Naval-Short	5.2022	1.8637	144		
Naval-Long	5.8374	1.8637	156		

WP = waste package; BWR = boiling water reactor; DHLW = defense high-level radioactive waste; MCO = multicanister overpack; CR = control rod; AP = absorber plate.

Table 6.7-7 – Simplified Inventory

WP Configuration	Effective Length (m)	Total Length (m)	# Packages	Percent	
PWR	5.0436	22984	4557	42.0%	
BWR	5.0244	14646	2915	26.8%	
Naval	5.5325	1660	300	3.0%	
HLW	4.5193	15420	3412	28.2%	
Total		54709	11184	100%	

where Total Length is given by package length times number of packages, summed over each package type in the group.

Effective length is given by Total length / Total number of packages in group % = Total length for that group / Total length for all groups

The PWR group includes the 21-PWR AP, 21-PWR CR, and 12-PWR AP Long packages.

The BWR group includes the 44-BWR AP and the 24-BWR AP packages.

The Naval group includes the Naval Long and Naval Short packages.

The HLW ground includes all DHLW packages.

WP = waste package; BWR = boiling water reactor, HLW = high-level radioactive waste, DHLW = defense high-level radioactive waste; CR = control rod; AP = absorber plate.

Table 6.7-9. Fault Exceedance Probabilities for Waste Package Failure

Using DTN: MO0401MWDRPSHA.000 [DIRS 166962], along with the maximum allowable fault displacements for each simplified waste package group as summarized in Table 6.7-8 of Section 6.7.4, one can determine the exceedance probability required to cause failure for each waste package type.

This is done as follows:

- the allowable fault displacement is given by the value from Table 6.7-8 (w/ drift collapse)
- using figures 8-4 (Drill Hole Wash) and 8-6 (Sundance), the exceedance probability associated with that magnitude of fault displacement is determined from the mean value curve for each waste package group.
- note that relative to the accuracy of these figures, the BWR and PWR groups are

Shown with the same probability.

- The Drill Hole Wash results apply to Pagany Wash and Sever Wash

Fault	PWR	BWR	Naval	HLW
Sundance	$< 2 \times 10^{-8}$	$< 2 \times 10^{-8}$	$< 3 \times 10^{-8}$	$< 5 \times 10^{-8}$
Drill Hole Wash	$< 5 \times 10^{-8}$	$< 5 \times 10^{-8}$	$< 1 \times 10^{-7}$	$< 2 \times 10^{-7}$
Pagany Wash	$< 5 \times 10^{-8}$	$< 5 \times 10^{-8}$	$< 1 \times 10^{-7}$	$< 2 \times 10^{-7}$
Sever Wash	$< 5 \times 10^{-8}$	$< 5 \times 10^{-8}$	$< 1 \times 10^{-7}$	$< 2 \times 10^{-7}$
Sites 7a/8a	N/A	N/A	N/A	$< 2 \times 10^{-8}$

Table 6.7-10 - Expected Number of Waste Packages Emplaced on Faults

Table 6.7-4 in Section 6.7.2.1 of the main report can be used to determine the total number of waste packages impacted by each fault in the lithophysal zones (based on number of fault intersections with each tunnel). The results in Table 6.7-7 can then be used to calculate the expected number of waste packages in each group that would be on a fault.

These results are summarized below.

	Total	PWR	BWR	Naval	HLW
Sundance	2	0.84	0.54	0.06	0.56
Drill Hole, etc.	20	8.40	5.35	0.61	5.64
Sites 7a/8a	119.85	50.3	32.1	3.64	33.8

Table 6.7-11 - Waste Packages Failed Versus Annual Exceedance Probability

The results of Table 6.7-9 and Table 6.7-10 in Section 6.7.4 of the main report can now be combined to provide the expected number of packages failed vs. the annual exceedance probability.

Annual Exceed. Prob. (1/yr)	Expected Number of Waste Package Failures				
	PWR	BWR	Naval	HLW	Total
$> 2 \times 10^{-7}$	0	0	0	0	0.00
1×10^{-7} to 2×10^{-7}	0	0	0	5.64	5.64
5×10^{-8} to 1×10^{-7}	0	0	0.61	5.64	6.24
3×10^{-8} to 5×10^{-8}	8.40	5.35	0.61	6.20	20.56
2×10^{-8} to 3×10^{-8}	8.40	5.35	0.67	6.20	20.62
1×10^{-8} to 2×10^{-8}	9.24	5.89	0.67	39.98	55.78

Table 6.7-13 - Parameters for Simplified Inventory for Criticality

Table 6.7-13 is a modified version of Table 6.7-7 with 10 waste package types

BSC 2004 [DIRS 169472] Table 1 for nominal length, Table 11 for nominal quantity.

WP Type	WP Length (m)	Nominal Quantity (-)	Total Length for Package Type (m)	Fraction of WP (% Total Length)
21-PWR AP	5.0244	4299	21600	39.48%
21-PWR CR	5.0244	95	477.32	0.87%
12-PWR AP Long	5.5604	163	906.35	1.66%
44-BWR AP	5.0244	2831	14224	26.00%
24-BWR AP	5.0244	84	422.05	0.77%
5 DHLW Short/1 DOE SNF Short	3.4528	1147	3960.4	7.24%
5 DHLW/DOE Long[1]	5.0594	2116	10706	19.57%
2 MCO/2 DHLW	5.0594	149	753.85	1.38%
Naval Short	5.2022	144	749.12	1.37%
Naval Long	5.8374	156	910.63	1.66%
TOTALS		11184	54709	100.00%

[1]The 5 DHLW/DOE Long category includes the 5 DHLW Long/1 DOE SNF - Long, the 5 DHLW Long/1 DOE SNF - Short, and the 5 HLW Long Only package types.

(-)=dimensionless; WP = waste package; BWR = boiling water reactor; DHLW = defense high-level radioactive waste; MCO = multicanister overpack ; CR = control rod; AP = absorber plate.

Table 6.7-14 - Maximum Allowable Displacement With Tunnel Collapse Before Waste Package Is Pinned

Table 6.7-14 is a modified version of Table 6.7-3. Outer diameter of outer barrier of waste package defined by drawings identified in BSC 2004 [DIRS 169472], Table 1. Interior height of drip shield is defined in BSC 2004 [DIRS 168489], Figure 1.

Waste Package Type	WP Outer Diameter (mm)	Max. Allowable Displ. With Collapse (mm)
21-PWR AP	1637.0	1079
21-PWR CR	1637.0	1079
12-PWR AP Long	1313.2	1403
44-BWR AP	1675.1	1041
24-BWR AP	1294.1	1422
5 DHLW Short/1 DOE SNF Short	2044.7	671
5 DHLW/DOE Long	2044.7	671
2 MCO/2 DHLW	1749.4	967
Naval Short	1863.7	852
Naval Long	1863.7	852

WP = waste package; MCO = multicanister overpack; PWR = pressurized water reactor; BWR = boiling water reactor; CR = control rod; AP = absorber plate.

Table 6.7-15 - Fault Exceedance Frequencies (Per Year) That Cause Failure in Lithophysal Zones

Table 6.7-15 is a modified version of Table 6.7-9 with 10 waste package types. The interpolated values on the fault displacement hazard curves for Sites 3, 5, 7a, and 8a are calculated first.

PSHA displacement hazard curve for Site 5 (Sundance fault) is based on DTN: MO0401MWDRPSHA.000 [DIRS 166962], file: */displ/tot_haz/s5.frac_mean.gz*.

Displacement (cm)	Mean Exceedance Frequency (1/yr)	Allowable Displ. (from Table 6.7-13) (cm)	Interpolated Exceedance Frequency (1/yr)
1.00E-01	9.54E-06	6.710E+01	4.23E-08
2.00E-01	8.28E-06	8.520E+01	2.77E-08
5.00E-01	6.32E-06	9.670E+01	2.21E-08
1.00E+00	4.34E-06	1.041E+02	1.92E-08
2.00E+00	2.68E-06	1.079E+02	1.79E-08
5.00E+00	1.11E-06	1.403E+02	1.06E-08
1.00E+01	5.40E-07	1.422E+02	1.03E-08
2.00E+01	2.53E-07		
5.00E+01	7.14E-08		
1.00E+02	2.09E-08		
2.00E+02	5.21E-09		

PSHA displacement hazard curve for Site 3 (Drill Hole Wash fault) is based on DTN: MO0401MWDRPSHA.000 [DIRS 166962], file: */displ/tot_haz/s3.frac_mean.gz***.**

Displacement (cm)	Mean Exceedance Frequency (1/yr)	Allowable Displ. (from Table 6.7-13) (cm)	Interpolated Exceedance Frequency (1/yr)
1.00E-01	8.57E-06	6.710E+01	1.21E-07
2.00E-01	7.86E-06	8.520E+01	7.89E-08
5.00E-01	6.91E-06	9.670E+01	6.30E-08
1.00E+00	5.98E-06	1.041E+02	5.49E-08
2.00E+00	4.87E-06	1.079E+02	5.13E-08
5.00E+00	3.06E-06	1.403E+02	3.09E-08
1.00E+01	1.69E-06	1.422E+02	3.01E-08
2.00E+01	7.38E-07		
5.00E+01	2.03E-07		
1.00E+02	5.94E-08		
2.00E+02	1.56E-08		

PSHA displacement hazard curve for Site 7a (100m East of SC, Cum. Displ.=2m)

DTN: MO0401MWDRPSHA.000 [DIRS 166962], file: */displ/tot_haz/s7a.frac_mean.gz.*

Displacement (cm)	Mean Exceedance Frequency (1/yr)	Allowable Displ. (from Table 6.7-13) (cm)	Interpolated Exceedance Frequency (1/yr)
1.00E-01	7.02E-06	6.710E+01	1.19E-08
2.00E-01	5.47E-06	8.520E+01	7.44E-09
5.00E-01	3.11E-06	9.670E+01	5.80E-09
1.00E+00	1.72E-06	1.041E+02	4.55E-09
2.00E+00	1.04E-06	1.079E+02	3.89E-09
5.00E+00	4.58E-07	1.403E+02	1.24E-09
1.00E+01	2.10E-07	1.422E+02	1.17E-09
2.00E+01	8.63E-08		
5.00E+01	2.12E-08		
1.00E+02	5.43E-09		
2.00E+02	2.63E-10		

PSHA displacement hazard curve for Site 8a (Between SC and GD, Cum. Displ.=2*m*). DTN: MO0401MWDRPSHA.000 [DIRS 166962], file: */displ/tot_haz/s8a.frac_mean.gz.*

Displacement (cm)	Mean Exceedance Frequency (1/yr)	Allowable Displ. (from Table 6.7-13) (cm)	Interpolated Exceedance Frequency (1/yr)
1.00E-01	6.72E-06	6.710E+01	1.33E-08
2.00E-01	5.26E-06	8.520E+01	8.41E-09
5.00E-01	3.05E-06	9.670E+01	6.59E-09
1.00E+00	1.70E-06	1.041E+02	5.12E-09
2.00E+00	1.02E-06	1.079E+02	4.34E-09
5.00E+00	4.52E-07	1.403E+02	1.28E-09
1.00E+01	2.09E-07	1.422E+02	1.21E-09
2.00E+01	8.91E-08		
5.00E+01	2.36E-08		
1.00E+02	6.17E-09		
2.00E+02	2.48E-10		

The interpolated values for exceedance frequency correspond to the maximum allowable fault displacements before a waste package type is damaged. These interpolated values are maximum values for exceedance frequency because smaller frequencies have larger fault displacements. The maximum values of exceedance frequency are listed in the following table, rounded up to two significant figures. The exceedance frequency for Sites 7a/8a is the maximum value for the Site 7a and Site 8a hazard curves.

Waste Package Type	Sundance Fault	Drill Hole Wash, Pagany Wash, & Sever Wash Faults	Sites 7a/8a
21-PWR AP	1.8E-08	5.2E-08	5.0E-09
21-PWR CR	1.8E-08	5.2E-08	5.0E-09
12-PWR AP Long	1.1E-08	3.1E-08	2.0E-09
44-BWR AP	2.0E-08	5.5E-08	6.0E-09
24-BWR AP	1.1E-08	3.1E-08	2.0E-09
5-DHLW Short/1 DOE SNF Short	4.3E-08	1.3E-07	1.4E-08
5-DHLW/DOE Long	4.3E-08	1.3E-07	1.4E-08
2 MCO/2 DHLW	2.3E-08	6.4E-08	7.0E-09
Naval Short	2.8E-08	7.9E-08	9.0E-09
Naval Long	2.8E-08	7.9E-08	9.0E-09

PWR = pressurized water reactor; AP = absorber plate; CR = control rod; BWR = boiling water reactor; SNF = spent nuclear fuel; DHLW = defense high-level radioactive waste; MCO = multicanister overpack; DOE = U.S. Department of Energy.

Table 6.7-16 - Expected Number of Waste Package Types Emplaced on Faults

Table 6.7-16 is a modified version of Table 6.7-10 with 10 waste package types. There are 2 locations and 20 locations where the Sundance fault and the Drill Hole/Pagany Wash/ Sever Wash faults intersect emplacement drifts in the lithophysal zones (Table 6.74). The number of locations where Sites 7a/8a intersect emplacement drifts are rounded up from 119.85 to 120.

Waste Package Type	Sundance Fault	Drill Hole Wash, Pagany Wash, & Sever Wash Faults	Sites 7a/8a
21-PWR AP	0.7896	7.8962	47.3774
21-PWR CR	0.0174	0.1745	1.0470
12-PWR AP Long	0.0331	0.3313	1.9880
44-BWR AP	0.5200	5.1999	31.1992
24-BWR AP	0.0154	0.1543	0.9257
5 DHLW Short/1 DOE SNF Short	0.1448	1.4478	8.6867
5 DHLW/DOE Long	0.3914	3.9137	23.4820
2 MCO/2 DHLW	0.0276	0.2756	1.6535
Naval Short	0.0274	0.2739	1.6431
Naval Long	0.0333	0.3329	1.9974
TOTALS	2.0000	20.0000	120.00

Table 6.7-17 - Failure of Waste Package Types by Annual Exceedance Probability

Table 6.7-17 is a modified version of Table 6.7-11 with 10 waste package types.

Waste Package Type	$> 2\times10^{-7}$	1×10^{-7} to 2×10^{-7}	6×10^{-8} to 1×10^{-7}	4×10^{-8} to 6×10^{-8}	2×10^{-8} to 4×10^{-8}	1×10^{-8} to 2×10^{-8}
21-PWR AP	0.00	0.00	0.00	7.90	7.90	8.69
21-PWR CR	0.00	0.00	0.00	0.17	0.17	0.19
12-PWR AP Long	0.00	0.00	0.00	0.00	0.33	0.36
44-BWR AP	0.00	0.00	0.00	5.20	5.20	5.72
24-BWR AP	0.00	0.00	0.00	0.00	0.15	0.17
5 DHLW Short/1 DOE SNF Short	0.00	1.45	1.45	1.59	1.59	10.28
5 DHLW/DOE Long	0.00	3.91	3.91	4.31	4.31	27.79
2 MCO/2 DHLW	0.00	0.00	0.28	0.28	0.30	0.30
Naval Short	0.00	0.00	0.27	0.27	0.30	0.30
Naval Long	0.00	0.00	0.33	0.33	0.37	0.37
TOTALS	0.00	5.36	6.24	20.05	20.62	54.17

PWR = pressurized water reactor, AP =absorber plate, CR = control rod; BWR = boiling water reactor; DHLW = defense high-level radioactive waste; SNF = spent nuclear fuel; MCO = multicanister overpack.

INTENTIONALLY LEFT BLANK

APPENDIX F

REPRESENTATION OF ALEATORY AND EPISTEMIC UNCERTAINTY IN THE CALCULATION OF EXPECTED DOSE FROM SEISMIC EVENTS AT THE PROPOSED YUCCA MOUNTAIN FACILITY FOR THE DISPOSAL OF HIGH LEVEL RADIOACTIVE WASTE

F1. INTRODUCTION

The following presentation provides a conceptual description of the calculation of expected doses (mrem/yr) to reasonably maximally exposed individuals (RMEIs) that result from potential seismic events at the proposed Yucca Mountain facility for the disposal of HLW. A conceptual and representational distinction is made between the effects and implications of aleatory and epistemic uncertainty in the assessment of the effects of seismic events at the Yucca Mountain facility, with aleatory uncertainty arising from the many possible seismic events that could occur over a time period of interest (e.g., 0 to 10,000 yr) and epistemic uncertainty arising from a lack of knowledge with respect to quantities used in the characterization of aleatory uncertainty or in the calculation of doses given the occurrence of a seismic event (Kaplan and Garrick 1981 [DIRS 100557], Helton 1994 [DIRS 107739], Paté-Cornell 1996 [DIRS 107499], Helton 1997 [DIRS 107496]). Due to the low likelihood of seismic events at the Yucca Mountain facility, traditional, integration-based importance sampling is introduced as a means to facilitate the computational determination of expected doses (Rubinstein 1981 [DIRS 163476], Section 4.3.1).

The presentation is organized as follows. Initially, the calculation of expected doses that result from aleatory uncertainty in the occurrence and properties of seismic events is considered (Section F2). Such doses are defined by an integral over possible seismic events, and importance sampling is introduced as a means to accelerate the convergence of numerical approximations to this integral. Then, the calculation of expected doses that result from both aleatory uncertainty and epistemic uncertainty is considered (Section F3). These doses are defined by a double integral, with one integral over the possible seismic events that could occur and the other integral over imprecisely known analysis inputs. Thus, one integral relates to aleatory uncertainty, and the other integral relates to epistemic uncertainty. Two different, sampling-based strategies for the numerical evaluation of the double integral that defines expected dose from aleatory and epistemic uncertainty are described, and the prior use of these strategies in the determination of expected dose from igneous events at the Yucca Mountain facility is indicated. Finally, the presentation ends with a discussion of the representation of expected doses when synergisms between multiple seismic events are possible (Section F4).

This presentation is very formal, with expected doses being defined by integrals over various spaces related to aleatory and epistemic uncertainty. However, it is important to recognize that every integral and every quantity used in association with an integral in this presentation is an entity that must be defined, dealt with, and numerically evaluated in the actual computational implementation of a performance assessment for the Yucca Mountain facility. The formal representations given here can be used as a starting point in documentation that clearly connects the overall structure of analyses of expected doses from seismic events at the Yucca Mountain facility with descriptions that provide the necessary finer detail required for the complete and unambiguous specification of the individual parts of such an analysis. In particular, documentation can be written that provides two-way mapping (i.e., from general to specific and also from specific to general) between the overall structure of an analysis and detailed descriptions of specific parts of that analysis.

For example, dose to the reasonably maximally exposed individual (RMEI) at time τ from a seismic event at time t with a peak ground velocity of v appears simply as a function $D(\tau|\, t,\, v)$ in the integrals that define expected dose in this presentation. This usage clearly indicates how the dose $D(\tau|\, t,\, v)$ to the RMEI enters into the calculation of expected dose but tells nothing about how this dose is actually calculated. In a complete documentation of the analysis, a formal description of the overall analysis would provide a forward reference to where $D(\tau|\, t,\, v)$ was defined, and the location at which $D(\tau|\, t,\, v)$ was defined would provide a backward reference to the description of the overall analysis that clearly indicated the use of $D(\tau|\, t,\, v)$ in the calculation of expected dose and other summary quantities of interest. Further, complete analysis documentation would also describe the numerical procedures used to estimate both $D(\tau|\, t,\, v)$ and the integrals involving $D(\tau|\, t,v)$ that determine expected dose. In this way, the interested individual would be provided with a road map to the complete analysis that clearly tied general structure, specific detail, and numerical procedures together.

F2. EXPECTED DOSE FROM ALEATORY UNCERTAINTY

The development of results in this section and the next section (Section F3) relating to expected doses from seismic events at the Yucca Mountain facility is based on the following three assumptions: (i) dose to the RMEI at time τ (yr) from a seismic event occurring prior to τ depends only on the time of occurrence t (yr) and peak ground velocity (PGV) v (m/s) at the waste drifts associated with that seismic event (Assumption 5.4), (ii) the occurrence of a seismic event has no effect on the dose to the RMEI that derives from any subsequent seismic event, and (iii) the occurrence of seismic events follows a Poisson process (Assumption 5.4) characterized by a function $\lambda_A(v)$ (1/yr) of PGV v (Figure VI-1), where $\lambda_A(v)$ is the annual exceedance frequency for a PGV of size v (i.e., the mean hazard curve for PGV in Section 6.1.3 and 6.4) and

$$prob_A\left[n|\Delta t, \lambda_A(v)\right] = \left\{\left[\lambda_A(v)\,\Delta t\right]^n / n!\right\} \exp\left[-\lambda_A(v)\,\Delta t\right] \quad \text{(Eq. F-1)}$$

is the probability that exactly n seismic events with a PGV exceeding v occur over a time interval of length Δt (yr) (Hahn and Shapiro 1967 [DIRS 146529], pp. 172-173). The synergisms between multiple seismic events are considered in Section F4, so it is not included as formal assumption in Section 5 of the main body of this report.

With respect to notation, this presentation will use a subscript A to designate quantities that relate primarily to aleatory uncertainty and, beginning in Section F3, a subscript E to designate quantities that relate primarily to epistemic uncertainty. For notational convenience, the dose is represented as

$D(\tau|t, v)$ = dose (mrem/yr) to the RMEI at time τ from a seismic event at time t with a PGV of v (Eq. F-2)

and that $D(\tau|\, t,\, v) = 0$ mrem/yr for $\tau < t$. In the computational implementation of an actual analysis for the Yucca Mountain facility, the function $D(\tau|\, t,\, v)$ would be a complex model implemented through the linked operation of several computer programs. However, the functional representation in Equation F-2 is all that is needed for the present discussion.

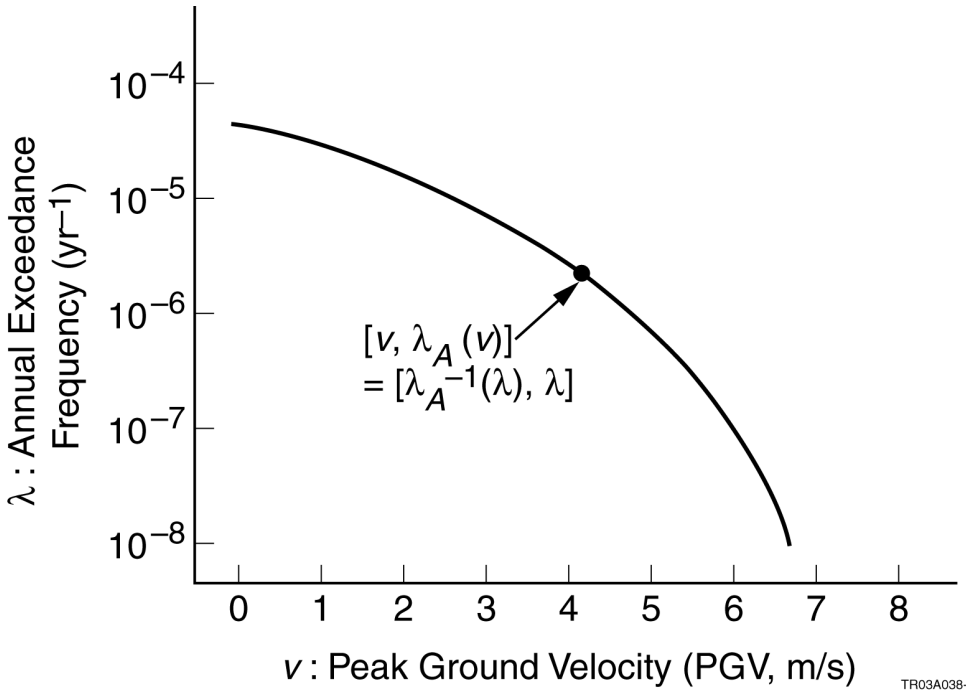

NOTE: Representation of aleatory uncertainty in PGV at disposal drifts induced by seismic events, with (1) [v, $\lambda_A(v)$] representing a point on the exceedance frequency curve, where v is a PGV from the abscissa and $\lambda_A(v)$ is the corresponding exceedance frequency on the ordinate, and (2) [$\lambda_A^{-1}(\lambda),\lambda$] representing the same point on the exceedance frequency curve, where λ is the exceedance frequency from the ordinate and $\lambda_A^{-1}(\lambda)$ is the corresponding PGV on the abscissa.

Figure F-1. Representation of Aleatory Uncertainty in PGV at Disposal Drifts Induced By Seismic Events

The Poisson process characterized by $\lambda_A(v)$ results in an unaccountably infinite number of possible dose curves [τ, $D(\tau|\ t,\ v)$], with one curve resulting for each possible occurrence time, PGV pair [t, v] (Figure F-2). One way to summarize these dose curves is by calculating an expected dose at each time τ. Given Assumptions 5.3 and 5.4, the expected dose $E_A[D(\tau|\ t,\ v)]$ to the RMEI at time τ from seismic events is given by

$$E_A\left[D\left(\tau|t,v\right)\right] = \int_{tMIN}^{\tau}\int_{vMIN}^{vMAX} D\left(\tau|t,v\right)\left[-d\lambda_A\left(v\right)/dv\right]dvdt \qquad \text{(Eq. F-3)}$$

$$= \int_{tMIN}^{\tau}\int_{\lambda MIN}^{\lambda MAX} D\left(\tau|t,\lambda_A^{-1}\left(\lambda\right)\right)d\lambda dt \qquad \text{(Eq. F-4)}$$

where (1) [*tMIN*, *tMAX*] defines the time interval under consideration (e.g., *tMIN* = 0 yr, *tMAX* = 10,000 yr) and $tMIN < \tau \leq tMAX$, (2) [*vMIN*, *vMAX*] and [λMIN, λMAX] define the ranges of PGVs and exceedance frequencies for PGVs, respectively, with $\lambda_A(vMIN) = \lambda MAX$

and $\lambda_A(vMAX) = \lambda MIN$ (e.g., $vMIN$ = 0.388 m/s, $vMAX$ = 10.73 m/s, $\lambda MIN = 10^{-8}$ yr^{-1}, $\lambda MAX = 10^{-4}$ yr^{-1}), (3) the double integral in Equation F-3 is defined by the limit of the approximating sums

$$
\begin{aligned}
E_A\left[D\left(\tau|t,v\right)\right] &\cong \sum_{i=1}^{nTM}\sum_{j=1}^{nPGV} D\left(\tau|t_i,v_j\right)\left[\lambda_A\left(v_{j-1}\right)-\lambda_A\left(v_j\right)\right]\Delta t_i \\
&= \sum_{i=1}^{nTM}\sum_{j=1}^{nPGV} D\left(\tau|t_i,v_j\right)\left[-\frac{\lambda_A\left(v_j\right)-\lambda_A\left(v_{j-1}\right)}{\Delta v_j}\right]\Delta v_j \Delta t_i \\
&\cong \sum_{i=1}^{nTM}\sum_{j=1}^{nPG} D\left(\tau|t_i,v_j\right)\left[-d\lambda_A\left(v\right)/dv\right]\Delta v_j \Delta t_i
\end{aligned}
\qquad \text{(Eq. F-5)}
$$

with $tMIN = t_0 < t_1 < \ldots < t_{nTM} = \tau$, $vMIN = v_0 < v_1 < \ldots < v_{nPGV} = vMAX$, $\Delta t_i = t_i - t_{i-1}$, and $\Delta v_j = v_j - v_{j-1}$, and (iv) the double integral in Equation F-4 follows from a change of variables in the integral involving PGV in Equation F-3. The validity of the integral representations for $E_A[D(\tau|\ t,\ v)]$ in Equations F-3 and F-4 depends on either assumption (ii) indicated in the first paragraph of this section being true or $\lambda MAX\ (\tau - tMIN)$ being sufficiently small to render the likelihood of two or more seismic events over the time interval $[tMIN, \tau]$ inconsequential (Eq. F-1).

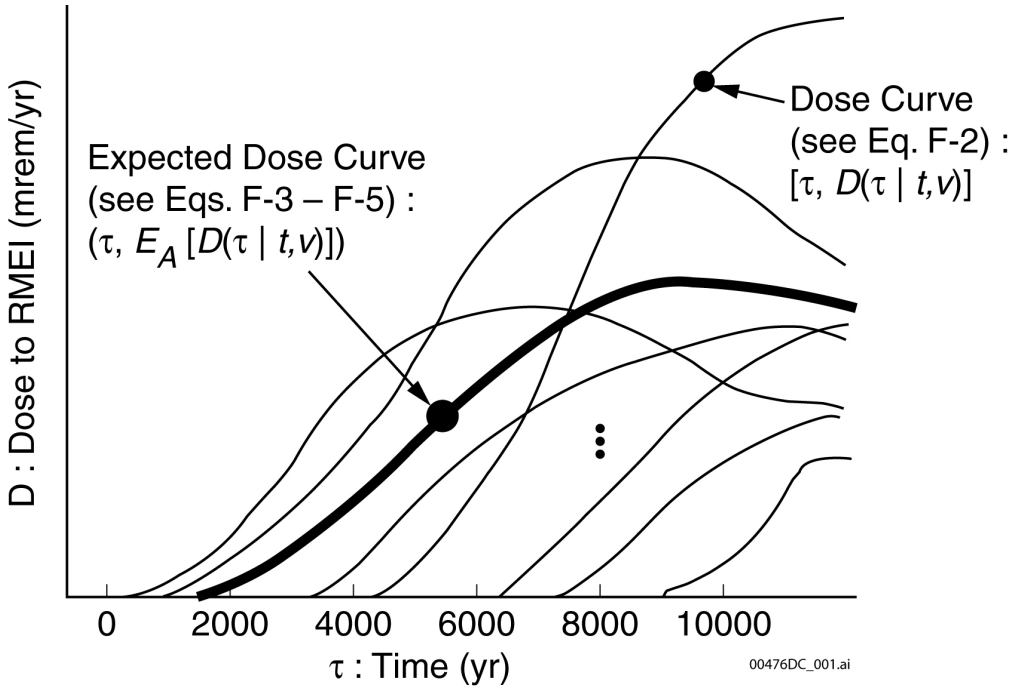

NOTE: Possible time-dependent dose curves $[\tau, D(\tau|\ t,\ v)]$ (Eq. F-2) to RMEI due to seismic events of different PGVs occurring at different times (note: due to the delays associated with groundwater transport, nonzero doses commence at a time subsequent to the occurrence of the initiating seismic events) and associated mean dose curve $(\tau, E_A[D(\tau|\ t,\ v)])$ (Eqs.F-4 – F-5).

Figure F-2. Possible Time-Dependent Dose Curves

As shown in Equations F-3 and F-4, expected dose $E_A[D(\tau|\ t,\ v)]$ is defined by double integrals involving time and PGV (i.e., Eq. F-3) or time and exceedance frequency λ (i.e., Eq. F-4). Thus, in concept, techniques for the numerical evaluation of integrals (e.g., appropriate forms of Simpson's rule or the trapezoidal rule) could be used to estimate $E_A[D(\tau|\ t,\ v)]$. An alternative approach to the estimation of $E_A[D(\tau|\ t,\ v)]$ is to use a Monte Carlo procedure for the evaluation of the integrals in Equations F-3 and F-4 (McKay et al. 1979 [DIRS 127905], Section 4.2.2), with this alternative approach currently favored for use in performance assessment for the Yucca Mountain facility.

The integral in Equation F-4 is used for illustration; analogous procedures can be applied to the integral in Equation F-3. Specifically, the representation for $E_A[D(\tau|\ t,\ v)]$ in Equation F-4 can be reformulated as

$$E_A\left[D\left(\tau|t,v\right)\right] = \int_{tMIN}^{tMAX}\int_{\lambda MIN}^{\lambda MAX} D\left(\tau|t,\lambda_A^{-1}\left(\lambda\right)\right) d\lambda dt \qquad \text{(Eq. F-6)}$$

$$= \int_{tMIN}^{tMAX}\int_{\lambda MIN}^{\lambda MAX}\left[\frac{D\left(\tau|t,\lambda_A^{-1}\left(\lambda\right)\right)}{\lambda IMP\left(\lambda\right) tIMP\left(t\right)}\right]\lambda IMP\left(\lambda\right) tIMP\left(t\right) d\lambda dt \qquad \text{(Eq. F-7)}$$

$$\cong \sum_{i=1}^{nIMP}\left[\frac{D\left(\tau|t_i,\lambda_A^{-1}\left(\lambda_i\right)\right)}{\lambda IMP\left(\lambda_i\right) tIMP\left(t_i\right)}\right]\Big/ nIMP \qquad \text{(Eq. F-8)}$$

where (1) Equation (F-6) is an immediate reformulation of Equation (F-4) based on the convention that $D(\tau|\ t,\ v) = 0$ mrem/yr for $\tau < t$ and is introduced so that the importance sampling procedure described in Equations (F-7) and (F-8) can sample on [*tMIN*, *tMAX*] rather than on [*tMIN*, τ], (2) Equation (F-7) is the standard important sampling transformation used in the Monte Carlo evaluation of an integral with $\lambda IMP(\lambda)$ and $tIMP(t)$ positive valued density functions defined on [λMIN, λMAX] and [*tMIN, tMAX*] (McKay et al. 1979 [DIRS 127905], Section 4.3.1), and (3) Eq. (F-8) is the importance sampling approximation to the integral defining $E_A[D(\tau|\ t,\ v)]$, and hence to $E_A[D(\tau|\ t,\ v)]$, obtained with a random or Latin hypercube sample $[t_i, \lambda_i]$, $i = 1, 2, \ldots, nIMP$, generated from [*tMIN*, *tMAX*] × [λMIN, λMAX] in consistency with the definitions of the density functions $tIMP(t)$ and $\lambda IMP(\lambda)$ (McKay et al. 1979 [DIRS 127905]) (Helton and Davis 2002 [DIRS 163475]). It is important to recognize that the distributions used in importance sampling have nothing to do with the treatment of uncertainty; they are simply numerical devices used to accelerate the convergence of Monte Carlo integration procedures and have no effect on the value of the integral being evaluated.

As examples, $\lambda IMP(\lambda)$ and $tIMP(t)$ often correspond to uniform or loguniform distributions. Specifically, uniform and loguniform importance sampling distributions for λ result in $\lambda IMP(\lambda)$ being defined by

$$\lambda IMP_u(\lambda) = \begin{cases} 1/(\lambda MAX - \lambda MIN) & \text{for } \lambda MIN \le \lambda \le \lambda MAX \\ 0 & \text{otherwise} \end{cases} \quad \text{(Eq. F-9)}$$

and

$$\lambda IMP_{lu}(\lambda) = \begin{cases} 1/[\lambda \ln(\lambda MAX/\lambda MIN)] & \text{for } \lambda MIN \le \lambda \le \lambda MAX \\ 0 & \text{otherwise,} \end{cases} \quad \text{(Eq. F-10)}$$

respectively. The density functions $tIMP_u(t)$ and $tIMP_{lu}(t)$ are defined analogously for uniform and loguniform sampling, respectively, on [$tMIN$, $tMAX$].

For uniform sampling on [λMIN, λMAX] and [$tMIN$, $tMAX$] in consistency with the density functions $\lambda IMP_u(\lambda)$ and $tIMP_u(t)$, the approximation to $E_A[D(\tau|\, t, v)]$ in Equation F-8 becomes

$$E_A[D(\tau|t,v)] \cong \left[\frac{(\lambda MAX - \lambda MIN)(tMAX - tMIN)}{nIMP}\right] \sum_{i=1}^{nIMP} D(\tau|t_i, \lambda_A^{-1}(\lambda_i)). \quad \text{(Eq. F-11)}$$

For loguniform sampling on [λMIN, λMAX] and [$tMIN$, $tMAX$] in consistency with the density functions $\lambda IMP_{lu}(\lambda)$ and $tIMP_{lu}(t)$, the approximation to $E_A[D(\tau|\, t, v)]$ in Equation F-8 becomes

$$E_A[D(\tau|t,v)] \cong \left[\frac{ln(\lambda MAX/\lambda MIN)\, ln(tMAX/tMIN)}{nIMP}\right] \sum_{i=1}^{nIMP} t_i \lambda_i\, D(\tau|t_i, \lambda_A^{-1}(\lambda_i)). \quad \text{(Eq. F-12)}$$

Other definitions for $\lambda IMP(\lambda)$ and $tIMP(t)$ result in analogous approximations to $E_A[D(\tau|\, t, v)]$.

The development of $E_A[D(\tau|\, t, v)]$ ends with a reminder that $E_A[D(\tau|\, t, v)]$ does not correspond to an actual dose received by the RMEI. Rather, $E_A[D(\tau|\, t, v)]$ is the expected (i.e., average) value of the infinitely many possible doses that the RMEI could receive at time τ from the infinitely many possible seismic events that could (but probably will not) occur before time τ. In particular, $E_A[D(\tau|\, t, v)]$ is the result of reducing all these possible doses and their associated "likelihood" to a single number through the integration processes described in Equations F-3 and F-4.

The character and likelihood of the actual doses that the RMEI could receive is preserved when the results of the analysis are presented as a distribution rather than as an expected value (Figure F-3). Exactly the same information is used in the development of distributions for dose

and expected values for dose; the only difference is in the details of the processing of this information. For example, the complementary cumulative distribution function for dose to the RMEI at time τ is defined by

$$prob_A\left[D(\tau|t,v) > D\right] = \int_{tMIN}^{\tau}\int_{vMIN}^{vMAX} \delta_D\left[D(\tau|t,v)\right]\left[-d\lambda_A(v)/dv\right] dvdt \quad \text{(Eq. F-13)}$$

$$= \int_{tMIN}^{\tau}\int_{\lambda MIN}^{\lambda MAX} \delta_D\left[D\left(\tau|t,\lambda_A^{-1}(\lambda)\right)\right] d\lambda dt, \quad \text{(Eq. F-14)}$$

where $prob_A[D(\tau|\ t,\ v) > D]$ is the probability that the RMEI will receive a dose at time τ (i.e., $D(\tau|\ t,\ v)$) that exceeds a dose of size D and the indicator function δ_D is defined by

$$\delta_D\left[D(\tau|t,v)\right] = \begin{cases} 1 & \text{if } D(\tau|t,v) > D \\ 0 & \text{otherwise.} \end{cases} \quad \text{(Eq. F-15)}$$

Except for the indicator function δ_D, the integrals defining $E_A[D(\tau|\ t,\ v)]$ in Equations F-3 and F-4 and the integrals defining $prob_A[D(\tau|\ t,\ v) > D]$ in Equations F-13 and F-14 are the same. Thus, the same evaluations of $D(\tau|\ t,\ v)$ that are used to estimate $E_A[D(\tau|\ t,\ v)]$ can also be used to estimate $prob_A[D(\tau|\ t,\ v) > D]$. In particular, the expected dose associated with the distribution defined by the complementary cumulative distribution function in Figure F-3 is the quantity $E_A[D(\tau|\ t,\ v)]$ defined in Equations F-3 – F-4; thus, the expected dose curve (τ, $E_A[D(\tau|\ t,\ v)]$) in Figure F-2 is a summary of the result of reducing distributions of the form shown in Figure F-3 to expected values.

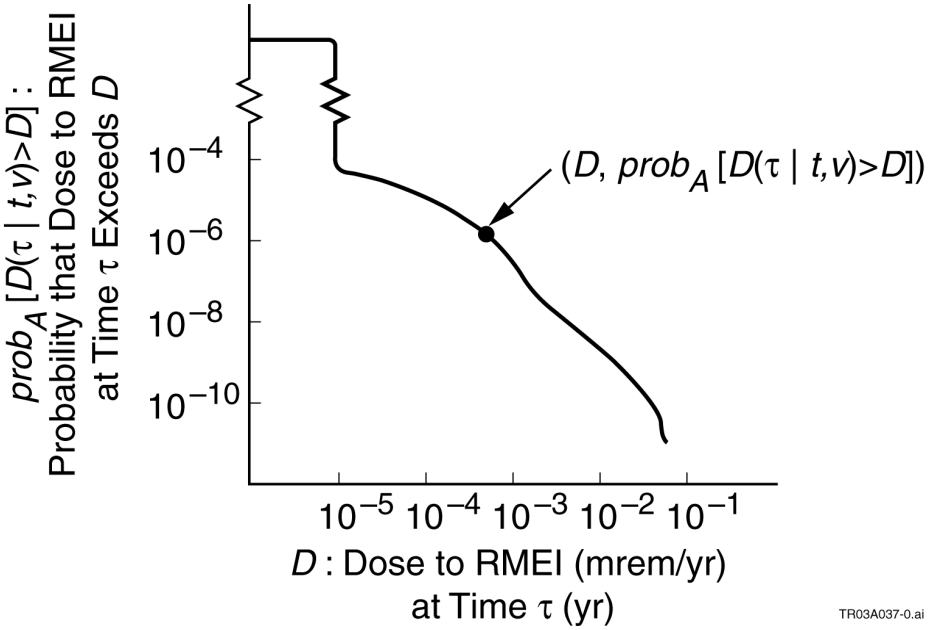

NOTE: i.e., a plot of (D, probA[D(τ| *t,* v) > D]).

Figure F-3. Illustration of Complementary Cumulative Distribution Function of Dose (mrem/yr) to RMEI at Time τ (yr)

As noted earlier, the integral representations for EA[D(τ| *t*, v)] in Equations F-3 and F -4 are only valid if either (1) the occurrence of a seismic event has no effect on the dose to the RMEI that derives from any subsequent seismic event or (2) λMAX (τ – tMIN) is sufficiently small to render the likelihood of two or more seismic events over the time interval [tMIN, τ] inconsequential. A stronger restriction is required for the validity of the integral representations of probA[D(τ| *t*, v) > D] in Equations F-13 and F-14. In particular, these representations are valid only if (2) above is satisfied. This constraint is necessary because the indicator function δD in Equations F-13 and F-14 is applied to the dose resulting from a single seismic event and thus the additive effects of two or more seismic events occurring before time τ is not incorporated into probA [D(τ| *t*, v) > D]. The appropriate formalism for the incorporation of the synergisms that could possibly exist in the determination of dose subsequent to multiple seismic events is discussed in a later section (Section F4).

F3. ALEATORY AND EPISTEMIC UNCERTAINTY

Section F2 introduces the calculation of expected dose $E_A[D(\tau|\, t,\, v)]$ at time τ from seismic events to the RMEI. The indicated expectation is over events that can occur in the future. As indicated in the Introduction (Section F1), uncertainty with respect to what can occur in the future is referred to as aleatory uncertainty, and in the example of the preceding section, its probabilistic nature was characterized by the function $\lambda_A(v)$. Specifically, aleatory uncertainty arises from the many possible seismic events that could occur over a time period of interest (e.g., 0 to 10,000 yr). If only aleatory uncertainty was present and $D(\tau|\, t,\, v)$ and $\lambda_A(v)$ were known with complete certainty, then the expected dose $E_A[D(\tau|\, t,\, v)]$ would derive solely from aleatory uncertainty and could be calculated with complete certainty.

Unfortunately, quantities such as $D(\tau|\, t,\, v)$ and $\lambda_A(v)$ can never be known with complete certainty in a PA as complex as the one that must be carried out for the Yucca Mountain facility. As a result, there is significant state of knowledge uncertainty with respect to how $D(\tau|\, t,\, v)$ and $\lambda_A(v)$ should be defined (Figure F4). This type of uncertainty is referred to as epistemic uncertainty to distinguish it from the previously introduced concept of aleatory uncertainty. Specifically, epistemic uncertainty arises from a lack of knowledge with respect to quantities used in the characterization of aleatory uncertainty or in the calculation of doses or other effects given the occurrence of a seismic event.

The notation introduced in the previous section (Section F2) for $D(\tau|\, t,\, v)$ and $\lambda_A(v)$ can be expanded to explicitly display a dependence on imprecisely known quantities. Specifically, $D(\tau|\, t,\, v)$ and $\lambda_A(v)$ can be represented by $D(\tau|\, t,\, v,\, \mathbf{e}_D)$ and $\lambda_A(v\,|\mathbf{e}_A)$, where

$$\mathbf{e}_D = \left[e_{D1}, e_{D2}, \ldots, e_{D,nD} \right] \qquad \text{(Eq. F-16)}$$

is a vector of imprecisely known variables required in the determination of $D(\tau|\, t,\, v)$, and

$$\mathbf{e}_A = \left[e_{A1}, e_{A2}, \ldots, e_{A,nA} \right] \qquad \text{(Eq. F-17)}$$

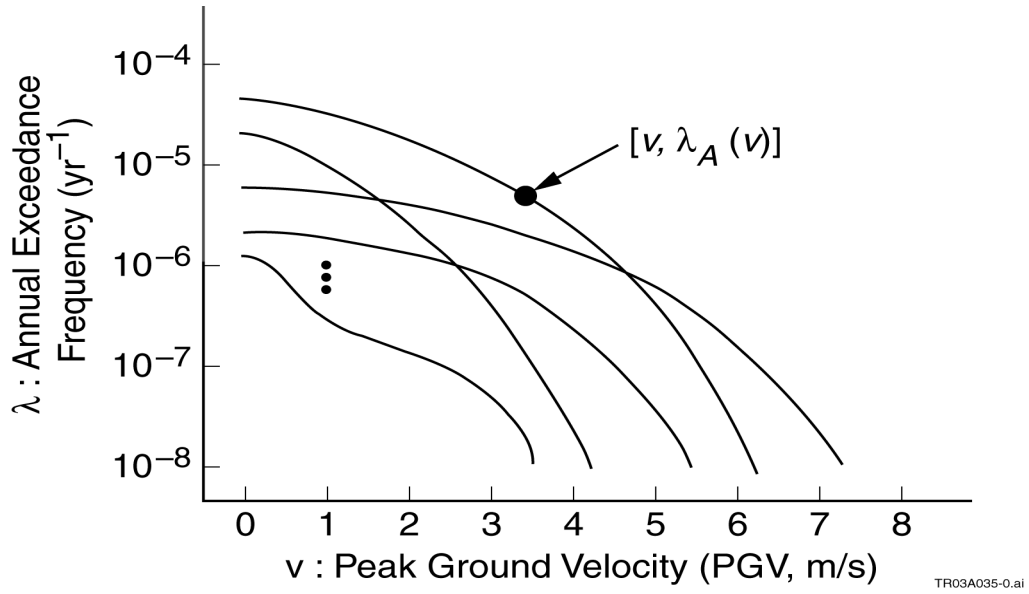

NOTE: Frequency curves $\lambda_A(v)$ resulting from epistemic uncertainty in PGV at disposal drifts induced by seismic events.

Figure F-4. Illustration of Multiple Exceedance Frequency Curves

is a vector of imprecisely known variables required in the definition of $\lambda_A(v)$. The fundamental idea is that the analysis has been developed to the point that it is believed that the elements of $\mathbf{e}_A$ and $\mathbf{e}_D$ should have fixed values and that appropriate analysis results would be obtained if these fixed values were known. Unfortunately, the appropriate values for these quantities are not known with certainty, and so there is epistemic uncertainty with respect to what their values should be. The elements of $\mathbf{e}_A$ and $\mathbf{e}_D$ can be interpreted generally enough to include imprecisely known functions and designators for alternative models. For notational convenience,

$$\mathbf{e} = [\mathbf{e}_A, \mathbf{e}_D] = [e_1, e_2, \ldots, e_{nE}] \qquad \text{(Eq. F-18)}$$

can be used to represent the vector of all imprecisely known variables.

Inclusion of a dependence on $\mathbf{e} = [\mathbf{e}_A, \mathbf{e}_D]$ results in the representations for $E_A[D(\tau|\, t,\, v)]$ in Equations F-3 and F-4 having the form

$$E_A\left[D\left(\tau|t, v, \mathbf{e}\right)\right] = \int_{tMIN}^{\tau}\int_{vMIN}^{vMAX} D\left(\tau|t, v, \mathbf{e}_D\right)\left[-d\lambda_A\left(v|\mathbf{e}_A\right)/dv\right] dvdt \qquad \text{(Eq. F-19)}$$

$$= \int_{tMIN}^{\tau}\int_{\lambda MIN}^{\lambda MAX} D\left(\tau|t, \lambda_A^{-1}\left(\lambda|\mathbf{e}_A\right), \mathbf{e}_D\right) d\lambda dt \,. \qquad \text{(Eq. F-20)}$$

The preceding notation emphasizes that the possible values for $\mathbf{e} = [\mathbf{e}_A, \mathbf{e}_D]$ result in different possible values for $\lambda_A(v\,|\mathbf{e}_A)$, $D(\tau\,|\,t,\, v,\, \mathbf{e}_D)$ and thus $E_A[D(\tau|\, t,\, v,\, \mathbf{e})]$. As $\mathbf{e}_D$ only affects the calculation of dose and $\mathbf{e}_A$ only affects the distributions that characterize aleatory uncertainty in t

and v, $E_A[D(\tau|\, t,\, v,\, \mathbf{e}_D) \mid \mathbf{e}_A]$ or $E_A[D(\tau|\, t,\, v) \mid \mathbf{e}_{\underline{A}},\, \mathbf{e}_D]$ are probably more conceptually correct notational representations for expected dose from aleatory uncertainty than $E_A[D(\tau|\, t,\, v,\, \mathbf{e})]$; however, for notational simplicity, the use of $E_A[D(\tau|\, t,\, v,\, \mathbf{e})]$ to represent this dose will be retained. Fortunately, the integrals in Equations F-19 and F-20 remove all ambiguity with respect to exactly what is represented by $E_A[D(\tau|\, t,\, v,\, \mathbf{e})]$.

Analyses for the Yucca Mountain facility, like most large performance assessments, use probability to characterize epistemic uncertainty. Specifically, distributions

$$D_1,\, D_2,\, \ldots,\, D_{nE}` \qquad \text{(Eq. F-21)}$$

are specified for the elements of $\mathbf{e}$, where D_k is the distribution assigned to e_k. Correlations and other restrictions involving pairs or larger groups of variables are also possible. These distributions and any associated restrictions provide a numerical quantification of what is known about individual variables and also the necessary starting structure to propagate this knowledge through the overall analysis. For notational convenience, the set of all possible values for $\mathbf{e}$ associated with the distributions in Equation F-21 will be represented by the set $\mathcal{E}$ (i.e., $\mathcal{E}$ is the sample space or universal set associated with epistemic uncertainty) and the corresponding density function defined on $\mathcal{E}$ will be represented by $d_E(\mathbf{e})$.

Each element $\mathbf{e}$ of $\mathcal{E}$ gives rise to a value for the expected dose $E_A[D(\tau|\, t,\, v,\, \mathbf{e})]$ indicated in Equations F-19 and F-20 and in Figure F-5. One way of describing the (epistemic) uncertainty in $E_A[D(\tau|\, t,\, v,\, \mathbf{e})]$ is to determine and present the range of values for $E_A[D(\tau|\, t,\, v,\, \mathbf{e})]$ that results from all possible values of $\mathbf{e}$ contained in $\mathcal{E}$. This is the simplest of all approaches to uncertainty analysis and is typically referred to as interval analysis.

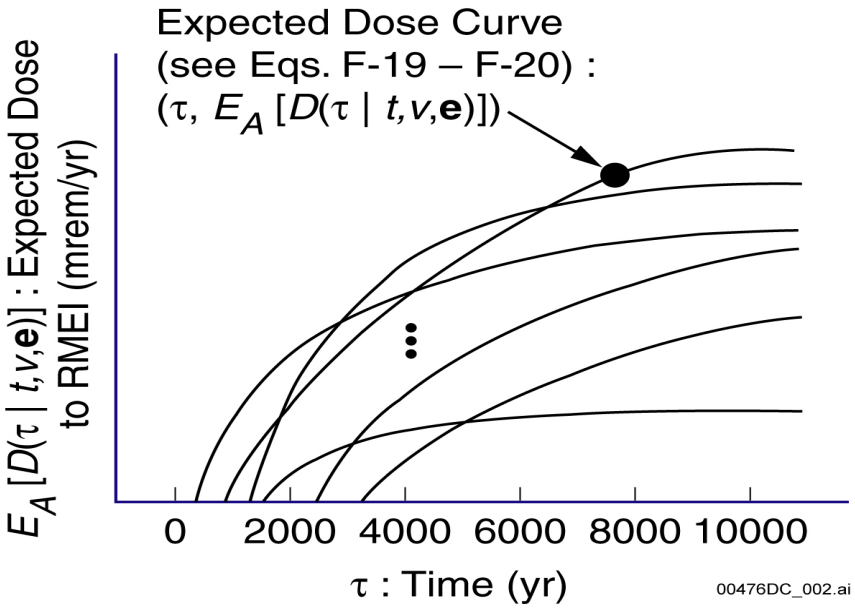

NOTE: Illustration of expected dose curves to RMEI resulting from epistemic uncertainty (i.e., plots of (τ, E_A[D(τ| t, v, **e**]) for $0 \le \tau \le 10{,}000$ yr and different values of **e**; see Eqs. F-19 – F-20.

Figure F-5. Illustration of Expected Dose Curves to RMEI Resulting From Epistemic Uncertainty

The specification of the distributions in Equation F-21 provides the necessary information to carry out more sophisticated uncertainty assessments than simple interval analysis. More specifically, the distributions in Equation F-21 provide the basis for calculating both the expected value and the distribution of $E_A[D(\tau|\, t,\, v,\, \mathbf{e})]$ that arise from possible values for **e**

(Figure F-6). In particular, the expected value $E_E(E_A[D(\tau|\, t,\, v,\, \mathbf{e})])$ of $E_A[D(\tau|\, t,\, v,\, \mathbf{e})]$ over epistemic uncertainty is given by:

$$E_E\left(E_A\left[D\left(\tau|t,v,\mathbf{e}\right)\right]\right) = \int_{\mathcal{E}} E_A\left[D\left(\tau|t,v,\mathbf{e}\right)\right] d_E\left(\mathbf{e}\right) dE \qquad \text{(Eq. F-22)}$$

$$= \int_{\mathcal{E}}\left[\int_{tMIN}^{tMAX}\int_{vMIN}^{vMAX} D\left(\tau|t,v,\mathbf{e}_D\right)\left[-d\lambda_A\left(v|\mathbf{e}_A\right)/dv\right] dvdt\right] d_E\left(\mathbf{e}\right) dE \qquad \text{(Eq. F-23)}$$

$$= \int_{\mathcal{E}}\left[\int_{tMIN}^{tMAX}\int_{\lambda MIN}^{\lambda MAX} D\left(\tau|t,\lambda_A^{-1}\left(\lambda|\mathbf{e}_A\right),\mathbf{e}_D\right) dvdt\right] d_E\left(\mathbf{e}\right) dE, \qquad \text{(Eq. F-24)}$$

where $\mathcal{E}$ and $d_E(\mathbf{e})$ are defined in conjunction with Equation F-21 and dE corresponds to an increment of volume from $\mathcal{E}$.

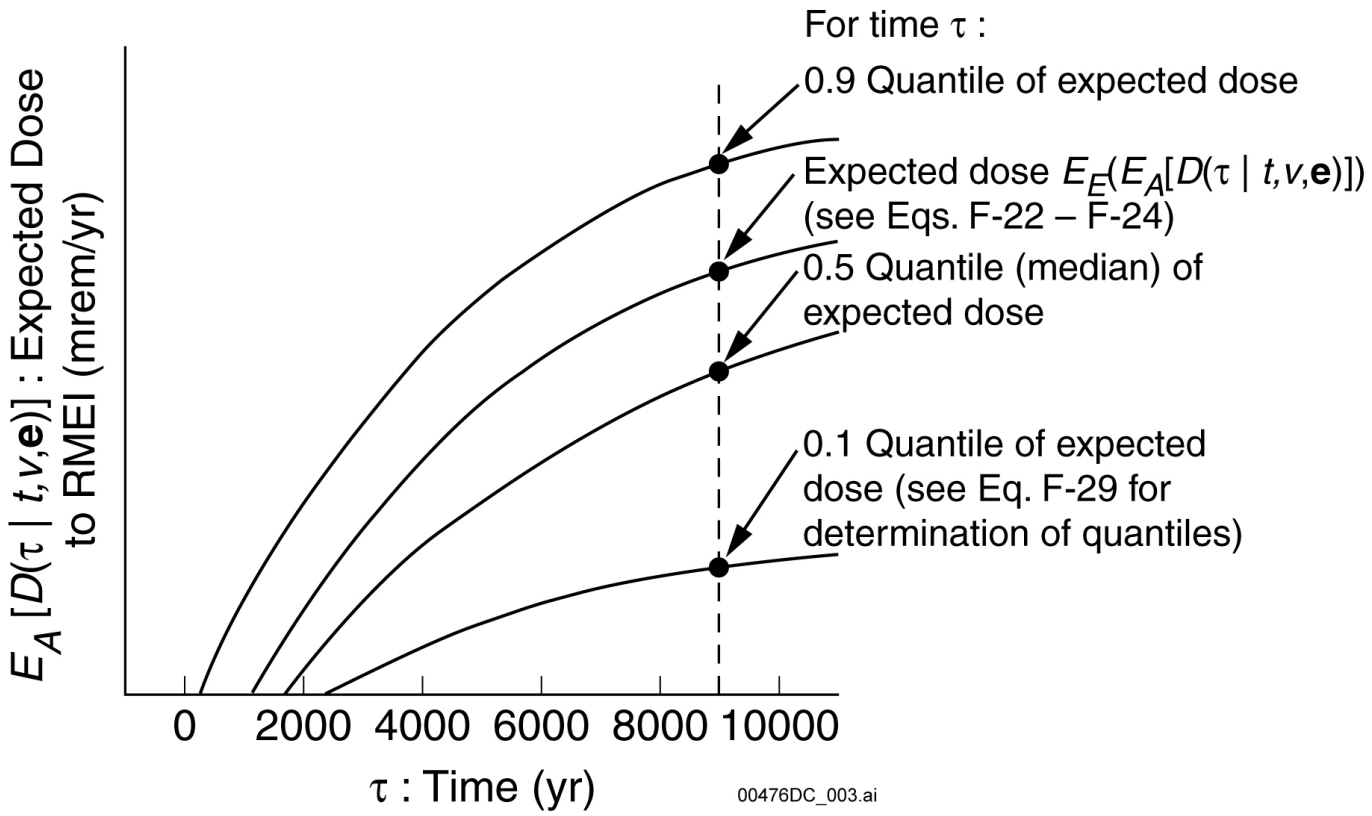

NOTE: Illustration of expected and selected quantile curves for distribution of expected (over aleatory uncertainty) dose curves resulting from epistemic uncertainty (i.e., the indicated expected and quantile curves derive from the epistemic uncertainty in **e** and result from integration over the set E of possible values for **e)**.

Figure F-6. Illustration of Expected and Selected Quantile Curves

Similarly, the epistemic (i.e., degree of belief) probability $prob_E(E_A[D(\tau|\, t,\ v,\ \mathbf{e})] > E)$ of exceeding an expected dose to the RMEI of size E is given by

$$prob_E\left(E_A\left[D\left(\tau|t,v,\mathbf{e}\right)\right]>E\right)=\int_{\mathcal{E}}\delta_E\left(E_A\left[D\left(\tau|t,v,\mathbf{e}\right)\right]\right)d_E\left(\mathbf{e}\right)dE \qquad \text{(Eq. F-25)}$$

$$=\int_{\mathcal{E}}\delta_E\left[\int_{tMIN}^{tMAX}\int_{vMIN}^{vMAX}D\left(\tau|t,v,\mathbf{e}_D\right)\left[-d\lambda_A\left(v|\mathbf{e}_A\right)/dv\right]dvdt\right]d_E\left(\mathbf{e}\right)dE \qquad \text{(Eq. F-26)}$$

$$=\int_{\mathcal{E}}\delta_E\left[\int_{tMIN}^{tMAX}\int_{\lambda MIN}^{\lambda MAX}D\left(\tau|t,\lambda_A^{-1}\left(\lambda|\mathbf{e}_A\right),\mathbf{e}_D\right)dvdt\right]d_E\left(\mathbf{e}\right)dE, \qquad \text{(Eq. F-27)}$$

where the indicator function δ_E is defined by

$$\delta_E\left(E_A\left[D\left(\tau|t,v,\mathbf{e}\right)\right]\right)=\begin{cases}1 & \text{if } E_A\left[D\left(\tau|t,v,\mathbf{e}\right)\right]>E\\ 0 & \text{otherwise}\end{cases} \qquad \text{(Eq. F-28)}$$

and plays the same role as the indicator function δ_D in Equations F-13 and F-14. The qth quantile (e.g., 0.1, 0.5, 0.9) for $E_A[D(\tau|\, t, v, \mathbf{e})]$ is obtained by solving the equation:

$$q = prob_E\left(E_A\left[D\left(\tau|t, v, \mathbf{e}\right)\right] > E\right) \qquad \text{(Eq. F-29)}$$

for E (see Figure F-6).

Two computational strategies for the estimation of $E_E(E_A[D(\tau|\, t, v, \mathbf{e})])$ are presented. The first strategy involves first approximating the integral over $\mathcal{E}$ and then approximating the integrals that define $E_A[D(\tau|\, t, v, \mathbf{e})]$. The second strategy involves treating $E_E(E_A[D(\tau|\, t, v, \mathbf{e})])$ as being defined by a single integral over the high dimensional space $\mathcal{AE}$ defined by:

$$\begin{aligned}\mathcal{AE} &= [tMIN, tMAX] \times [\lambda MIN, \lambda MAX] \times \mathcal{E} \\ &= \left\{\mathbf{ae} : \mathbf{ae} = [t, \lambda, \mathbf{e}], tMIN \le t \le tMAX, \lambda MIN \le \lambda \le \lambda MAX, \mathbf{e} \in \mathcal{E}\right\}\end{aligned} \qquad \text{(Eq. F-30)}$$

and then approximating this integral without drawing a distinction between the parts that derive from aleatory uncertainty and the parts that derive from epistemic uncertainty.

In Strategy 1, a random or Latin hypercube sample

$$\mathbf{e}_k = [\mathbf{e}_{Ak}, \mathbf{e}_{Dk}] = \left[e_{1k}, e_{2k}, \ldots, e_{nE,k}\right], k = 1, 2, \ldots, nS, \qquad \text{(Eq. F-31)}$$

is generated from $\mathcal{E}$ in consistency with the distributions indicated in Equation F-21. Then, $E_E(E_A[D(\tau|\, t, v, \mathbf{e})])$ is approximated by:

$$E_E\left(E_A\left[D\left(\tau|t, v, \mathbf{e}\right)\right]\right) \cong \sum_{k=1}^{nS} E_A\left[D\left(\tau|t, v, \mathbf{e}_k\right)\right] \Big/ nS. \qquad \text{(Eq. F-32)}$$

To complete the approximation of $E_E(E_A[D(\tau|\, t, v, \mathbf{e})])$, approximations $\hat{E}_A\ [D(\tau|\, t, v, \mathbf{e}_k)]$ to $E_A[D(\tau|\, t, v, \mathbf{e}_k)]$ for k = 1, 2, …, nS must be developed. Possibilities for the determination of $\hat{E}_A\,[D(\tau|\, t, v, \mathbf{e}_k)]$ include (1) use of the importance sampling procedures indicated in conjunction with Equations F-6 – F-12 and (2) development of computationally efficient procedures that depend on specific properties of the problem under consideration. Once the approximations $\hat{E}_A\,[D(\tau|\, t, v, \mathbf{e}_k)]$ to $E_A[D(\tau|\, t, v, \mathbf{e}_k)]$ are determined,

$$E_E\left(E_A\left[D\left(\tau|t, v, \mathbf{e}\right)\right]\right) \cong \sum_{k=1}^{nS} \hat{E}_A\left[D\left(\tau|t, v, \mathbf{e}_k\right)\right] \Big/ nS \qquad \text{(Eq. F-33)}$$

provides the final approximation to $E_E(E_A[D(\tau|\, t, v, \mathbf{e})])$.

With Strategy 1, the same numerical results used to estimate $E_E(E_A[D(\tau|\, t,\, v,\, \mathbf{e})])$ can also be used to estimate $prob_E(E_A[D(\tau|\, t,\, v,\, \mathbf{e})] > E)$. Specifically,

$$prob_E\left(E_A\left[D\left(\tau|t, v, \mathbf{e}\right)\right] > E\right) = \sum_{k=1}^{nS} \delta_E\left(\hat{E}_A\left[D\left(\tau|t, v, \mathbf{e}_k\right)\right]\right) \Big/ nS, \tag{Eq. F-34}$$

where the indicator function δ_E is defined in Equation F-28. Strategy 1 also provides the mapping:

$$\left(\mathbf{e}_k, \hat{E}_A\left[D\left(\tau|t, v, \mathbf{e}_k\right)\right]\right), k = 1, 2, \ldots, nS, \tag{Eq. F-35}$$

between uncertain analysis inputs (i.e., the $\mathbf{e}_k$) and analysis results (i.e., the $\hat{E}_A\ [D(\tau|\, t,\, v,\, \mathbf{e}_k)]$) that can be explored with a variety of sensitivity analysis procedures to determine the effects of individual uncertain analysis inputs on expected dose (Helton and Davis 2000 [DIRS 156572]).

In Strategy 2, a random or Latin hypercube sample:

$$\mathbf{ae}_k = \left[t_k, \lambda_k, \mathbf{e}_{Ak}, \mathbf{e}_{Dk}\right] = \left[t_k, \lambda_k, e_{1k}, e_{2k}, \ldots, e_{nE,k}\right], k = 1, 2, \ldots, nS, \tag{Eq. F-36}$$

is generated from $\mathcal{AE}$ (Equation F-29) in consistency with whatever sampling distributions are assigned to t and λ (Equations F-6 – F-12) and also in consistency with the distributions indicated in Equation F-21 for the elements of $\mathbf{e} = [\mathbf{e}_A,\ \mathbf{e}_D]$. Then, $E_E(E_A[D(\tau|\, t,\, v,\, \mathbf{e})])$ as represented in Equation F-24 is approximated by:

$$E_E\left(E_A\left[D\left(\tau|t, v, \mathbf{e}\right)\right]\right) \cong \sum_{k=1}^{nS}\left[\frac{D\left(\tau|t_k, \lambda_A^{-1}\left(\lambda_k|\mathbf{e}_{Ak}\right), \mathbf{e}_{Dk}\right)}{\lambda IMP\left(\lambda_k\right) tIMP\left(t_k\right)}\right] \Big/ nS, \tag{Eq. F-37}$$

where $\lambda IMP(\lambda)$ and $tIMP(t)$ are the sampling distributions for λ and t (Equations F-9) –F-12). In particular,

$$E_E\left(E_A\left[D\left(\tau|t, v, \mathbf{e}\right)\right]\right) \cong \left[\frac{\left(\lambda MAX - \lambda MIN\right)\left(tMAX - tMIN\right)}{nS}\right] \sum_{k=1}^{nS} D\left(\tau|t_k, \lambda_A^{-1}\left(\lambda_k|\mathbf{e}_{Ak}\right), \mathbf{e}_{Dk}\right), \tag{Eq. F- 38}$$

if $\lambda IMP(\lambda)$ and $tIMP(t)$ correspond to uniform distributions on $[\lambda MIN, \lambda MAX]$ and $[tMIN, tMAX]$ (Equations F-9 and F-11), and

$$E_E\left(E_A\left[D\left(\tau|t, v, \mathbf{e}\right)\right]\right) \cong \left[\frac{ln\left(\lambda MAX/\lambda MIN\right) ln\left(tMAX/tMIN\right)}{nS}\right] \sum_{k=1}^{nS} t_k \lambda_k D\left(\tau|t_k, \lambda_A^{-1}\left(\lambda_k|\mathbf{e}_{Ak}\right), \mathbf{e}_{Dk}\right) \tag{Eq. F-39}$$

if $\lambda IMP(\lambda)$ and $tIMP(t)$ correspond to loguniform distributions on $[\lambda MIN, \lambda MAX]$ and $[tMIN, tMAX]$ (Equations F-10 and F-12). Analogous approximations also hold for $E_E(E_A[D(\tau|\, t,\, v,\, \mathbf{e})])$ as represented in Equation F-23.

With Strategy 2, it is not possible to estimate the expected doses $E_A[D(\tau|\, t, v, \mathbf{e})]$ to the RMEI for different values of $\mathbf{e}$. This inability results from the concurrent variation of the aleatory variables t_k and $v_k = \lambda_A^{-1}\ (\lambda_k\,|\mathbf{e}_{Ak})$ and the epistemic variables $e_{1k}, e_{2k}, \ldots, e_{nE,k}$ associated with $\mathbf{e}_k = [\mathbf{e}_{Ak}, \mathbf{e}_{Dk}]$ in the determination of the doses:

$$D\left(\tau|t_k, \lambda_A^{-1}\left(\lambda_k|\mathbf{e}_{Ak}\right), \mathbf{e}_{Dk}\right), k = 1, 2, \ldots, nS, \qquad \text{(Eq. F-40)}$$

to the RMEI that are calculated for each sample element $\mathbf{ae}_k$ (Equation F-36) in Strategy 2. Specifically, because dose to the RMEI is known for only one pair $[t_k, v_k]$ of time, PGV values for each vector $\mathbf{e}_k = [\mathbf{e}_{Ak}, \mathbf{e}_{Dk}]$ of epistemic variable values, it is not possible to estimate the integral over time and PGV that defines the expected dose $E_A[D(\tau|\, t, v, \mathbf{e}_k)]$ associated with $\mathbf{e}_k$. As a result, Strategy 2 does not provide a basis to estimate the uncertainty in expected dose $E_A[D(\tau|\, t, v, \mathbf{e})]$ to the RMEI as defined by $prob_E(E_A[D(\tau|\, t, v, \mathbf{e})] > E)$ in Equations F-25 – F-27.

Strategy 2 does allow an estimate of the uncertainty in the dose to the RMEI due to both aleatory and epistemic uncertainty. In particular, this uncertainty is characterized by the probability:

$$prob_{EA}\left[D\left(\tau|t, v, \mathbf{e}_D\right) > D\right] = \int_E \int_{tMIN}^{tMAX} \int_{vMIN}^{vMAX} \delta_D\left[D\left(\tau|t, v, \mathbf{e}_D\right)\right]\left[-d\lambda_A\left(v|\mathbf{e}_A\right)/dv\right] d_E(\mathbf{e})\, dv dt\, dE \qquad \text{(Eq. F-41)}$$

$$= \int_E \int_{tMIN}^{tMAX} \int_{\lambda MIN}^{\lambda MAX} \delta_D\left[D\left(\tau|t, \lambda_A^{-1}\left(\lambda|\mathbf{e}_A\right), \mathbf{e}_D\right)\right] d_E(\mathbf{e})\, dv dt\, dE \qquad \text{(Eq. F-42)}$$

$$\cong \sum_{k=1}^{nS}\left[\frac{\delta_D\left[D\left(\tau|t_k, \lambda_A^{-1}\left(\lambda_k|\mathbf{e}_{Ak}\right), \mathbf{e}_{Dk}\right)\right]}{\lambda IMP(\lambda_k)\, tIMP(t_k)}\right] \Big/ nS, \qquad \text{(Eq. F-43)}$$

where (1) the indicator function δ_D is defined in Equation F-15, (2) the density functions $\lambda IMP(\lambda)$ and $tIMP(t)$ are the same as indicated in conjunction with Equations F-6 – F-12, and (3) the sample elements $\mathbf{ae}_k = [t_k, \lambda_k, \mathbf{e}_{Ak}, \mathbf{e}_{Dk}]$, $k = 1, 2, \ldots, nS$, correspond to the sample in Equation F-36. The preceding probability defines the complimentary cumulative distribution function for dose to the RMEI (i.e., $D(\tau \mid t, v, \mathbf{e}_D)$) that derives from both aleatory and epistemic uncertainty and is very different from the probability $prob_E(E_A[D(\tau|\, t, v, \mathbf{e})] > E)$ defined in Equations F-25 – F-27, which defines the complementary cumulative distribution function for expected dose to the RMEI (i.e., $E_A[D(\tau|\, t, v, \mathbf{e})]$) that derives from epistemic uncertainty.

Strategy 2 provides the following mapping from analysis inputs to analysis results:

$$\left[\mathbf{ae}_k, D\left(\tau|t_k, v_k, \mathbf{e}_{Dk}\right)\right], k = 1, 2, \ldots, nS, \qquad \text{(Eq. F-44)}$$

where $v_k = \lambda_A^{-1}\ (\lambda_k \mid \mathbf{e}_{Ak})$. Like the mapping in Equation F-35 associated with Strategy 1, this mapping can be explored with a variety of sensitivity analysis procedures (Helton 1994 [DIRS 107739] and Paté-Cornell 1996 [DIRS 107499]). However, the interpretation of any

results obtained in such a sensitivity analysis would be very different from the interpretation of results obtained from a sensitivity analysis of the mapping in Equation F-35 for two reasons. First, the mapping in Equation 35 obtained with Strategy 1 involves expected dose to the RMEI (i.e., $E_A[D(\tau|\ t,\ v,\ \mathbf{e})]$) while the mapping in Equation F-44 obtained with Strategy 2 involves dose to the RMEI (i.e., $D(\tau|\ t,\ v,\ \mathbf{e})$). Hence, the dependent variables under study are not the same. Second, the mapping obtained with Strategy 1 involves only epistemic uncertainty while the mapping obtained with Strategy 2 involves both epistemic uncertainty and aleatory uncertainty. Thus, the uncertainty spaces being sampled from (i.e., $\mathcal{E}$ and $\mathcal{AE}$) are fundamentally different.

If implemented correctly and with sufficiently large sample sizes to assure convergence, both strategies will produce the same value for the expected dose $E_E(E_A[D(\tau|\ t,\ v,\ \mathbf{e})])$. Strategy 1 has the advantage that it permits uncertainty and sensitivity studies of the effects of epistemic uncertainty on the expected dose to the RMEI (i.e., $E_A[D(\tau|\ t,\ v,\ \mathbf{e})]$); such studies are not possible with Strategy 2. Strategy 2 has the advantage that it is likely to be more computationally efficient (i.e., require fewer evaluations of $D(\tau|\ t,\ v,\ \mathbf{e})$) in the determination of $E_E(E_A[D(\tau|\ t,\ v,\ \mathbf{e})])$ than Strategy 1.

Both computational strategies are used in the determination of expected dose to the RMEI from igneous events at the Yucca Mountain facility. In particular, the expected dose $E_E(E_A[D(\tau|\ t,\ v,\ \mathbf{e})])$ from the eruptive component of igneous events is calculated with Strategy 1, and the expected dose $E_E(E_A[D(\tau|\ t,\ v,\ \mathbf{e})])$ from the groundwater release component of igneous events is calculated with Strategy 2. Thus, when viewed at a sufficiently high-level, the calculation of expected doses $E_E(E_A[D(\tau|\ t,\ v,\ \mathbf{e})])$ from seismic events, the eruptive component of igneous events, and the groundwater component of igneous events is conceptually the same, although the uncertain variables, the representation of aleatory uncertainty, and the dose models are at least partially different for these three cases.

F4. EXPECTED DOSE FROM ALEATORY AND EPISTEMIC UNCERTAINTY INCLUDING SYNERGISMS

The computational procedures for the calculation of expected doses presented in the two preceding sections (Sections F2, F3) are predicated on the assumption that the occurrence of a seismic event has no effect on doses that derive from any subsequent seismic event. Further, the computational procedures presented for the determination of distributions of doses do not include the possibility of multiple seismic events occurring before a given time. This section briefly presents the formal representations for expected dose and distribution of expected dose that includes the possibility of synergisms between multiple seismic events on dose subsequent to these events.

For this representation, the occurrence of multiple seismic events between *tMIN* and *tMAX* is possible. The properties of a sequence of seismic event occurring between *tMIN* and *tMAX* is represented by a vector:

$$\mathbf{a} = [\mathbf{a}_1, \mathbf{a}_2, \ldots, \mathbf{a}_{nO}], \tag{Eq. F-45}$$

where

$$\mathbf{a}_i = [\mathbf{a}_{i1}, \mathbf{a}_{i2}, \ldots, \mathbf{a}_{i,nP}] \tag{Eq. F-46}$$

is the vector of properties (e.g., time of occurrence, PGV, extent of rock fall, …) that, in essence, defines the i^{th} seismic event occurring between *tMIN* and *tMAX*. If time of occurrence and PGV are the only two defining characteristics of a seismic event, then $\mathbf{a}_i$ would be defined by:

$$\mathbf{a}_i = [t_i, v_i], \tag{Eq. F-47}$$

where t_i and v_i are the time of occurrence and PGV associated with the i^{th} seismic event, and $\mathbf{a}$ would be defined by

$$\begin{aligned} \mathbf{a} &= [\mathbf{a}_{i1}, \mathbf{a}_{i2}, \ldots, \mathbf{a}_{nO}] \\ &= [t_1, v_1, t_2, v_2, \ldots, t_{nO}, v_{nO}]. \end{aligned} \tag{Eq. F-48}$$

For completeness, $\mathbf{a}_0$ can be used to represent the degenerate vector (i.e., the vector with no components) that corresponds to no seismic events occurring between *tMIN* and *tMAX*. Then, the set $\mathcal{A}$ containing $\mathbf{a}_0$ and all possible vectors $\mathbf{a}$ of the form indicated in Equation F-45 corresponds to the universe (i.e., sample space) of all possible sequences of seismic events that could occur over the time interval [*tMIN*, *tMAX*].

Aleatory uncertainty with respect to the potential occurrence of the sequences of seismic events represented by the elements of $\mathcal{A}$ is characterized by a probability distribution defined on $\mathcal{A}$. For notational convenience, this distribution is represented by its density function $d_A(\mathbf{a})$, where the probability $prob_A(\mathcal{U})$ of a subset $\mathcal{U}$ of $\mathcal{A}$ is given by:

$$prob_A(\mathcal{U}) = \int_{\mathcal{U}} d_A(\mathbf{a})\, dA. \tag{Eq. F-49}$$

For example, if the elements of $\mathcal{A}$ are of the form indicated in Equation F-48, then $d_A(\mathbf{a})$ could derive from a function $\lambda_A(v)$ of the form considered in the two preceding sections (Sections F2, F3).

The expected dose $E_A[D(\tau|\mathbf{a})]$ to the RMEI at time τ would then be defined by:

$$E_A[D(\tau|\mathbf{a})] = \int_{\mathcal{A}} D(\tau|\mathbf{a})\, d_A(\mathbf{a})\, dA, \tag{Eq. F-50}$$

where $D(\tau|\mathbf{a})$ = dose (mrem/yr) to the RMEI at time τ from the sequence of seismic events represented by $\mathbf{a}$.

The representation for $D(\tau|\mathbf{a})$ allows the potential for synergistic interactions involving two or more seismic events. Similarly, the probability $prob_A[D(\tau|\mathbf{a}) > D]$ that the dose to the RMEI at time τ will exceed a dose of size D is given by:

$$prob_A\left[D(\tau|\mathbf{a}) > D\right] = \int_{\mathcal{A}} \delta_D\left[D(\tau|\mathbf{a})\right] d_A(\mathbf{a})\, dA, \tag{Eq. F-51}$$

where

$$\delta_D\left[D(\tau|\mathbf{a})\right] = \begin{cases} 1 & \text{if } D(\tau|\mathbf{a}) > D \\ 0 & \text{otherwise.} \end{cases} \tag{Eq. F-52}$$

Unlike the representation for probA[D(τ| t, v)] in Equations F-13 and F-14, in which a = [t, v] corresponds to a single seismic event and $D(\tau|\ t,\ v)$ corresponds to the dose from this single event, the preceding representation for $prob_A[D(\tau|\mathbf{a}) > D]$ incorporates the possibility that $\mathbf{a}$ corresponds to multiple seismic events and that $D(\tau|\mathbf{a})$ is affected by some form of interaction (i.e., synergism) involving these events.

As before, epistemic uncertainty exists in the elements of a vector $\mathbf{e} = [\mathbf{e}_A,\ \mathbf{e}_D]$ of the form defined in Equation F-18 with (1) this uncertainty characterized by probability distributions D_1, D_2, …, D_{nE} for the elements of $\mathbf{e}$ as indicated in Eq. F-21, (2) the set of all possible values for $\mathbf{e}$ constituting a set $\mathcal{E}$, and (3) the distributions D_1, D_2, …, D_{nE} giving rise to a density function $d_E(\mathbf{e})$ defined on $\mathcal{E}$. With the introduction of epistemic uncertainty in the elements of $\mathbf{e}$, dose $D(\tau|\mathbf{a},\ \mathbf{e}_D)$ to the RMEI is a function of $\mathbf{e}_D$, and expected dose $E_A[D(\tau|\mathbf{a},\ \mathbf{e})]$ to the RMEI arising from aleatory uncertainty is a function of both $\mathbf{e}_A$ and $\mathbf{e}_D$. In particular, the density function $d_A(\mathbf{a}|\mathbf{e}_A)$ and also possibly the sample space $\mathcal{A}(\mathbf{e}_A)$ associated with aleatory uncertainty can change as a function of $\mathbf{e}_A$. As a result, expected dose $E_A[D(\tau|\mathbf{a},\ \mathbf{e})]$ arising from aleatory uncertainty now has the form

$$E_A\left[D(\tau|\mathbf{a},\mathbf{e})\right] = \int_{\mathcal{A}(\mathbf{e}_A)} D(\tau|\mathbf{a},\mathbf{e}_D)\, d_A(\mathbf{a}|\mathbf{e}_A)\, dA, \tag{Eq. F-53}$$

and the expected value $E_E(E_A[D(\tau|\mathbf{a},\ \mathbf{e})])$ of $E_A[D(\tau|\mathbf{a},\ \mathbf{e})]$ over epistemic uncertainty has the form

$$E_E\left(E_A\left[D(\tau|\mathbf{a},\mathbf{e})\right]\right) = \int_{\mathcal{E}} E_A\left[D(\tau|\mathbf{a},\mathbf{e})\right] d_E(\mathbf{e})\, dE \tag{Eq. F-54}$$

$$= \int_{\mathcal{E}}\left[\int_{\mathcal{A}(\mathbf{e}_A)} D(\tau|\mathbf{a},\mathbf{e}_D)\, d_A(\mathbf{a}|\mathbf{e}_A)\, dA\right] d_E(\mathbf{e})\, dE. \tag{Eq. F-55}$$

The preceding results are analogous to those in Equations F-19 and F-20 and Equations F-22 - F-24 with a more general dependence on the properties of the seismic events under consideration now incorporated into the representation of dose and expected dose.

The probability $prob_E(E_A[D(\tau|\mathbf{a}, \mathbf{e})] > E)$ that an expected dose of size E will be exceeded is now given by:

$$prob_E\left(E_A\left[D\left(\tau|\mathbf{a}, \mathbf{e}\right)\right] > E\right) = \int_{\mathcal{E}} \delta_E\left(E_A\left[D\left(\tau|\mathbf{a}, \mathbf{e}\right)\right]\right) d_E\left(\mathbf{e}\right) dE \quad \text{(Eq. F-56)}$$

$$= \int_{\mathcal{E}} \delta_E\left(\int_{\mathcal{A}(\mathbf{e}_A)} D\left(\tau|\mathbf{a}, \mathbf{e}_D\right) d_A\left(\mathbf{a}|\mathbf{e}_A\right) dA\right) d_E\left(\mathbf{e}\right) dE, \quad \text{(Eq. F-57)}$$

where

$$\delta_E\left(E_A\left[D\left(\tau|\mathbf{a}, \mathbf{e}\right)\right]\right) = \begin{cases} 1 & \text{if } E_A\left[D\left(\tau|\mathbf{a}, \mathbf{e}\right)\right] > E \\ 0 & \text{otherwise.} \end{cases} \quad \text{(Eq. F-58)}$$

The preceding result is analogous to the results in Equations F-25 – F-27 except, as already explained, a more general dependence of dose on the properties of seismic events is allowed.

Computational Strategies 1 and 2 described in the preceding section (Section F3) for the evaluation of expected dose $E_E(E_A[D(\tau|\mathbf{a}, \mathbf{e})])$ with $\mathbf{a} = [t, v]$ can also be applied to the evaluation of expected dose with the more complex forms introduced in this section for $\mathbf{a}$ and the dose that derives from $\mathbf{a}$. The procedures are conceptually the same for both cases and will not be repeated here. However, the same caveats as presented at the end of Section F3 still apply. Further, if the probabilistic structure of the set $\mathcal{A}$ is complicated, the actual construction of iterated integrals and associated density functions for integration over $\mathcal{A}$ can be a difficult task.

INTENTIONALLY LEFT BLANK

APPENDIX G

LISTING OF ELECTRONIC FILES ON CD (APPENDIX H)

The files listed in Table G-1 are provided on CD with this document. These files provide electronic versions of the spreadsheets presented in Appendices A, B, and E of this report.

Table G-1. Listing of Electronic Files on CD (Appendix H)

File Name	Date and Time	Size	Contents
Appendix A Rev01 Final.xls	9/21/2004 4:48 PM	45 KB	Electronic version of Appendix A
Appendix B Rev01 Final.xls	9/21/2004 5:08 PM	63 KB	Electronic version of Appendix B
Appendix E Rev01 Final.xls	9/22/2004 8:16 AM	50 KB	Electronic version of Appendix E

INTENTIONALLY LEFT BLANK

APPENDIX H

CD WITH ELECTRONIC FILES

INTENTIONALLY LEFT BLANK